frontiers | Research Topics

Immune-boosting effects of dietary bioactive polysaccharides

Edited by
Baojun Xu, Ammad Ahmad Farooqi and Bin Du

Published in
Frontiers in Nutrition
Frontiers in Immunology

FRONTIERS EBOOK COPYRIGHT STATEMENT

The copyright in the text of individual articles in this ebook is the property of their respective authors or their respective institutions or funders. The copyright in graphics and images within each article may be subject to copyright of other parties. In both cases this is subject to a license granted to Frontiers.

The compilation of articles constituting this ebook is the property of Frontiers.

Each article within this ebook, and the ebook itself, are published under the most recent version of the Creative Commons CC-BY licence. The version current at the date of publication of this ebook is CC-BY 4.0. If the CC-BY licence is updated, the licence granted by Frontiers is automatically updated to the new version.

When exercising any right under the CC-BY licence, Frontiers must be attributed as the original publisher of the article or ebook, as applicable.

Authors have the responsibility of ensuring that any graphics or other materials which are the property of others may be included in the CC-BY licence, but this should be checked before relying on the CC-BY licence to reproduce those materials. Any copyright notices relating to those materials must be complied with.

Copyright and source acknowledgement notices may not be removed and must be displayed in any copy, derivative work or partial copy which includes the elements in question.

All copyright, and all rights therein, are protected by national and international copyright laws. The above represents a summary only. For further information please read Frontiers' Conditions for Website Use and Copyright Statement, and the applicable CC-BY licence.

ISSN 1664-8714
ISBN 978-2-83251-073-5
DOI 10.3389/978-2-83251-073-5

About Frontiers

Frontiers is more than just an open access publisher of scholarly articles: it is a pioneering approach to the world of academia, radically improving the way scholarly research is managed. The grand vision of Frontiers is a world where all people have an equal opportunity to seek, share and generate knowledge. Frontiers provides immediate and permanent online open access to all its publications, but this alone is not enough to realize our grand goals.

Frontiers journal series

The Frontiers journal series is a multi-tier and interdisciplinary set of open-access, online journals, promising a paradigm shift from the current review, selection and dissemination processes in academic publishing. All Frontiers journals are driven by researchers for researchers; therefore, they constitute a service to the scholarly community. At the same time, the *Frontiers journal series* operates on a revolutionary invention, the tiered publishing system, initially addressing specific communities of scholars, and gradually climbing up to broader public understanding, thus serving the interests of the lay society, too.

Dedication to quality

Each Frontiers article is a landmark of the highest quality, thanks to genuinely collaborative interactions between authors and review editors, who include some of the world's best academicians. Research must be certified by peers before entering a stream of knowledge that may eventually reach the public - and shape society; therefore, Frontiers only applies the most rigorous and unbiased reviews. Frontiers revolutionizes research publishing by freely delivering the most outstanding research, evaluated with no bias from both the academic and social point of view. By applying the most advanced information technologies, Frontiers is catapulting scholarly publishing into a new generation.

What are Frontiers Research Topics?

Frontiers Research Topics are very popular trademarks of the *Frontiers journals series*: they are collections of at least ten articles, all centered on a particular subject. With their unique mix of varied contributions from Original Research to Review Articles, Frontiers Research Topics unify the most influential researchers, the latest key findings and historical advances in a hot research area.

Find out more on how to host your own Frontiers Research Topic or contribute to one as an author by contacting the Frontiers editorial office: frontiersin.org/about/contact

Immune-boosting Effects of Dietary Bioactive Polysaccharides

Topic editors

Baojun Xu — United International College, China

Ammad Ahmad Farooqi — Institute of Biomedical and Genetic Engineering (IBGE), Pakistan

Bin Du — Hebei Normal University of Science and Technology, China

Citation

Xu, B., Farooqi, A. A., Du, B., eds. (2023). *Immune-boosting effects of dietary bioactive polysaccharides*. Lausanne: Frontiers Media SA.

doi: 10.3389/978-2-83251-073-5

Table of contents

frontiers | Frontiers in Nutrition

TYPE Editorial
PUBLISHED 02 December 2022
DOI 10.3389/fnut.2022.1102641

Check for updates

OPEN ACCESS

EDITED AND REVIEWED BY
Willem Van Eden,
Utrecht University, Netherlands

*CORRESPONDENCE
Baojun Xu
baojunxu@uic.edu.cn

SPECIALTY SECTION
This article was submitted to Nutritional Immunology, a section of the journal Frontiers in Nutrition

RECEIVED 19 November 2022
ACCEPTED 23 November 2022
PUBLISHED 02 December 2022

CITATION
Du B and Xu B (2022) Editorial: Immune-boosting effects of dietary bioactive polysaccharides. *Front. Nutr.* 9:1102641. doi: 10.3389/fnut.2022.1102641

COPYRIGHT
© 2022 Du and Xu. This is an open-access article distributed under the terms of the Creative Commons Attribution License (CC BY). The use, distribution or reproduction in other forums is permitted, provided the original author(s) and the copyright owner(s) are credited and that the original publication in this journal is cited, in accordance with accepted academic practice. No use, distribution or reproduction is permitted which does not comply with these terms.

Editorial: Immune-boosting effects of dietary bioactive polysaccharides

Bin Du[1] and Baojun Xu[2]*

[1]Hebei Key Laboratory of Natural Products Activity Components and Function, Hebei Normal University of Science and Technology, Qinhuangdao, China, [2]Food Science and Technology Program, Department of Life Sciences, BNU–HKBU United International College, Zhuhai, China

KEYWORDS

immunomodulation, polysaccharides, cell signaling, molecular pathways, cellular mechanisms

Editorial on the Research Topic
Immune-boosting effects of dietary bioactive polysaccharides

In recent year, polysaccharides currently represent a hot research field. Dietary bioactive polysaccharides have attracted more attention due to its non-harmful and non-toxic properties (1, 2). Abundant studies have identified valuable biological activities of dietary bioactive polysaccharides, especially immunomodulating activity (3, 4). Previous studies have shown that the mechanisms involved in immunomodulating effects are due to the modulation of innate immunity and macrophage function (5). However, the underlying cellular signaling and molecular mechanisms of their immune-boosting activity are not clear.

This Research Topic is aimed at collecting and summarizing the immune-boosting effects of dietary bioactive polysaccharides (such as inulin, dietary gum, fucoidan, glucan, glucomannan, heteropolysaccharides, etc.) from different natural sources (such as fruits and vegetables, cereal grains, edible mushrooms, sea foods, medicinal plants) in immune cells, animal study and clinical study as well.

In this special e-collection there are nine papers covering the above-mentioned aspects. Roselli et al. investigated the anti-inflammatory activity of galactooligosaccharide in an *in vitro* model of ulcerative colitis (UC)-like inflamed intestinal cells. The findings indicated that Bimuno GOS at different concentrations, while not affecting cell monolayer permeability, was shown to counteract UC-like intestinal inflammatory responses and damages induced by DSS. Indeed, Bimuno GOS was able to counteract the detrimental effects of DSS on cell permeability, determined by transepithelial electrical resistance, phenol red apparent permeability, and tight- and adherent junction protein distribution. Furthermore, Bimuno GOS inhibited the DSS-induced NF-kB nuclear translocation and pro-inflammatory cytokine secretion. Further analyses showed that Bimuno GOS was able to revert the expression levels of most of the proteins involved in the NF-κB cascade to control levels (Roselli et al.).

Lycium barbarum polysaccharides have been widely explored for their potential health properties. Zhang et al. tested the mechanisms of *L. barbarum* residue (RW) and fermented *L. barbarum* residue (RFW) on meat quality and immunity of sheep. Fifty-four Tan sheep were randomly divided into control, RFW or RW treatments. Data showed that RFW and RW increased the carcass weight, fat content, ash content and reduced the cooking loss of lamb. RFW performed more significant effects on activating immune-related genes than those of RW. The expression of chemokines and immune-related pathways, such as signaling pathways of interleukin-17 signaling pathway and NOD-like receptor signaling pathway, were elevated in sheep fed RFW. RW increased the diversity in rumen metabolites, especially compositions of lipids, organic acids and organ heterocyclic compounds (Zhang et al.).

Park et al. assessed the immune-enhancing effect of co-treatment with *Kalopanax pictus Nakai* Bark and *Nelumbo nucifera* Gaertner leaf extract (KPNN) in a cyclophosphamide (Cy)-induced immunosuppressed rat model. KPNN significantly increased phospho-NF-κB and phospho-ERK protein levels and cell viability in macrophages. KPNN significantly increased the NK cell activity in splenocytes compared to that in the control. Cy treatment decreased tumor necrosis factor (TNF)-α, interleukin (IL)-6, and interferon-γ production. In the Cy-induced immunosuppression rat model, KPNN-treated rats had significantly higher body weights and tissue weights than the Cy-treated rats. Additionally, KPNN treatment restored the immune-related factors, such as total leukocyte, lymphocyte, and intermediate cell contents, to their normal levels in the blood. The blood cytokines (TNF-α and IL-6) were increased, and spleen tissue damage was significantly alleviated (Park et al.).

In this Research Topic, there are two papers covering the fucoidan research. Fucoidan is a type of polysaccharide rich in sulfuric acid groups and is mainly found in brown algae. In this study, the effect of sterile fucoidan on the T-cell response and the subsequent modulation of osteogenesis is investigated. The physicochemical features of fucoidan treated by high-temperature autoclave sterilization are characterized by UV–visible spectroscopy, X-ray diffraction, Fourier transform infrared and nuclear magnetic resonance analysis. It is demonstrated that high-temperature autoclave treatment resulted in fucoidan depolymerization, with no change in its key bioactive groups. Further, sterile fucoidan promotes T cells proliferation and the proportion of differentiated T cells decreases with increasing concentration of fucoidan. In addition, the supernatant of T cells co-cultured with fucoidan greatly suppresses the osteogenic differentiation of MC3T3-E1 by downregulating the formation of alkaline phosphatase and calcium nodule compared with fucoidan (Huang et al.).

In another study, the effects of *Laminaria japonica* fucoidan (LF) on immune regulation and intestinal microflora in cyclophosphamide (CTX)-treated mice were investigated in this work. Results indicated that LF significantly enhanced the spleen and thymus indices, promoted spleen lymphocyte and peritoneal macrophages proliferation, and increased the immune-related cytokines production in serum. Moreover, LF could regulate intestinal flora composition, increasing the abundance of *Lactobacillaceae* and *Alistipes*, and inhibiting *Erysipelotrichia*, *Turicibacter*, *Romboutsia*, *Peptostreptococcaceae*, and *Faecalibaculum* (Tang et al.).

Yang et al. investigated the structural characterization and immunological activity *in vitro* and *in vivo* of a polysaccharide from the rhizome of *Menispermum dauricum*. A new polysaccharide named MDP was isolated from the rhizome of *M. dauricum* by hot water extraction, ethanol precipitation, anion-exchange, and gel-filtration chromatography. MDP was homogeneous and had a molecular weight of 6.16×10^3 Da, and it was an α-D-glucan containing a (1→ 6)-linked backbone, with a glucosyl residue at the C-3 position along the main chain. MDP exhibited immunological activity *in vitro*, which could significantly promote the proliferation and phagocytosis of RAW264.7 cells and the release of TNF-α and IL-6 factors. MDP also could significantly increase the thymus and spleen indices, enhance the macrophage function, increase the level of cytokine (IL-6 and TNF-α) and immunoglobulin IgM in the serum and regulate T lymphocyte subsets (Yang et al.).

Both edible and medicinal mushrooms possess strong therapeutic and biological activities (6). There are two papers covering the immune-boosting effects of mushroom polysaccharides in this special e-collection. *Flammulina velutipes* polysaccharides could improve gut health through gut microbiota and metabolism regulation. Data from Liang et al. showed that compared with the model group, *F. velutipes* polysaccharide could increase thymus and spleen indices and improve thymus tissue structure in mice; IL-2 and IL-4 contents were significantly increased and IL-6 and TNF-α contents were significantly decreased; serum acid phosphatase (ACP), lactate dehydrogenase (LDH) and total antioxidant capacity (T-AOC) activities were increased ($P < 0.05$); in the liver, superoxide dismutase (SOD) and catalase (CAT) activities were increased ($P < 0.001$), while malondialdehyde (MDA) content was decreased ($P < 0.001$). Proteomics discovered that *F. velutipes* polysaccharides may exert immune modulatory effects by participating in signaling pathways such as immune diseases, transport and catabolism, phagosomes and influenza A, regulating the immune-related proteins Transferrin receptor protein 1 (TFRC) and Radical S-adenosyl methionine domain-containing protein 2 (RSAD2), etc. Gut microbial studies showed that *F. velutipes* polysaccharides could increase the abundance of intestinal flora and improve the flora structure (Liang et al.).

Furthermore, to investigate the effect of *F. velutipes* polysaccharides (FVPs) on mice intestinal inflammation, FVPs were extracted from *F. velutipes* (FV) using a solid anaerobic fermentation technique. The antioxidant and anti-inflammatory

capacities of FVP and fermented FVP (FFVP) induced by lipopolysaccharide (LPS) were investigated *in vitro* and *in vivo*. The results showed that the yield of FFVP (9.44%) was higher than that of FVP (8.65%), but the molecular weight (MW) of FFVP (15,702 Da) was lower than that of FVP (15,961 Da). The antioxidant and anti-inflammatory capacities of FFVP were higher than that of FVP in preventing mice diarrhea, enhancing antioxidant capacities, and reducing the secretion and mRNA expression of interleukin-1β (IL-1β), IL-6, IL-18, and tumor necrosis factor-α (TNF-α). The anti-inflammatory mechanisms of FVP and FFVP were analyzed by inhibiting the activation of the NLRP3 signaling pathway using an LPS-induced mice model (Ma et al.).

Li et al. employed RNA-sequencing (RNA-seq) to determine the level and function of differentially expressed genes (DEGs) and further explore the mechanism of the HRP anti-inflammatory and immune process. The differential expression analysis indicated that 3622, 1216, and 2100 DEGs in the IPEC-J2 cells were identified in C vs. L, L vs. H6-L, and C vs. H6-L, respectively. The Kyoto Encyclopedia of Genes and Genomes (KEGG) enrichment analysis found six identified pathways related to the immune system. Additionally, the authors used the Science, Technology, Engineering, and Math (STEM) program to categorize the 3,134 DEGs that were differentially expressed in H2-L, H4-L and H6-L into eight possible expression profiles, in which 612 were clustered into two profiles. The accuracy and consistency of RNA-seq data were validated by the results of qRT-PCR of the nuclear factor of kappa light polypeptide gene enhancer in B-cells 2 (NFKB2), MAP kinase interacting serine/threonine kinase 2 (MKNK2), mitogen-activated protein kinase 1 (MAP2K1), mitogen-activated protein kinase kinase kinase 8 (MAP3K8), Ras-related protein R-Ras (RRAS), TNF receptor-associated factor 1 (TRAF1), NF-kappa-B inhibitor alpha (NFKBIA), interleukin 8 (IL8), tumor necrosis factor, alpha-induced protein 3 (TNFAIP3), and transforming growth factor beta-1 (TGFB1). Transcriptome sequencing also indicated that HRP reduced the expression levels of related DEGs and inhibited the activation of the mitogen-activated protein kinase (MAPK)/nuclear factor kappa-B (NF-κB) signaling pathway (Li et al.).

In summary, the results of the above-mentioned studies will fill the gap between the knowledge on significant therapeutic immune-boosting activities of dietary polysaccharides and their underlying cellular signaling and molecular mechanisms. It also aims to accumulate new knowledge and methods for discovery and development of novel therapeutic agents and adjuvants that exhibit beneficial immune-boosting properties.

Author contributions

BD wrote the introduction and the conclusion. BX wrote the central part with comments to the cited papers and references. Both authors contributed to the article and approved the submitted version.

Conflict of interest

The authors declare that the research was conducted in the absence of any commercial or financial relationships that could be construed as a potential conflict of interest.

Publisher's note

All claims expressed in this article are solely those of the authors and do not necessarily represent those of their affiliated organizations, or those of the publisher, the editors and the reviewers. Any product that may be evaluated in this article, or claim that may be made by its manufacturer, is not guaranteed or endorsed by the publisher.

References

1. Wang XY, Zhang DD, Yin JY, Nie SP, Xie MY. Recent developments in *Hericium erinaceus* polysaccharides: extraction, purification, structural characteristics and biological activities. *Crit Rev Food Sci Nutr.* (2019) 59:S96–S115. doi: 10.1080/10408398.2018.1521370

2. Zhang J, Liu Y, Tang Q, Zhou S, Feng J, Chen H. Polysaccharide of ganoderma and its bioactivities. *Adv Exp Med Biol.* (2019) 1181:107–34. doi: 10.1007/978-981-13-9867-4_4

3. Ye YF, Zhang BW, Liu Y, Wang JH. Purification, structural characterization and immunostimulatory activity of polysaccharides from *Umbilicaria esculenta*. *Int J Biol Macromol.* (2021) 181:743–51. doi: 10.1016/j.ijbiomac.2021.03.176

4. Aipire A, Yuan P, Aimaier A, Cai S, Mahabati M, Lu J, et al. Preparation, characterization, and immuno-enhancing activity of polysaccharides from *Glycyrrhiza uralensis*. *Biomolecules.* (2020) 10:159. doi: 10.3390/biom10010159

5. Cai Q, Li Y, Pei G. Polysaccharides from *Ganoderma lucidum* attenuate microglia-mediated neuroinflammation and modulate microglial phagocytosis and behavioural response. *J Neuroinflammation.* (2017) 14:63. doi: 10.1186/s12974-017-0839-0

6. Du B, Zhu FM, Xu BJ. An insight into the anti-inflammatory properties of edible and medicinal mushrooms. *J Functional Food.* (2018) 47:334–42. doi: 10.1016/j.jff.2018.06.003

frontiers in Nutrition

ORIGINAL RESEARCH
published: 28 January 2022
doi: 10.3389/fnut.2022.841230

The Effect of *Flammulina velutipes* Polysaccharide on Immunization Analyzed by Intestinal Flora and Proteomics

Qiongxin Liang[1,2†], *Qingchun Zhao*[1,2†], *Xuting Hao*[1], *Jinmei Wang*[1,2], *Changyang Ma*[1,2,3*], *Xuefeng Xi*[1,4*] *and Wenyi Kang*[1,2,3*]

[1] National R&D Center for Edible Fungus Processing Technology, Henan University, Kaifeng, China, [2] Functional Food Engineering Technology Research Center, Kaifeng, China, [3] Joint International Research Laboratory of Food & Medicine Resource Function, Kaifeng, China, [4] College of Physical Education, Henan University, Kaifeng, China

Proteomics and intestinal flora were used to determine the mechanism of immune modulatory effects of *Flammulina velutipes* polysaccharide on immunosuppressed mice. The results showed that compared with the model group, *F. velutipes* polysaccharide could increase thymus and spleen indices and improve thymus tissue structure in mice; IL-2 and IL-4 contents were significantly increased and IL-6 and TNF-α contents were significantly decreased; serum acid phosphatase (ACP), lactate dehydrogenase (LDH) and total antioxidant capacity (T-AOC) activities were increased ($P < 0.05$); in the liver, superoxide dismutase (SOD) and catalase (CAT) activities were increased ($P < 0.001$), while malondialdehyde (MDA) content was decreased ($P < 0.001$). Proteomics discovered that *F. velutipes* polysaccharides may exert immune modulatory effects by participating in signaling pathways such as immune diseases, transport and catabolism, phagosomes and influenza A, regulating the immune-related proteins Transferrin receptor protein 1 (TFRC) and Radical S-adenosyl methionine domain-containing protein 2 (RSAD2), etc. Gut microbial studies showed that *F. velutipes* polysaccharides could increase the abundance of intestinal flora and improve the flora structure. Compared to the model group, the content of short-chain fatty acids (SCFAs) and the relative abundance of SCFA-producers *Bacteroides* and *Alloprevotella* were increased in the *F. velutipes* polysaccharide administration group, while *Lachnospiraceae_NK4A136_group* and *f_Lachnospiraceae_Unclassified* decreased in relative abundance. Thus, *F. velutipes* polysaccharide may play an immunomodulatory role by regulating the intestinal environment and improving the balance of flora.

Keywords: ***Flammulina velutipes*, *Flammulina velutipes* polysaccharide, immunomodulation, proteomics, intestinal flora**

OPEN ACCESS

Edited by:
Bin Du,
Hebei Normal University of Science and Technology, China

Reviewed by:
Lijun Sun,
Northwest A and F University, China
Qiang Yu,
Nanchang University, China

***Correspondence:**
Changyang Ma
macaya1024@sina.com
Xuefeng Xi
xuefeng350286@sina.com
Wenyi Kang
kangweny@hotmail.com

† These authors have contributed equally to this work

Specialty section:
This article was submitted to Nutritional Immunology, a section of the journal Frontiers in Nutrition

Received: *22 December 2021*
Accepted: *06 January 2022*
Published: *28 January 2022*

Citation:
Liang Q, Zhao Q, Hao X, Wang J, Ma C, Xi X and Kang W (2022) The Effect of Flammulina velutipes Polysaccharide on Immunization Analyzed by Intestinal Flora and Proteomics. Front. Nutr. 9:841230. doi: 10.3389/fnut.2022.841230

INTRODUCTION

Immunosuppression is a distinctive feature of immune disorders (1), which predispose to the development of tumors, infections, cardiovascular diseases and diabetes, so the improvement of immune modulatory effects has become an urgent problem. Edible mushrooms are collected and/or cultivated worldwide and considered to be an important part of a healthy human diet (2, 3). In

recent years, the immune modulatory effect of edible mushrooms polysaccharides has attracted much attention (4). *Schizophyllum commune* polysaccharides can increase RAW264.7 cell activity and promote the production of large amounts of NO by cells to exert immune effects (5). *Hericium erinaceus* polysaccharide (HEP) can improve immune function by enhancing cellular and humoral immunity, macrophage phagocytosis and NK cell activity in mice, in addition, Sheng et al. found that HEP can upregulate intestinal SIgA secretion and activate MAPK and AKT cell signaling pathways (6).

Flammulina velutipes is one of the most popular edible mushrooms that contain triterpenes, polysaccharides, sterols and vitamins. *F. velutipes* polysaccharides have anti-inflammatory, antioxidant, anti-aging, immune modulatory, and intestinal flora activities (7–10). Earlier experiments of our group found that *F. velutipes* polysaccharides were non-toxic and could promote intestinal motility and improve constipation in rats (11). Liang obtained two polysaccharides CHFVP-1 (24.44 kDa) and CHFVP-2 (1,497 kDa) from *F. velutipes* and found that CHFVP-1 had procoagulant activity *in vitro* (12). A review of the literature shows that *F. velutipes* polysaccharides can modulate the intestinal microbiota of healthy mice and has potential immunomodulatory abilities (13, 14). However, the target proteins of immunomodulatory effects of this biologically active polysaccharide in immunocompromised mice remains to be investigated.

Proteomics can elucidate the composition of proteins and their action patterns in tissues and cells at a holistic level, can rapidly and precisely identify the key functional proteins between polysaccharides and immunity, lay the foundation for the study of disease mechanisms, drug action targets and new drug development (15–18). Zhao et al. investigated the key proteins and immune-related pathways stimulated by LPS after pretreatment with Hippophae rhamnoides polysaccharide in IPEC-J2 cells by proteomics techniques, and identified 42 key proteins related to immune pathways, and MAPKs/NF-κB signaling pathway may be the target for the efficacy of the drug (19). Yang et al. analyzed the effect of Taishan *Pinus massoniana* pollen polysaccharide on chicken peripheral blood lymphocyte proteome and identified 10 differentially expressed candidate proteins. Candidate proteins, and some differentially expressed proteins were associated with host innate immune response, stress-induced immune response and lipid synthesis-related pathways (20). The intestine is the largest immune organ and contains a large number of immune cells (21). The intestinal flora and its metabolites can play an important role in host immune homeostasis by promoting the development of the immune system, activating the immune response and regulating immune cell function (22). Numerous studies have shown that a variety of plant-derived polysaccharides can act directly as prebiotics or indirectly induce changes in the intestinal flora (23). Chen et al. found that *food* polysaccharide could reduce intestinal damage in immunosuppressed mice, regulate the composition of intestinal microorganisms, increase the levels of SCFAs, and exert intestinal immunomodulatory effects (24). *Coptis chinensis* Franch polysaccharides, when utilized by the intestinal flora, dynamically regulates the diversity, composition and distribution of the intestinal flora and has a regulatory effect on the intestinal immune microenvironment (25). The use of proteomic techniques and flora analysis will help to explore the mechanism of action of polysaccharide immunomodulation. Therefore, the immunosuppression model was established to investigate the immune modulatory mechanism of *F. velutipes* polysaccharides in immunocompromised mice, and to infer the target proteins of *F. velutipes* polysaccharides by proteomics *in vivo*.

MATERIALS AND METHODS

Materials and Reagents

Cyclophosphamide: Jiangsu Hengrui Pharmaceutical Co., Ltd (batch number: 20031125); *Lentinus edodes* Polysaccharide Tablets: Hubei Guangren Pharmaceutical Co., Ltd (batch number: 1909080); Biochemical kit: Nanjing Jiancheng Institute of Biological Engineering; ELISA kit: Beijing Si Zhengbai Biotechnology Co., Ltd; Paraformaldehyde fixative: Wuhan Xavier Biotechnology Co., Ltd; antibody TFRC: abcam; antibody RSAD2: Wuhan Sanying Biotechnology Co. Multiskan GO full wavelength enzyme standardizer: Thermo Fisher; Analytical balance: Sartorius.

Extraction of Polysaccharides

Flammulina velutipes polysaccharides was extracted according to the literature (26) with the extraction rate of 1.49%.

Animals

Specific pathogen free (SPF) grade, male, Kunming (KM) mice, 4–5 weeks old, 18–22 g. All mice were placed in a light-dark cycle at 24 ± 2°C for 12 h. Mice were acclimated for 7 d before the start of the experiment and were fed standard chow and had free access to water. Animals were acclimatized and fed for 1 week. The study received ethical approval from the Ethics Committee of Henan University School of Medicine (HUSOM2021-76) and was conducted in accordance with the guidelines of the Ethics Committee of the Animal Experimentation Ethics Committee.

Establishment of Immunosuppressed Mouse Model

Fifty-four mice were randomly divided into 6 groups of 9 mice each according to body weight, namely, blank group (BC), model group (MC), positive control group (PC), high-dose group (HD, 200 mg/kg), medium-dose group (MD, 100 mg/kg) and low-dose group (LD, 50 mg/kg) of *F. velutipes* polysaccharide. The BC and MC groups were given saline (0.1 mL/10 g) daily by gavage, the PC group was administered *Lentinus edodes* polysaccharide tablets by gavage at 3 mg/kg body weight as a positive control once daily for 21 d. Except for the BC group, which was administered saline intraperitoneally, the remaining groups were molded with CTX at 80 mg/kg intraperitoneally on days 18, 19, 20, and 21 of the experiment.

Measurement of Organ Indices

The mice were fasted for 12 h after the last administration, and the body weight of each group was weighed. After removing the

eyeballs, they were executed. The thymus and spleen tissues of the mice were immediately taken, washed with PBS solution, blotted dry on filter paper and weighed. The immune organ indices of mice were calculated according to the following formula.

$$\text{Immune organ index} = \text{weight of thymus or spleen (mg)} / \text{body weight(g*10)}$$

Determination of Lactate Dehydrogenase and Acid Phosphatase Activity

The prepared sera were taken and the activity of LDH and ACP were determined by microplate method and microenzymatic assay, respectively, according to the instructions of the kit.

Determination of Cytokine Content in Mice Serum

Blood was taken into 1.5 mL EP tubes by the eyeball removal method, and serum was prepared by centrifugation at 4°C and 3,500 r/min for 10 min. The cytokines interleukin 2 (IL-2), interleukin 4 (IL-4), interleukin 6 (IL-6), and tumor necrosis factor α (TNF-α) were detected in the serum by ELISA according to the kit instructions.

Determination of Antioxidant Stress Capacity

The prepared serum was taken and the total antioxidant capacity (T-AOC) level in mice was determined according to the kit instructions. The mouse liver tissues were weighed accurately, and 10% tissue homogenate was prepared by homogenization method under ice water bath conditions according to the ratio of weight (g) to volume (mL) of 1:9, and the supernatant was centrifuged at 2,500 rpm/min for 10 min. The supernatant was taken and the malondialdehyde (MDA), superoxide dismutase (SOD) and catalase (CAT) were measured in mouse liver tissues according to the kit instructions, respectively.

Pathological Observation

The mouse thymus specimens were rinsed with PBS, placed in 4% paraformaldehyde solution for fixation, dehydrated with gradient ethanol solution, and paraffin-embedded sections. H&E staining was performed by hematoxylin-eosin for 5 min, followed by dehydration, sealing of the sections with neutral gum, microscopic examination, and image acquisition for analysis.

Proteomics Studies

The spleens of mice in the BC, MC, and HD groups were taken, and after washing, the spleen tissues of each three mice were combined into one sample, and the obtained samples were subjected to proteomic assay (27).

Western Blotting Analysis

According to the amount of protein supernatant, 1/4 of loading buffer was added and mixed, and then heated at 100°C for 10 min. Forty microgram of sample protein solution was taken and analyzed by SDS-PAGE method for protein TFRC and RSAD2.

Diversity Sequencing of Cecum Contents Flora

Under aseptic conditions, the cecum contents of mice were taken, the contents of three mice from each group were pooled, and the obtained samples were sequenced for flora diversity analysis (28).

Content Determination of SCFAs

The contents of acetic acid, propionic acid and butyric acid in cecum contents were analyzed with reference to literature (29).

Bioinformatics Analysis

The identified proteins and peptides were firstly obtained under a filtering criterion of 1% FDR (PSM-level FDR $\leq$ 0.01). The differential proteins were clustered and analyzed by Euclidean distance and systematic clustering method (Hierarchical Cluster). The identified differential proteins were also subjected to GO functional annotation, Pathway enrichment analysis, protein interactions analysis, and subcellular localization analysis.

The forward and reverse reads obtained from double-end sequencing were spliced two-by-two, and after quality filtering to remove chimeric sequences, the final valid sequences obtained were subjected to OTU clustering analysis by Vsearch (1.9.6) (sequence similarity was set to 97%), and the reference database Silva 132 was used for sequence comparison analysis, and the representative sequences of OTU were analyzed for species taxonomy. Based on the analysis results obtained from OTU, sample Alpha diversity analysis, Beta diversity analysis, and colony function prediction were performed.

Statistical Analysis

The results were expressed after arithmetic mean and standard deviation, and the data were statistically compared for significant differences by one-way analysis of variance (One-Way ANOVA) using SPSS 19.0 software.

RESULTS

Effect of *Flammulina velutipes* Polysaccharide on Thymus Index and Spleen Index of Mice

In **Table 1**, compared with the BC group, the thymus index and spleen index of the MC group was decreased, indicating the model was established. Compared with the MC group, the spleen index of mice in the polysaccharide administration group and the thymus index in the PC and HD groups were significantly increased, the thymus index in the MD and LD groups had no the significant level, but it was an increasing trend compared with the MC group. It showed that *F. velutipes* polysaccharide could improve the atrophy of immunosuppressed mice constructed by CTX, and promote their development and enhance the immunity of the organism.

TABLE 1 | Effect of *F. velutipes* polysaccharide on the index of immune organs.

Group	Thymus index (mg/10*g)	Spleen index (mg/10*g)
BC	10.96 ± 4.66	26.77 ± 2.14
MC	5.54 ± 1.31***	21.28 ± 3.80*
PC	9.37 ± 4.06##	24.09 ± 3.27
HD	9.63 ± 3.38##	30.63 ± 4.53###
MD	6.72 ± 0.95	26.91 ± 4.10#
LD	6.19 ± 0.99	30.83 ± 8.22###

*Compared with BC group: ***$P < 0.001$, *$P < 0.05$; Compared with MC group: ###$P < 0.001$, ##$P < 0.01$, #$P < 0.05$.*

TABLE 2 | Effect of *F. velutipes* polysaccharide on serum ACP and LDH activity.

Group	ACP (unit/100 mL)	LDH (U/L)
BC	7.75 ± 1.26	5703.86 ± 529.04
MC	4.94 ± 1.22***	4814.77 ± 706.42*
PC	5.27 ± 1.32	5736.72 ± 431.79#
HD	6.79 ± 2.00##	6761.14 ± 1148.80###
MD	5.39 ± 0.80	6376.81 ± 722.82###
LD	4.46 ± 0.74	5989.80 ± 1041.74##

*Compared with BC group: ***$P < 0.001$, *$P < 0.05$; Compared with MC group: ###$P < 0.001$, ##$P < 0.01$, #$P < 0.05$.*

Effect of *Flammulina velutipes* Polysaccharide on ACP and LDH Activity in Mice

In **Table 2**, the ACP and LDH activity in serum of MC group was significantly reduced compared with BC group. After the administration treatment, the ACP vitality in the HD group was significantly increased compared with the MC group, and the LDH vitality in both the PC group and the administered group was improved, especially in the polysaccharide administered group. It indicated that the *F. velutipes* polysaccharide is beneficial to improve the ACP and LDH activity in mice.

Effect of *Flammulina velutipes* Polysaccharide on the Content of Cytokines in Mice Serum

In **Figure 1**, the levels of IL-2 and IL-4 were significantly decreased and the levels of IL-6 and TNF-α were extremely significantly increased in the MC group compared with the BC group ($P < 0.001$), indicating that cyclophosphamide could suppress immune activity in mice. The levels of IL-2, IL-4, IL-6, and TNF-α were improved by administration of the drug, and the best results were achieved in the HD group with highly significant levels ($P < 0.001$). It showed that *F. velutipes* polysaccharide could restore cyclophosphamide-induced immunosuppression and improve immune activity by regulating the levels of cytokines.

Effect of *Flammulina velutipes* Polysaccharide on Antioxidant Capacity of Mice

In **Figure 2**, compared with the BC group, the T-AOC content and SOD and CAT activity in the MC group were highly significant decreased ($P < 0.001$) and the MDA activity was significantly increased ($P < 0.001$), indicating the model was established. Compared with the MC group, T-AOC content and SOD and CAT viability values were significantly increased and MDA activity was significantly decreased in the PC group and the high and medium dose administration groups, and SOD viability was significantly increased and MDA activity was highly significantly decreased in the low dose group, and it proved that *F. velutipes* polysaccharide had antioxidant capacity.

Effect of *Flammulina velutipes* Polysaccharide on Pathological Changes of Mouse Thymus Organs

In **Figure 3**, the thymus cells of mice in BC group were abundant and well-arranged, there were no abnormalities, and the thymus staining was darker. Compared with the BC group, the thymus cells in the MC group were arranged in a disorganized and irregular manner with unclear edges, and the decrease of thymus cells led to the overall lighter staining of the thymus. Compared with the MC group, the treatment of *F. velutipes* polysaccharide alleviated the CTX-induced pathological changes in the thymus of mice, indicating that polysaccharide could alleviate the atrophy of the thymus caused by CTX and protect the thymus of mice.

Protein Identification and Protein GO (Gene Ontology) Annotation Analysis

A total of 717,312 secondary spectra were generated for the 3 sets of samples in this experiment. A total of 31,743 peptides and 5,975 proteins were identified under the "1% FDR" filtering criteria. The differentially expressed proteins between groups were compared by screening for differential ploidy and significance. In **Figure 4A**, the protein quantification results statistics were presented in the form of volcano plots. One hundred and thirty four differentially expressed proteins were identified in the MC group compared with the BC group, of which 52 were up-regulated and 82 were down-regulated. Compared with the MC group, there were 46 differentially expressed proteins after administration of *F. velutipes* polysaccharide treatment, of which 30 were up-regulated and 16 were down-regulated. The reproducibility of the quantification was assessed by the CV value, CV = standard deviation SD/mean, the lower the value, the better the reproducibility. In **Figure 4B**, the mean CV value was equal to 0.091 and the percentage of proteins with CV values within 20% was 93.6%, and the results indicated that the biological reproducibility was good between sample groups.

All the identified proteins were compared with NR database for GO gene function annotation and enrichment analysis, and it was found that they mainly have molecular functions

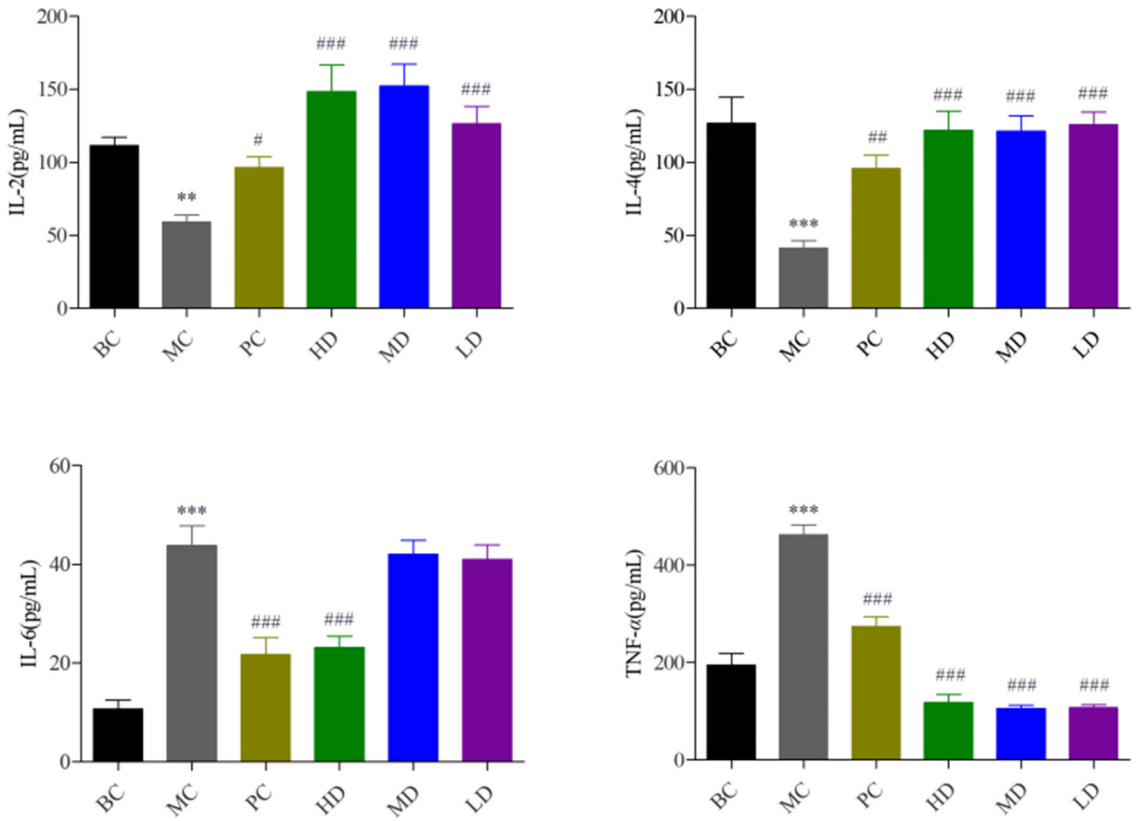

FIGURE 1 | Effect of *F. velutipes* polysaccharide on serum cytokine content. Compared with BC group: $^{***}P < 0.001$, $^{**}P < 0.01$; Compared with MC group: $^{\#\#\#}P < 0.001$, $^{\#\#}P < 0.01$, $^{\#}P < 0.05$.

such as binding, catalytic activity, molecular function regulator, transcription regulator activity, etc.; contain cellular components such as cell, cell part, organelle, membrane, macromolecular complex, etc.; participate in cellular process, metabolic process, biological regulation, regulation of biological process, signaling, immune system process and other biological processes, as shown in **Figure 4C**.

GO Enrichment Analysis of Differential Proteins

The GO entries with significant enrichment of differential proteins were analyzed by clustering in **Figure 5A**, the horizontal axis represents the GO annotation entries, and the vertical axis represents the up- and down-regulated differential proteins. In **Figure 5A**, the GO functional classification of differential proteins in the HD group was more up-regulated compared with the MC group, among which cellular process, cell part, cell, binding was the more the GO entries were significantly different. The relationship network was used to observe the relationship between each GOterm in **Figure 5B**, the significantly enriched GOterms in the HD group and MC group were mainly related to the biological process function.

Differential Protein Pathway Enrichment Analysis and Subcellular Localization

Pathway enrichment analysis of differential proteins was performed by the Kyoto Encyclopedia of Genes and Genomes. In **Figure 6A**, the differentially expressed proteins in the HD and MC groups were mainly involved in transport and catabolism, signal transduction, infectious diseases: viral, immune diseases, carbohydrate metabolism, immune system and other metabolic pathways. The analysis revealed that TFRC (Transferrin receptor protein (1) and RSAD2 (Radical S-adenosyl methionine domain-containing protein (2) protein content changed significantly. The number of differential proteins annotated to the pathway was divided by all the proteins identified to the pathway as the RichFactor, and the larger the value, the larger the proportion of differential proteins in the pathway, and the size of its point represents the number of differential proteins annotated to the pathway. In **Figure 6B**, differential proteins could play a role in phagosome, antigen processing and presentation, autoimmune thyroid disease, and intestinal immune network for IgA production by participating in the pathway immune modulatory effects.

Subcellular localization of proteins is an important part of protein function annotation. Protein subcellular localization prediction was performed by WoLF PSORT software. In

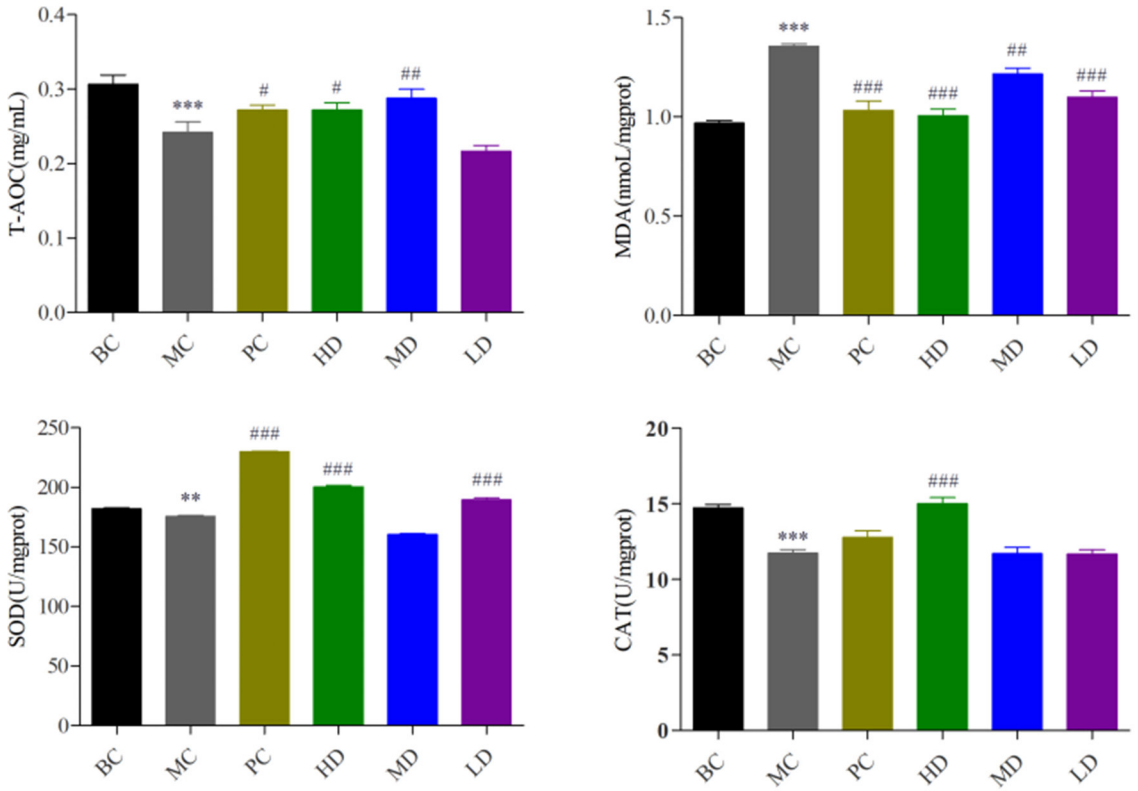

FIGURE 2 | Effect of *F. velutipes* polysaccharide on antioxidant capacity of mice. Compared with BC group: $^{***}P < 0.001$, $^{**}P < 0.01$; Compared with MC group: $^{\#\#\#}P < 0.001$, $^{\#\#}P < 0.01$, $^{\#}P < 0.05$.

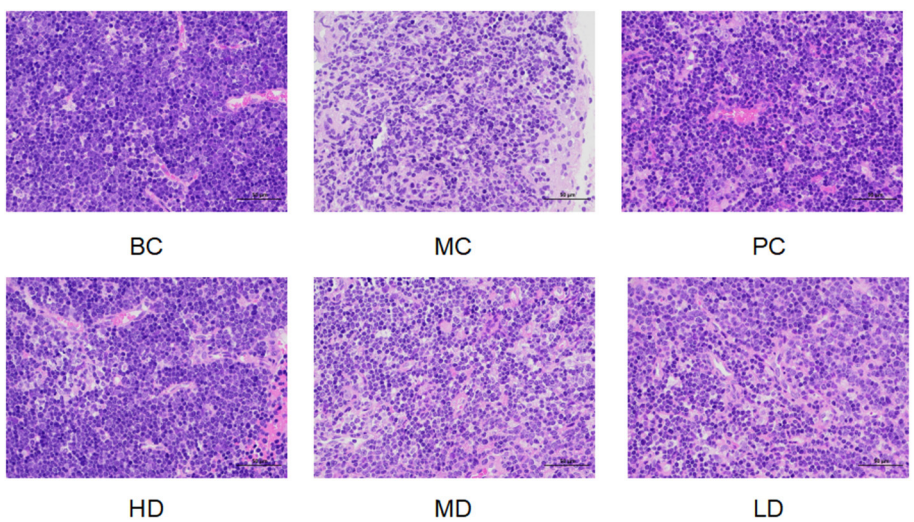

FIGURE 3 | Effect of *F. velutipes* polysaccharide on thymus organ in mice.

Figure 6C, the differential protein subcellular localization of HD and MC differential proteins were more distributed in cyto (cytosol), nucl (nucleus), plas (plasma membrane) and extr (extracellular).

Protein Validation

In **Figure 7**, the protein expression in the spleen of TFRC and RSAD2 mice was highly significantly down-regulated in the MC group compared with the BC group ($P < 0.001$), and highly

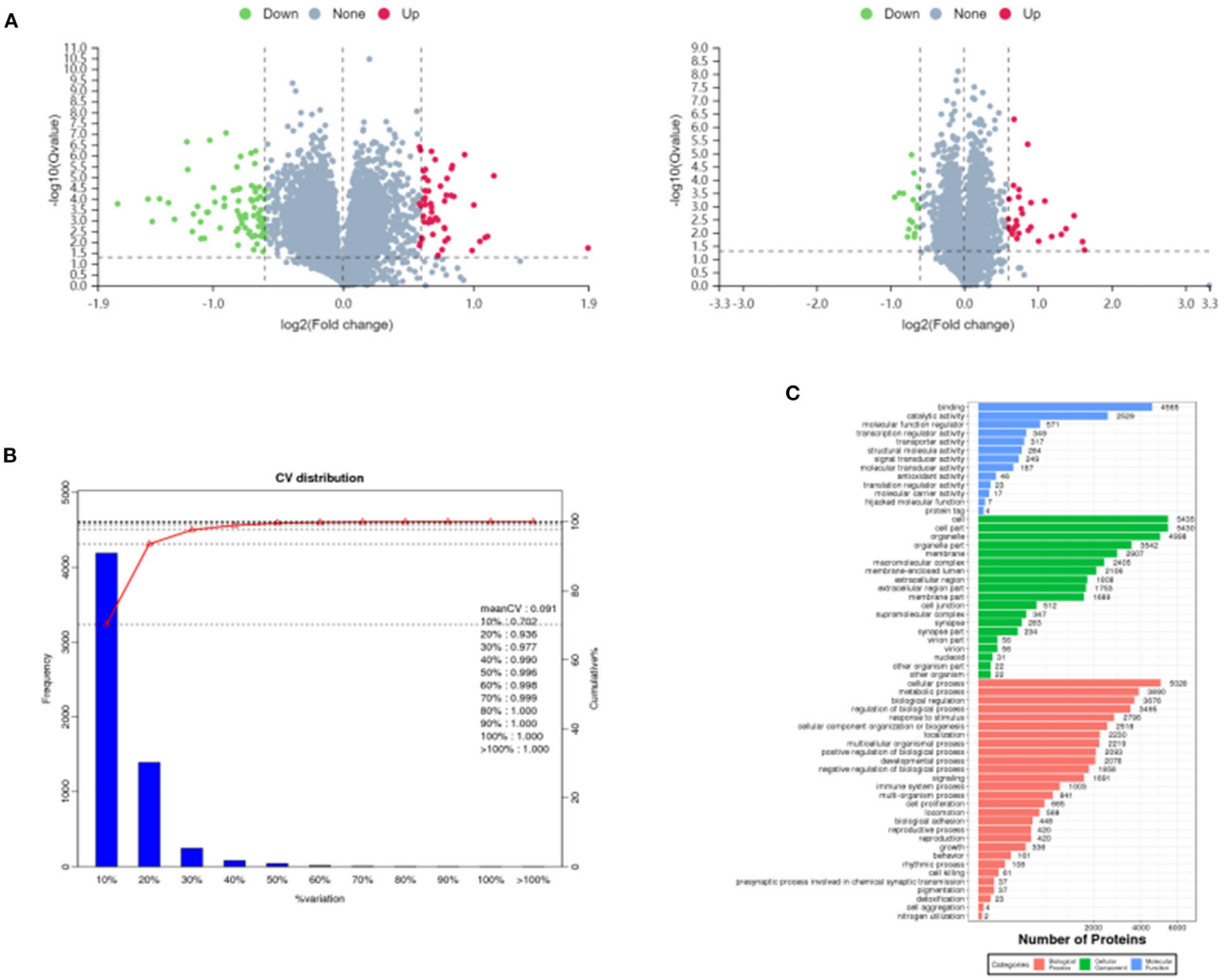

FIGURE 4 | Volcano plots of differentially expressed proteins in MC/BC (left) and HD/MC (right) **(A)**, distribution of CV values of replicate experiments **(B)** and GO annotation histogram **(C)**.

significantly up-regulated in the HD group compared with the MC group ($P < 0.001$), which is consistent with the results of proteomics.

Taxonomic Analysis of Intestinal Flora Species

OTUs clustering analysis was performed on mouse intestinal microorganisms, and the Top 30 dominant species were selected for analysis by comparing the database for Silva_132 16S rRNA database. In **Figure 8A**, at the phylum level, the phylum *Firmicutes* and the phylum *Bacteroidetes* were the major dominant groups in the mouse intestinal flora, accounting for more than 95% of all bacteria, followed by the phylum *Proteobacteria*. The relative abundance of *Firmicutes* decreased, the relative abundance of *Bacteroidetes* increased and *Proteobacteria* showed no significant change in the *F. velutipes* polysaccharide administration group compared with the MC group.

To further understand the changes in the intestinal flora, the relative abundance of the dominant flora was analyzed at the genus level in **Figure 8B**. Compared to the MC group, the relative abundance of *Lachnospiraceae_NK4A136_group* and *f_Lachnospiraceae_Unclassified* was reduced in the blank and high and medium dose administration groups. While the relative abundance of *f_Muribaculaceae_Unclassified*, *Bacteroides*, and *Alloprevotella* was relatively increased in the HD and MD groups compared with the MC group.

Colony Diversity Analysis and PICRUSt Functional Prediction Analysis

The alpha diversity of the flora was carried out by randomly sampling the sample sequences. Alpha diversity allows assessment of species abundance and diversity. In **Figure 9A**, the Chao1 index was higher in the HD and LD groups than in

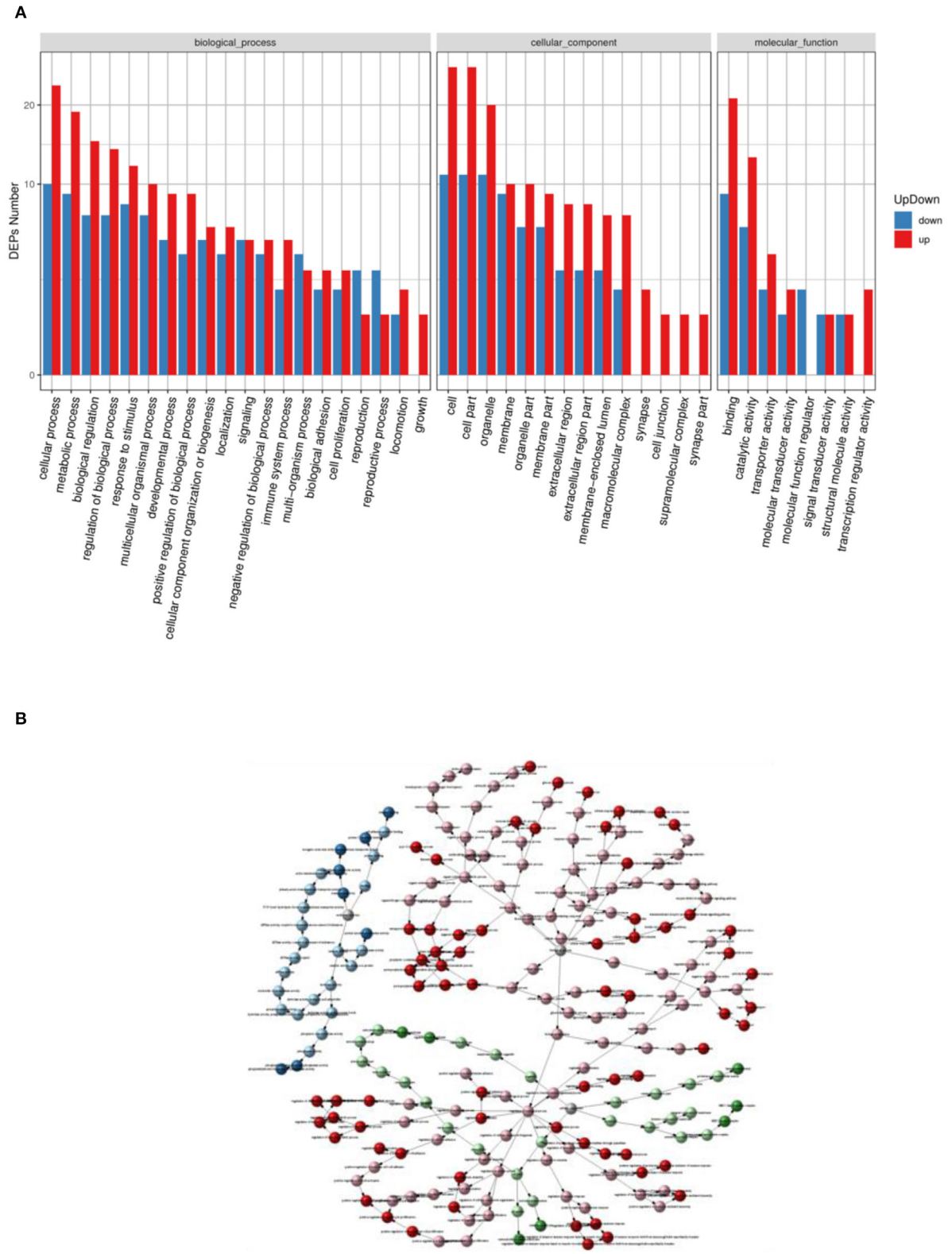

FIGURE 5 | Statistical graph of up- and down-regulation of GO functional classification of differential proteins in HD and MC groups **(A)** and GOterm relationship network graph **(B)**.

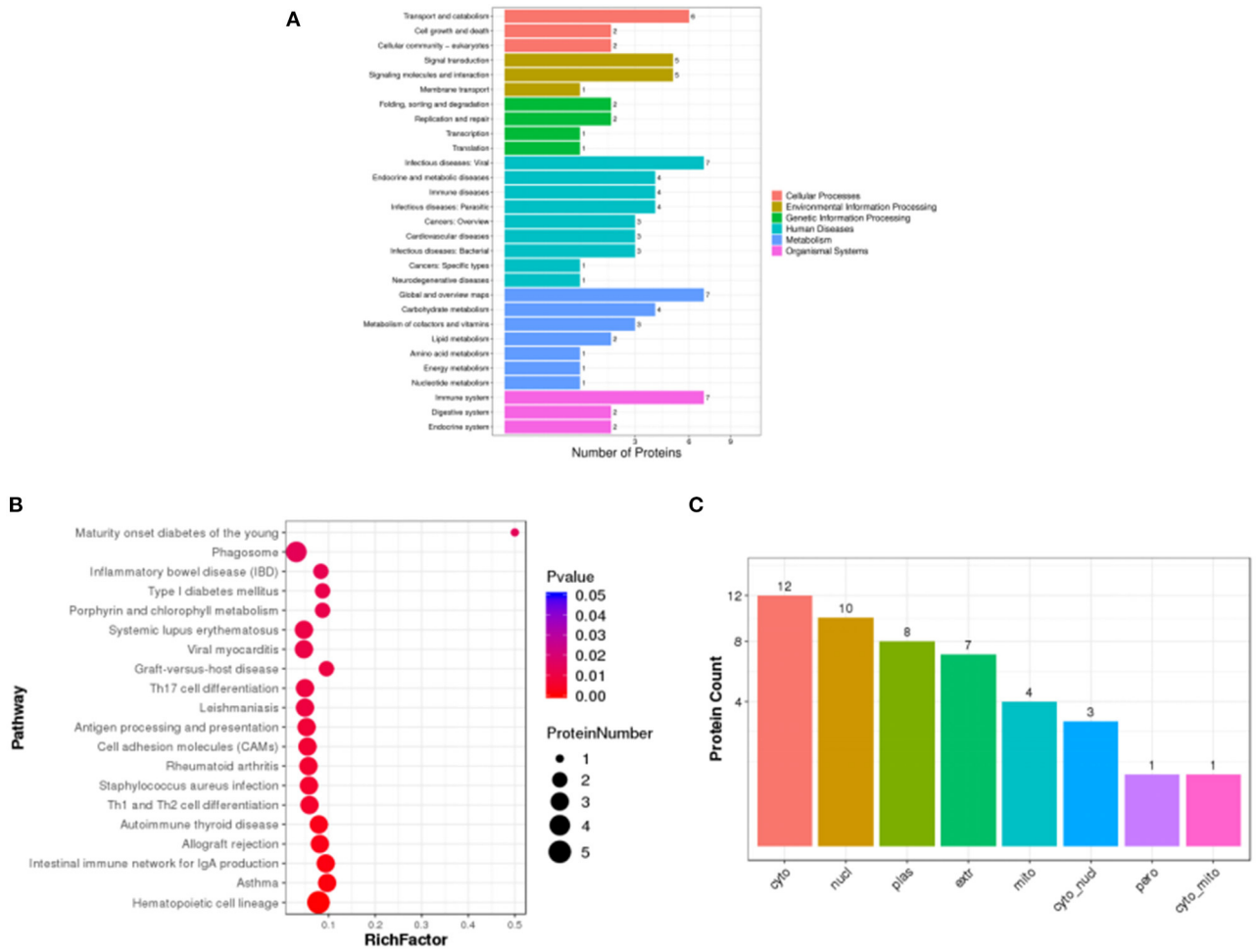

FIGURE 6 | Statistical plots of Pathway classification of differential proteins **(A)**, statistical plots of significantly enriched pathway **(B)** and histogram of subcellular localization **(C)** in HD and MC groups.

the MC group, indicating that the high and low dose groups of *F. velutipes* polysaccharide could increase the abundance of intestinal flora in immunosuppressed mice. **Figure 9B** showed that the Shannon index value increased in the LD group compared with the MC group, and there was no significant change in the HD and MD groups, indicating that the low-dose administration group could improve the diversity of intestinal flora in mice.

In order to reflect the diversity differences among different samples, the samples were analyzed by beta diversity between groups. In **Figure 9C**, the composition of intestinal flora of immunosuppressed mice treated with *F. velutipes* polysaccharide was significantly different from that of mice in the MC group, indicating that *F. velutipes* polysaccharide had a good effect on the structural composition of intestinal microorganisms in immunosuppressed mice.

PICRUSt Functional Prediction Analysis

The metabolic functions of the colony were predicted based on the PICRUSt analysis platform. In **Figure 10**, the metabolic functions of the colony were concentrated in energy production and conversion, amino acid transport and metabolism, carbohydrate transport and metabolism, lipid transport and metabolism, signal transduction mechanisms, etc. It can be predicted that the intestinal flora may play a regulatory role by affecting the signaling pathways of amino acid, carbohydrate, lipid transport and metabolism and signal transduction.

Effect of *Flammulina velutipes* Polysaccharide on the Content of SCFAs

The effects of *F. velutipes* polysaccharide on the content of SCFAs were determined by extracting SCFAs from the intestine of mice. In **Table 3**, compared with BC, the contents of acetic acid, propionic acid and butyric acid were all down-regulated in the MC group, and the contents of acetic acid and butyric acid reached a significant level ($P < 0.05$), indicating that CTX had an inhibitory effect on the production of SCFAs. Compared with the MC group, the content of SCFAs was improved in both the PC and polysaccharide treatment groups,

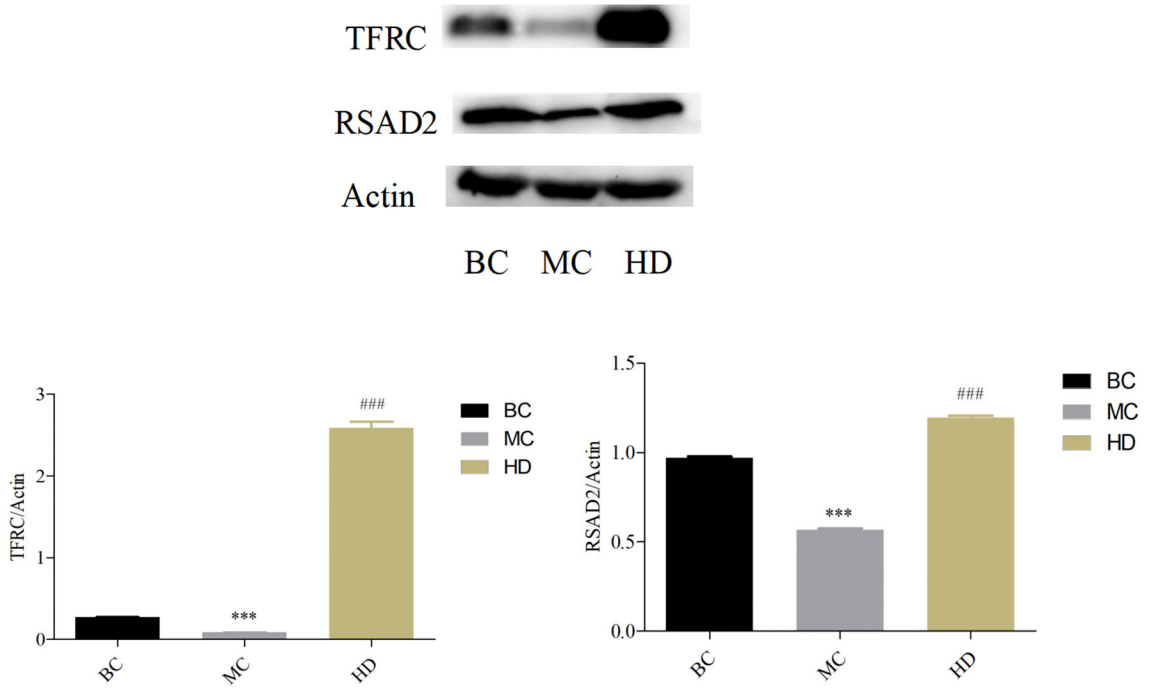

FIGURE 7 | Effect of *F. velutipes* polysaccharide on the expression levels of TFRC and RSAD2 proteins in mouse spleen. Compared with BC group: $^{***}P < 0.001$; Compared with MC group: $^{\#\#\#}P < 0.001$.

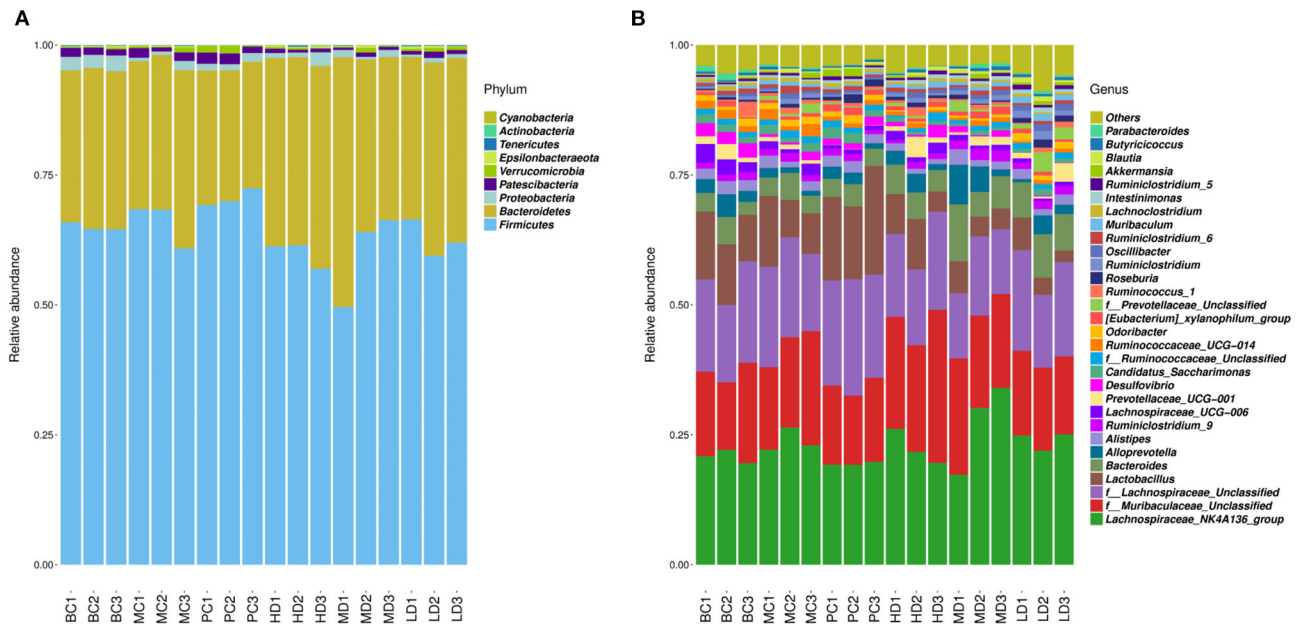

FIGURE 8 | Relative abundance of dominant groups at phylum **(A)** and genus **(B)** level.

with the content of acetic acid, propionic acid and butyric acid reaching significant levels in the HD group. It was speculated that *F. velutipes* polysaccharide might regulate the changes of intestinal microbial composition by improving the content of SCFAs, with the most obvious improvement in the high-dose group.

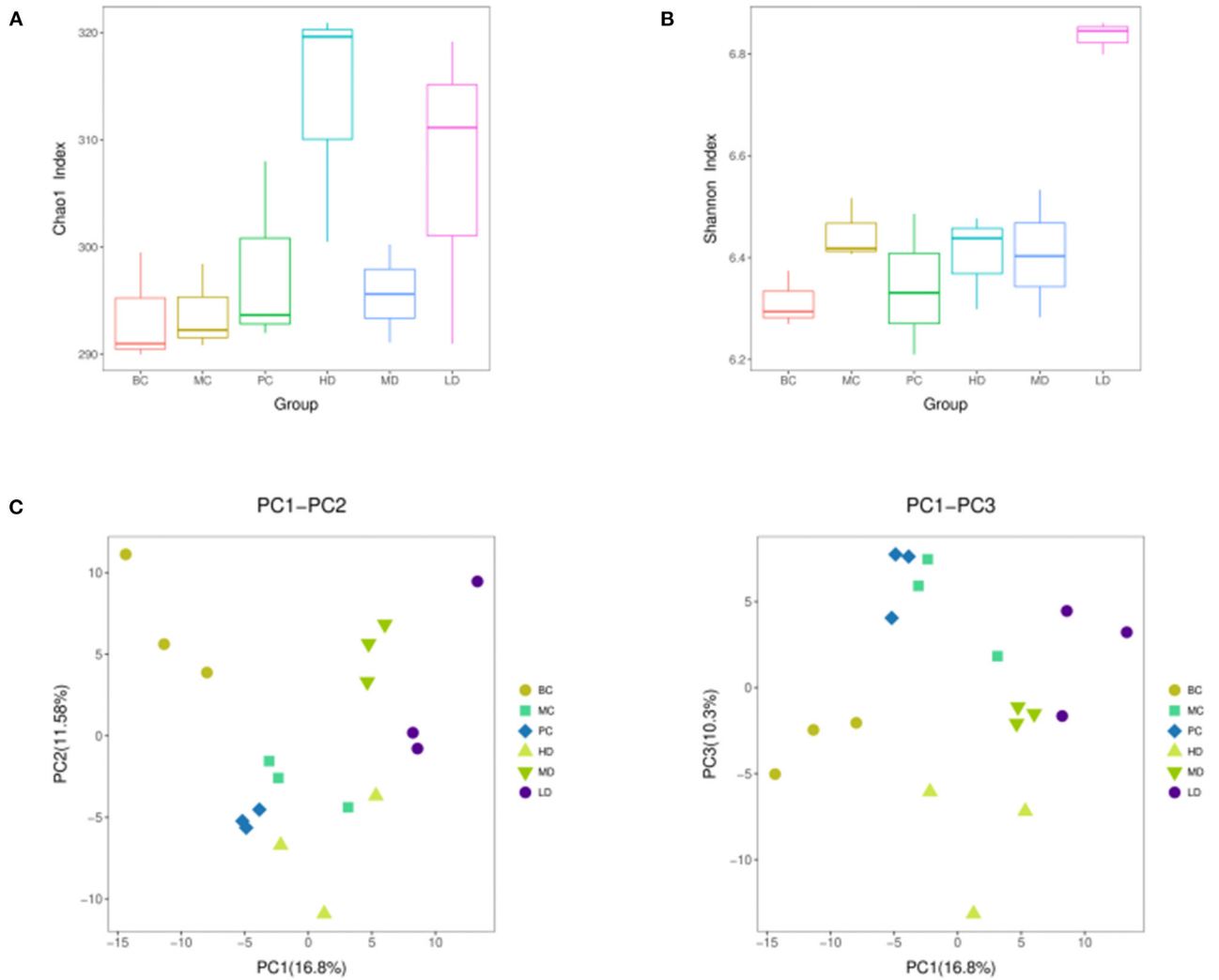

FIGURE 9 | Chao 1 index **(A)**, Shannon index **(B)** based on alpha diversity analysis, PCA analysis performed on the distribution of strain communities **(C)**.

DISCUSSION

Thymus and spleen are two important immune organs for the proliferation and growth of human immune cells, and the immune organ index is known as the main indicator of immune function (30). It has been shown that polysaccharide can significantly increase thymus index and spleen index in immunosuppressed mice (31, 32). CTX is a chemotherapeutic drug that has a suppressive effect on the body's immune system, which is manifested by a decrease in spleen and thymus index (1). It was found that the thymus and spleen indices of mice in the MC group were significantly lower than those of normal mice, indicating that the immune function of mice was suppressed by CTX, and when the polysaccharide was gavaged, the thymus and spleen indices of mice in each dose group increased to different degrees, and the spleen indices of the polysaccharide administration group and the thymus indices of the HD group increased significantly, and the thymus tissue structure was improved, indicating that *F. velutipes* polysaccharide could improve the immune organ damage and enhance the immunity of the organism, which is consistent with the results of Zhang et al. (33). *Panax japonicus* polysaccharide can improve spleen and thymus indices of immunosuppressed mice induced by cyclophosphamide.

Macrophages arise from the differentiation of monocytes and play a unique role in the immune system with the function of activating the innate immune response (34). Macrophage enzyme activity can reflect the functional status of macrophages. ACP is the marker enzyme of macrophage lysosomal enzymes in higher animals, and its activity reflects the degree of macrophage activation. LDH is an enzyme necessary for intracellular glucose enzymes, and the energy required by phagocytes is also derived from glycolysis. Lactic acid produced during LDH enzymes can cause a decrease in intracellular pH in macrophages, which

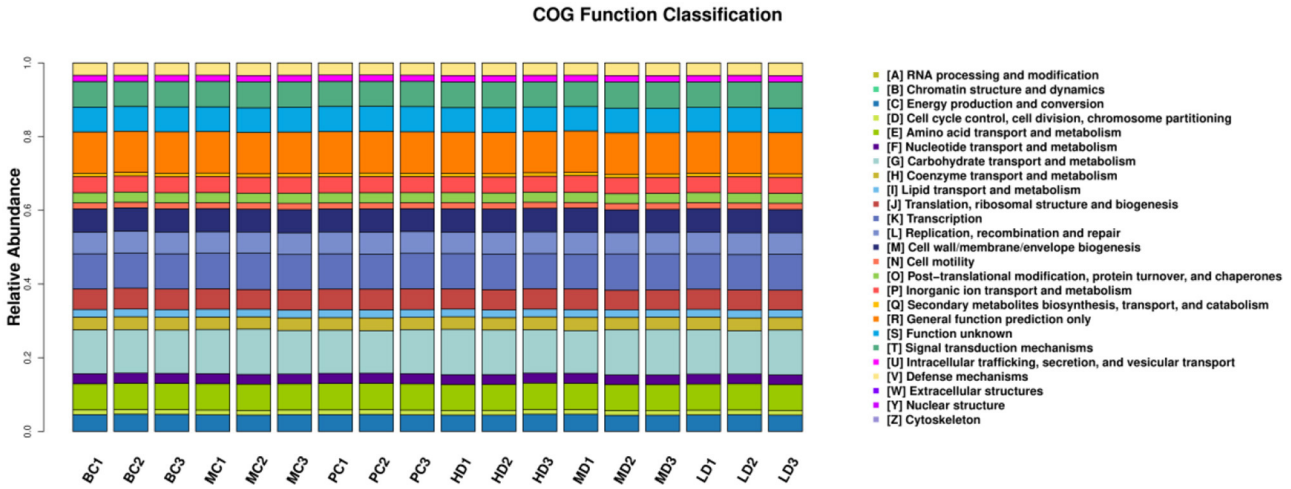

FIGURE 10 | Bar distribution of COG functional abundance.

TABLE 3 | Effect of *F. velutipes* polysaccharide on the content of SCFAs.

	BC	MC	PC	HD	MD	LD
Acetic acid	1.58 ± 0.84	0.35 ± 0.05*	1.15 ± 1.11	1.68 ± 1.86#	1.14 ± 0.82	0.8 ± 0.55
Propionic acid	3.17 ± 0.47	2.09 ± 0.73	4.47 ± 3.71#	5.9 ± 0.77###	3.71 ± 0.69	4.11 ± 0.59#
Butyric acid	4.54 ± 1.16	2.6 ± 0.87*	4.03 ± 2.4	5.32 ± 1.43##	3.47 ± 0.69	3.55 ± 1.02

Compared with BC group: $^{*}P < 0.05$; Compared with MC group: $^{###}P < 0.001$, $^{##}P < 0.01$, $^{#}P < 0.05$.

facilitates the immune response of macrophages and is one of the hallmarks of macrophage activation (35). *Paecilomyces sinensis* polysaccharides can increase the activity of LDH and ACP in rat and human monocytes AMϕ and PMϕ (36). Water-soluble *Ginseng marc* polysaccharide can activate macrophages by regulating the activity of lysosomal phosphatases, affecting the ability of lysosomal enzymes to respond appropriately to exogenous substances and increasing the proportion of phagocytic macrophages (37). The ACP activity in the HD group and LDH in the polysaccharide administration group were significantly increased after the administration treatment, indicating that ACP and LDH activities in immunocompromised mice can be regulated by the *F. velutipes* polysaccharide.

Cytokines have an important regulatory role in cell growth, cell differentiation and cell-cell interactions and have a significant effect on the immune inflammatory response (38). In this experiment, IL-2 and IL-4 levels were significantly decrease and TNF-α and IL-6 levels were significantly increase in the MC group compared to the BC group, indicating that CTX has a suppressive effect on the immune function of the body. IL-2 is mainly expressed by Th1 cells and is a soluble factor that mediates T cell proliferation and has an important role in the innate and adaptive immune system (39). IL-4 is mainly expressed by Th2 cells and is an important anti-inflammatory cytokine that plays an important role in humoral immunity and has an important regulatory role in the immune function and inflammatory process of the body. Wen et al. found that low molecular-weight seleno-aminopolysaccharides significantly increased cyclophosphamide-induced secretion of serum cytokines IL-2 and IL-4 in immunosuppressed mice to restore immune function (40). It is consistent with our research, *F. velutipes* polysaccharides can significantly increase the levels of serum cytokines IL-2 and IL-4 to exert immune modulatory effects. IL-6 and TNF-α have dual effects on the body. Moderate concentrations can enhance the immune function of the organism, regulate a variety of immune cells, and have a protective effect on the organism, but large production and release can disrupt the immune balance of the organism, produce an overly violent immune response, present toxic effects, and cause damage to the organism (41, 42). Cheng et al. (43) showed that *Bupleurum smithii var. Parvifolium* polysaccharides can inhibit lipopolysaccharide induced production of pro-inflammatory cytokines IL-6 and TNF-α. It has been reported that CTX can induce elevation of inflammatory cytokines TNF-α, IL-6 through activation of nuclear factor-κB (NF-κB) and p38 mitogen-activated protein kinase (p38-MAPK) (44–46). *F. velutipes* polysaccharides could exert immune modulatory effects by inhibiting the CTX-induced increase in the levels of pro-inflammatory cytokines IL-6 and TNF-α.

CTX causes immunosuppression along with damage to the liver and antioxidant enzymes, induces oxidative stress in the body, generates large amounts of ROS, causes oxidative damage to immune cells (47–49), and further decreases the immune function of the body. Excess ROS leads to an increase

in the membrane lipid peroxidation product MDA (50, 51), which reflects the overall level of lipid peroxidation. SOD is an important oxygen radical scavenger widely present in living organisms, catalyzing the disproportionation of superoxide anions and converting them into hydrogen peroxide, which is decomposed into H_2O and O_2 catalyzed by CAT (52–54). Antioxidant the proteins SOD and CAT can act as cellular detoxification systems to prevent ROS damage (55). T-AOC represents the total antioxidant capacity of the organism. It has been shown that polysaccharides can enhance antioxidant activity in immunosuppressed mice (26). Our research found that *F. velutipes* polysaccharide could reduce the level of MDA and alleviate oxidative stress in the body by increasing the activity of SOD, CAT and T-AOC, which is consistent with the results of Xu et al. (56).

Proteomics research involves the large-scale detection, identification and characterization of proteins, making it highly promising for biomarker discovery in many diseases (57). Chen et al. (58) investigated the effect of *Sargassum fusiforme* polysaccharides (SFP) on the antioxidant capacity of liver tissue in mice by proteomics techniques. The effect of SFP on the antioxidant capacity of mouse liver tissues was investigated by proteomic techniques, and 38 out of 49 protein spots were found to be up-regulated and 11 down-regulated. Functional analysis revealed that the differentially expressed proteins were mainly involved in redox, amino acid metabolism and energy metabolism, and the results indicated that SFP could regulate antioxidant enzymes to scavenge excess free radicals and prevent oxidative damage. Jiang et al. investigated the immune modulatory function of *Durio zibethinus* Rind polysaccharide at the proteomic level and found a total of 13 shared differential proteins by comparing the differential proteins in untreated, immunosuppressed and *D. zibethinus* Rind polysaccharide-treated mice. These shared differential proteins were mostly associated with biological functions such as lolalization, biological regulation and immune system process. Liang et al. (59) used proteomics to find that *Nigella sativa* seed polysaccharides could participate in immune regulation by regulating metabolism-related pathways such as Autoimmune thyroid disease, Primary immunodeficiency, and PI3K-Akt signaling pathway through the regulation of differential proteins such as PI3K and PTEN. The aim of this study was to investigate the immune modulatory effects of *F. velutipes* polysaccharide at the proteomic level through the quantitative technique of homogeneous isotope labeling. By comparing the differential proteins in spleen tissues of different treated mice, 52 differential proteins were up-regulated and 82 differential proteins were down-regulated in the MC group compared with the BC group, and 30 differential proteins were up-regulated and 16 differential proteins were down-regulated in *F. velutipes* polysaccharide treated group compared with the MC group. These differential proteins were mostly associated with functions such as biological regulation, immune system process and signal transducer activity, and were involved in transport and catabolism, infectious diseases: viral, immune diseases, phagosome and other pathways to play immune regulatory roles. Differential protein function enrichment analysis revealed that among the immune-related proteins, TFRC and RSAD2 were significantly upregulated in HD compared with MC group. Iron is essential for the generation of immune responses and is required for the growth, proliferation and differentiation of immune cells (60). Iron deficiency leads to a decrease in the number of T cells, a lower proportion of mature T cells and suppressed cytokine synthesis (61–63). Cellular iron uptake is largely dependent on iron transporters (64, 65). The transferrin receptor is a cell surface receptor that mediates iron uptake through receptor-mediated endocytosis and is required for cellular iron uptake (66, 67). It has been suggested that mutations in the transferrin receptor gene may lead to severe combined immunodeficiency (68). Promoting the expression of transferrin receptor protein (TFRC) increases cellular iron uptake and helps to enhance host antitumor immunity (69). RSAD2 is a key enzyme of the innate immune response, localized to the cytoplasmic face of the endoplasmic reticulum (70) and/or to lipid droplets via the N-terminal hydrophobic structural domain (71), and its expression is induced by interferon-dependent or non-dependent pathways (72). The inhibition of GAPDH activity by the ddhCTP product of RSAD2 radical SAM activity may improve the rate of NADPH regeneration by affecting upstream metabolic pathways and increasing the flux of the pentose phosphate pathway (PPP). It is also able to increase the rate of reduction of glutathione disulfide (GSSG) to reduced glutathione (GSH), thus protecting cells from reactive oxygen species (ROS) damage (73). In macrophages, the cellular activity of RSAD2 may provide a protective mechanism for cells against viral infection or other conditions that increase ROS levels (74). The results of the present study showed that *F. velutipes* polysaccharide may alleviate CTX-induced oxidative stress capacity as well as increase the body's iron uptake and immune response through upregulation of TFRC and RSAD2 protein expression, and exert immune modulatory effects through drug metabolism-related pathways such as immune diseases, transport and catabolism, phagosomes and influenza A.

The intestinal flora has an important role in immune system development and regulation of immune function (75). Dysfunctional gut microbial structure affects physiological processes such as energy metabolism, immune regulation and liver injury in humans (76–78). Niu et al. evaluated the effect of *Pinus massoniana* pollen polysaccharides (PPPS) on the intestinal flora of mice by 16S rRNA high-throughput sequencing technology and showed that PPPS can regulate the composition of mouse intestinal microorganisms and increase the proportion of probiotic bacteria, and also regulate the systemic immune system by modulating the immunosuppressive status of lymphocytes in Peyer's patches (79). *N. sativa* seed polysaccharides can exert immune modulatory effects by improving the structure of the intestinal flora, increasing flora diversity, and regulating metabolic pathways such as lipid metabolism, polysaccharide synthesis and signal transduction (59). The results of the present study showed that *F. velutipes* polysaccharides improved the composition and diversity of the intestinal flora of mice in a CTX-induced immunosuppression model. At the phylum level, the thick-walled phylum *Firmicutes* and *Bacteroidetes* were the predominant intestinal flora in mice, it

is consistent with the Tremaroli et al. research. *Bacteroidetes* and *Firmicutes* accounted for more than 90% of the total intestinal microorganisms (80). It has been shown that *Bacteroidetes* can interact with cellular receptors using lipopolysaccharide and flagellin components to enhance the immune response through cytokine synthesis (81), and that an increase in thick-walled *Bacteroidetes* promotes energy absorption by the body, leading to obesity (82). In the present study, *F. velutipes* polysaccharides decreased the relative abundance of *Firmicutes* and increased the relative abundance of *Bacteroidetes*, which had a beneficial regulatory effect on the intestinal flora. The literature reports that intestinal microorganisms have a large system of carbohydrate-active enzymes that can further utilize polysaccharides (83). After entering the intestine, polysaccharides are converted into SCFAs by microbial metabolism (84). Short-chain fatty acids are not only an important source of energy for intestinal epithelial cells, but it also regulates the production of inflammatory factors and reduces intestinal inflammation and tumorigenesis (85, 86). Among the various microbial metabolites, acetic acid, butyric acid, and propionic acid are the key bacterial metabolites that promote the development and maintenance of the immune system (87). In the present study, it was found that *F. velutipes* polysaccharides increased the content of acetic acid, propionic acid, and butyric acid, with the most significant increase in the high-dose administration group. Tan et al. (88) found that the intervention of *Bacteroides* reduced the destruction of intestinal flora by LPS treatment, maintained the integrity of the intestinal epithelium, had a role in promoting intestinal homeostasis, and its content was proportional to the acetic acid content in short-chain fatty acids (89). Propionate is a health-promoting microbial fermentation metabolite in the human gut that provides energy to the intestine and plays an inhibitory role in the development of disease (90). Butyrate is the preferred source of energy for colon cells and is locally consumed, and has been more extensively studied in inflammation and cancer, where it inhibits colorectal cancer and inflammation (87). *Alloprevotella* belongs to the genus *Bacteroides* of the phylum *Synechococcus* and is SCFA-producers, whose abundance is negatively correlated with obesity and diabetes (91, 92). *Lachnospiraceae_NK4A136 group* is a discriminatory feature of intestinal dysfunction (93), and Wang et al. (94) studied found that *Chrysanthemum morifolium* polysaccharides could improve intestinal dysfunction by decreasing the abundance of *Lachnospiraceae_NK4A136_group* flora and increasing the relative abundance of beneficial bacteria. In the present study, the relative abundance of *Lachnospiraceae_NK4A136_group* flora was decreased and the relative abundance of *Bacteroides* and *Alloprevotella* was increased in the group administered with high and medium doses of *F. velutipes* polysaccharide compared with the MC group, which regulated the balance of flora in the intestine of mice.

In conclusion, *F. velutipes* polysaccharide can protect immune organs of immunosuppressed mice, improve serum cytokine levels, enhance the antioxidant capacity of the body, promote the increase of intestinal SCFAs content, regulate the expression of proteins TFRC and RSAD2, promote energy metabolism, increase the abundance of flora, improve the structure of flora and maintain the homeostasis of the intestinal environment. The results suggest that *F. velutipes* polysaccharide has potential immune modulatory effects.

DATA AVAILABILITY STATEMENT

The original contributions presented in the study are included in the article/supplementary material, further inquiries can be directed to the corresponding author/s.

ETHICS STATEMENT

The animal study was reviewed and approved by Ethics Committee of Henan University School of Medicine (HUSOM2021-76).

AUTHOR CONTRIBUTIONS

QL and QZ: conceptualization, investigation, methodology, software, and writing-original draft preparation. XH and JW: data curation, formal analysis, and visualization. CM and XX: supervision, software, and validation. WK: resources, funding acquisition, project administration, and writing-reviewing and editing. All authors contributed to the article and approved the submitted version.

FUNDING

This work was supported by Major Public Welfare Projects in Henan Province (201300110200), Research on Precision Nutrition and Health Food, Department of Science and Technology of Henan Province (CXJD2021006), and The Key Project in Science and Technology Agency of Henan Province (212102110019 and 202102110283).

REFERENCES

1. Zhu GX, Jiang Y, Yao Y, Wu N, Luo J, Hu MW, et al. Ovotransferrin ameliorates the dysbiosis of immunomodulatory function and intestinal microbiota induced by cyclophosphamide. *Food Funct.* (2019) 10:1109–22. doi: 10.1039/C8FO02312C
2. Barzee TJ, Cao L, Pan ZL, Zhang RH. Fungi for future foods. *J. Funct Foods.* (2021) 1:25–37. doi: 10.1016/j.jfutfo.2021.09.002
3. USDA. *Dietary Guidelines for Americans, 2020-2025*. 9th ed (2020). Available online at: DietaryGuidelines.gov (accessed August 26, 2021).
4. Yin ZH, Liang ZH, Li CQ, Wang JM, Ma CY, Kang WY. Immunomodulatory effects of polysaccharides from edible fungus: a review. *Food Sci Hum Well.* (2021) 10:393–400. doi: 10.1016/j.fshw.2021.04.001
5. Yelithao K, Surayot U, Lee CS, Palanisamy S, Prabhu NM, Lee JH, et al. Studies on structural properties and immune-enhancing activities of

glycomannans from Schizophyllum commune. *Carbohydr Polym.* (2019) 218:37–45. doi: 10.1016/j.carbpol.2019.04.057
6. Sheng XT, Yan JM, Meng Y, Kang YY, Han Z, Tai GH, et al. Immunomodulatory effects of *Hericium erinaceus* derived polysaccharides are mediated by intestinal immunology. *Food Funct.* (2017) 8:1020–7. doi: 10.1039/C7FO00071E
7. Wu DM, Duan WQ, Liu Y, Cen Y. Anti-inflammatoryeffect of the polysaccharides of golden needle mushroom in burnedrats. *Int J Biol Macromol.* (2010) 46:100–3. doi: 10.1016/j.ijbiomac.2009.10.013
8. Zhang ZF, Lv GY, He WQ, Shi LG, Pan HJ, Fan LF. Effects of extraction methods on the antioxidant activities of polysaccharides obtained from *Flammulina velutipes*. *Carbohydr Polym.* (2013) 98:1524–31. doi: 10.1016/j.carbpol.2013.07.052
9. Yuan FF, Gao Z, Liu WB, Li HP, Zhang YW, Feng Y, et al. Characterization, antioxidant, anti-aging and organ protective effects of sulfated polysaccharides from *Flammulina velutipes*. *Molecules.* (2019) 24:3517. doi: 10.3390/molecules24193517
10. Ye JF, Wang XD, Wang K, Deng YD, Yang YC, Ali R, et al. A novel polysaccharide isolated from *Flammulina velutipes*, characterization, macrophage immunomodulatory activities and its impact on gut microbiota in rats. *J Anim Physiol Anim Nutr.* (2020) 104:735–48. doi: 10.1111/jpn.13290
11. Xin X, Zheng KW, Niu YY, Song MM, Kang WY. Effect of *Flammulina velutipes* (golden needle mushroom, eno-kitake) polysaccharides on constipation. *Open Chem*. (2018) 16:155–62. doi: 10.1515/chem-2018-0017
12. Liang ZH, Zheng KW, Zhao QC, Shao WJ, Li CQ, Wang JM, et al. Structural identification and coagulation effect of *Flammulina Velutipes* polysaccharides. *App Sci.* (2021) 11:1736. doi: 10.3390/app11041736
13. Zhao RQ, Fang DL, Ji Y, Chen X, Ma GX, Su AX, et al. *In vitro* and *in vivo* functional characterization of an immune activation *Flammulina velutipes* polysaccharide based on gut microbiota regulation. *Food Agric Immunol.* (2020) 1:667–86. doi: 10.1080/09540105.2020.1754345
14. Zhao RQ, Hu QH, Ma GX, Su AX, Xie MH, Li XF, et al. Effects of *Flammulina velutipes* polysaccharide on immune response and intestinal microbiota in mice. *J Funct Foods.* (2019) 56:255–64. doi: 10.1016/j.jff.2019.03.031
15. Kahn P. From genome to proteome: looking at a cell's proteins. *Science*. (1995) 270:369–70. doi: 10.1126/science.270.5235.369
16. Pandey A, Mann M. Proteomics to study genes and genomes. *Nature*. (2000) 405:837–46. doi: 10.1038/35015709
17. Almeida AM, Bassols A, Bendixen E, Bhide M, Ceciliani F, Cristobal S, et al. Animal board invited review: advances in proteomics for animal and food sciences. *Animal.* (2014) 9:1–17. doi: 10.1017/S1751731114002602
18. Nanjundan M, Byers LA, Carey MS, Siwak DR, Raso MG, Diao LX, et al. Proteomic profiling identifies pathways dysregulated in non-small cell lung cancer and an inverse association of AMPK and adhesion pathways with recurrence. *J Thorac Oncol.* (2010) 5:1894–904. doi: 10.1097/JTO.0b013e3181f2a266
19. Zhao L, Geng TT, Sun KC, Su S, Zhao Y, Bao N, et al. Proteomic analysis reveals the molecular mechanism of *Hippophae rhamnoides* polysaccharide intervention in LPS-induced inflammation of IPEC-J2 cells in piglets. *Int J Biol Macromol.* (2020) 164:3294–304. doi: 10.1016/j.ijbiomac.2020.08.235
20. Yang SF, Zhao ZC, Zhang AY, Jia FJ, Song MX, Huang ZL, et al. Proteomics analysis of chicken peripheral blood lymphocyte in Taishan *Pinus massoniana* pollen polysaccharide regulation. *PloS ONE.* (2018) 13:e0208314. doi: 10.1371/journal.pone.0208314
21. Round JL, Mazmanian SK. The gut microbiota shapes intestinal immune responses during health and disease. *Nat Rev Immunol.* (2009) 9:313–23. doi: 10.1038/nri2515
22. Thomas S, Izard J, Walsh E, Batich K, Chongsathidkiet P, Clarke G, et al. The host microbiome regulates and maintains human health: a primer and perspective for non-microbiologists. *Cancer Res.* (2017) 77:1783–812. doi: 10.1158/0008-5472.CAN-16-2929
23. Tropini C, Earle KA, Huang KC, Sonnenburg JL. The gut microbiome: connecting spatial organization to function. *Cell Host Microbe.* (2017) 21:433–42. doi: 10.1016/j.chom.2017.03.010
24. Chen SP, Wang JQ, Fang QY, Nan D, Fang QY, Cui SW, et al. A polysaccharide from natural *Cordyceps sinensis* regulates the intestinal immunity and gut microbiota in mice with cyclophosphamide-induced intestinal injury. *Food Funct.* (2021) 12:6271–82. doi: 10.1039/D1FO00596K
25. Chen QQ, Ren RR, Zhang QQ, Wu JJ, Zhang YF, Xue MS, et al. *Coptis chinensis* Franch polysaccharides provide a dynamically regulation on intestinal microenvironment, based on the intestinal flora and mucosal immunity. *J Ethnopharmacol.* (2020) 267:113542. doi: 10.1016/j.jep.2020.113542
26. Niu YY, Dong J, Jiang HM, Wang JM, Liu ZH, Ma CY, et al. Effects of polysaccharide from *Malus halliana Koehne* flowers in cyclophosphamide-induced immunosuppression and oxidative stress on mice. *Oxidative Med Cell Longev.* (2020) 2020:1603735. doi: 10.1155/2020/1603735
27. Jiang HM, Wang JM, Liang QX, Jiang SJ, Ma CY, Zhang, et al. Mechanism of intestinal flora and proteomics on regulating immune function of *Durio zibethinus* rind polysaccharide. *Oxid Med Cell Longev.* (2021) 2021:6614028. doi: 10.1155/2021/6614028
28. Jiang HM, Dong J, Jiang SJ, Liang QX, Zhang Y, Liu ZH, et al. Effect of *Durio zibethinus* rind polysaccharide on functional constipation and intestinal microbiota in rats. *Food Res Int.* (2020) 136:109316. doi: 10.1016/j.foodres.2020.109316
29. Dong J, Liang QX, Niu Y, Jiang SJ, Zhou L, Wang JM, et al. Effects of *Nigella sativa* seed polysaccharides on type 2 diabetic mice and gut microbiota. *Int J Biol Macromol.* (2020) 159:725–38. doi: 10.1016/j.ijbiomac.2020.05.042
30. Sun H, Ni XQ, Song X, Wen B, Zhou Y, Zou FQ, et al. Fermented Yupingfeng polysaccharides enhance immunity by improving the foregut microflora and intestinal barrier in weaning rex rabbits. *Appl Microbiol Biotechnol.* (2016) 100:8105–20. doi: 10.1007/s00253-016-7619-0
31. Gong Y, Wu J, Li ST. Immuno-enhancement effects of *Lycium ruthenicum* Murr. polysaccharide on cyclophosphamide-induced immunosuppression in mice. *Int J Clin Exp Med*. (2015) 8:20631–7.
32. Li WJ, Li L, Zhen WY, Wang LF, Pan M, Lv JQ, et al. *Ganoderma atrum* polysaccharide ameliorates ROS generation and apoptosis in spleen and thymus of immunosuppressed mice. *Food Chem Toxicol.* (2017) 99:199–208. doi: 10.1016/j.fct.2016.11.033
33. Zhang J, Li CY, Li JP, Guo R, Wang H, Pan J, et al. Immunoregulation on mice of low immunity and effects on five kinds of human cancer cells of *Panax japonicus* polysaccharide. *Evid Based Complement Altern Med.* (2015) 2015:839697. doi: 10.1155/2015/839697
34. Cui LN, Chen L, Yang G, Li YK, Qiao ZH, Liu Y, et al. Structural characterization and immunomodulatory activity of a heterogalactan from *Panax ginseng* flowers. *Food Res Int.* (2021) 140:109859. doi: 10.1016/j.foodres.2020.109859
35. Chen HR. *Study on immunological enhancemen and free radical pharmacology of potentilla anserine polysaccharide*. [dissertation]. Gansu Agricultural University, Lanzhou, China (2008).
36. Chen XM, Lu JX, Zhang YD, He JT, Guo XZ, Tian GY, et al. Studies of macrophage immuno-modulating activity of polysaccharides isolated from *Paecilomyces tenuipes*. *Int J Biol Macromol.* (2008) 43:252–6. doi: 10.1016/j.ijbiomac.2008.06.004
37. Lim TS, Na K, Choi EM, Chung JY, Hwang JK. Immunomodulating activities of polysaccharides isolated from *Panax ginseng*. *J Med Food.* (2004) 7:1–6. doi: 10.1089/109662004322984626
38. Aringer M, Smolen JS. Cytokine expression in lupus kidneys. *Lupus*. (2005) 14:13–18. doi: 10.1191/0961203305lu2053oa
39. Yang Y, Lundqvist A. Immunomodulatory effects of IL-2 and IL-15; implications for cancer immunotherapy. *Cancers.* (2020) 12:3586. doi: 10.3390/cancers12123586
40. Wen ZS, Tang Z, Gu LX, Xiang XW, Qu YL. Immunomodulatory effect of low molecular-weight seleno-aminopolysaccharide on immunosuppressive mice. *Int J Biol Macromol.* (2019) 123:1278–88. doi: 10.1016/j.ijbiomac.2018.10.099
41. Baumeister D, Akhtar R, Ciufolini S, Pariante CM, Mondelli V. Childhood trauma and adulthood inflammation: a meta-analysis of peripheral C-reactive protein, interleukin-6 and tumour necrosis factor-α. *Mol Psychiatry.* (2016) 21:642–9. doi: 10.1038/mp.2015.67
42. Cleynen I, Moerkercke WV, Billiet T, Vandecandelaere P, Vande Casteele NV, Breynaert C, et al. Characteristics of skin lesions associated with anti-tumor necrosis factor therapy in patients with inflammatory bowel disease: a cohort study. *Ann Intern Med.* (2016) 164:10–22. doi: 10.7326/M15-0729
43. Cheng XQ, Li H, Yue XL, Xie J, Zhang YY, Di HY, et al. Macrophage immunomodulatory activity of the polysaccharides from the roots of *Bupleurum smithii var. parvifolium*. *J Ethnopharmacol.* (2010) 130:363–8. doi: 10.1016/j.jep.2010.05.019

44. El-Kholy AA, Elkablawy MA, El-Agamy DS. Lutein mitigates cyclophosphamide induced lung and liver injury via NF-κB/MAPK dependent mechanism. *Biomed Pharmacother.* (2017) 92:519–27. doi: 10.1016/j.biopha.2017.05.103
45. Iqubal A, Syed MA, Haque MM, Najmi AK, Ali J, Haque SE. Effect of nerolidol on cyclophosphamide-induced bone marrow and hematologic toxicity in Swiss albino mice. *Exp Hematol.* (2020) 82:24–32. doi: 10.1016/j.exphem.2020.01.007
46. Iqubal A, Syed MA, Najmi AK, Azam F, Barreto GE, Iqubal MK, et al. Nano-engineered nerolidol loaded lipid carrier delivery system attenuates cyclophosphamide neurotoxicity-Probable role of NLRP3 inflammasome and caspase-1. *Exp Hematol.* (2020) 334:113464. doi: 10.1016/j.expneurol.2020.113464
47. Tong J, Mo QG, Ma BX, Ge LL, Zhou G, Wang YW. The protective effects of *Cichorium glandulosum* seed and cynarin against cyclophosphamide and its metabolite acrolein-induced hepatotoxicity *in vivo* and *in vitro*. *Food Funct.* (2017) 8:209–19. doi: 10.1039/C6FO01531J
48. Singh C, Prakash C, Tiwari KN, Mishra S, Kumar V. *Premna integrifolia* ameliorates cyclophosphamide-induced hepatotoxicity by modulation of oxidative stress and apoptosis. *Biomed Pharmacother.* (2018) 107:634–43. doi: 10.1016/j.biopha.2018.08.039
49. Nafees S, Ahmad ST, Arjumand W, Rashid S, Ali N, Sultana S. Modulatory effects of gentisic acid against genotoxicity and hepatotoxicity induced by cyclophosphamide in Swiss albino mice. *J Pharm Pharmacol.* (2012) 64:259–67. doi: 10.1111/j.2042-7158.2011.01393.x
50. Shi AM, Shi HT, Wang Y, Liu X, Cheng Y, Li H, et al. Activation of Nrf2 pathway and inhibition of NLRP3 inflammasome activation contribute to the protective effect of chlorogenic acid on acute liver injury. *Int Immunopharmacol.* (2018) 54:125–30. doi: 10.1016/j.intimp.2017.11.007
51. Lu Y, Hu DM, Ma SB, Zhao X, Wang S, Wei G, et al. Protective effect of wedelolactone against CCl4-induced acute liver injury in mice. *Int Immunopharmacol.* (2016) 34:44–52. doi: 10.1016/j.intimp.2016.02.003
52. Kebieche M, Lakroun Z, Lahouel M, Bouayed J, Meraihi Z, Soulimani R. Evaluation of epirubicin-induced acute oxidative stress toxicity in rat liver cells and mitochondria, and the prevention of toxicity through quercetin administration. *Exp Toxicol Pathol.* (2009) 61:161–7. doi: 10.1016/j.etp.2008.06.002
53. Wang QF, Nie P, Hou YH, Wang YT. Purification, biochemical characterization and DNA protection against oxidative damage of a novel recombinant superoxide dismutase from psychrophilic bacterium *Halomonas* sp. ANT108. *Protein Expres Purif.* (2020) 173:105661. doi: 10.1016/j.pep.2020.105661
54. Hou RL, Liu X, Wu XP, Zheng MF, Fu, JS. Therapeutic effect of natural melanin from edible fungus *Auricularia auricula* on alcohol-induced liver damage *in vitro* and *in vivo*. *Food Sci Hum Well.* (2021) 10:514–22. doi: 10.1016/j.fshw.2021.04.014
55. Lin XH, Yang F, Huang J, Jiang S, Tang YP, Li JR. Ameliorate effect of pyrroloquinoline quinone against cyclophosphamide-induced nephrotoxicity by activating the Nrf2 pathway and inhibiting the NLRP3 pathway. *Life Sci.* (2020) 256:117901. doi: 10.1016/j.lfs.2020.117901
56. Xu YY, Li YH, Lu YX Feng XB Tian GT, Liu QH. Antioxidative and hepatoprotective activities of a novel polysaccharide (LSAP) from *Lepista sordida* mycelia, *Food Sci Hum Well.* (2021) 10:536–44. doi: 10.1016/j.fshw.2021.04.016
57. Chan PP, Wasinger VC, Leong RW. Current application of proteomics in biomarker discovery for inflammatory bowel disease. *World J Gastrointest Pathophysiol.* (2016) 7:27–37. doi: 10.4291/wjgp.v7.i1.27
58. Chen PC, Zhang Y, Xu M, Chen HJ, Zou HX, Zhang X, et al. Proteomic landscape of liver tissue in old male mice that are long-term treated with polysaccharides from *Sargassum fusiforme*. *Food Funct.* (2020) 11:3632. doi: 10.1039/D0FO00187B
59. Liang QX, Dong J, Wang SY, Shao WJ, Ahmed AF, Zhang Y, et al. Immunomodulatory effects of *Nigella sativa* seed polysaccharides by gut microbial and proteomic technologies. *Int J Biol Macromol.* (2021) 184:483–496. doi: 10.1016/j.ijbiomac.2021.06.118
60. Beard JL. Iron biology in immune function, muscle metabolism and neuronal functioning. *J Nutr.* (2001) 131:568–80S. doi: 10.1093/jn/131.2.568S
61. Bonaccorsi-Riani E, Danger R, Lozano JJ, Martinez-Picola M, Kodela E, Mas-Malavila R, et al. Iron deficiency impairs intra-hepatic lymphocyte mediated immune response. *PLoS ONE.* (2015) 10:e0136106. doi: 10.1371/journal.pone.0136106
62. Kuvibidila SR, Velez M, Gardner R, Penugonda K, Chandra LC, Yu L. Iron deficiency reduces serum and *in vitro* secretion of interleukin-4 in mice independent of altered spleen cell proliferation. *Nutr Res.* (2012) 32:107–15. doi: 10.1016/j.nutres.2011.12.005
63. Kuvibidila SR, Kitchens D, Baliga BS. *In vivo* and *in vitro* iron deficiency reduces protein kinase C activity and translocation in murine splenic and purified T cells. *J Cell Biochem.* (1999) 74:468–78.
64. Arosio P, Elia L, Poli M. Ferritin, cellular iron storage and regulation. *IUBMB Life.* (2017) 69:414–22. doi: 10.1002/iub.1621
65. Gao GF, Li J, Zhang YT, Chang YZ. Cellular iron metabolism and regulation. *Adv Exp Med Biol.* (2019) 1173:21–32. doi: 10.1007/978-981-13-9589-5_2
66. Levy JE, Jin O, Fujiwara Y, Kuo F, Andrews NC. Transferrin receptor is necessary for development of erythrocytes and the nervous system. *Nat. Genet.* (1999) 21:369. doi: 10.1038/7727
67. Shen Y, Li X, Dong DD, Zhang B, Xue YR. Shang P, Transferrin receptor 1 in cancer: a new sight for cancer therapy. *Am J Cancer Res.* (2018) 8:916–31.
68. Jabara HH, Boyden SE, Chou J, Ramesh N, Massaad MJ, Benson H, et al. A missense mutation in TFRC, encoding transferrin receptor 1, causes combined immunodeficiency. *Nat Genet.* (2016) 48:74–8. doi: 10.1038/ng.3465
69. Song J, Liu TT, Yin Y, Zhao W, Lin ZQ, Yin YX, et al. The deubiquitinase OTUD1 enhances iron transport and potentiates host antitumor immunity. *EMBO Rep.* (2021) 22:e51162. doi: 10.15252/embr.202051162
70. Hinson ER, Cresswell P. The N-terminal amphipathic a-helix of viperin mediates localization tothe cytosolic face of the endoplasmic reticulum and inhibits protein secretion. *J Biol Chem.* (2009) 284:4705–4712. doi: 10.1074/jbc.M807261200
71. Hinson ER, Cresswell P. The antiviral protein, viperin, localizes to lipid droplets via its Nterminal amphipathic a-helix. *Proc Natl Acad Sci USA.* (2009) 106:20452–7. doi: 10.1073/pnas.0911679106
72. Severa M, Coccia EM, Fitzgerald KA. Toll-like receptor-dependent and -independent viperin gene expression and counter-regulation by PRDI-binding factor-1/BLIMP1. *J Biol Chem.* (2006) 281:26188–95. doi: 10.1074/jbc.M604516200
73. Ebrahimi KH, Vowles J, Browne C, McCullagh J, James WS. ddhCTP produced by the radical-SAM activity of RSAD2 (viperin) inhibits the NAD^+-dependent activity of enzymes to modulate metabolism. *FEBS Lett.* (2020) 594:1631–44. doi: 10.1002/1873-3468.13778
74. Schwarz KB. Oxidative stress during viral infection: a review. *Free Radic Biol Med.* (1996) 21:641–9. doi: 10.1016/0891-5849(96)00131-1
75. Kamada N, Seo SU, Chen GY, Núñez G. Role of the gut microbiota in immunity and inflammatory disease. *Nat Rev Immunol.* (2013) 13:321–35. doi: 10.1038/nri3430
76. Zhang XW, Ma CW, Xu PP, Tang J, Xu XF. Gut microbiota, host health, and polysaccharides. *Biotechnol Adv.* (2013) 31:237–318. doi: 10.1016/j.biotechadv.2012.12.009
77. Liu CJ, Cheng LY, Ji LL, Li F, Zhan YX, Wu BT, et al. Intestinal microbiota dysbiosis play a role in pathogenesis of patients with primary immune thrombocytopenia. *Thromb Res.* (2020) 190:11–19. doi: 10.1016/j.thromres.2020.03.012
78. Hong YZ, Shen MY, Huang LX, Wu T, Xie JH. *Mesona chinensis* Benth polysaccharides alleviates liver injury by beneficial regulation of gut microbiota in cyclophosphamide-induced mice. *Food Sci Hum Well.* (2022) 11:74–84. doi: 10.1016/j.fshw.2021.07.009
79. Niu XY, Shang HQ, Chen SY, Chen RC, Huang J, Miao YQ, et al. Effects of *Pinus massoniana pollen* polysaccharides on intestinal microenvironment and colitis in mice. *Food Funct.* (2020) 12:252–66. doi: 10.1039/D0FO02190C
80. Tremaroli V, Bäckhed F. Functional interactions between the gut microbiota and host metabolism. *Nature.* (2012) 489:242–9. doi: 10.1038/nature11552
81. Stojanov S, Berlec A, Štrukelj B. The influence of probiotics on the *Firmicutes*/*Bacteroidetes* ratio in the treatment of obesity and inflammatory bowel disease. *Microorganism.* (2020) 8:1715–31. doi: 10.3390/microorganisms8111715

82. Roy TL, Llopis M, Lepage P, Bruneau A, Rabot S, Bevilacqua C, et al. Intestinal microbiota determines development of non-alcoholic fatty liver disease in mice. *Gut.* (2013) 62:1787–94. doi: 10.1136/gutjnl-2012-303816
83. Kaoutari AE, Armougom F, Gordon JI, Raoult D, Henrissat B. The abundance and variety of carbohydrate-active enzymes in the human gut microbiota. *Nat. Rev. Microbiol.* (2013) 11:497–504. doi: 10.1038/nrmicro3050
84. Lovegrove A, Edwards CH, Noni ID, Patel H, EI SN, Grassby T, et al. Role of polysaccharides in food, digestion, and health. *Crit Rev Food Sci.* (2017) 57:237. doi: 10.1080/10408398.2014.939263
85. Donohoe DR, Garge N, Zhang XX, Sun W, O'Connell TM, Bunger MK, et al. The microbiome and butyrate regulate energy metabolism and autophagy in the mammalian colon. *Cell Metab.* (2011) 13:517–26. doi: 10.1016/j.cmet.2011.02.018
86. Inagaki A, Sakata T. Dose-dependent stimulatory inhibitory effects of luminal serosal n-butyric acid on epithelial cell proliferation of pig distal colonic mucosa. *J Nutr Sci Vitaminol.* (2005) 51:156–60. doi: 10.3177/jnsv.51.156
87. Koh A, Vadder F D, Kovatcheva-Datchary P, Bäckhed F. From dietary fiber to host physiology: short-chain fatty acids as key bacterial metabolites. *Cell.* (2016) 165:1332–45. doi: 10.1016/j.cell.2016.05.041
88. Tan HZ, Zhao JX, Zhang H, Zhai QX, Chen W. Novel strains of *Bacteroides fragilis* and *Bacteroides ovatus* alleviate the LPS-induced inflammation in mice. *Appl Microbiol Biotechnol.* (2019) 103:2353–65. doi: 10.1007/s00253-019-09617-1
89. Rui Y, Wan P, Chen GJ, Xie MH, Sun Y, Zeng XX, et al. Simulated digestion and fermentation *in vitro* by human gut microbiota of intra- and extra-cellular polysaccharides from *Aspergillus cristatus*. *LWT Food Sci Technol.* (2019) 116:108508–17. doi: 10.1016/j.lwt.2019.108508
90. Hosseini E, Grootaert C, Verstraete W, Wiele TV. Propionate as a health-promoting microbial metabolite in the human gut. *Nutr. Rev.* (2011) 69:245–58. doi: 10.1111/j.1753-4887.2011.00388.x
91. Hu RK, Guo WL, Huang ZR, Li L, Liu B, Lv XC, et al. Anti-diabetic effect of aloin *via* JNK-IRS1/PI3K pathways and regulation of gut microbiota. *J Funct Foods.* (2018) 46:403–12. doi: 10.1016/j.jff.2018.05.020
92. Shang QS, Song GR, Zhang MF, Shi JJ, Xu CY, Hao JJ, et al. Dietary fucoidan improves metabolic syndrome in association with increased *Akkermansia* population in the gut microbiota of high-fat diet-fed mice. *J Funct Foods.* (2017) 28:138–46. doi: 10.1016/j.jff.2016.11.002
93. Caparrós-Martín JA, Lareu RR, Ramsay JP, Peplies J, Reen FJ, Headlam HA, et al. Statin therapy causes gut dysbiosis in mice through a PXR-dependent mechanism. *Microbiome.* (2017) 5:95. doi: 10.1186/s40168-017-0312-4
94. Wang JM, Liang QX, Zhao QC, Tang Q, Ahmed AF, Zhang Y, et al. The effect of microbial composition and proteomic on improvement of functional constipation by *Chrysanthemum morifolium* polysaccharide. *Food Chem. Toxicol.* (2021) 153:112305. doi: 10.1016/j.fct.2021.112305

Conflict of Interest: The authors declare that the research was conducted in the absence of any commercial or financial relationships that could be construed as a potential conflict of interest.

Publisher's Note: All claims expressed in this article are solely those of the authors and do not necessarily represent those of their affiliated organizations, or those of the publisher, the editors and the reviewers. Any product that may be evaluated in this article, or claim that may be made by its manufacturer, is not guaranteed or endorsed by the publisher.

Copyright © 2022 Liang, Zhao, Hao, Wang, Ma, Xi and Kang. This is an open-access article distributed under the terms of the Creative Commons Attribution License (CC BY). The use, distribution or reproduction in other forums is permitted, provided the original author(s) and the copyright owner(s) are credited and that the original publication in this journal is cited, in accordance with accepted academic practice. No use, distribution or reproduction is permitted which does not comply with these terms.

frontiers | Frontiers in Immunology

ORIGINAL RESEARCH
published: 08 April 2022
doi: 10.3389/fimmu.2022.889436

Integrated Metabolomics and Transcriptome Revealed the Effect of Fermented *Lycium barbarum* Residue Promoting *Ovis aries* Immunity

Yajun Zhang[1†], *Yansheng Guo*[1†], *Yulong Luo*[2], *Min Du*[3], *Xin Yin*[4], *Xiaochun Xu*[5] *and Guijie Zhang*[1*]

[1] Departments of Animal Science, School of Agriculture, Ningxia University, Yinchuan, China, [2] School of Food and Wine, Ningxia University, Yinchuan, China, [3] Nutrigenomics and Growth Biology Laboratory, Department of Animal Sciences, Washington State University, Pullman, WA, United States, [4] State Key Laboratory of Veterinary Biotechnology, Harbin Veterinary Research Institute, The Chinese Academy of Agricultural Sciences, Harbin, China, [5] Collaborative Innovation Center for Food Production and Safety, North Minzu University, Yinchuan, China

Lycium barbarum residue contains abundant bioactive nutrients which can be used as feed supplement. The fermentation treatment of plant residue can promote the utilization of nutrients, rumen digestion, and the growth and immunity of animals. Based on ultra-performance liquid chromatography-tandem mass spectrometry (UPLC-MS/MS) metabolomics and in-depth transcriptome analysis, the study tested the mechanisms of *Lycium barbarum* residue (RW) and fermented *Lycium barbarum* residue (RFW) on meat quality and immunity of sheep. Fifty-four Tan sheep were randomly divided into control, RFW or RW treatments. Data showed that RFW and RW increased the carcass weight, fat content, ash content and reduced the cooking loss of lamb. RFW performed more significant effects on activating immune-related genes than those of RW. The expression of chemokines and immune-related pathways, such as signaling pathways of interleukin-17 signaling pathway and NOD-like receptor signaling pathway, were elevated in sheep fed RFW. RW increased the diversity in rumen metabolites, especially compositions of lipids, organic acids and organ heterocyclic compounds. RFW affected numerous compounds which are closely correlated with the activation of immune genes. In conclusion, RFW could represent a valuable strategy to improve growth performance and immunity of sheep.

Keywords: ***Lycium barbarum*** **residue, immune response, immunity, immune system, transcriptomic patterns, fermentation, sheep, metabolomics**

OPEN ACCESS

Edited by:
Bin Du,
Hebei Normal University of Science and Technology, China

Reviewed by:
Jingzhang Geng,
Shaanxi University of Technology, China
Guang Xin,
Shenyang Agricultural University, China

***Correspondence:**
Guijie Zhang
guijiezhang@nxu.edu.cn

†These authors have contributed equally to this work and share first authorship

Specialty section:
This article was submitted to Nutritional Immunology, a section of the journal Frontiers in Immunology

Received: *04 March 2022*
Accepted: *17 March 2022*
Published: *08 April 2022*

Citation:
Zhang Y, Guo Y, Luo Y, Du M, Yin X, Xu X and Zhang G (2022) Integrated Metabolomics and Transcriptome Revealed the Effect of Fermented Lycium barbarum Residue Promoting Ovis aries Immunity. Front. Immunol. 13:889436. doi: 10.3389/fimmu.2022.889436

1 INTRODUCTION

Disease resistance and meat quality are critically important for Tan sheep production. Bioactive metabolites from plants have gained increasing interest as being developed as growth-promoting antibiotics for ruminant animals (1). Various plants have been used as fodder additives for their particular metabolites with antimicrobial, antioxidant, anti-inflammatory and promoting immunity activities (2–5). Thus, developing effective plant-derived fodder additives will improve the production of ruminant animals.

Lycium barbarum is one of the important agricultural species, and has been widely used in traditional Chinese medicine. *Lycium barbarum* contains amino acids, polysaccharide (LBP), flavonoids, betaine, vitamins and other active nutrients (6). A wealth of vitamins in *Lycium barbarum* can promote the proliferation of hepatocytes, enhance non-specific immunity, and improve disease resistance and the phagocytosis of phagocytes. In addition, the by-products of *Lycium barbarum* contain a variety of nutrients that could be used as high-quality feed materials for animal. Previous studies have confirmed that the addition of *Lycium barbarum* residue in feed could improve the immunity and growth performance of animals (7). Chemical, physical and biological fermentation could break down the cellulose, hemicellulose, and lignin of plant residues, improving the utilization of nutrients and the efficiency of the animal production. Fermentation technology has been shown to effectively improve the nutrient utilization rate of *Lycium barbarum* and to reduce the feed/gain ratio (8–10). Remarkably, it also can provide readily available nutrients for rumen microorganisms (11, 12), and enhance animal immunity by increasing the levels of immunoglobulin G (IgG), immunoglobulin M (IgM) and interleukin-10 (IL-10) (13). The fermentation treatment of plant residue further promotes the absorption of nutrients and rumen digestion by animals, and has various effects on the growth and immunity of ruminants. Thus, elucidating the mechanisms of *Lycium barbarum* residue and its fermented products on animal immunity and meat quality would contribute to make full use of them and improve animal productivity.

Overall, *Lycium barbarum* residue has the characteristics of green pollution-free, no drug resistance, and can be used as feed ingredients to improve immunity and disease resistance. Although the effect of *Lycium barbarum* residue on the growth and immunity of animals has been investigated, only simple indicators of immunity were revealed, which does not elaborate the mechanism that are sufficient enough to realize the effect of *Lycium barbarum* residue. An integrated investigation of the detailed mechanism of *Lycium barbarum* residue before and after fermentation on sheep immunity remains to be tested.

Recently, with the advancement of multi-omics technology, the changes of animal immune system and meat quality under different conditions can be systematically evaluated, which provides the opportunity for us to deeply understanding the biological process of fermented products *in vivo* (14–17). Based on ultra-performance liquid chromatography-tandem mass spectrometry (UPLC-MS/MS) metabolomics and in-depth transcriptome analysis, the present study investigated the mechanisms of *Lycium barbarum* residue (RW) and fermented *Lycium barbarum* residue (RFW) on meat quality and immunity of sheep. This study aimed to provide the theoretical basis and method for rational utilization of *Lycium barbarum* residue as feed sources.

2 MATERIALS AND METHODS

The experimental protocols were approved by the Institutional Animal Care and Use Committee of Ningxia University (NXUC20200618).

2.1 Sample Collection and Preparation

In total, fifty-four ram Tan sheep (120 days, 19.86 ± 0.62 kg) with similar genetic background were selected and randomly divided into 3 experimental groups. Three experimental groups of sheep were feed with basal diet (RCON), basal diet supplemented with *Lycium barbarum* residue (RW) and basal diet supplemented with fermented *Lycium barbarum* residue (RFW) for 70 days. During the feeding trial, sheep were fed twice at 8:00 and 16:00 every day with free access to drinking water. At the end of trial, six biological replicates of sheep in each treatment were selected and slaughtered for further experiment analysis. All sheep were fasted for 16 h before slaughter. Carcass weight was obtained. The rumen was collected for metabolomics and transcriptome analyses, and venous blood was obtained from the jugular vein. The 10 mL venous blood of each sheep was collected. After the blood was fully coagulated, the serum was obtained by centrifugation at 2500 r/min for 15 min and stored at -20°C, then series serum immune indexes were determined, including the contents of immunoglobulin A (IgA), immunoglobulin G (IgG), immunoglobulin M (IgM), interleukin-1β (IL-1β) and interleukin-6 (IL-6).

2.2 RNA Extraction

Total RNA was extracted from the rumen of each sample using a total RNA extraction kit (#AM1561, Ambion), following the manufacturer's instructions. RNA purity was checked using the NanoPhotometer® spectrophotometer (IMPLEN, CA, USA). An Agilent Bioanalyzer 2100 (Agilent Technologies) was used to ensure RNA integrity by determining the RNA integrity number. The sequencing reagent was prepared according to the HiSeq 2500 user guide. Then, clusters were generated.

2.3 Transcriptome Sequencing and Assembly

A total amount of 1.5 μg RNA per sample was used as input material for the RNA sample preparations. Sequencing libraries were generated using NEBNext® Ultra™ RNA Library Prep Kit for Illumina® (NEB, USA) following manufacturer's recommendations and index codes were added to attribute sequences to each sample. The library fragments were purified with AMPure XP system (Beckman Coulter, Beverly, USA) to select cDNA fragments of preferentially 250~300 bp in length. Then 3 μL USER Enzyme (NEB, USA) was used with size-

selected, adaptor-ligated cDNA at 37°C for 15 min followed by 5 min at 95°C before PCR. Then PCR was performed with Phusion High-Fidelity DNA polymerase, Universal PCR primers and Index (X) Primer. At last, PCR products were purified (AMPure XP system). The library quality was assessed on the Agilent Bioanalyzer 2100 system.

Raw data (raw reads) of fastq format were firstly processed through in-house perl scripts. In this step, clean data (clean reads) were obtained by removing reads containing adapter, reads containing ploy-N and low quality from raw data. At the same time, Q20, Q30, GC-content and sequence duplication level of the clean data were calculated. All the downstream analyses were based on clean data with high quality. Transcriptome assembly was accomplished based on the left.fq and right.fq using trinity with min kmer cov set to 2 by default and all other parameters set default (18).

2.4 Differential Expression Analysis

Gene expression levels were estimated by RSEM for each sample. Clean data were mapped back onto the assembled transcriptome, and read count for each gene was obtained from the mapping results. Differential expression analysis of two conditions/groups was performed using the DESeq R package (1.10.1). DESeq provide statistical routines for determining differential expression in digital gene expression data using a model based on the negative binomial distribution. The resulting *P* values were adjusted using the Benjamini and Hochberg's approach for controlling the false discovery rate. Genes with FDR < 0.05 and $|\log_2 FC| > 1$ found by DESeq were assigned as differentially expressed.

2.5 Function Analysis of Differentially Expressed Genes

Genes were classified by GO annotation into three categories: biological process, cellular compartment and molecular function. For each category, a two-tailed Fisher's exact test was employed to test the enrichment of the differentially expressed proteins against all identified genes. KEGG database was used to identify enriched pathways by a two-tailed Fisher's exact test to test the enrichment of the differentially expressed genes against all identified genes. The pathways and GO terms with $P < 0.05$ were considered significant. All differentially expressed genes were searched against the STRING database for protein-protein interaction analysis. All interactions with a confidence score ≥ 0.7 (high confidence) were used.

2.6 LC-MS/MS Analysis

In total, 1g of rumen from each sample was transferred to an EP tube. After the addition of 400 μL of extract solution (acetonitrile: methanol = 1: 1, containing isotopically-labelled internal standard mixture), the samples were vortexed for 30 s, sonicated for 10 min in ice-water bath, and incubated for 1 h to precipitate proteins. Then the sample was centrifuged at 12,000r/min for 15 min. The supernatant was transferred to a fresh glass vial for analysis. The quality control (QC) sample was prepared by mixing an equal aliquot of the supernatants from all of the samples (19).

LC-MS/MS analyses were performed using an UHPLC system (Vanquish, Thermo Fisher Scientific) with a UPLC BEH Amide column (2.1 mm × 100 mm, 1.7 μm) coupled to Q Exactive HFX mass spectrometer (Orbitrap MS, Thermo). The mobile phase consisted of 25 mmol/L ammonium acetate and 25 ammonia hydroxides in water (pH = 9.75) (A) and acetonitrile (B). The auto-sampler temperature was 4°C, and the injection volume was 3 μL (20). The raw data were converted to the mzXML format using ProteoWizard and processed with an in-house program, which was developed using R and based on XCMS, for peak detection, extraction, alignment, and integration. Then an in-house MS2 database (BiotreeDB) was applied in metabolite annotation. The cutoff for annotation was set at 0.3 (21).

2.7 Analysis of Metabolomics Profiles

The analysis of data variation was performed by R packages XCMS software. The Principal Component Analysis (PCA) and pathway enrichment analysis were performed by Metaboanalyst 3.0. PCA was performed on the three-dimensional metabolic data involving the metabolite name, sample name and normalized peak area. The data were further treated through mean centering and unit variance scaling. The PCA plots were generated to interpret cluster separation. And the therapy $P < 0.05$ and fold change (FC) > 2 was used for identification of significantly differential metabolites.

3 RESULTS

3.1 Dramatic Variations Between RW and RFW in the Transcriptomic Patterns of Sheep

To investigate the effect of RW and RFW on the sheep, rumen with six replicates for each treatment were collected for transcriptome sequencing, and the rumen with basic ration was used as control. In total, 823,571,490 paired-end reads were generated from high-throughput sequencing of all samples, and 44,415,297 clean reads were obtained from 45,753,971 per library in average (**Table 1**). All reads were mapped to the reference genome of sheep (Oar_rambouillet_v1.0), and 95.95% of clean reads were aligned to the genome of sheep in average. Finally, 35,671 genes were obtained for further functional analysis to elucidate the effect of RW and RFW on the transcriptomic pattern of sheep (**Table 1**).

Subsequently, based on the transcriptome profiles of the three experimental treatments of RW, RCON and RFW, two algorithms, correlation analysis and PCA, were further used to study the overall impact of RW and RFW treatments on the transcriptome profiles of sheep (**Figure 1**). The correlation analysis displayed an obvious cluster containing all samples from RFW treatment, whereas samples from other two treatments (RW and RCON) irregularly clustered into another cluster (**Figure 1A**). This suggests that RFW treatment caused more significant variations in transcriptomic patterns of sheep than those of RW and RCON treatment. Further PCA analysis

TABLE 1 | Characteristics of sheep transcriptome assembly under RFW and RW treatments.

Sample	Raw reads	Clean reads	Clean bases	Total map
RCON1	45232800	44092650	6.61G	42788762 (97.04%)
RCON2	42219944	40888960	6.13G	39591387 (96.83%)
RCON3	43444466	41659558	6.25G	40050506 (96.14%)
RCON4	42946476	41714970	6.26G	40189419 (96.34%)
RCON5	45723612	44575256	6.69G	43235768 (96.99%)
RCON6	45899104	44166626	6.62G	42598564 (96.45%)
RW1	45946156	44674048	6.7G	42923559 (96.08%)
RW2	53574850	51574902	7.74G	49474581 (95.93%)
RW3	44084436	42681690	6.4G	41138358 (96.38%)
RW4	47272822	45844162	6.88G	44022901 (96.03%)
RW5	47793996	46327334	6.95G	44360148 (95.75%)
RW6	46289582	45130724	6.77G	43245909 (95.82%)
RFW1	46547690	45206554	6.78G	42911105 (94.92%)
RFW2	44450046	43092694	6.46G	40130860 (93.13%)
RFW3	46325768	45126570	6.77G	43229285 (95.8%)
RFW4	46189858	44887138	6.73G	43013512 (95.83%)
RFW5	46195812	44935596	6.74G	43096286 (95.91%)
RFW6	43434072	42895926	6.43G	41031677 (95.65%)

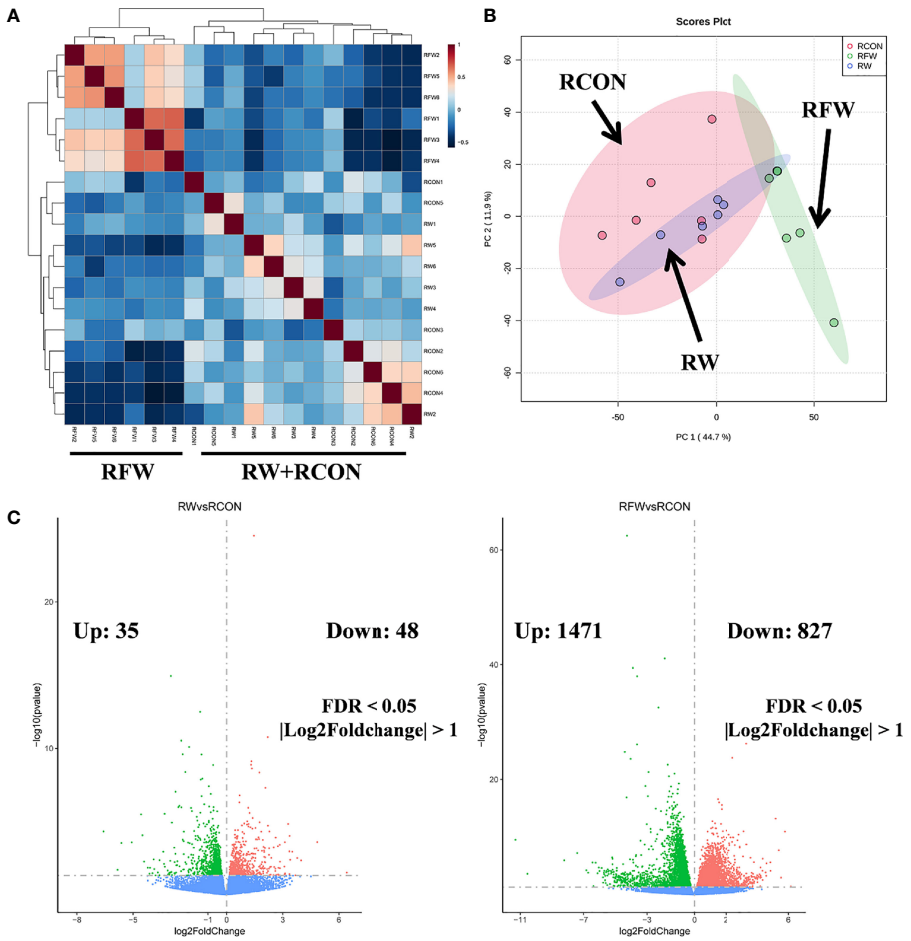

FIGURE 1 | Landscape of the transcriptomic patterns of sheep after RFW and RW treatments. **(A)** Correlation analysis on all samples showing two distinct clades: samples of RFW and RW+RCON. The correlation value between samples were represented by the color of each cell. **(B)** Principal component analysis (PCA) on the metabolic profiles of sheep after RFW and RW treatments. Three regions within 95% confidence intervals were formed in the PCA plots, including RCON, RW and RFW. **(C)** Volcano plots showed the differentially expression genes in RW *vs.* RCON (left) and RFW *vs.* RCON (right) pairwise comparisons. The upregulated and downregulated genes were shown in pink and green, respectively, whereas blue dots represented the genes without significance in each comparison.

reached a consensus with the correlation analysis that all RW and RCON samples distributed into one region, whereas RFW samples separated with both groups and formed another region (**Figure 1B**). The top two components of PCA analysis explained 44.7% and 11.9% of the variances caused by RFW and RW treatments, represented by principal component PC1 and PC2 (**Figure 1B**). PCA analysis supported that RFW caused more transcriptomic variations of sheep than those of RW treatment. Then, we set threshold value of FDR < 0.05 and $|\log_2 FC| > 1$ to identified the differentially expression genes (DEGs) in two pairwise comparisons (**Figure 1C**). Compared with RCON, 83 genes were altered to differentially express in RW treatments, with 35 upregulated genes and 48 downregulated genes (**Figure 1C**). By contrast, RFW dramatically induced variations in gene expression of 2,298 genes, with 1,471 upregulated genes and 827 downregulated genes (**Figure 1C**). Thus, these DEGs from both pairwise comparisons were used for further function analysis to elucidate the detailed effects of RW and RFW treatments on sheep.

3.1.1 RW Altered Transcription Patterns of Metabolisms Relevant to Amino Acids and Fatty Acids

To investigate the function of genes of RW treatments, we performed Gene Ontology (GO) enrichment analysis on the 83 DEGs. Functional enrichment results showed that these DEGs (FDR < 0.05) were involved in 805 GO categories, with 35 significant GO terms among three main groups, including biological process, molecular function and cellular component (**Supplementary Table 1**, $P < 0.05$). Two significantly enriched terms relevant to cellular component were ribosome and ribonucleoprotein complex (**Figure 2A**). Among molecular function categorizes, 13 terms were significantly enriched in the RW *vs.* RCON comparison, including structural constituent of ribosome, structural molecule activity, RNA binding, unfolded protein binding, translation initiation factor activity, translation factor activity, RNA binding, transcription regulator activity, DNA binding transcription factor activity, isomerase activity, rRNA binding, oxidoreductase activity,

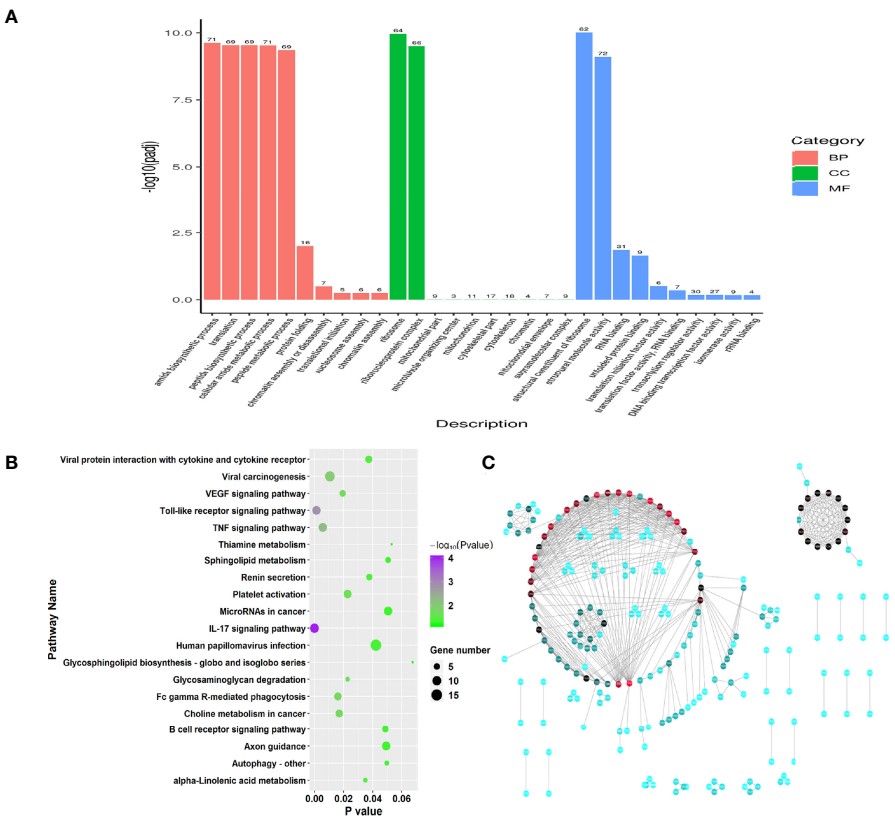

FIGURE 2 | Function enrichment analysis on the significant differential genes in RW *vs.* RCON comparison. **(A)** Gene ontology enrichment analysis on all differential genes in RW *vs.* RCON comparison. Three main kinds of terms relevant to biological process, cellular component and molecular function were shown in pink, green and blue, respectively. The vertical coordinate represented the *P* value of each GO term. **(B)** Dot plots showing the results of KEGG pathway enrichment analysis on upregulated genes upon RW treatment. The dot size represented the gene number involved in each pathway, whereas the dot color represented the *P* value of each pathway. The abscissa represented the *P* value. **(C)** Protein-protein interaction network of RW-associated genes. The dot color represented the importance of each gene in this topological network.

chemokine activity and chemokine receptor binding (**Figure 2A**). We noted that RW mainly altered genes with chemokine and transcription activity, demonstrating that RW might affect the chemokine production of sheep. For biological processes, 20 categories were significantly identified, especially genes with protein modification and transcription activity, such as amide biosynthetic process, translation, peptide biosynthetic process, cellular amide metabolic process, peptide metabolic process, protein folding, chromatin assembly or disassembly, translational initiation, nucleosome assembly, chromatin assembly, protein-DNA complex assembly and regulation of hydrolase activity (**Figure 2A**).

Subsequently, pathway enrichment analysis was performed on the upregulated and downregulated genes in RW *vs.* RCON comparison based KEGG database. 35 upregulated genes were enriched in 257 pathways, with 16 significant pathways (**Figure 2B**, $P < 0.05$). We noted various immune-related pathways were significantly activated upon RW treatment, such as IL-17 signaling pathway, Toll-like receptor signaling pathway, TNF signaling pathway, autophagy and phagocytosis, as well as the expression of cytokines (**Figure 2B**). In addition, RW also altered the gene expression relevant to metabolisms, such as glycosaminoglycan degradation and alpha-linolenic acid metabolism (**Figure 2B**). Further pathway analysis on 48 downregulated genes showed that RW-suppressed genes mainly functioned in pathways relevant to metabolisms. Various pathways relevant to amino acid and fatty acid metabolisms, such as valine, leucine and isoleucine degradation, butanoate metabolism, sulfur metabolism, fatty acid degradation, propanoate metabolism, tryptophan metabolism and fatty acid elongation, thiamine metabolism, were significantly enriched (**Supplementary Figure 1A**). Meanwhile, these genes involved in a duplicated interaction network *in vivo*, suggesting that RW altered transcriptional patterns in sheep on a global scale, leading to activation and metabolic redirection of immune-related genes associated with fatty acids and amino acids in sheep (**Figure 2C**).

3.1.2 RFW Triggered Expression of Genes Involved in Sheep Immune System

Similarly, GO and pathway enrichment analysis were also performed in RFW *vs.* RCON comparison to investigate the effect of RFW on transcriptomic variations of the sheep. GO enrichment analysis on 2,298 DEGs showed that RFW mainly altered 157 GO terms among biological process, molecular function and cellular component (**Supplementary Table 2**, $P <$

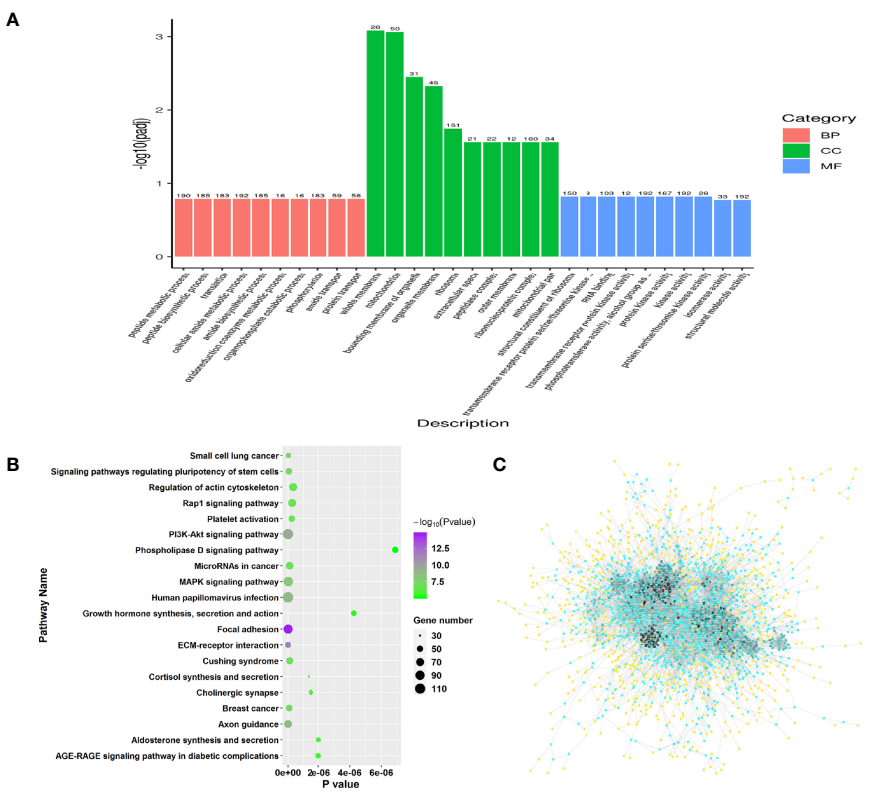

FIGURE 3 | Genes triggered by RFW treatments mainly involved in the immune system of sheep. **(A)** GO enrichment analysis on all DEGs from RFW *vs.* RCON comparison. Biological process, cellular component and molecular function terms were shown in pink, green and blue, respectively. The vertical coordinate represented the *P* value of each GO terms. **(B)** Dot plots showing the results of KEGG pathway enrichment analysis on upregulated genes upon RFW treatment. The dot size and color represented the gene number and *P* value of each pathway, respectively. The abscissa represented the *P* value. **(C)** Protein-protein interaction network of RFW-associated genes. The dot color represented the importance of each gene in this topological network.

0.05). For biological process, various terms relevant to transcription and metabolisms were affected by RFW treatment, including peptide metabolic process, translation, amide biosynthetic process, phosphorylation, nucleoside phosphate catabolic process, protein localization, intracellular transport, pyridine nucleotide biosynthetic process, ATP metabolic process, cation homeostasis, purine ribonucleotide biosynthetic process, cell differentiation, coenzyme biosynthetic process and lipid catabolic process (**Figure 3A**). The various related cellular component terms were significantly enriched, including whole membrane, mitochondrion, organelle membrane, ribosome, extracellular space, peptidase complex, mitochondrial outer membrane, envelope, cytoplasmic vesicle part and golgi-associated vesicles (**Figure 3A**). Similarly, RFW also affected various genes with transcription function. Numerous molecular function related terms were significantly identified in RFW treatment, such as structural constituent of ribosome, transmembrane receptor protein serine/threonine kinase activity, RNA binding, protein kinase activity, 5'-3' RNA polymerase activity, RNA polymerase activity and ferric iron binding (**Figure 3A**).

Remarkably, the pathway analysis of 1,471 upregulated genes were mainly involved in various immune-related pathways, such as, IL-17 signaling pathway, NOD-like receptor signaling pathway and Chemokine signaling pathway (**Figure 3B**). Various studies have well documented these pathways in animal immune system (22–25). The 1,471 upregulated genes also involved in a complex interaction network (**Figure 3C**), demonstrating the effect of RFW on the sheep immune system were comprehensive. Remarkably, RFW activated more immune-related pathways and the activation degree was more significant than RW treatment (**Figure 3B**). In parallel, among the 827 downregulated genes, pathway analysis showed that some metabolism-related pathways were significantly inhibited *in vivo*, while immune-related pathways have not identified significantly in RFW treatment (**Supplementary Figure 1B**). Furthermore, we determined the levels of immune indexes under RW and RFW treatments. The results showed that both RW and RFW treatments could increase the IgG, IgA, IgM and GLB levels. The effect of RFW was more significant in increasing immune-related factors, with 242 μg/mL of IgG, 135 μg/mL of IgA, 105 μg/mL of IgM and 34.9 μg/mL of GLB (**Table 2**). It supported that RFW could trigger the expression of more immune-related genes in sheep.

3.1.3 Effects of RFW and RW on Acting Immune-Related Genes

To investigate whether RFW and RW could trigger common immune-related response, we identified the 60 DEGs that were common in RFW *vs.* RCON and RW *vs.* RCON comparisons. As shown in **Figure 4A**, RFW and RW specifically affected 2,238 and 23 genes, respectively. Notably, RFW and RW had similar effects on these genes, which were both induced or suppressed by RFW or RW in sheep (**Figure 4B**). Protein-protein interaction analysis showed that these genes were involved in a simple network with only 11 proteins that could interact with others (**Figure 4C**). Further pathway enrichment analysis of these genes showed that these genes were mainly involved in ribosome, and no obvious immune or metabolism-related pathways were identified in these 60 genes (**Table 3**). These results suggested that RFW could specifically trigger the immune response and promote the immunity of sheep. Although RW could also trigger immune-related genes *in vivo*, its effects were not as obvious as RFW. RW mainly altered the metabolic flux of sheep, which may cause differences in meat quality.

3.2 Dramatic Variations Between RW and RFW in the Metabolic Patterns of Sheep

Presently, we found that RFW and RW treatment could increase the carcass weight, fat content and ash content (**Table 4**). The increase of these three indicators was higher in RFW than in RW treatment. Meanwhile, RFW and RW treatments could reduce the cooking loss of sheep (**Table 4**). Thus, we concluded that RFW and RW could affect the meat quality. Numerous indicators of meat quality were closely associated with the changes in metabolisms *in vivo*. Considering the influences of RFW and RW on metabolisms of sheep at transcription levels, we performed metabolomics analysis on the rumen in RFW and RW treatment after 70 days (**Figure 5**). Ten replicates of each treatment were collected for metabolomics analysis based on high resolution LC-MS platform. The rumen with basic ration was set as control (RCON). Totally, 329 and 1,034 metabolites were identified in negative and positive modes, respectively (**Figure 5**). As shown in **Figure 5A**, PCA analysis was conducted on the metabolic profiles among three treatments. The results indicated that the metabolic patterns of three treatments were significantly different, and the three treatments were distributed in different regions. The differences

TABLE 2 | Influences of RFW and RW on the immune indicators of sheep.

Name	RCON	RW	RFW	SEM	*P*-value
IgG μg/mL	170.56[a]	200.03[b]	242.28[b]	39.61	0.04
IgA μg/mL	102.48	110.03	135.49	23.55	0.26
IgM μg/mL	53.54[a]	76.72[ab]	105.04[b]	20.67	0.01
GLB g/L	29.58[a]	31.00[b]	34.95[b]	2.48	0.04

[a,b]*Different letters within a row means values with significantly different (P < 0.05).*

TABLE 3 | Pathway enrichment results of genes involved in the protein-protein interaction network.

Pathway	Gene count	FDR	Matching proteins in your network (labels)
Ribosome	5	0.00036	RPL9, ENSOARP00000004395, RPS15A, LOC101103232, RPL35A

TABLE 4 | Effects of RFW and RW treatments on slaughter performance of sheep.

Term	RCON	RW	RFW	SEM	*P*-values
Carcass weight (kg)	15.32[a]	16.83[b]	16.88[b]	0.53	0.04
Pure meat percentage (%)	63.54	61.81	63.04	2.34	0.87
Cooking lost (%)	46.91[a]	44.39[b]	44.05[b]	0.48	0.02
Water content (%)	74.17[a]	75.37[b]	75.05[b]	0.48	0.04
Fat (%)	14.85[a]	17.17[b]	18.47[b]	1.76	0.02
Ash content (%)	4.01[a]	4.57[b]	4.61[b]	0.07	0.03

[a,b]*Different letters within a row means values with significantly different (P < 0.05).*

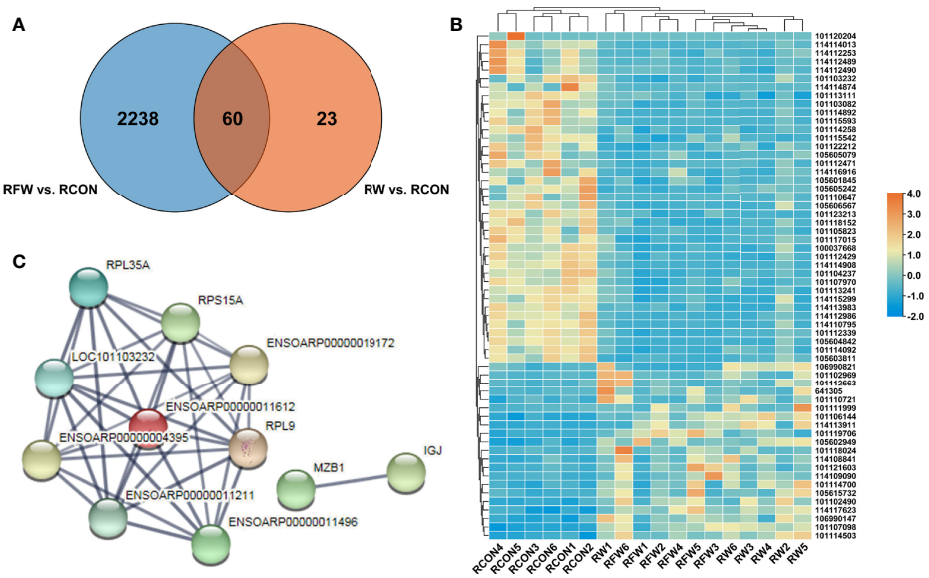

FIGURE 4 | Immune-related genes were shared in RFW *vs.* RCON and RW *vs.* RCON comparisons. **(A)** Venn diagram showed that genes shared in RFW *vs.* RCON and RW *vs.* RCON pairwise comparisons. The DEGs from RFW *vs.* RCON and RW *vs.* RCON were represented by blue and orange circles, respectively. **(B)** Heatmap displayed the expression pattern of 60 DEGs shared in RFW *vs.* RCON and RW *vs.* RCON pairwise comparisons. The up- and down-regulated genes were shown in red and blue, respectively. The gene expression levels were represented by the normalized FPKM values of gene in each sample. **(C)** The protein-protein interaction network of the genes shared in both comparisons.

may be concentrated in a few highly affected metabolites or may exist in all metabolic patterns. Remarkably, the region of RFW-treated samples was close to the RCON region, indicating similar metabolic patterns between the two groups (**Figure 5A**). However, RW-treated samples distinctly separated with RCON and RFW, which was consistent with the transcriptomic results that RW altered more genes involved in metabolic pathways than those of RFW and RCON treatments (**Figure 5A**). The top two main components could explain 54.5% of the RFW/RW-associated variations in the data (**Figure 5A**). Further unsupervised hierarchical clustering analysis was performed to identify the variances of metabolic patterns among both RFW *vs.* RCON and RW *vs.* RCON pairwise comparisons (**Figure 5B**). Data showed that all samples under the same treatments were closely clustered on one branch, and the comparison difference between RW *vs.* RCON was more significant than that between RFW *vs.* RCON (**Figure 5B**). These data were in good agreement with the PCA results.

Subsequently, we set threshold ($|\log_2 FC| > 1$, *P*-value < 0.05, and VIP > 1) to identified differential metabolites in both comparisons (**Figure 5C**). The VIP values of each metabolite were calculated from the PLS-DA model. A total of 508 metabolites changed significantly between the RW and RCON treatment, with 31 downregulated metabolites and 477 upregulated metabolites (**Figure 5C**). However, RFW only significantly altered the levels of 199 metabolites, with 189 metabolites decreased and 10 metabolites increased (**Figure 5C**). Therefore, we concluded that the metabolic patterns of sheep in

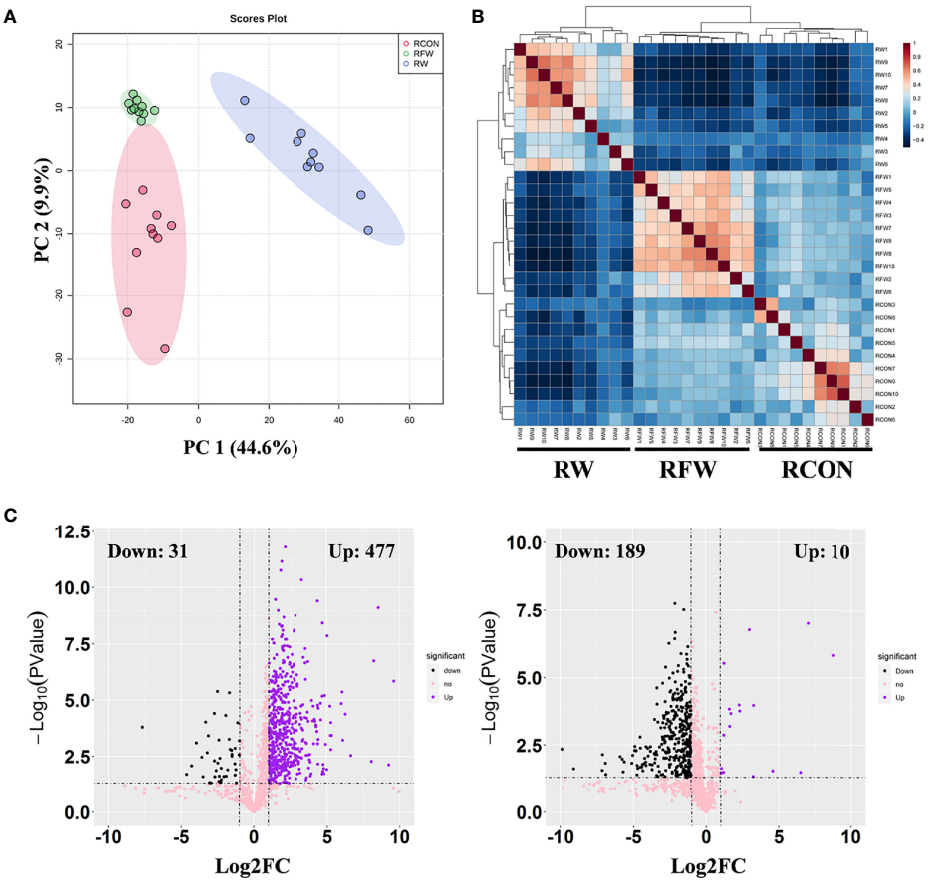

FIGURE 5 | Overview of metabolic profiles of rumen after RFW and RW treatments. **(A)** Principal component analysis on the metabolic profiles from three experiment treatments. The PCA plots showed the separation of three treatments and stability of replicates from same treatment. Each dot represented a sample. Three ellipses were the 95% confidence intervals formed in the PCA plots, representing RCON, RW and RFW treatments. PC1 for metabolomics explains 44.6% of variance and PC2 explains 9.9% of variance using integral metabolomics data. **(B)** Heatmap showing the square of Pearson correlation coefficient between samples. The correlation analysis showed tree clades in the heatmap, representing biological replicates from three experiment treatments. **(C)** Volcano plots of differential metabolites in RFW *vs.* RCON and RW *vs.* RCON pairwise comparisons. Each plot represented a metabolite identified in metabolomics profiles. The increased and decreased metabolites were shown in purple and black dots. The metabolites without significance were shown in pink.

RFW and RW treatments were significantly different, and RW had a greater impact on the metabolic patterns of sheep.

3.2.1 Compositions of Fatty Acids and Amino Acids in Rumen

In this study, we identified 338 and 176 metabolites which were closely associated with RW and RFW treatment, respectively (**Figure 6A**). Among 338 RW-related metabolites, 297 compounds were specifically induced by RW treatment that they increased to high levels (**Figures 6A, C**). 18 metabolites were specifically decreased in RW treatment (**Figures 6A, C**). 10 metabolites were commonly upregulated in RW and RFW treatment, while 13 metabolites were commonly downregulated in RW and RFW treatment (**Figures 6A, C**). Additionally, we identified 176 metabolites in the RFW treatment (**Figure 6A**). Among these 176 metabolites, 6 compounds were specifically decreased in RFW treatment, whereas 170 metabolites were downregulated by RFW treatment and upregulated by RW treatment (**Figures 6A, D**). We recognized these 176 metabolites as the candidate metabolites which contributed to activation of immune responses by RFW treatment. The 338 metabolites were the candidate compounds which explained the influences of RW on the metabolic pattern of sheep.

Subsequently, we analyzed the categorizes of these two sets of metabolites (**Figure 6B**). The results showed that among 338 RW-related metabolites, lipid, organic acid and organ heterocyclic compound-related metabolites were the main components, of which 108 and 82 compounds belonged to both categorizes of metabolites (**Figure 6B**). Thus, it suggested that RW could alter the composition of lipid and organic acid to affect the meat quality of sheep. It has been reported that alterations in lipid, amino acid and organic acid-related metabolites could affect the meat quality of various ruminant animal (26, 27). Additionally, benzenoids, organic oxygen compounds and nucleotides also accounted for a certain percentage (**Figure 6B**). By contrast, RFW had no significant

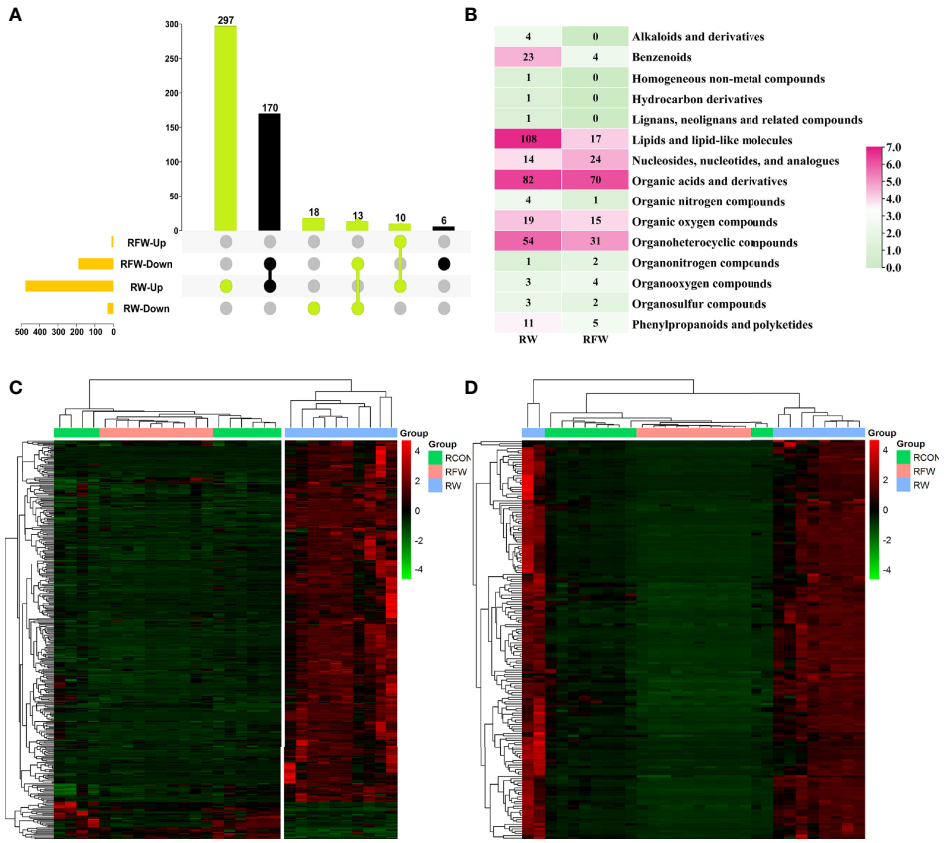

FIGURE 6 | Identification of candidate RFW- and RW-associated metabolites. **(A)** Upset diagram showed the specific metabolites identified in RFW *vs.* RCON and RW *vs.* RCON pairwise comparisons. RFW- and RW-associated metabolites were shown in black and light green, respectively. **(B)** Classifications of metabolites closely correlated with RFW and RW treatments. The color represented the metabolite number in each classification, and the number were shown in each cell. **(C, D)** Heatmap displayed the relative level of RW **(C)** and RFW -associated **(D)** metabolites. The metabolites with high levels were shown in red, whereas the metabolites with low levels were shown in green. The normalized peak area of each metabolite was used to represent the levels.

effect on lipid composition in sheep, only on 17 lipid levels (**Figure 6B**). Similarly, RFW also significantly affected the levels of 70 organic acid and 31 organ heterocyclic compound-related metabolites (**Figure 6B**). However, the overall metabolic changes caused by RFW were significantly less than those of RW treatment.

3.2.2 The Immune System and Metabolism Network

KEGG pathway enrichment analysis was performed to investigate the detailed pathways involved in these RFW and RW-related metabolites *in vivo* (**Figure 7** and **Table 5**). The results showed that RW-related metabolites were involved in 43 biosynthetic pathways, in which the biosynthesis of valine, leucine and isoleucine and the metabolism of linoleic acid were all highly enriched (**Figure 7A**). The biosynthesis of valine, leucine and isoleucine was the most significant pathway, $P < 0.05$ (**Figure 7A**), indicating that RW mainly altered the biosynthesis of valine, leucine and isoleucine in sheep, resulting in changes in meat quality. Remarkably, the top 10 related pathways mainly involved in amino acid and fatty acid metabolism, including valine, leucine and isoleucine biosynthesis, linoleic acid metabolism, glycerophospholipid metabolism, pyrimidine metabolism, lysine degradation, ascorbate and aldarate metabolism, phenylalanine, tyrosine and tryptophan biosynthesis, caffeine metabolism, alpha-linolenic acid metabolism, cysteine and methionine metabolism and arginine and proline metabolism (**Figure 7A**). Subsequently, pathway analysis results also displayed overrepresentation of pathways involved in primary biosynthesis based on RFW-related metabolites (**Figure 7B**). Series amino acid-related pathways were significantly affected by RFW treatments, including histidine metabolism, arginine biosynthesis, phenylalanine, tyrosine and tryptophan biosynthesis, alanine, aspartate and glutamate metabolism, arginine and proline metabolism and D-Glutamine and D-glutamate metabolism (**Figure 7B**). It suggested that RFW also affected the meat quality by redirecting amino acid composition and may trigger immune-related genes through this strategy. Additionally, glycine, serine and threonine metabolism, valine, leucine and isoleucine biosynthesis, glutathione metabolism, beta-alanine metabolism and phenylalanine metabolism were also altered (**Figure 7B**). However, we did not identify fatty acid-related

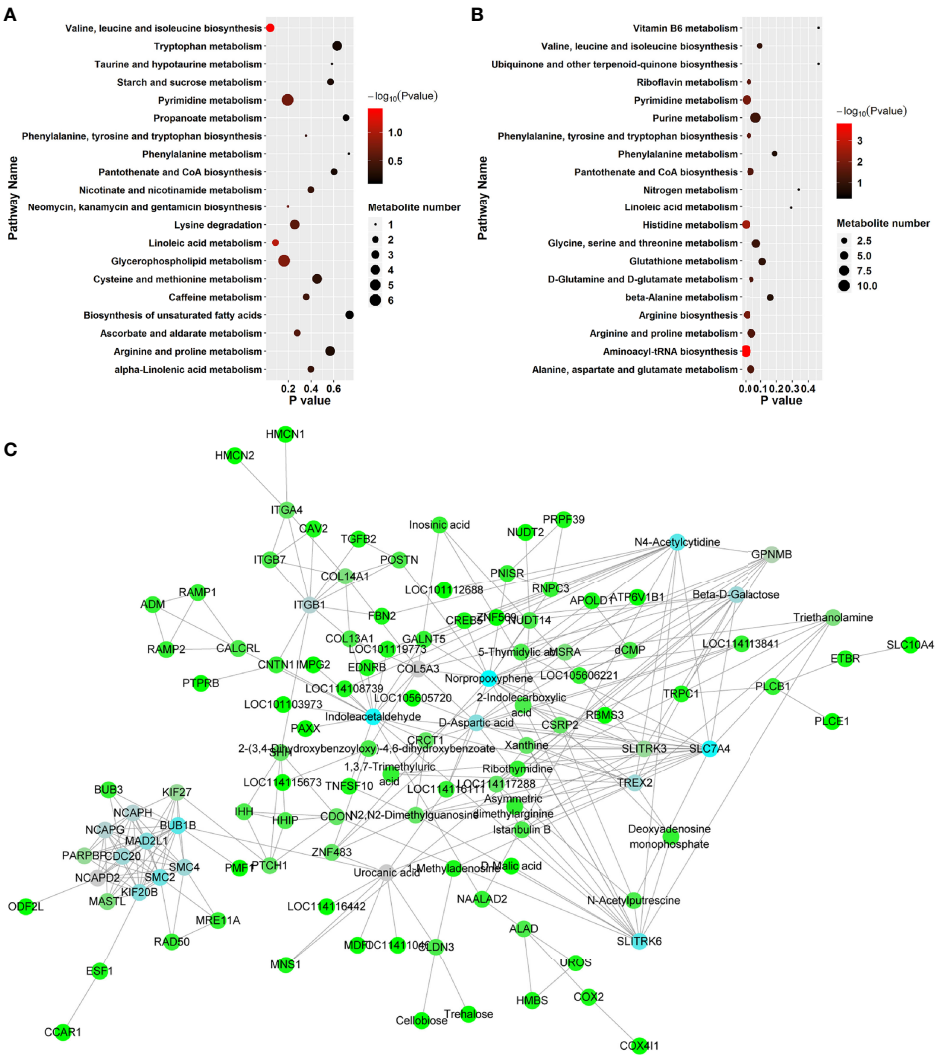

FIGURE 7 | RFW and RW treatments exhibited different effects on metabolic compositions and immune system of sheep. **(A, B)** Top 20 of enriched pathways of RW- **(A)** and RFW-associated **(B)** metabolites; The size of circle represented the number of metabolites in the related pathways. And the significance was shown in different color (high: black, low: red, $P < 0.05$). **(C)** Coexpression network of RFW-associated metabolites and RFW-triggered immune genes. The hub metabolites and genes in the topological network were shown in blue.

pathways in RFW-related metabolites (**Figure 7B**), indicating that RFW did not affected the meat quality by changing fatty acid composition *in vivo*. The aminoacyl-tRNA biosynthesis pathway was the most significantly affected pathway in RFW treatment, $P < 0.01$ (**Figure 7B**). Various researches suggested that aminoacyl-tRNA biosynthesis could influenced the immune responses (28–30). Thus, we analyzed the correlation between RFW-related metabolites and RFW-triggered immune genes (**Figure 7C**). The coexpression network analysis revealed that the metabolites were closely associated with immune-related genes (**Figure 7C**), suggesting that RFW could reorganize the transcriptome to influence metabolic composition and trigger immune-related responses. Furthermore, we identified 71 hub metabolites such as 2-(3,4-Dihydroxybenzoyloxy)-4,6-dihydroxybenzoate, triethanolamine, indoleacetaldehyde, urocanic acid, istanbulin B, 2-Indolecarboxylic acid, norpropoxyphene and Beta-D-galactose, which may be related to the activation of immune-related genes (**Supplementary Table 3** and **Figure 7C**). These metabolites mainly derived from purine metabolism and pyrimidine metabolism, and some metabolites were derived from amino acid metabolisms (**Supplementary Table 3** and **Figure 4**). In conclusion, both RFW and RW treatments affected amino acid composition, and RW could also affect fatty acid composition. RFW may change the serial metabolism of purines and pyrimidines in sheep, thereby exerting its immune system-promoting effect.

TABLE 5 | Pathway enrichment results on hub metabolites involved in the topological network.

Pathway	Hits	*P*-value	Impact
Purine metabolism	3	0.046	0.156
Pyrimidine metabolism	2	0.080	0.086
Caffeine metabolism	1	0.141	0.000
Histidine metabolism	1	0.184	0.123
Starch and sucrose metabolism	1	0.204	0.000
Alanine, aspartate and glutamate metabolism	1	0.300	0.000
Arginine and proline metabolism	1	0.385	0.023
Tryptophan metabolism	1	0.408	0.013

4 DISCUSSION

4.1 The Effects of RFW on IgA and IgG of Sheep

Traditional technology for the usage of plant-derived feed resources could not meet the development of animal feeding industry. However, the advanced fermentation technology contributed the usage of plant-derived fodder source, improving resource utilization rate and saving feed costs. Although this study did not reveal the mechanism of how fermented *Lycium barbarum* residue improves meat productivity of sheep without changing rumen metabolism, it provided plenty of evidences to decipher the detailed metabolic changes of rumen caused by fermented and non-fermented *Lycium barbarum* residue. Importantly, the addition of RFW can effectively improve the overall immunity of sheep, which is conducive to improving the resistance of sheep to a variety of pathogenic microbial and diseases in production sheep. Fermented feed refers to artificially controlled feed with microorganisms and enzymes as starter agents. The nutrients and anti-nutritional factors of feed raw materials could be decomposed or transformed into biological feed containing microbial protein and bioactive peptide amino acids, which were easy for animals to digest and absorb without toxic effects. *Lycium barbarum* residue is rich in nutrients and beneficial metabolites, which are more conducive to animal rumen digestion and absorption after fermentation. It could improve animal growth performance, daily gain, composition of rumen microflora and reduce the ratio of feed consumption to gain (8–10). Importantly, the use of *Lycium barbarum* residue and its fermented products can effectively improve animal immunity. The levels of immunoglobulin in animal blood directly reflect the immune activity of animals. Previous studies found that *Lycium barbarum* residue can increase the levels of IgA and IgG in serum of Tibetan sheep, thereby improving immunity (31, 32). Similarly, our results also showed that fermented *Lycium barbarum* could promote the levels of IgA and IgG of sheep.

4.2 The Effects of RFW on Acting Immune-Related Genes

Various studies have shown that the increases in immunoglobulin *in vivo* is mainly caused by the high levels of *Lycium barbarum* polysaccharide (1, 31). Our study showed that RFW-induced multiple carbohydrates are involved in the network of immune-related genes and metabolites, such as cellobiose, Beta-D-galactose and trehalose. Researcher proved that *Lycium barbarum*-related polysaccharide protein complex (LBP3P) can promote the expression of interleukins and TNF-α at mRNA and protein levels, regulate the immune response of animal, and improve immune performance (32). Additionally, our results showed that RFW triggered various immune-related genes involved in PI3K-Akt signaling pathway, Rap1 signaling pathway, Hedgehog signaling pathway, Wnt signaling pathway, Hippo signaling pathway, IL-17 signaling pathway, and Chemokine signaling pathway. As an important part of cellular immunity, cytokines are divided into anti-inflammatory cytokines and pro-inflammatory cytokines (IL-1β, IL-6 and tumor necrosis factor α, TNF-α), which have the functions of regulating immunity, hematopoiesis and anti-inflammatory effect (33). Immunoglobulin is an important part of humoral immunity and plays an important role in the body's immune defense. Similarly, researchers showed that fermented wheat bran increased the levels of IgG, IgM and interleukin-10, but did not affect the levels of IL-1β, IL-6 and TNF-α, indicating that fermented wheat bran could stimulate the secretion of immunoglobulin and anti-inflammatory cytokines (13). The researchers also confirmed that fermented feed can significantly increase the serum IgG and IgM levels of sheep, as well as the level of IL-6. The above results showed that fermented feed can improve the immune level of sheep to a certain extent, which may be because fermentation promotes the absorption of nutrients, thereby improving the immunity of animals. Thus, we proposed that RFW has specific metabolic components and is more advantageous than RW in improving immunity in sheep.

4.3 The Effects of RFW and RW on Ruminal Metabolic Patterns

We compared the effects of RW and RFW on ruminal metabolic patterns. RW induced more striking variations in metabolic patterns than that of RFW treatment. We assumed that this variation is mainly caused by the degradation of *Lycium barbarum* residue caused by fermentation. Indeed, fermentation could enormously change the physical and chemical properties of plant residues, leading more conducive absorption of nutrients which have been degraded into macromolecules with more comfortable solubility and sizes (34). *Bacillus siamensis* involved fermentation could make the soybean residue loosened and poriferous, leading increases of crude protein and small peptide and decreases of antinutritional factor globulins in fermented soybean residue, which improved the digestibility of

sheep (35). Meanwhile, the crude fat content in fermented corn and soybean meal mixture were lower than that in unfermented feed, leading increases of ash, calcium and total phosphorus contents of pig meats during lactation (36). Similarly, RFW and RW also caused the increases of carcass weight, fat and ash contents. Considering the degradation of 80% anti-nutritional factors in soybean residue caused by fermentation (36), thus we proposed that RFW also promoted the degradation of anti-nutritional factors and macromolecular fat, which provided a shortcut for nutrients uptake and economized energy expense in comparison to RW treatment. Indeed, non-fermented *Lycium barbarum* residue will also be fermented in rumen of ruminants for further absorption of nutrients. Due to the large number and variety of microorganisms in the rumen, it is a natural anaerobic fermenter and is also the main place for material degradation and nutrient absorption (37). Meanwhile, rumen also provides a suitable environment for the development of microbes, in return these microbials further functioned *in vivo* to affect the host immunity and homeostasis (38). Considering the conducive nutrient absorption of RFW, the microbials could deploy the nutrient more fully in rumen, resulting in the promotion of sheep immunity and meat performance. However, RW treatment also compelled rumen to burden the task for disintegration of organic macromolecules, which could be dealt by fermentation. Integrated metabolomics and transcriptome showed the activation of series nutrient and energy-related pathway in RW treatment, supporting our hypothesis that rumen need to deploy more resources to participate in the assimilation process and nutrient absorption. Overall, RWF treatment could improve the physicochemical properties and structure of *Lycium barbarum* residue and optimize its nutrient composition, contributing to the utilization efficiency of nutrients and resources.

5 CONCLUSION

In conclusion, we performed integrated transcriptome and metabolomics on the rumen fed with RW and RFW. RFW significantly increased levels of IgG, IgA, IgM and GLB, and induced the expression levels of immune-related pathway genes, thereby improving the immunity of sheep. Although RW could also induce some immune-related genes, its effect was far less than that of RFW. Remarkably, both RFW and RW treatment significantly increased sheep carcass weight, fat content and ash content. RW significantly affected the metabolic patterns of rumen, mainly altering the compositions of lipid acids, organic acids and organ heterocyclic compounds, thereby affecting meat quality. However, RFW only altered the compositions of organic acids and organ heterocyclic compounds in the rumen, and had little effect on the level of lipid acid. In summary, both RW and RFW could improve the production performance of sheep. RFW could further promote overall immunity in sheep. Our results illustrated the mechanism of the effect of RW and RFW on the immunity and production performance of sheep, and provided a theoretical basis and strategy for the rational utilization of *Lycium barbarum* residue feed resources.

DATA AVAILABILITY STATEMENT

The original contributions presented in the study are publicly available. This data can be found here: https://www.ncbi.nlm.nih.gov/ accession number PRJNA815909 and https://www.ebi.ac.uk/metabolights/ accession number MTBLS4507.

ETHICS STATEMENT

The animal study was reviewed and approved by Institutional Animal Care and Use Committee of Ningxia University (NXUC20200618).

AUTHOR CONTRIBUTIONS

YZ and YG drafted the original manuscript and prepared the table and figure. GZ designed the experiments. YL, XY, MD, and XX provided critical feedback. All authors read and approved the submitted version.

FUNDING

This study was supported by the National Natural Science Foundation of China (31960672), Top Discipline Construction Project of Pratacultural Science (NXYLXK2017A01) and the Key Research and Development Program of Ningxia Hui Autonomous Region (2021BBF02034).

ACKNOWLEDGMENTS

The financial supports from the National Natural Science Foundation of China and Ningxia University are gratefully acknowledged.

SUPPLEMENTARY MATERIAL

The Supplementary Material for this article can be found online at: https://www.frontiersin.org/articles/10.3389/fimmu.2022.889436/full#supplementary-material

Supplementary Figure 1 | Pathway analysis on RW- and RFW-suppressed genes. Scatter plots showing the results of KEGG pathway enrichment analysis on downregulated genes upon RW **(A)** or RFW **(B)** treatment. The dot size and color represented the gene number and P value of each pathway.

REFERENCES

1. Wang B, Ma MP, Diao QY, Tu Y. Saponin-Induced Shifts in the Rumen Microbiome and Metabolome of Young Cattle. *Front Microbiol* (2019) 10:356. doi: 10.3389/fmicb.2019.00356
2. Martins N, Petropoulos S, Ferreira ICFR. Chemical Composition and Bioactive Compounds of Garlic (Allium Sativum L.) as Affected by Pre- and Post-Harvest Conditions: A Review. *Food Chem* (2016) 211:41–50. doi: 10.1016/j.foodchem.2016.05.029
3. Castrica M, Menchetti L, Balzaretti CM, Branciari R, Ranucci D, Cotozzolo E, et al. Impact of Dietary Supplementation With Goji Berries (*Lycium Barbarum*) on Microbiological Quality, Physico-Chemical, and Sensory Characteristics of Rabbit Meat. *Foods* (2020) 9(10):1480. doi: 10.3390/foods9101480
4. Panyod S, Wu WK, Ho CT, Lu KH, Liu CT, Chu YL, et al. Diet Supplementation With Allicin Protects Against Alcoholic Fatty Liver Disease in Mice by Improving Anti-Inflammation and Antioxidative Functions. *J Agric Food Chem* (2016) 64(38):7104–13. doi: 10.1021/acs.jafc.6b02763
5. Wanapat M, Cherdthong A, Phesatcha K, Kang S. Dietary Sources and Their Effects on Animal Production and Environmental Sustainability. *Anim Nutr* (2015) 1(3):96–103. doi: 10.1016/j.aninu.2015.07.004
6. Lu F, Zhai R, Ruan S, Yang X, Alenyorege EA, Wang Y, et al. Enhancement of Ultrasound on the Dynamic Decolorization of Wolfberry (*Lycium Barbarum*) Polysaccharides. *Lwt* (2021) 145:111384. doi: 10.1016/j.lwt.2021.111384
7. Abdallah A, Zhang P, Zhong Q, Sun Z. Application of Traditional Chinese Herbal Medicine By-Products as Dietary Feed Supplements and Antibiotic Replacements in Animal Production. *Curr Drug Metab* (2018) 20(1):54–64. doi: 10.2174/1389200219666180523102920
8. Choi Y, Rim JS, Na Y, Lee SR. Effects of Dietary Fermented Spent Coffee Ground on Nutrient Digestibility and Nitrogen Utilization in Sheep. *Asian-Australasian J Anim Sci* (2018) 31(3):363–8. doi: 10.5713/ajas.17.0654
9. Naseer R, Hashmi AS, Zulfiqar-ul-Hassan, Rehman H, Naveed S, Masood F, et al. Assessment of Feeding Value of Processed Rice Husk for Lohi Sheep in Growing Phase. *Pak J Zool* (2017) 49(5):1725–9. doi: 10.17582/journal.pjz/2017.49.5.1725.1729
10. Su Y, Chen G, Cai Y, Gao B, Zhi X, Chang F. Effects of Broussonetia Papyrifera-Fermented Feed on the Growth Performance and Muscle Quality of Hu Sheep. *Can J Anim Sci* (2020) 100(4):771–80. doi: 10.1139/cjas-2018-0167
11. Haro AN, Carro MD, de Evan T, González J. Protecting Protein Against Ruminal Degradation Could Contribute to Reduced Methane Production. *J Anim Physiol Anim Nutr (Berl)* (2018) 102(6):1482–7. doi: 10.1111/jpn.12973
12. Liu C, Zhang L, Yang J, Zhang W, Wang Q, Zhang J, et al. Study on the Nutritional Value and Ruminal Degradation Characteristics of Fermented Waste Vinegar Residue by N. Sitophila. *Trop Anim Health Prod* (2019) 51(6):1449–54. doi: 10.1007/s11250-019-01822-4
13. Wang Y, Wang R, Hao X, Hu Y, Guo T, Zhang J, et al. Growth Performance, Nutrient Digestibility, Immune Responses and Antioxidant Status of Lambs Supplemented With Humic Acids and Fermented Wheat Bran Polysaccharides. *Anim Feed Sci Technol* (2020) 269:114644. doi: 10.1016/j.anifeedsci.2020.114644
14. Arreola-Ramírez JL, Vargas DMH, Manjarrez-Gutiérrez G, Alquicira J, Gutiérrez J, Córdoba G, et al. Modifications of Plasma 5-HT Concentrations During the Allergic Bronchoconstriction in Guinea Pigs. *Exp Lung Res* (2013) 39(7):269–74. doi: 10.3109/01902148.2013.805855
15. Lechin F, van der Dijs B, Orozco B, Jara H, Rada I, Lechin ME, et al. Neuropharmacologic Treatment of Bronchial Asthma With the Antidepressant Tianeptine: A Double-Blind, Crossover Placebo-Controlled Study. *Clin Pharmacol Ther* (1998) 64(2):223–32. doi: 10.1016/S0009-9236(98)90156-4
16. Berger M, Gray JA, Roth BL. The Expanded Biology of Serotonin. *Annu Rev Med* (2009) 60:355–66. doi: 10.1146/annurev.med.60.042307.110802
17. Cloutier N, Allaeys I, Marcoux G, Machlus KR, Mailhot B, Zufferey A, et al. Platelets Release Pathogenic Serotonin and Return to Circulation After Immune Complex-Mediated Sequestration. *Proc Natl Acad Sci USA* (2018) 115(7):1550–9. doi: 10.1073/pnas.1720553115
18. Martin JA, Wang Z. Next-Generation Transcriptome Assembly. *Nat Rev Genet* (2011) 12(10):671–82. doi: 10.1038/nrg3068
19. Dunn WB, Broadhurst D, Begley P, Zelena E, Francis-Mcintyre S, Anderson N, et al. Procedures for Large-Scale Metabolic Profiling of Serum and Plasma Using Gas Chromatography and Liquid Chromatography Coupled to Mass Spectrometry. *Nat Protoc* (2011) 6(7):1060–83. doi: 10.1038/nprot.2011.335
20. Wang J, Zhang T, Shen X, Liu J, Zhao D, Sun Y, et al. Serum Metabolomics for Early Diagnosis of Esophageal Squamous Cell Carcinoma by UHPLC-QTOF/Ms. *Metabolomics* (2016) 12(7):116. doi: 10.1007/s11306-016-1050-5
21. Smith CA, Want EJ, O'Maille G, Abagyan R, Siuzdak G. XCMS: Processing Mass Spectrometry Data for Metabolite Profiling Using Nonlinear Peak Alignment, Matching, and Identification. *Anal Chem* (2006) 78(3):779–87. doi: 10.1021/ac051437y
22. Brubaker SW, Bonham KS, Zanoni I, Kagan JC. Innate Immune Pattern Recognition: A Cell Biological Perspective. *Annu Rev Immunol* (2015) 33(1):257–90. doi: 10.1146/annurev-immunol-032414-112240
23. Reeves RK, Li H, Jost S, Blass E, Li H, Schafer JL, et al. Antigen-Specific NK Cell Memory in Rhesus Macaques. *Nat Immunol* (2015) 16(9):927–32. doi: 10.1038/ni.3227
24. Kaufmann E, Sanz J, Dunn JL, Khan N, Mendonça LE, Pacis A, et al. BCG Educates Hematopoietic Stem Cells to Generate Protective Innate Immunity Against Tuberculosis. *Cell* (2018) 172(1-2):176–90. doi: 10.1016/j.cell.2017.12.031
25. Sun JC, Madera S, Bezman NA, Beilke JN, Kaplan MH, Lanier LL. Proinflammatory Cytokine Signaling Required for the Generation of Natural Killer Cell Memory. *J Exp Med* (2012) 209(5):947–54. doi: 10.1084/jem.20111760
26. McCormick RJ. The Flexibility of the Collagen Compartment of Muscle. *Meat Sci* (1994) 36(1-2):79–91. doi: 10.1016/0309-1740(94)90035-3
27. Smith SB, Johnson BJ. 0794 Marbling: Management of Cattle to Maximize the Deposition of Intramuscular Adipose Tissue. *J Anim Sci* (2016) 94(suppl_5):382–2. doi: 10.2527/jam2016-0794
28. Moutiez M, Belin P, Gondry M. Aminoacyl-tRNA-Utilizing Enzymes in Natural Product Biosynthesis. *Chem Rev* (2017) 117(8):5578–618. doi: 10.1021/acs.chemrev.6b00523
29. Mun CH, Kim JO, Ahn SS, Yoon T, Kim SJ, Ko E, et al. Atializumab, a Humanized anti-aminoacyl-tRNA Synthetase-Interacting Multifunctional Protein-1 (AIMP1) Antibody Significantly Improves Nephritis in (NZB/NZW) F1 Mice. *Biomaterials* (2019) 220:119408. doi: 10.1016/j.biomaterials.2019.119408
30. Li L, Boniecki MT, Jaffe JD, Imai BS, Yau PM, Luthey-Schulten ZA, et al. Naturally Occurring Aminoacyl-tRNA Synthetases Editing-Domain Mutations That Cause Mistranslation in Mycoplasma Parasites. *Proc Natl Acad Sci USA* (2011) 108(23):9378–83. doi: 10.1073/pnas.1016460108
31. Planchais C, Mouquet H. Easy Pan-Detection of Human IgA Immunoglobulins. *J Immunol Methods* (2020) 484:112833. doi: 10.1016/j.jim.2020.112833
32. Gan L, Zhang SH, Liu Q, Xu HB. A Polysaccharide-Protein Complex From *Lycium Barbarum* Upregulates Cytokine Expression in Human Peripheral Blood Mononuclear Cells. *Eur J Pharmacol* (2003) 471(3):217–22. doi: 10.1016/S0014-2999(03)01827-2
33. Turner MD, Nedjai B, Hurst T, Pennington DJ. Cytokines and Chemokines: At the Crossroads of Cell Signalling and Inflammatory Disease. *Biochim Biophys Acta - Mol Cell Res* (2014) 1843(11):2563–82. doi: 10.1016/j.bbamcr.2014.05.014
34. Bhatia SK, Jagtap SS, Bedekar AA, Bhatia RK, Rajendran K, Pugazhendhi A, et al. Renewable Biohydrogen Production From Lignocellulosic Biomass Using Fermentation and Integration of Systems With Other Energy Generation Technologies. *Sci Total Environ* (2021) 765:144429. doi: 10.1016/j.scitotenv.2020.144429
35. Lio J, Wang T. Solid-State Fermentation of Soybean and Corn Processing Coproducts for Potential Feed Improvement. *J Agric Food Chem* (2012) 60(31):7702–9. doi: 10.1021/jf301674u
36. Wang C, Lin C, Su W, Zhang Y, Wang F, Wang Y, et al. Effects of Supplementing Sow Diets With Fermented Corn and Soybean Meal Mixed Feed During Lactation on the Performance of Sows and Progeny. *J Anim Sci* (2018) 96(1):206–14. doi: 10.1093/jas/skx019

37. Jami E, Israel A, Kotser A, Mizrahi I. Exploring the Bovine Rumen Bacterial Community From Birth to Adulthood. *ISME J* (2013) 7(6):1069–79. doi: 10.1038/ismej.2013.2
38. Nur Atikah I, Alimon AR, Yaakub H, Abdullah N, Jahromi MF, Ivan M, et al. Profiling of Rumen Fermentation, Microbial Population and Digestibility in Goats Fed With Dietary Oils Containing Different Fatty Acids. *BMC Vet Res* (2018) 14(1):1–9. doi: 10.1186/s12917-018-1672-0

Conflict of Interest: The authors declare that the research was conducted in the absence of any commercial or financial relationships that could be construed as a potential conflict of interest.

Publisher's Note: All claims expressed in this article are solely those of the authors and do not necessarily represent those of their affiliated organizations, or those of the publisher, the editors and the reviewers. Any product that may be evaluated in this article, or claim that may be made by its manufacturer, is not guaranteed or endorsed by the publisher.

Copyright © 2022 Zhang, Guo, Luo, Du, Yin, Xu and Zhang. This is an open-access article distributed under the terms of the Creative Commons Attribution License (CC BY). The use, distribution or reproduction in other forums is permitted, provided the original author(s) and the copyright owner(s) are credited and that the original publication in this journal is cited, in accordance with accepted academic practice. No use, distribution or reproduction is permitted which does not comply with these terms.

frontiers | Frontiers in Nutrition

ORIGINAL RESEARCH
published: 14 April 2022
doi: 10.3389/fnut.2022.862974

Galactooligosaccharide Treatment Alleviates DSS-Induced Colonic Inflammation in Caco-2 Cell Model

Marianna Roselli[1], *Aleksandra Maruszak*[2], *Roberta Grimaldi*[2], *Lucien Harthoorn*[2] *and Alberto Finamore*[1]*

[1] Research Centre for Food and Nutrition, CREA (Consiglio per la ricerca in agricoltura e l'analisi dell'economia agraria), Rome, Italy, [2] Clasado Biosciences Ltd., Reading, United Kingdom

The biological activities of dietary bioactive polysaccharides have been largely explored. Studies on the immunomodulating effects of oligosaccharides and polysaccharides have shown that they are able to modulate innate immunity. Prebiotics are a class of poorly digested carbohydrates that are mainly produced from dietary fibers, which are carbohydrate polymers with ten or more monomeric units as defined by the Codex Alimentarius Commission in 2009. Considering the capacity of prebiotics in reducing gut inflammation, the aim of this study was to investigate the anti-inflammatory activity of galactooligosaccharide (Bimuno® GOS) in an *in vitro* model of ulcerative colitis (UC)-like inflamed intestinal cells. Differentiated Caco-2 cells were exposed to 2 % dextran-sulfate-sodium salt (DSS) to induce inflammation, and then with different concentrations of Bimuno GOS (1–1,000 μg/ml). Cell monolayer permeability, tight- and adherent junction protein distribution, pro-inflammatory cytokine secretion, and NF-kB cascade were assessed. Bimuno GOS at different concentrations, while not affecting cell monolayer permeability, was shown to counteract UC-like intestinal inflammatory responses and damages induced by DSS. Indeed, Bimuno GOS was able to counteract the detrimental effects of DSS on cell permeability, determined by transepithelial electrical resistance, phenol red apparent permeability, and tight- and adherent junction protein distribution. Furthermore, Bimuno GOS inhibited the DSS-induced NF-kB nuclear translocation and pro-inflammatory cytokine secretion. Further analyses showed that Bimuno GOS was able to revert the expression levels of most of the proteins involved in the NF-kB cascade to control levels. Thus, the prebiotic Bimuno GOS can be a safe and effective way to modulate the gut inflammatory state through NF-kB pathway modulation, and could possibly further improve efficacy in inducing remission of UC.

Keywords: Inflammatory Bowel Disease, ulcerative colitis, prebiotic, galactooligosaccharides, cytokines, gut barrier, gut inflammation

OPEN ACCESS

Edited by:
Bin Du,
Hebei Normal University of Science and Technology, China

Reviewed by:
Ding-Tao Wu,
Chengdu University, China
Oswaldo Hernandez-Hernandez,
Spanish National Research Council (CSIC), Spain
Jiali Chen,
Jinan University, China

***Correspondence:**
Alberto Finamore
alberto.finamore@crea.gov.it

Specialty section:
This article was submitted to Nutritional Immunology, a section of the journal Frontiers in Nutrition

Received: *26 January 2022*
Accepted: *04 March 2022*
Published: *14 April 2022*

Citation:
Roselli M, Maruszak A, Grimaldi R, Harthoorn L and Finamore A (2022) Galactooligosaccharide Treatment Alleviates DSS-Induced Colonic Inflammation in Caco-2 Cell Model. Front. Nutr. 9:862974. doi: 10.3389/fnut.2022.862974

INTRODUCTION

Inflammatory Bowel Disease (IBD), including Crohn's disease (CD) and ulcerative colitis (UC), are chronic inflammatory disorders characterized by a progressive disease course involving the gastrointestinal tract. Traditionally, IBD has been considered as a disease of the Western world, however, data from the last 10 years describe a continuous increase of its incidence in newly

industrialized geographies such as Asia and Latin America (1, 2). The etiology of UC is still not completely known, multiple factors such as genetic background, environmental factors, microbiota, and mucosal immune dysregulation seem to be involved in its onset (3, 4). UC generally affects the colon and rectum with a relapsing and remitting pattern. It is an idiopathic intestinal inflammatory disease presenting typical symptoms (3), such as rectal bleeding, bloody and mucous diarrhea, and abdominal pain, however, the presence of extra-intestinal manifestations is also known and used for the diagnosis of UC (5). UC characteristic pathophysiology involves epithelial barrier and increased uptake of luminal antigens caused by defects in colonic mucin secretion and tight junctions damages (6). An increased number of activated and mature dendritic cells with a high expression of Toll-Like Receptor (TLR)2 and TLR4 has been observed in the lamina propria of patients affected by IBD (7), and loss of negative regulation of TLR signaling has been associated with the disruption of intestinal homeostasis (8). An atypical T-helper (Th)-cell response, as well as a specific pro-inflammatory cytokine pattern, have been shown to exist in patients affected by UC (9). Conventional therapies consist of pharmacologic agents including aminosalicylates and corticosteroids, which are able to induce remission and mucosal healing and to prevent relapses to avoid colectomy in patients affected by UC. New pharmacological strategies such as monoclonal antibodies targeted to specific pro-inflammatory cytokines, adhesion molecules, T-cell activation, as well as agents inducing anti-inflammatory cytokines [i.e., IL-10, transforming growth factor (TGF)-β], have been also used, however, they are often associated with adverse effects including headache, nausea, abdominal pain and cramping, loss of appetite, vomiting and rash (10).

Clinical and animal studies indicate that UC pathophysiology is strongly associated with changes in the gut microbiota composition (11, 12) including reduced species richness (13). Microbiome dysbiosis in UC plays a critical role in the innate intestinal immunity, however, whether these changes are a cause, or a consequence of the disease remains to be elucidated (14). Overall, considering the close connection between intestinal microbiota and UC pathogenesis, several studies have shown that intestinal dysbiosis contributes to the pathogenesis of this disease (13).

In animal models, experimental colitis is commonly induced by dextran sodium sulfate (DSS) dissolved in drinking water. Rodents treated with DSS exhibit clinical features very similar to those observed in humans affected by UC, including increased intestinal mucosal permeability and gut inflammation characterized by the secretion of specific cytokines (15). Moreover *in vitro* models of intestinal cells treated with DSS are also used to investigate mechanisms associated with UC pathogenesis (16–18). In particular, it has been shown that DSS alters Caco-2 cell tight junctions, cell cycle metabolism, as well as cytokine release (18). DSS in Caco-2 cells leads to an increased pro-inflammatory cytokine expression pattern (IL-2, IL-8, TNF-α) and gut barrier damages characterized by loss of zonula occludens-1 (ZO-1), occludin, and claudin-1, that are similar to the changes observed in *in vivo* models and patients with UC (19).

Considering that on one hand, IBD patients have been shown to have dysbiosis and reduced microbiota diversity, and on the other hand, a relationship between UC and gut microbiota has been observed, several studies investigated if microbiota modulation can ameliorate UC symptoms. There is growing evidence that probiotic and prebiotic supplementation can positively modulate gut microbiota composition by inducing microbiota restitution, which is fundamental to ensure gut health maintenance and immune homeostasis in UC patients.

Prebiotics are defined as "a substrate that is selectively utilized by host microorganisms conferring a health benefit" (20). Prebiotics are a substrate for beneficial gut bacteria able to produce short-chain fatty acids (SCFAs), which have been shown to play a key role in the suppression of inflammation in IBD (21). Thus, prebiotics or fiber-rich diets lead to an increase in SCFAs-producing microbiota.

Prebiotics include galactooligosaccharides (GOS), fructo-oligosaccharides (FOS), inulin, and β-glucans (22). The potential use of prebiotics in IBD has been suggested since they are able to promote probiotic microorganisms' growth and stimulate innate immunity (23). GOS is a term indicating a group of carbohydrates composed of oligo-galactose with lactose molecules and glucose monomers (24). The products of lactose extension are classified into two smaller groups, the GOS with excess galactose at C3, C4, or C6 and the GOS manufactured from lactose through enzymatic trans-glycosylation (25). A recent study demonstrated normalization of stools and a reduction of the incidence and severity of loose stools alongside lower urgency and a specific prebiotic effect by GOS in a cohort of patients with UC (26). Some preclinical and clinical studies highlighted that prebiotics may exert beneficial effects on UC symptoms (27) including a reduction of gut inflammation (28), bloating, diarrhea, constipation, abdominal pain, fecal pH reduction, as well as promoting regular intestinal peristalsis and preventing the mucus layer degradation (27). It has been recognized that one of the SCFA, butyrate, is associated with decreased inflammation and may alleviate UC symptoms (29). For the above-described reasons, prebiotics can be considered a valid alternative to conventional UC therapies.

A reduction of markers of intestinal inflammation, such as fecal calprotectin, has also been observed in patients with UC with active disease after supplementation with inulin (30). Experimental evidence suggests that GOS are metabolized by bacteria that possess β-galactosidases, such as Bifidobacterium species (31, 32). In particular, the major bifidogenic effect has been observed with a specific GOS (Bimuno GOS) (33, 34). This GOS has an important role in the immune function modulation, as observed in a study on a population of elderly supplemented with the GOS, where it induced IL-10 increase and reduction of IL-1β. This specific GOS has also been shown to reduce serum IL-8, C-Reactive Protein (CRP), and to improve NK cell activity (34).

In *in vitro* models, GOS has also been shown to modulate the epithelial barrier function by inducing differentiation and epithelial wound repair, and by promoting the growth of specific

gut bacteria, associated with changes in SCFA profiles (35). The effect of GOS on epithelial cells has been further confirmed by a transcriptomic analysis performed on Caco-2 cells, showing that GOS was able to modulate the expression of several genes implicated in digestion and transepithelial transport, which contribute to intestinal cell integrity and function (36).

Several studies have suggested that prebiotics, in addition to the ability to modulate the intestinal microbiota, can also exert a direct action on the intestinal epithelium through the induction of an anti-inflammatory response (37–39). In the present study, we aimed to analyze the direct effect of a specific GOS (Bimuno) in an *in vitro* model of UC-like inflammation. We treated the intestinal Caco-2 cells with DSS to mimic the inflammatory state present in the intestinal mucosa of UC patients, and we identified the possible mechanisms associated with GOS treatment for improvement of the inflammatory status in the context of UC.

MATERIALS AND METHODS

Epithelial Cell Culture

The Caco-2/TC7 cells, a clone derived from parental human intestinal Caco-2 cell line at late passage, were a kind gift from Dr. Monique Rousset (Institute National de la Santé et de la Recherche Médicale, INSERM, France). These cells are characterized by a more homogeneous expression of differentiation traits with more developed intercellular junctions and have been observed to exhibit higher metabolic and transport activities, being more similar to enterocytes of the small intestine than the original cell line (40).

Caco-2/TC7 cells were maintained at 37°C in an atmosphere of 5% CO_2/95% air at 90% relative humidity on plastic tissue culture flasks (75 cm^2 growth area, Becton Dickinson, Milan, Italy), in Dulbecco's modified minimum essential medium (DMEM; 3.7 g/L $NaHCO_3$), supplemented with 4 mm glutamine, 10% heat-inactivated fetal calf serum, 1% non-essential amino acids, 10^5 U/L penicillin, and 100 mg/L streptomycin. The cell culture media and reagents were purchased from Euroclone (Milan, Italy). The cells were used between 80 and 105 passages. For the experimental assays, the cells were seeded at a density of 1×10^6 cells/filter on polyethylene terephthalate semipermeable filters (Transwell®, 12 mm diameter,0.45 μm pore size, Becton Dickinson), which allow epithelial differentiation between apical (AP) and basolateral (BL) compartments. After reaching confluency, the cells were left for 17–21 days to allow full differentiation. The medium was changed 3 times a week. To induce inflammation, differentiated Caco-2/TC7 cells were exposed to dextran sulfate sodium salt (DSS, MW: 40.000; Sigma, Milan, Italy). Preliminary experiments were performed to choose the optimal DSS concentration in the 0.05–5 % range, as well as the suitable time of treatment.

Cell Permeability Assessments

Cell membrane permeability was assayed by measuring the transepithelial electrical resistance (TEER), according to Ferruzza et al. (41). TEER was monitored every day until differentiation using a Millicell Electrical Resistance system (Merck Millipore, Darmstadt, Germany), and expressed as Ohm (resistance) × cm^2 (surface area of the filter), after subtracting the resistance value of the filter without cell monolayer. The TEER was checked before each experimental assay, and only cell monolayers with TEER values higher than 1,000 Ohm × cm^2 were used, as this TEER value was identified in preliminary experiments as indicative of correct differentiation in Caco-2/TC7 cells. During the experiments, TEERs were recorded every 30–60 min. Cell permeability was also measured at the end of treatments by measuring phenol red passage, as reported by Ferruzza et al. (41). Briefly, after three washes with phosphate buffered saline (PBS) containing Ca^{++} and Mg^{++} (PBS^{++}), 0.5 ml 1 mm phenol red was added to the AP compartment of cell monolayers, whereas 1 ml PBS^{++} was added in the BL compartment. After 1 h incubation at 37°C, 0.9 ml, the BL medium was collected, added with 0.1 ml 0.1 N NaOH, and read at 560 nm to determine the phenol red concentration (Tecan Infinite M200 microplate reader, Tecan Italia, Milan, Italy). This concentration was used to calculate the phenol red apparent permeability coefficient (Papp) by applying the following formula: $Papp = Ct \times V_{BL}/\Delta t \times C_0 \times A$, where V_{BL} is the volume of the BL compartment (cm^3), A is the filter area (cm^2), Δt is the time interval (s), Ct is the phenol red concentration in the BL compartment at the end of time interval, and C_0 is the phenol red concentration in the AP compartment at the beginning. The tight junctions were considered open and indicative of an absence of cell monolayer integrity when the phenol red Papp values were above 1×10^{-6} cm/s, as evaluated by previous reports in the literature (42). Differences observed among samples with such values of phenol red Papp were thus considered biologically irrelevant, irrespective of statistical significance.

GOS Preparation

Bimuno® in powder form with a content of 80% active GOS, 14% lactose, 5% glucose, and ∼1% galactose on dry matter, was supplied by Clasado Biosciences Ltd. (Reading, UK). The composition of the active GOS in terms of the degree of polymerization (DP), which refers to the number of monomeric units, was as follows: DP2 25%, DP3 41%, DP4 20%, DP5 9%, and DP>5 5%. Final concentrations of active GOS were made from 1 to 1,000 μg/ml by dissolving it as a powder in a serum free-cell culture medium.

Cell Toxicity of GOS

Several GOS concentrations were tested on Caco-2/TC7 cells differentiated on Transwell filters to assay the potential toxicity, by measuring TEER every 60 min for 24 h and phenol red Papp at the end of treatment. The concentrations tested ranged from 1 to 1,000 μg/ml (calculated from the percentage of active GOS). The cell monolayers were kept in the serum-free medium overnight before the experiments, to avoid possible interferences with serum proteins.

Inflammation Induction by DSS

Dextran-sulfate-sodium salt was used to induce inflammation in differentiated Caco-2/TC7 cells. In order to identify the suitable concentration of DSS to activate inflammatory status without inducing serious damages to cell monolayers, different

concentrations of DSS, ranging from 0.05 to 5 % were tested for 5.5 h, and TEER, phenol red Papp, and induction of NF-kB activation were measured.

Cell Treatment With DSS and Bimuno GOS

There were three different experimental setups: differentiated Caco-2/TC7 cells were either: 1-untreated cells (Blank Control; C), 2- treated with 2% DSS alone (6 h, positive control; DSS), 3-treated with 2 % DSS for 2 h, then several concentrations of Bimuno GOS (1–1,000 μg/ml) were added for further 4 h, or 4-treated with different Bimuno GOS concentrations alone (4 h). The different time points, according to the different experiments performed, are shown in **Figure 1**.

Western Blot Assay of TLR4 Signaling Proteins

Differentiated Caco-2/TC7 cells were treated according to the three different experimental setups, with GOS concentrations 100 or 200 μg/ml. At the end of treatments, the cells were washed with cold PBS and lysed in a cold radioimmunoprotein assay buffer (RIPA: 20 mM Tris-HCl pH 7.5, 150 mM NaCl, 0.1% SDS, 1% Na deoxy-cholate, 1% Triton X-100) supplemented with 1 mm phenylmethylsulphonyl fluoride, and protease inhibitor (Complete Mini, Roche, Milan, Italy) and phosphatase inhibitor (PhosSTOP, Roche) cocktails, according to Finamore et al. (43). Cell lysates (50 μg total proteins) were dissolved in sample buffer (50 mM Tris-HCl pH 6.8, 2 % SDS, 10 % glycerol, 100 g/L bromophenol blue, 10 mm β-mercaptoethanol), heated for 5 min, fractionated by SDS-polyacrylamide gel (4–20% gradient) electrophoresis and transferred to nitrocellulose filters (Trans-Blot Turbo, Biorad, Milan, Italy). Membranes were incubated with the following primary antibodies: rabbit polyclonal anti-human TLR4, MyD88, IKKα, IKKβ, phospho(P)-IKKα/β, IkBα, P-IkBα, NF-kB p65, P-p65, IRAK-M, Tollip, from Cell Signaling Technology (Danvers, MA), mouse monoclonal α-tubulin. Proteins were detected with horseradish peroxidase-conjugated secondary antibodies (Cell Signaling Technology) and enhanced chemiluminescence reagent (ECL kit Lite Ablot Extend, Euroclone), followed by the analysis of chemiluminescence with the charge-coupled device camera detection system Las4000 Image Quant (GE Health Care Europe GmbH, Milan, Italy). Relative levels of TLR4, MyD88, Tollip, and IRAK-M were normalized to α-tubulin, whereas the phosphorylated proteins were normalized to their corresponding unphosphorylated forms.

Cytokine Secretion

Differentiated Caco-2/TC7 cells were treated according to the three different experimental setups, with GOS concentrations 1–200 μg/ml. Secretion of pro-inflammatory cytokines IL-1β, IL-6, IL-8. and TNF-α was measured by ELISA (Biolegend, San Diego, CA) in the cell supernatants collected from the AP compartments at the end of treatments, following the manufacturer's instruction. Supernatants were centrifuged at 650×g for 5 minin at 4°C to remove cell debris, aliquoted, and immediately frozen at −80°C. In the preliminary experiments, cytokines were measured also in the culture media collected from the (BL) compartment, but results showed undetectable levels (data not shown).

Localization of TJ (ZO-1 and Occludin) Proteins, AJ (E-Cadherin and β-Catenin) Proteins, and P-P65

Differentiated Caco-2/TC7 cells were treated according to the three different experimental setups, with GOS concentrations 100 or 200 μg/ml. The effect of GOS on membrane damage induced by DSS was assessed by evaluating tight and adherent junctions' principal proteins immunolocalization, as well as P-p65 immunolocalization. Briefly, at the end of the experiments, Caco-2/TC7 cells were washed with cold PBS++, fixed in ice-cold methanol for 3 mins, and then incubated with rabbit polyclonal anti-ZO-1 and mouse monoclonal anti-occludin, or mouse monoclonal anti-β-catenin and rabbit polyclonal anti-E-cadherin antibodies (Zymed Laboratories, San Francisco, CA), or rabbit polyclonal anti-P-p65 antibody (Cell Signaling Technology, Danvers, MA) for 1 h. For secondary detection, cells were incubated with fluorescein isothiocyanate (FITC) or tetramethylrhodamine isothiocyanate (TRITC) conjugated secondary antibodies (Jackson Immunoresearch, Milan, Italy), for 1 h. 4′,6-diamidino-2-phenylindole (DAPI) was used to label DNA in nuclei. Stained monolayers were mounted on glass slides using the Prolong Gold antifade reagent (Molecular Probes, Invitrogen, Milan, Italy) and analyzed using a confocal fluorescence microscope (LSM 700, Zeiss, Jena, Germany).

Statistical Analysis

All experiments were performed at least in triplicate. The statistical significance of the differences was evaluated by one-way ANOVA followed by a *post-hoc* Tukey HSD test, after verifying the normality and homogeneity of variance by Shapiro–Wilk's and Levene's tests, respectively. Statistical significance was set at $P < 0.005$. In the figures, mean values with different superscript letters significantly differ. $P < 0.01$ or 0.001 are indicated, where appropriate. In TEER figures, only final and initial time points were compared for statistical analysis. The statistical analyses were executed with the "Statistica" software package (version 5.; StatSoftInc., Tulsa, OK, USA).

RESULTS

The different experimental setups and different timepoints are shown in **Figure 1**.

Effect of GOS and DSS on Caco-2/TC7 Cell Permeability

Preliminary experiments were performed to evaluate the toxicity of GOS on Caco-2 cells. TEER and phenol red Papp were measured in differentiated Caco-2 cells after treatment with several GOS concentrations for up to 24 h. The results show that GOS treatment did not affect cell permeability, except for the highest GOS concentration, which induced a TEER drop after 3 h, which was maintained until the end of the experiment (**Figure 2A**). However, this TEER decrease was not associated

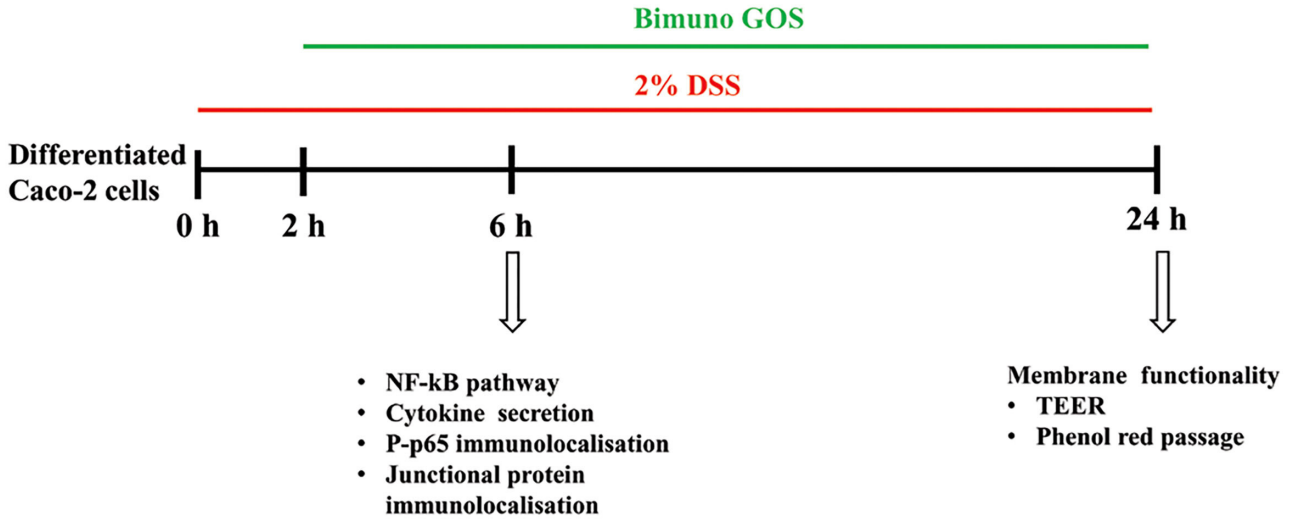

FIGURE 1 | Experimental design. Three different experimental setups were employed, as differentiated Caco-2 cells were: (1) treated with 2% dextran-sulfate-sodium salt (DSS) alone (6 or 24 h), (2) treated with 2% DSS for 2 h, then several Bimuno galactooligosaccharides (GOS) concentrations (1–1,000 μg/ml) were added for further 4 or 22 h, or (3) treated with different Bimuno GOS concentrations alone (4 or 20 h). The different analyses performed at each time point are indicated.

with a biologically relevant phenol red Papp increase, as the values were all below 1×10^{-6} cm/s, indicating that the tight junctions were not open. On the contrary 2% DSS treatment induced a strong increase on phenol red passage ($P < 0.001$, **Figure 2B**; **Supplementary Table S1**).

Dextran-sulfate-sodium salt was used to induce inflammation in differentiated Caco-2 cells. In order to determine the DSS concentration able to trigger inflammation without inducing serious damages to the cell monolayer, different DSS concentrations were tested for 5.5 h, by measuring TEER and phenol red passage (**Figures 3A,B**). Treatment with DSS concentrations ranging between 0.05 and 1% did not alter cell permeability, as shown by both TEER measurements and phenol red Papp (**Figures 3A,B**, respectively). On the contrary, 3 and 5% DSS induced a dramatic TEER drop starting from 2.5 h until 5.5 h (**Figure 3A**), which was accompanied by a phenol red Papp higher than 1×10^{-6} cm/s (**Figure 3B**). The 2% DSS induced a lower TEER drop as compared to 3 and 5% (**Figure 3A**), and a slight increase of phenol red passage, borderline with the threshold value of 1×10^{-6} cm/s (**Figure 3B**; **Supplementary Table S2**), thus this concentration was chosen for further experiments, as supposed to be able to induce inflammation, without seriously damaging cell monolayers.

GOS Exerted a Protective Effect Against DSS-Induced Membrane Barrier Damage

To induce inflammation differentiated Caco-2 cells were pre-treated with 2 % DSS for 2 h, then GOS was added for additional 4 h, to test its protective effect. TEER analysis showed that GOS concentrations ranging from 50 to 1,000 μg/ml were able to prevent the TEER decrease induced by DSS, whereas 1 and 10 μg/ml concentrations only partially protected the cells from the DSS-induced TEER drop (**Figure 4A**). Analysis of phenol red Papp showed that all GOS concentrations were able to protect the cells from DSS damage, except for the lowest one (1 μg/ml, **Figure 4B**; **Supplementary Table S3**). Based on these data, the 100 and 200 μg/ml GOS concentrations were chosen for further experiments, considering that these concentrations were not detrimental for cell monolayers and were able to protect cells against DSS-induced cell damages.

GOS Reduced the DSS-Induced Pro-Inflammatory Cytokine Secretion

Considering the role of pro-inflammatory cytokines in the mucosal damages occurring in patients with UC, the principal cytokines involved in the UC pathogenesis were investigated in Caco-2 cells. In particular, secretion of IL-1β, IL-6, IL-8, and TNF-α was analyzed in Caco-2 cell culture supernatants after treatment with DSS alone, GOS alone, or first with DSS for 2 h and then GOS for the following 4 h. GOS alone did not induce apical secretion of IL-1β, IL-6, IL-8, and TNF-α by Caco-2 cells, while DSS induced a significant increase ($P < 0.01$) of all the pro-inflammatory cytokines, as compared to control untreated cells (**Figure 5**; **Supplementary Tables S4a–d**).

GOS at concentrations from 1 to 50 μg/ml administered 2 h after DSS did not change IL-1β secretion in comparison to DSS-treated cells, whereas 100 and 200 μg/ml GOS significantly reduced IL-1β secretion induced by DSS ($P < 0.05$) compared to DSS alone. However, this reduction in IL-1β secretion was still significantly higher compared to the control ($P < 0.05$, **Supplementary Table S4a**).

Similar results were obtained for IL-6, which was induced by DSS as compared to the control ($P < 0.01$), and was significantly reduced in cells first treated with DSS and then either with 100 or 200 μg/ml GOS ($P < 0.01$, **Supplementary Table S4b**).

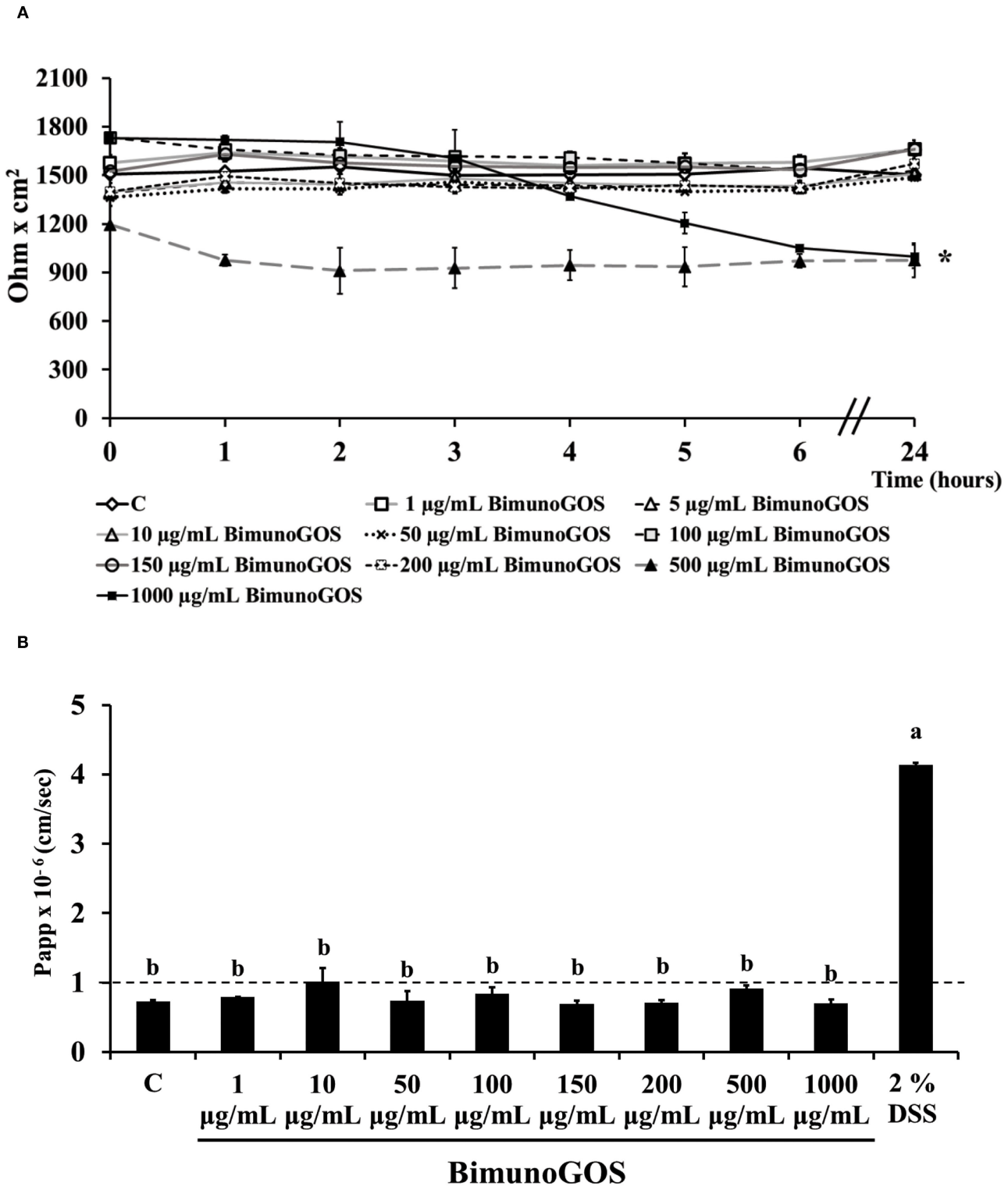

FIGURE 2 | Bimuno GOS effects on membrane barrier of Caco-2 cells. Transepithelial electrical resistance (TEER) **(A)** and phenol red apparent permeability (Papp) **(B)**. Cells were untreated (Control, C), treated with different Bimuno GOS concentrations (1–1,000 µg/ml), or treated with 2% DSS. TEER values are reported as Ohm × cm^2. Phenol red Papp was measured after 24 h treatment with Bimuno GOS or after 6 h treatment with DSS, and values are reported as cm/s. Values represent mean ± SD of at least three independent experiments, carried out in triplicate. **(A)** *Stands for significant difference between T0 and T24 ($P < 0.001$). **(B)** Means without a common letter significantly differ, $P < 0.001$.

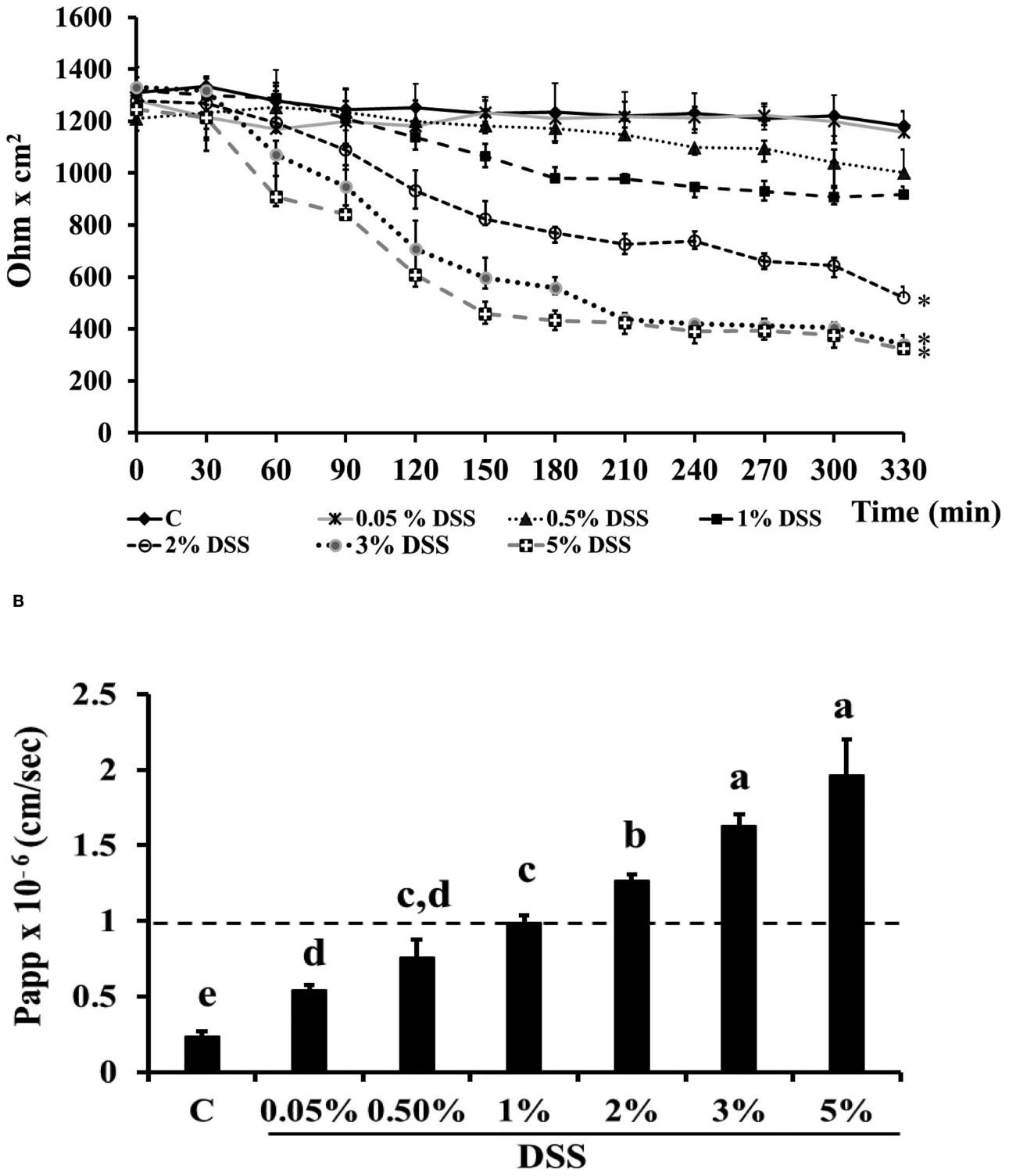

FIGURE 3 | DSS effects on membrane barrier of Caco-2 cells. Transepithelial electrical resistance (TEER) **(A)** and phenol red apparent permeability (Papp) **(B)**. Cells were either untreated (Control, C) or treated with different DSS concentrations (0.05–5%) for 330 min. TEER values are reported as Ohm × cm^2. Phenol red Papp was measured at end of TEER measurements, and values are reported as cm/sec. Values represent mean ± SD of at least three independent experiments, carried out in triplicate. **(A)** *Stands for significant difference between T0 and T330 ($P < 0.001$). **(B)** Means without a common letter significantly differ, $P < 0.05$.

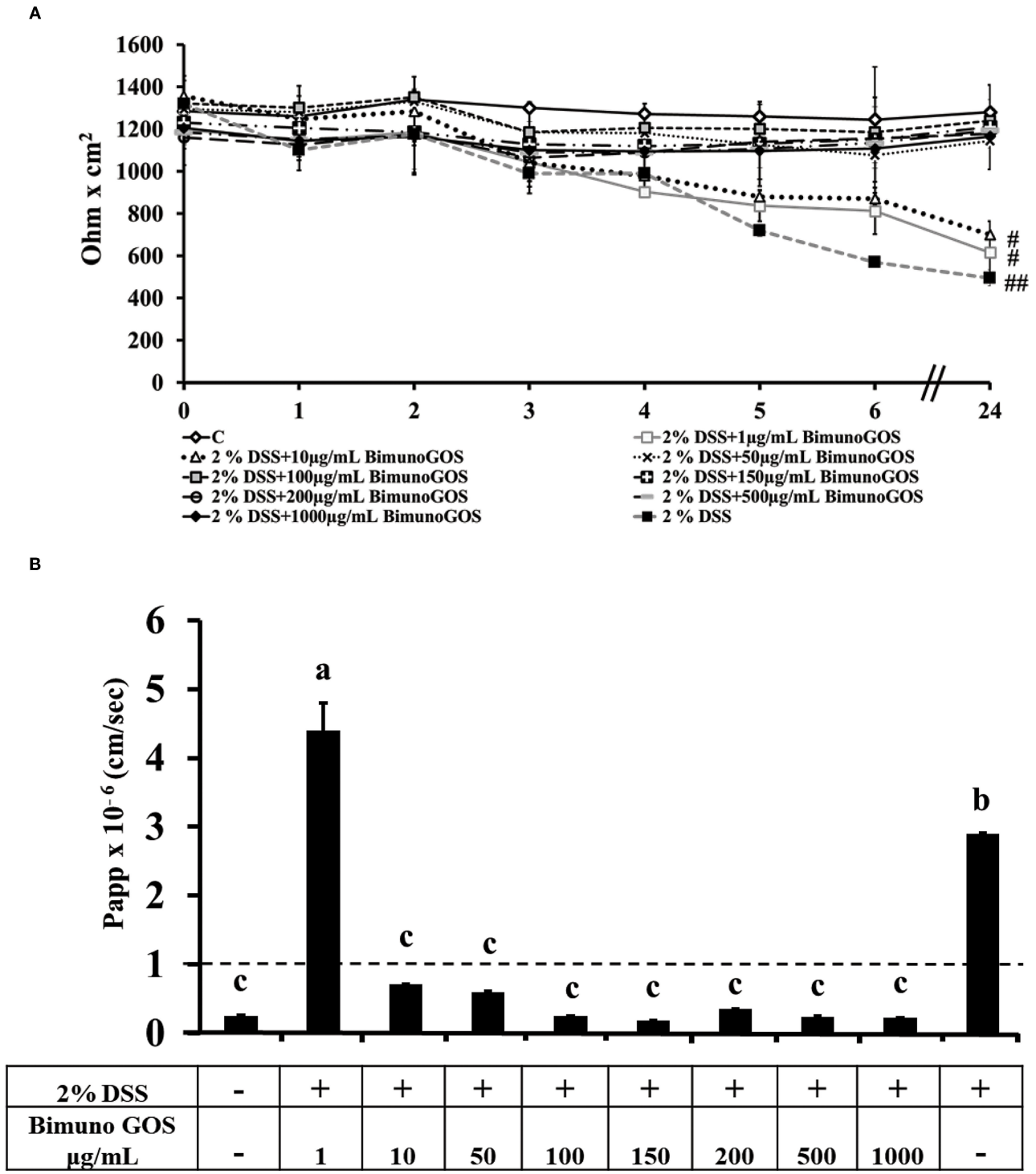

FIGURE 4 | Protective effect of Bimuno GOS against membrane barrier damages induced by DSS in Caco-2 cells. Transepithelial electrical resistance (TEER) **(A)** and phenol red apparent permeability (Papp) **(B)**. Cells were either untreated (C) or treated with 2% DSS for 2 h and then with several Bimuno GOS concentrations (1–1,000 µg/ml) up to 24 h. TEER values are reported as Ohm × cm^2. Phenol red Papp values are reported as cm/s. Values represent mean ± SD of at least three independent experiments, carried out in triplicate. **(A)** #,##Stand for significant difference between T0 and T24 ($P < 0.01$ and $P < 0.001$, respectively). Values represent mean ± SD of at least three independent experiments, carried out in triplicate. **(B)** Means without a common letter significantly differ, $P < 0.05$.

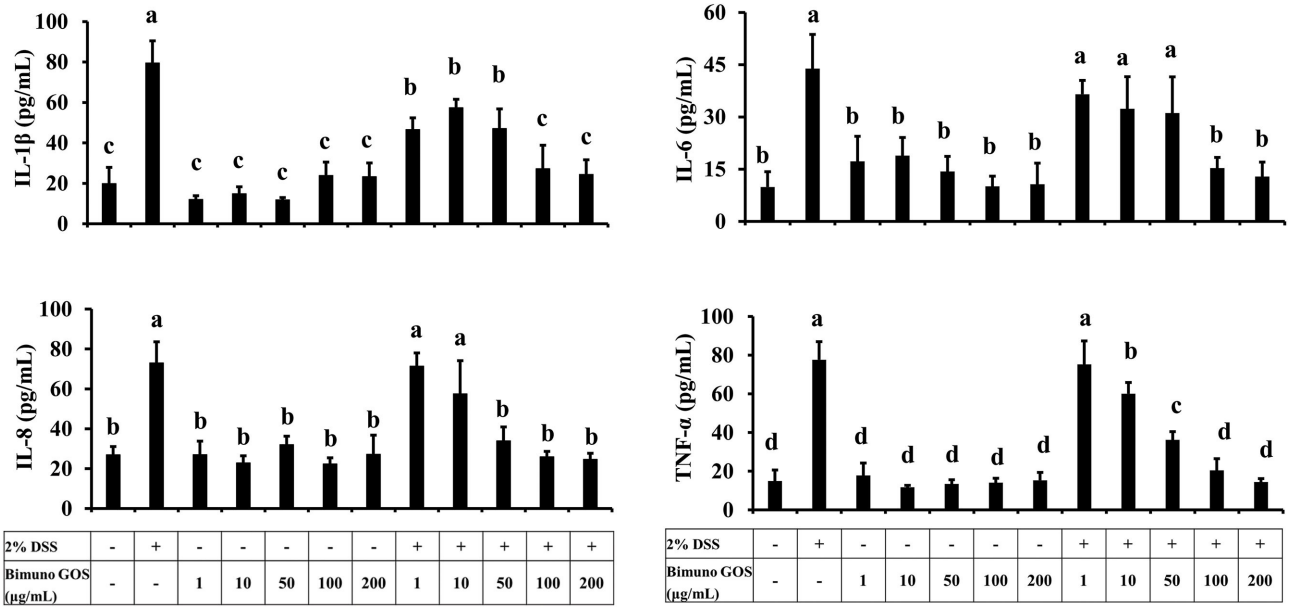

FIGURE 5 | Pro-inflammatory cytokine secretion in presence of different concentrations of Bimuno GOS and/or DSS in Caco-2 cells. Cells were untreated, or treated with 2% DSS alone for 6 h, or treated with 100 or 200 μg/ml Bimuno GOS alone for 4 h, or treated with 2% DSS for 2 h and then with 100 or 200 μg/ml Bimuno GOS for further 4 h. Values represent means ± SD of three independent experiments, carried out in triplicate. Means without a common letter significantly differ, $P < 0.05$.

DSS salt significantly increased IL-8 secretion, as compared to the control ($P < 0.01$). GOS concentrations ranging from 50 to 200 μg/ml were effective in reducing the IL-8 secretion in DSS-treated Caco-2 cells ($P < 0.01$), whereas GOS concentrations from 1 to 10 μg/ml were not able to counteract the DSS-induced IL-8 secretion (**Supplementary Table S4c**).

DSS salt also induced TNF-α secretion as compared to the control ($P < 0.01$), this increase was partially reduced by 50 μg/ml GOS ($P < 0.05$), and totally inhibited by treatment with 100 or 200 μg/ml GOS ($P < 0.01$, **Supplementary Table S4d**).

Overall, 100 and 200 μg/ml GOS concentrations were the most effective in reducing the pro-inflammatory cytokine secretion induced by DSS. In particular, we observed that treatment with 100 or 200 μg/ml GOS was able to reduce to control level IL-6, IL-8, and TNF-α (**Figure 5**).

GOS Inhibited NF-kB Pathway Signaling Induced by DSS

In order to clarify the mechanism of action of this specific GOS on the inflammatory cascade, the expression level of the key proteins involved in the activation of the NF-kB pathway was analyzed by Western blot. DSS induced a significant increase of expression of TLR4, MyD88, P-IKKα, P-IKKβ ($P < 0.05$), P-IkBα, and P-p65 ($P < 0.01$), as compared to the control (**Figure 6A**; **Supplementary Tables S5a–f**). In addition, the expression of Tollip and IRAK-M, negative regulators of NF-kB cascade, was significantly reduced ($P < 0.01$) as compared to the control (**Figure 6B**; **Supplementary Tables S5g,h**). No significant differences for all the analyzed proteins could be observed in cells treated with 100 or 200 μg/ml GOS alone, as compared to the control.

On the other hand, Caco-2 cells treated first with DSS and then with GOS had similar expression levels of all the activator proteins involved in the NF-kB inflammatory pathway (**Figure 6A**) and of Tollip and IRAK-M negative regulators (**Figures 6B,C**), as compared to control cells.

Data on P-p65 protein expression levels were confirmed by immunolocalization analysis. Immunolabeling of P-p65 showed that treatment with DSS induced a strong migration into the nucleus of P-p65, as indicated by the high fluorescence signal intensity, whereas in control cells or in cells treated with 100 or 200 μg/ml GOS alone the positive signal into the nucleus was slight or absent. In agreement with the results of Western blot analysis, treatment with 100 or 200 μg/ml GOS was able to inhibit the P-p65 migration induced by DSS treatment (**Figure 7**).

All these results indicate that GOS was able to counteract the DSS-induced inflammatory NF-kB cascade activation.

Maintenance of Tight and Adherent Junction Protein Localization by GOS

In order to evaluate the ability of the GOS to counteract the membrane barrier damage induced by DSS in Caco-2 cells, immunolocalization of the principal tight and adherent junction proteins was performed. As reported in **Figure 8A**, DSS induced several damages in both ZO-1 and occludin protein distribution, as ZO-1 resulted in discontinuous cell boundaries, whereas occludin disappeared from cell boundaries and partly localized in the cell cytoplasm. Several damages induced by DSS were also present in the adherens junctions. Indeed, DSS induced the

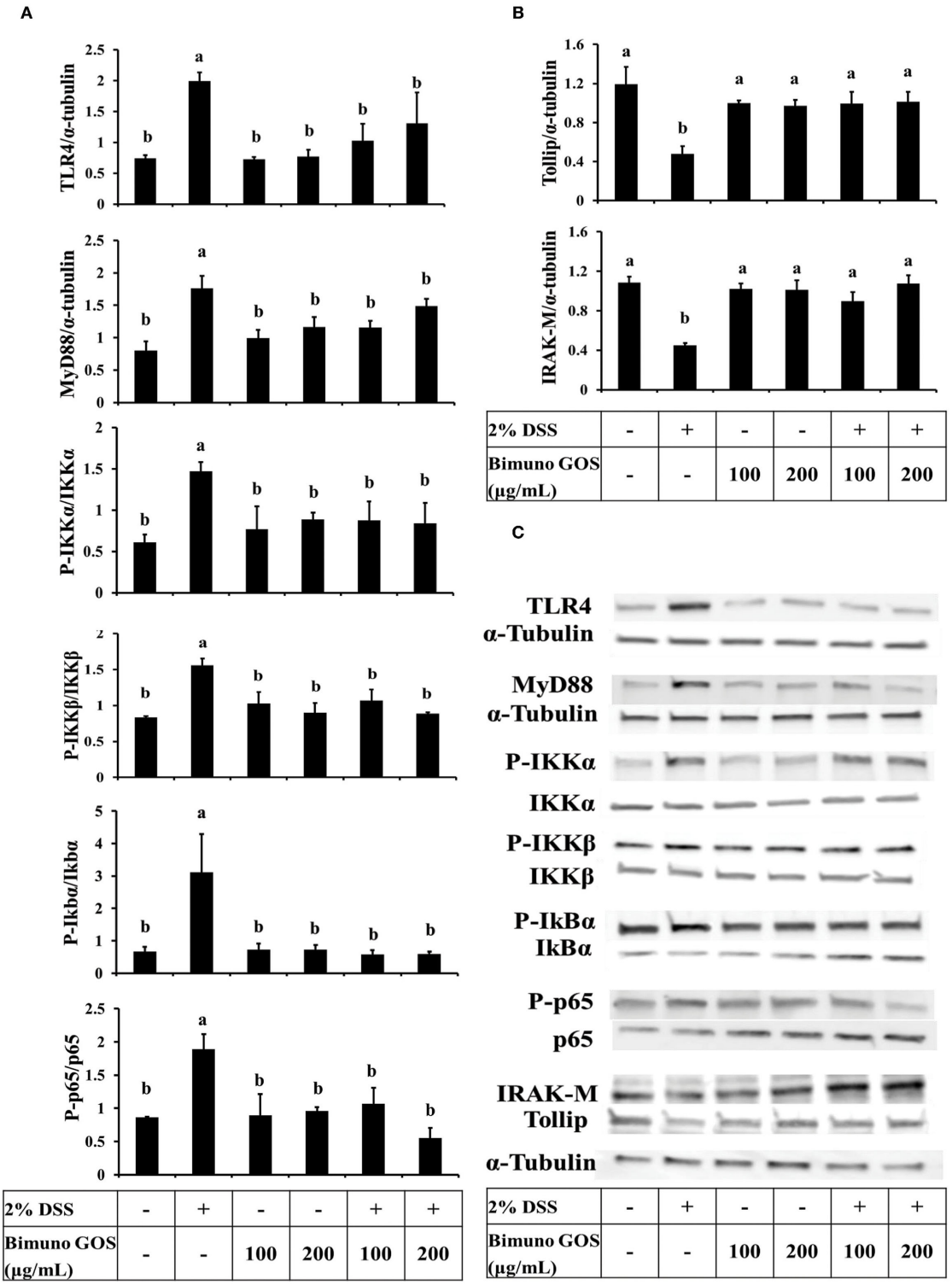

FIGURE 6 | Inhibition of DSS induced-NF-kB signaling pathway by Bimuno GOS in Caco-2 cells. Cells were untreated, or treated with 2% DSS alone for 6 h, or treated with 2% DSS for 2 h and then with Bimuno GOS (100 or 200 μg/ml) for a further 4 h, or treated with 100 or 200 μg/ml Bimuno GOS alone for 4 h. Protein expression was analyzed by Western blot. The relative expression levels of TLR4, MyD88, Tollip, and IRAK-M were normalized to α-tubulin, whereas the phosphorylated IKK-α, IKK-β, IkB-α, and p65 were normalized to their corresponding unphosphorylated forms. **(A)** TLR4, MyD88, P-IKK-α, P-IKK-β, P-IkB-α, P-p65 (densitometric values). **(B)** Tollip and IRAK-M (densitometric values). **(C)** Representative Western blot of the analyzed proteins. Values represent means ± SD of three independent experiments, carried out in triplicate. Means without a common letter significantly differ, $P < 0.05$.

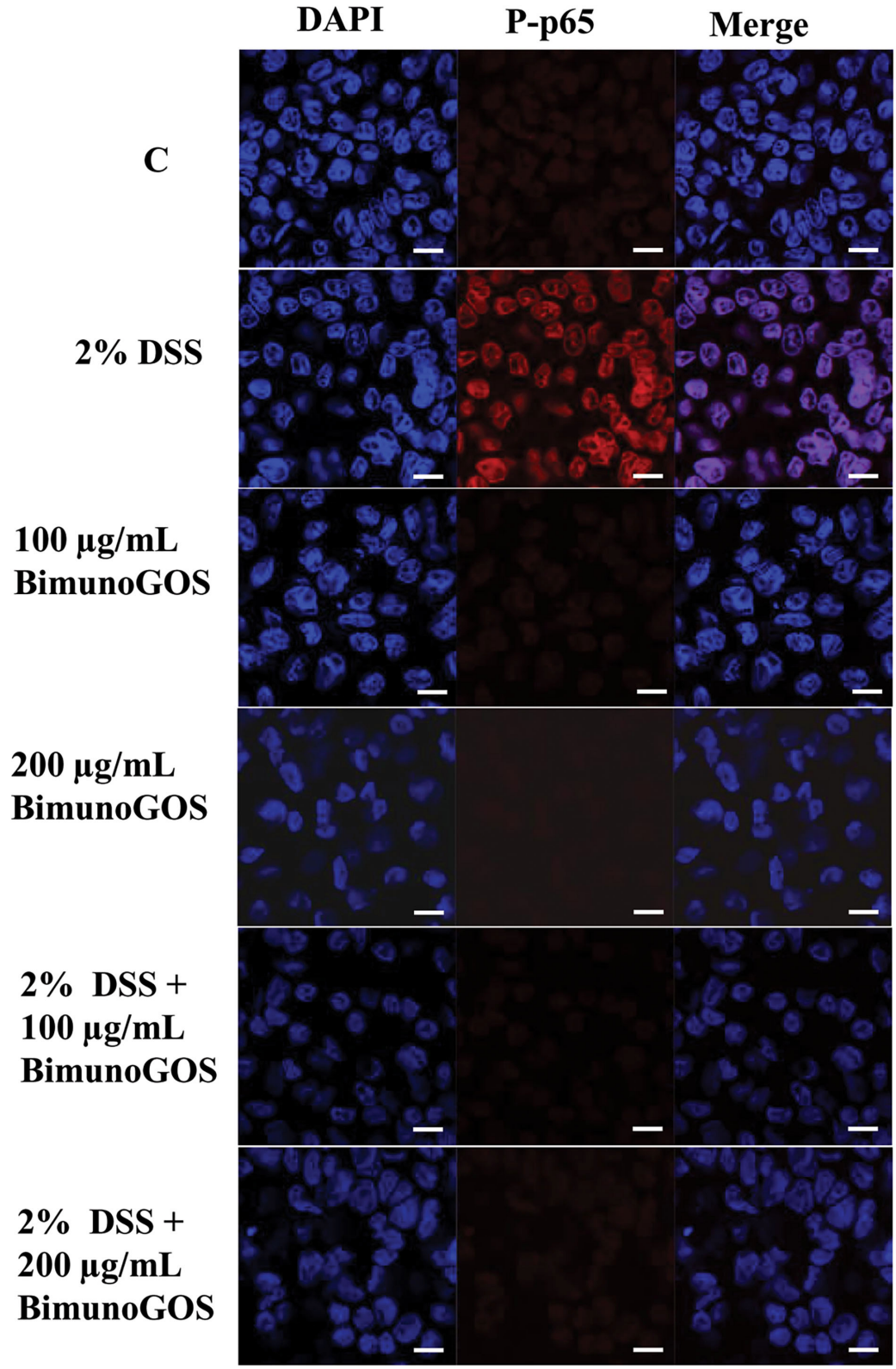

FIGURE 7 | Inhibition of DSS induced-P-p65 translocation by Bimuno GOS in Caco-2 cells. Cells were untreated (C), or treated with 2% DSS for 6 h, or treated with Bimuno GOS (100 or 200 µg/ml) for 4 h, or treated with 2% DSS for 2 h and then with Bimuno GOS (100 or 200 µg/ml) for further 4 h. Cell nuclei were stained with DAPI, while P-p65 was labeled with rabbit polyclonal anti-P-p65 antibody, followed by TRITC-conjugated secondary antibody. Each figure is representative of three independent assays (63× magnification). Bars represent 10 µm.

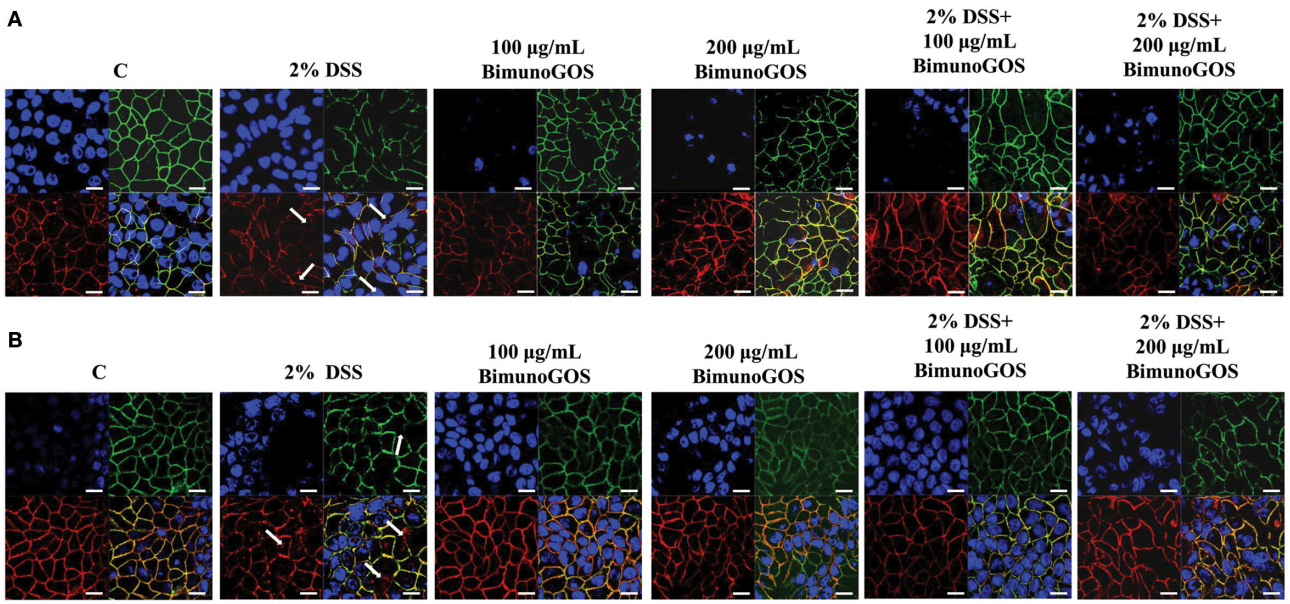

FIGURE 8 | Localization of tight and adherent junction proteins in Caco-2 cells. Cells were either untreated (C), or treated with 2% DSS for 6 h, or treated with Bimuno GOS (100 or 200 µg/ml) for 4 h, or treated with 2% DSS for 2 h and then with Bimuno GOS (100 or 200 µg/ml) for further 4 h. Cells were labeled with specific primary antibodies for tight **(A)** and adherent **(B)** junction proteins, followed by TRITC- and FITC-conjugated secondary antibodies for occludin and ZO-1, and for β-catenin and E-cadherin, respectively. Cell nuclei were stained with DAPI. Dissociation of occludin from the membrane is indicated by arrows. Each figure is representative of three independent immunofluorescence assays (63× magnification). Bars represent 10 µm.

disappearance of both E-cadherin and β-catenin from the cell boundaries associated with a loss of co-localization of the two proteins. A total of 100 and 200 µg/ml GOS were able to rescue the damages induced by DSS in both tight and adherent junction protein distribution, as shown in **Figure 8B**.

DISCUSSION

In this study, the potential benefits of a specific GOS (Bimuno GOS) for UC were tested in an established cell culture model of gut inflammation, i.e., the Caco-2 intestinal cell line, where DSS was used to induce gut inflammation and cell damage.

This study demonstrates that the specific GOS tested can counteract UC-like inflammatory characteristics, gut permeability markers, and tissue damages induced by DSS in the *in vitro* model. Several *in vivo* and *in vitro* studies have shown that in UC cellular junctions damages are associated with increased permeability of intestinal mucosa (44, 45). In line with these studies, we observed that DSS treatment induced cell junction opening, increased monolayer permeability, and the disappearance of tight and adherent junction proteins. Importantly, we observed that GOS on its own did not affect membrane permeability, as indicated by TEER and Papp measurements, which is essential for being a safe and potentially effective way of improving the gut inflammatory state in IBD. All damages induced by DSS to the epithelial barrier were reversed after treatment with GOS, including the DSS-induced cell damage and permeability determined by the localization of the tight junction proteins ZO-1 and occludin, and the adherent junction proteins E-cadherin and β-catenin. This demonstrates that the specific GOS could be beneficial in preventing gut barrier disruption in challenging conditions such as gut inflammation.

In active UC, expression of pro-inflammatory cytokines such as IL-1β, IL-6, IL-8, and TNF-α is usually increased, and pro-inflammatory cytokines have been clearly demonstrated to play a key role in epithelial junction remodeling and disruption (46, 47). In the present study, we demonstrated that GOS on its own did not induce the secretion of pro-inflammatory cytokines IL-1β, IL-6, IL-8, and TNF-α, whereas DSS alone as the pro-inflammatory stimulant triggered secretion of all these cytokines through the activation of the NF-kB pathway, as indicated by translocation of the phosphorylated form of p65 into the nucleus. The secretion of IL-1β, IL-6, IL-8, and TNF-α was significantly decreased when GOS was added to DSS-treated cells, compared to the DSS treatment alone. Our results are in agreement with those obtained by Hwang and colleagues, who observed that inflammatory status induced in Caco-2 cells by LPS challenge was reduced by treatment with low-molecular-weight polysaccharides showing prebiotic activity (48). It was also shown that low-molecular-weight fucoidan and high-stability fucoxanthin were able to inhibit IL-1β and TNF-α secretion to promote IL-10 and IFN-γ secretion in cells treated with LPS, indicating that these compounds could exert anti-inflammatory activity on intestinal cells. In this study, the most effective GOS concentrations in dampening pro-inflammatory cytokine secretion were 100 and 200 µg/ml. A more detailed analysis demonstrated that proteins of the NF-kB signaling pathway were involved in the pro-inflammatory cascade induced by DSS.

Indeed, 2% DSS induced the NF-kB inflammatory pathway, as shown by the increase of TLR4, MyD88, P-IKKα, P-IKKβ, P-IkBα, and P-p65 and the reduction of negative regulators Tollip and IRAK-M protein expression levels. Bimuno GOS inhibited the DSS-induced expression levels of TLR4, MyD88, P-IKKα, P-IKKβ, P-IkBα, and P-p65, which were restored to control levels.

Our results are in agreement with those shown in a previous study conducted by Wu et al., where Caco-2 cells were treated with several pro-inflammatory agents, however, other prebiotics, such as inulin or FOS, were used (38). Interestingly, we also observed that GOS was able to restore the expression levels of NF-kB negative regulators, Tollip and IRAK-M. Although the role of Tollip and IRAK-M in IBD is not yet clarified, in a study conducted on biopsies from CD and UC patients, Fernandes et al. reported a reduced Tollip expression, similar to our findings (49). However, in contrast to our data reported here, these authors observed an increase in IRAK-M, and concluded that the up-regulation of IRAK-M was a mechanism to counteract the high level of inflammation. Nevertheless, the role of IRAK-M has been highlighted in the IRAK-M $^{-/-}$ mice model orally treated with DSS (50). In line with our findings, the authors showed that IRAK-M plays a key role in downregulating the induction and progression of DSS colitis through the modulation of proinflammatory cytokines such as TNF-α and IL-6. The role of IRAK-M has been extensively investigated in several studies reporting its role in LPS and DSS inflammatory state induction. Both LPS and DSS act through TLR4 signaling and modulate NF-kB and MAPK cascade in *in vitro* and *in vivo* studies. IRAK-M deficiency was shown to be responsible for the intestinal inflammation onset, suggesting a possible impairment in the negative regulation of TLR signaling causing IBD (51, 52). In our model, the ability of GOS to modulate the expression of both negative regulators Tollip and IRAK-M is important, since they were able to block the pro-inflammatory NF-kB pathway by inhibiting the transcription of inflammatory mediators.

The role of pro-inflammatory cytokines such as IL-1β, IL-6, IL-8, and TNF-α in UC pathogenesis has been well described in the literature. These cytokines are involved in pro-inflammatory responses through immune cells recruitment, followed by amplification and propagation of inflammation (53). In our model, Caco-2 cells exposed to DSS showed increased secretion of all the analyzed pro-inflammatory cytokines, as compared to the control. GOS was able to abolish the increase of pro-inflammatory cytokines induced by DSS and this indicates that GOS is able to reduce inflammation. The involvement of cytokines in the epithelial damages of UC is well known, however, only a few studies have analyzed the effect of prebiotic molecules on inflammatory process repair, as well as their ability to modulate cellular response without involving microbiota (38, 48, 54). In all these studies, the authors showed that prebiotics was able to induce an immunomodulatory effect by modulating the NF-kB pathway and cytokine secretion. Pistol and colleagues reported that in LPS-pretreated Caco-2 cells a synbiotic (grape extract plus lactobacilli mixture) treatment for 24 h induced a decrease of inflammatory cytokine secretion associated with the prevention of MAPK and NF-kB markers induction. In addition, Wu and colleagues (38) showed in an *in vitro* model of Caco-2 cells treated with FOS, prebiotics could directly influence the signal transduction mediated by protein kinases.

Prebiotics have been also tested in the context of irritable bowel syndrome (IBS). In an *in vitro* model of IBS, obtained by infection of Caco-2 cells with *Salmonella typhimurium* and post-infection treatment with a prebiotic blend (FOS plus GOS), prebiotics were shown to inhibit the pro-inflammatory cytokine secretion by suppressing inflammation, and this activity was not mediated by microbiota (55). Similarly, in our study, we show that GOS was able to reduce the inflammatory status in an *in vitro* UC-like model by acting in a microbiota-independent way. From all our data we can speculate that in DSS treated cells, GOS was able to counteract the inflammatory status and the membrane barrier damage induced by inflammatory cytokines that reverted to control level. The ability of GOS to regulate immune response was previously suggested, as it has been shown to be effective in modulating cytokine secretion in intestinal cells through TLR4 binding (56), as well as through a direct effect on intestinal cell transcriptome by modulating the expression of several genes, including some involved in antimicrobial activity and inflammatory response (36). According to previous studies, our results strongly suggest that a specific prebiotic can have a direct effect on the regulation of inflammation.

Overall, the present study identifies mechanisms of how GOS can support gut cells by improving their function, including gut barrier function, and decreasing inflammation in the context of UC, through modulation of the NF-kB pathway and pro-inflammatory cytokine secretion. The current study, although with the limitations of being a preclinical experimental setup, shows the potential of the specific GOS for the management of a challenging condition such as IBD, where gut barrier integrity and function are compromised by chronic inflammation.

We used differentiated Caco-2 epithelial cells as a suitable, reliable, and widely used model of intestinal barrier, that mimics the *in vivo* intestinal mucosa and allows the understanding of some mechanisms of action. We demonstrated that Bimuno GOS has direct effects in such model, by reducing pro-inflammatory cytokines and damage caused by DSS. It is noteworthy that in addition to direct effects, the Bimuno GOS used in this study has been demonstrated to have potent indirect effects involving growth stimulation of beneficial gut bacteria such as bifidobacteria (26, 33) on gut microbiota modulation, which in turn have been associated with immune system modulation (57). The gut-immune interplay is pivotal in the induction and maintenance of a non-inflammatory status and a local tolerogenic environment (58, 59). A recent study in a cohort of patients with UC demonstrated that the administration of Bimuno GOS for 6 weeks results in overall normalization of stools and reduced incidence and severity of loose stools, in addition to decreased urgency (26). A subset of patients in the remission stage had increased bifidobacterial counts. Although Wilson et al. study (26) did not investigate immune markers in patients with UC, it demonstrated a clinical improvement. The results from the current study, using the DSS model suggest a potential mechanism of action for the observed clinical outcomes in Wilson et al. (26). It remains to be explored how the

immune markers are affected in the cohort of UC patients taking a prebiotic.

Finally, it is common knowledge that GOS is a mixture of multiple oligosaccharide structures. The specific GOS in this study had a relatively high abundance of the lower DP fractions, which is inherent to the manufacturing of GOS by enzymatic processes. Interestingly, a previous study conducted by Newburg and colleagues (60) has shown that trisaccharide (DP3) structures in particular and at a relatively high quantity in this GOS have strong immunological, i.e., anti-inflammatory responses in different human intestinal cell lines. This warrants further research into the specific structure—bioactivity relationships of individual GOS structures to further understand their contribution to biological, and thus immune activities. More detailed GOS structure analyses and comparisons between different GOS's, including Bimuno GOS used in the present study, have previously been published by Hernandez-Hernandez et al. (61) and Van Leeuwen et al. (62). Further to that, it should also be emphasized that generic extrapolation of effects between different GOS's cannot be made. Structure analyses have shown clear differences between individual GOS types (61, 62), and therefore each GOS product or GOS-derived fraction should be tested separately for their biological properties and activities in future research.

CONCLUSIONS

In conclusion, using DSS-treated Caco-2 cells as an *in vitro* UC model, we suggest that the specific GOS tested in this study can be a safe and effective way not only to modulate gut inflammation but also to potentially prevent or restore gut barrier disruption and further improve efficacy in inducing remission, although *in vivo* validation is necessary. Currently, various pharmaceutical options are available for the treatment of IBD, however, all with their own limitations related to efficacy, side effects, and costs (10, 63). A prebiotic supplement such as the specific GOS tested in this study could be an attractive therapeutic agent or an add-on to other treatment options including enteral nutrition for managing IBD.

DATA AVAILABILITY STATEMENT

The raw data supporting the conclusions of this article will be made available by the authors, without undue reservation.

AUTHOR CONTRIBUTIONS

AF and RG: conceptualization, methodology, and validation. AF and MR: investigation, formal analysis, visualization, writing—original draft, supervision, project administration, and funding acquisition. AM and LH: writing—review and editing. All authors have read and approved the final version of the manuscript and participated to the decision to submit the manuscript for publication.

FUNDING

The authors declare that this study received part of the funding from Clasado Biosciences Ltd.

ACKNOWLEDGMENTS

The authors would like to thank Dr. G. Tzortzis for his contribution to the study initiation.

SUPPLEMENTARY MATERIAL

The Supplementary Material for this article can be found online at: https://www.frontiersin.org/articles/10.3389/fnut.2022.862974/full#supplementary-material

REFERENCES

1. GBD 2017. Inflammatory Bowel Disease Collaborators. The global, regional, and national burden of inflammatory bowel disease in 195 countries and territories, 1990-2017: a systematic analysis for the Global Burden of Disease Study 2017. *Lancet Gastroenterol Hepatol.* (2020) 5:17–30. doi: 10.1016/S2468-1253(19)30333-4
2. Gasparini RG, Sassaki LY, Saad-Hossne R. Inflammatory bowel disease epidemiology in São Paulo State, Brazil. *Clin Exp Gastroenterol.* (2018) 11:423–9. doi: 10.2147/CEG.S176583
3. Roselli M, Finamore A. Use of synbiotics for ulcerative colitis treatment. *Curr Clin Pharmacol.* (2020) 15:174–82. doi: 10.2174/1574884715666191226120322
4. Kobayashi T, Siegmund B, Le Berre C, Wei SC, Ferrante M, Shen B et al. Ulcerative colitis. *Nat Rev Dis Primers.* (2020) 6:74. doi: 10.1038/s41572-020-0205-x
5. Finamore A, Peluso I, Cauli O. Salivary stress/immunological markers in crohn's disease and ulcerative colitis. *Int J Mol Sci.* (2020) 21:8562. doi: 10.3390/ijms21228562
6. Schulzke JD, Ploeger S, Amasheh M, Fromm A, Zeissig S, Troeger H et al. Epithelial tight junctions in intestinal inflammation. *Ann N Y Acad Sci.* (2009) 1165:294–300. doi: 10.1111/j.1749-6632.2009.04062.x
7. Szebeni B, Veres G, Dezsõfi A, Rusai K, Vannay A, Mraz M et al. Increased expression of Toll-like receptor (TLR) 2 and TLR4 in the colonic mucosa of children with inflammatory bowel disease. *Clin Exp Immunol.* (2008) 151:34–41. doi: 10.1111/j.1365-2249.2007.03531.x
8. Steinbach EC, Plevy SE. The role of macrophages and dendritic cells in the initiation of inflammation in IBD. *Inflamm Bowel Dis.* (2014) 20:166–75. doi: 10.1097/MIB.0b013e3182a69dca
9. Candia E, Díaz-Jiménez D, Langjahr P, Núñez LE. de la Fuente M, Farfán N, et al. Increased production of soluble TLR2 by lamina propria mononuclear cells from ulcerative colitis patients. *Immunobiology.* (2012) 217:634–42. doi: 10.1016/j.imbio.2011.10.023
10. Mowat C, Cole A, Windsor A, Ahmad T, Arnott I, Driscoll R et al. IBD Section of the british society of gastroenterology. Guidelines for the management of inflammatory bowel dis-ease in adults. *Gut.* (2011) 60:571–607. doi: 10.1136/gut.2010.224154
11. Guo XY, Liu XJ, Hao JY. Gut microbiota in ulcerative colitis: insights on pathogenesis and treatment. *J Dig Dis.* (2020) 21:147–59. doi: 10.1111/1751-2980.12849
12. Pei LY, Ke YS, Zhao HH, Wang L, Jia C, Liu WZ et al. Role of colonic microbiota in the pathogenesis of ulcerative colitis. *BMC Gastroenterol.* (2019) 19:10. doi: 10.1186/s12876-019-0930-3

13. Alam MT, Amos GCA, Murphy ARJ, Murch S, Wellington EMH, Arasaradnam RP. Microbial imbalance in inflammatory bowel disease patients at different taxonomic levels. *Gut Pathog.* (2020) 12:1. doi: 10.1186/s13099-019-0341-6
14. Manichanh C, Borruel N, Casellas F, Guarner F. The gut microbiota in IBD. *Nat Rev Gastroenterol Hepatol.* (2012) 9:599–608. doi: 10.1038/nrgastro.2012.152
15. Li YH, Adam R, Colombel JF, Bian ZX, A. characterization of pro-inflammatory cytokines in dextran sulfate sodium-induced chronic relapsing colitis mice model. *Int Immunopharmacol.* (2018) 60:194–201. doi: 10.1016/j.intimp.2018.05.001
16. Toutounji M, Wanes D, El-Harakeh M, El-Sabban M, Rizk S, Naim HY. Dextran sodium sulfate-induced impairment of protein trafficking and alterations in membrane composition in intestinal Caco-2 cell line. *Int J Mol Sci.* (2020) 21:2726. doi: 10.3390/ijms21082726
17. Li Q, Liang X, Guo N, Hu L, Prasad EM, Wu Y et al. Protective effects of Bee pollen extract on the Caco-2 intestinal barrier dysfunctions induced by dextran sulfate sodium. *Biomed Pharmacother.* (2019) 117:109200. doi: 10.1016/j.biopha.2019.109200
18. Araki Y, Sugihara H, Hattori T. In vitro effects of dextran sulfate sodium on a Caco-2 cell line and plausible mechanisms for dextran sulfate sodium-induced colitis. *Oncol Rep.* (2006) 16:1357–62. doi: 10.3892/or.16.6.1357
19. Kang EA, Choi HI, Hong SW, Kang S, Jegal HY, Choi EW et al. Extracellular vesicles derived from kefir grain lactobacillus ameliorate intestinal inflammation via regulation of proinflammatory pathway and tight junction integrity. *Biomedicines.* (2020) 8:522. doi: 10.3390/biomedicines8110522
20. Gibson GR, Hutkins R, Sanders ME, Prescott SL, Reimer RA, Salminen SJ et al. Expert consensus document: the international scientific association for probiotics and prebiotics (ISAPP) consensus statement on the definition and scope of prebiotics. *Nat Rev Gastroenterol Hepatol.* (2017) 14:491–502. doi: 10.1038/nrgastro.2017.75
21. Gibson GR, Probert HM, Van Loo J, Rasrall RA, Roberfroid MB. Dietary modulation of the human colonic microbiota: introducing the concept of prebiotics. *Nutr Res Rev.* (2004) 17:259–75. doi: 10.1093/jn/125.6.1401
22. Roberfroid M. Dietary fiber, inulin, and oligofructose: a review comparing their physiological effects. *Crit Rev Food Sci Nutr.* (1993) 33:103–48. doi: 10.1080/10408399309527616
23. Novak M, Vetvicka V. Beta-glucans, history, and the present: immunomodulatory aspects and mechanisms of action. *J Immunotoxicol.* (2008) 5:47–57. doi: 10.1080/15476910802019045
24. Niittynen L, Kajander K, Korpela R. Galacto-oligosaccharides and bowel function. *Scand J Food Nutr.* (2007) 51:62–6. doi: 10.1080/17482970701414596
25. Davani-Davari D, Negahdaripour M, Karimzadeh I, Seifan M, Mohkam M, Masoumi SJ, et al. Prebiotics: Definition, Types, Sources, Mechanisms, and Clinical Applications. *Foods.* (2019) 8:92. doi: 10.3390/foods8030092
26. Wilson B, Eyice Ö, Koumoutsos I, Lomer MC, Irving PM, Lindsay JO et al. Prebiotic galactooligosaccharide supplementation in adults with ulcerative colitis: exploring the impact on peripheral blood gene expression, gut microbiota, and clinical symptoms. *Nutrients.* (2021) 13:3598. doi: 10.3390/nu13103598
27. Guarino MPL, Altomare A, Emerenziani S, Di Rosa C, Ribolsi M, Balestrieri P et al. Mechanisms of action of prebiotics and their effects on gastro-intestinal disorders in adults. *Nutrients.* (2020) 12:1037. doi: 10.3390/nu12041037
28. Akram W, Garud N, Joshi R. Role of inulin as prebiotics on inflammatory bowel disease. *Drug Discov Ther.* (2019) 13:1–8. doi: 10.5582/ddt.2019.01000
29. Parada Venegas D. De la Fuente MK, Landskron G, González MJ, Quera R, Dijkstra G, et al. Short Chain Fatty Acids (SCFAs)-mediated gut epithelial and immune regulation and its relevance for inflammatory bowel diseases. *Front Immunol.* (2019) 10:277. doi: 10.3389/fimmu.2019.00277
30. Casellas F, Borruel N, Torrejon A, Varela E, Antolin M, Guarner F et al. Oral oligofructose-enriched inulin supplementation in acute ulcerative colitis is well tolerated and associated with lowered faecal calprotectin. *Aliment Pharmacol Ther.* (2007) 25:1061–7. doi: 10.1111/j.1365-2036.2007.03288.x
31. Brummer Y, Kaviani M, Tosh SM. Structural and functional characteristics of dietary fibre in beans, lentils, peas and chickpeas. *Food Res Int.* (2015) 67:117–25. doi: 10.1016/j.foodres.2014.11.009
32. Vulevic J, Rastall RA, Gibson GR. Developing a quantitative approach for determining the in vitro prebiotic potential of dietary oligosaccharides. *FEMS Microbiol Lett.* (2004) 236:153–9. doi: 10.1016/j.femsle.2004.05.036
33. Depeint F, Tzortzis G, Vulevic J, I'anson K, Gibson GR. Prebiotic evaluation of a novel galactooligosaccharide mixture produced by the enzymatic activity of *Bifidobacterium bifidum* NCIMB 41171, in healthy humans: a randomized, double-blind, crossover, placebo-controlled intervention study. *Am J Clin Nutr.* (2008) 87:785–91. doi: 10.1093/ajcn/87.3.785
34. Vulevic J, Juric A, Walton GE, Claus SP, Tzortzis G, Toward RE et al. Influence of galacto-oligosaccharide mixture (B-GOS) on gut microbiota, immune parameters and metabonomics in elderly persons. *Br J Nutr.* (2015) 114:586–95. doi: 10.1017/S0007114515001889
35. Perdijk O, van Baarlen P, Fernandez-Gutierrez MM, van den Brink E, Schuren FHJ, Brugman S et al. Sialyllactose and galactooligosaccharides promote epithelial barrier functioning and distinctly modulate micro-biota composition and short chain fatty acid production in vitro. *Front Immunol.* (2019) 10:94. doi: 10.3389/fimmu.2019.00094
36. Lafontaine GMF, Fish NM, Connerton IF. In vitro evaluation of the effects of commercial prebiotic GOS and FOS products on human colonic Caco-2 cells. *Nutrients.* (2020) 12:1281. doi: 10.3390/nu12051281
37. Lehmann S, Hiller J, van Bergenhenegouwen J, Knippels LM, Garssen J, Traidl-Hoffmann C. In vitro evidence for immune-modulatory properties of non-digestible oligosaccharides: direct effect on human monocyte derived dendritic cells. *PLoS ONE.* (2015) 10:e0132304. doi: 10.1371/journal.pone.0132304
38. Wu RY, Määttänen P, Napper S, Scruten E, Li B, Koike Y et al. Non-digestible oligosaccharides directly regulate host kinome to modulate host inflammatory responses without alterations in the gut microbiota. *Microbiome.* (2017) 5:135. doi: 10.1186/s40168-017-0357-4
39. Del Fabbro S, Calder PC, Childs CE. Microbiota-independent immunological effects of non-digestible oligosaccharides in the context of inflammatory bowel diseases. *Proc Nutr Soc.* (2020) 2020:1–11. doi: 10.1017/S0029665120006953
40. Sambuy Y, De Angelis I, Ranaldi G, Scarino ML, Stammati A, Zucco F. The Caco-2 cell line as a model of the intestinal barrier: influence of cell and culture-related factors on Caco-2 cell functional characteristics. *Cell Biol Toxicol.* (2005) 21:1–26. doi: 10.1007/s10565-005-0085-6
41. Ferruzza S, Sambuy Y, Onetti-Muda A, Nobili F, Scarino ML. Copper toxicity to tight junctions in the human intestinal Caco-2 cell line BT. In: Massaro EJ, editor. *Handbook of Copper Pharmacology and Toxicology*. Totowa, NJ: Humana Press (2002). p. 397–416
42. Hubatsch I, Ragnarsson EG, Artursson P. Determination of drug permeability and prediction of drug absorption in Caco-2 monolayers. *Nat Protoc.* (2007) 2:2111–9. doi: 10.1038/nprot.2007.303
43. Finamore A, Roselli M, Imbinto A, Seeboth J, Oswald IP, Mengheri E. Lactobacillus amylovorus inhibits the TLR4 inflammatory signaling triggered by enterotoxigenic Escherichia coli via modulation of the negative regulators and involvement of TLR2 in intestinal Caco-2 cells and pig explants. *PLoS ONE.* (2014) 9:e94891. doi: 10.1371/journal.pone.0094891
44. Lechuga S, Ivanov AI. Disruption of the epithelial barrier during intestinal inflammation: quest for new molecules and mechanisms. *Biochim Biophys Acta Mol Cell Res.* (2017) 1864:1183–94. doi: 10.1016/j.bbamcr.2017.03.007
45. Kucharzik T, Walsh SV, Chen J, Parkos CA, Nusrat A. Neutrophil transmigration in inflammatory bowel disease is associated with differential expression of epithelial inter-cellular junction proteins. *Am J Pathol.* (2001) 159:2001–9. doi: 10.1016/S0002-9440(10)63051-9
46. Leppkes M, Neurath MF. Cytokines in inflammatory bowel diseases - Update 2020. *Pharmaco Res.* (2020) 158:104835. doi: 10.1016/j.phrs.2020.104835
47. Luissint AC, Parkos CA, Nusrat A. Inflammation and the intestinal barrier: leukocyte-epithelial cell interactions, cell junction remodeling, and mucosal repair. *Gastroenterology.* (2016) 151:616–32. doi: 10.1053/j.gastro.2016.07.008
48. Hwang PA, Phan NN, Lu WJ, Ngoc Hieu BT, Lin YC. Low-molecular-weight fucoidan and high-stability fucoxanthin from brown seaweed exert prebiotics and an-ti-inflammatory activities in Caco-2 cells. *Food Nutr Res.* (2016) 60:32033. doi: 10.3402/fnr.v60.32033

49. Fernandes P, MacSharry J, Darby T, Fanning A, Shanahan F, Houston A et al. Differential expression of key regulators of Toll-like receptors in ulcerative colitis and Crohn's disease: a role for Tollip and peroxisome proliferator-activated receptor gamma? *Clin Exp Immunol.* (2016) 183:358–68. doi: 10.1111/cei.12732
50. Berglund M, Melgar S, Kobayashi KS, Flavell RA, Hörnquist EH, Hultgren OH. IL-1 receptor-associated kinase M downregulates DSS-induced colitis. *Inflamm Bowel Dis.* (2010) 16:1778–51. doi: 10.1002/ibd.21287
51. Hubbard LL, Moore BB, IRAK-M. regulation and function in host defense and immune homeostasis. *Infect Dis Rep.* (2010) 2:e9. doi: 10.4081/idr.2010.e9
52. Ren G, Sun A, Deng C, Zhang J, Wu X, Wei X et al. The anti-inflammatory effect and potential mechanism of cardamonin in DSS-induced colitis. *Am J Physiol Gastrointest Liver Physiol.* (2015) 309:G517–27. doi: 10.1152/ajpgi.00133.2015
53. Sanchez-Munoz F, Dominguez-Lopez A, Yamamoto-Furusho JK. Role of cytokines in inflammatory bowel disease. *World J Gastroenterol.* (2008) 14:4280–8. doi: 10.3748/wjg.14.4280
54. Pistol GC, Marin DE, Dragomir C, Taranu I. Synbiotic combination of prebiotic grape pomace extract and probiotic Lactobacillus sp. reduced important intestinal inflammatory markers and in-depth signalling mediators in lipopolysaccharide-treated Caco-2 cells. *Br J Nutr.* (2019) 121:291–305. doi: 10.1017/S0007114518003410
55. Chen Q, Ren Y, Lu J, Bartlett M, Chen L, Zhang Y et al. A novel prebiotic blend product prevents irritable bowel syndrome in mice by improving gut microbiota and modulating immune response. *Nutrients.* (2017) 9:1341. doi: 10.3390/nu9121341
56. Ortega-González M, Ocón B, Romero-Calvo I, Anzola A, Guadix E, Zarzuelo A et al. Nondigestible oligosaccharides exert nonprebiotic effects on intestinal epithelial cells enhancing the immune response via activation of TLR4-NFκB. *Mol Nutr Food Res.* (2014) 58:384–93. doi: 10.1002/mnfr.201300296
57. Vulevic J, Drakoularakou A, Yaqoob P, Tzortzis G, Gibson GR. Modulation of the fecal microflora profile and immune function by a novel trans-galactooligosaccharide mixture (B-GOS) in healthy elderly volunteers. *Am J Clin Nutr.* (2008) 88:1438–46. doi: 10.3945/ajcn.2008.26242
58. Geuking MB, Cahenzli J, Lawson MA, Ng DC, Slack E, Hapfelmeier S et al. Intestinal bacterial colonization induces mutualistic regulatory T cell responses. *Immunity.* (2011) 34:794–806. doi: 10.1016/j.immuni.2011.03.021
59. Zoumpopoulou G, Tsakalidou E, Dewulf J, Pot B, Grangette C. Differential crosstalk between epithelial cells, dendritic cells and bacteria in a co-culture model. *Int J Food Microbiol.* (2009) 131:40–51. doi: 10.1016/j.ijfoodmicro.2008.12.037
60. Newburg DS, Ko JS, Leone S, Nanthakumar NN. Human milk oligosaccharides and synthetic galactosyloligosaccharides contain 3′-, 4′-, and 6′-Galactosyllactose and attenuate inflammation in human T84, NCM-460, and H4 cells and intestinal tissue ex vivo. *J Nutr.* (2016) 146:358–67. doi: 10.3945/jn.115.220749
61. Hernández-Hernández O, Calvillo I, Lebrón-Aguilar R, Moreno FJ, Sanz ML. Hydrophilic interaction liquid chromatography coupled to mass spectrometry for the characterization of prebiotic galactooligosaccharides. *J Chromatogr A.* (2012) 1220:57–67. doi: 10.1016/j.chroma.2011.11.047
62. Van Leeuwen SS, Kuipers BJH, Dijkhuizen L, Kamerling JP. Comparative structural characterization of 7 commercial galacto-oligosaccharide (GOS) products. *Carbohydrate Res.* (2016) 425:48–58. doi: 10.1016/j.carres.2016.03.006
63. Dignass A, Eliakim R, Magro F, Maaser C, Chowers Y, Geboes K et al. Crohns Colitis. Second European evidence-based consensus on the diagnosis and management of ulcerative colitis part 1: definitions and diagnosis. *Crohn's Colitis.* (2012) 6:965–90. doi: 10.1016/j.crohns.2012.09.003

Conflict of Interest: AM and LH are currently employees of Clasado Biosciences. RG was an employee of Clasado Biosciences when the work was performed. AM, LH, and RG had no access to raw data and they did not participate in data analysis. The authors declare that this study received funding from Clasado Biosciences. The funder had the following involvement with the study: Clasado co-founded the study but was not involved in the data collection and analysis, as well as interpretation of data. Clasado indeed participated to writing and revision of the present manuscript and agreed to submit it for publication.

The remaining authors declare that the research was conducted in the absence of any commercial or financial relationships that could be construed as a potential conflict of interest.

Publisher's Note: All claims expressed in this article are solely those of the authors and do not necessarily represent those of their affiliated organizations, or those of the publisher, the editors and the reviewers. Any product that may be evaluated in this article, or claim that may be made by its manufacturer, is not guaranteed or endorsed by the publisher.

Copyright © 2022 Roselli, Maruszak, Grimaldi, Harthoorn and Finamore. This is an open-access article distributed under the terms of the Creative Commons Attribution License (CC BY). The use, distribution or reproduction in other forums is permitted, provided the original author(s) and the copyright owner(s) are credited and that the original publication in this journal is cited, in accordance with accepted academic practice. No use, distribution or reproduction is permitted which does not comply with these terms.

frontiers | Frontiers in Nutrition

ORIGINAL RESEARCH
published: 19 May 2022
doi: 10.3389/fnut.2022.898417

Immune-Enhancing Effects of Co-treatment With *Kalopanax pictus* Nakai Bark and *Nelumbo nucifera* Gaertner Leaf Extract in a Cyclophosphamide-Induced Immunosuppressed Rat Model

*Young Mi Park[1], Hak Yong Lee[1], Dong Yeop Shin[1], Dae Sung Kim[2], Jin Joo Yoo[2], Hye Jeong Yang[3], Min Jung Kim[3] and Jun Sang Bae[4]**

[1] INVIVO Co., Ltd., Nonsan-si, South Korea, [2] Central Research and Development, Hanpoong Pharm & Foods Co., Ltd., Wanju-gun, South Korea, [3] Korea Food Research Institute, Wanju-gun, South Korea, [4] Department of Pathology, College of Korean Medicine, Wonkwang University, Iksan, South Korea

OPEN ACCESS

Edited by:
Bin Du,
Hebei Normal University of Science and Technology, China

Reviewed by:
Xiaojun Huang,
Nanchang University, China
Jingzhang Geng,
Shaanxi University of Technology, China

***Correspondence:**
Jun Sang Bae
jsbae78@wku.ac.kr

Specialty section:
This article was submitted to Nutritional Immunology, a section of the journal Frontiers in Nutrition

Received: 17 March 2022
Accepted: 29 April 2022
Published: 19 May 2022

Citation:
Park YM, Lee HY, Shin DY, Kim DS, Yoo JJ, Yang HJ, Kim MJ and Bae JS (2022) Immune-Enhancing Effects of Co-treatment With Kalopanax pictus Nakai Bark and Nelumbo nucifera Gaertner Leaf Extract in a Cyclophosphamide-Induced Immunosuppressed Rat Model. Front. Nutr. 9:898417. doi: 10.3389/fnut.2022.898417

Objective: Immune system disorders can result in various pathological conditions, such as infections and cancer. Identifying therapies that enhance the immune response might be crucial for immunocompromised individuals. Therefore, we assessed the immune-enhancing effect of co-treatment with *Kalopanax pictus* Nakai Bark and *Nelumbo nucifera* Gaertner leaf extract (KPNN) in a cyclophosphamide (Cy)-induced immunosuppressed rat model.

Materials and Methods: For *in vitro* studies, macrophages and splenocytes were treated with various KPNN doses in the presence or absence of Cy. Macrophage viability, nitric oxide production, splenocyte viability, cytokine production and natural killer (NK) cell activity were analyzed. For *in vivo* studies, analysis of weekly body weight, dietary intake, tissue weight, immune-related blood cell count, cytokine levels, and spleen biopsy was performed in a Cy-induced immunocompromised animal model.

Results: KPNN significantly increased phospho-NF-κB and phospho-ERK protein levels and cell viability in macrophages. KPNN significantly increased the NK cell activity in splenocytes compared to that in the control. Cy treatment decreased tumor necrosis factor (TNF)-α, interleukin (IL)-6, and interferon-γ production. In the Cy-induced immunosuppression rat model, KPNN-treated rats had significantly higher body weights and tissue weights than the Cy-treated rats. Additionally, KPNN treatment restored the immune-related factors, such as total leukocyte, lymphocyte, and intermediate cell contents, to their normal levels in the blood. The blood cytokines (TNF-α and IL-6) were increased, and spleen tissue damage was significantly alleviated.

Conclusions: Collectively, KPNN exerts an immune-enhancing effect suggesting their potential as an immunostimulatory agent or functional food.

Keywords: *Kalopanax pictus* Nakai Bark, *Nelumbo nucifera* Gaertner, immune enhancement, cyclophosphamide, macrophage, immunosuppressed rat, ERK, NF-κB

INTRODUCTION

An underactive immune system, caused by conditions such as immunodeficiency, is more prone to infection by pathogenic organisms. Thus, immune system disorders can provoke the development of various pathological conditions, such as infections and cancers (1–3). Therefore, identifying therapies that enhance the immune response are vital for immunocompromised individuals.

The immune monitoring function in humans plays a vital role as a biological host defense mechanism against the development of cancer and the proliferation of tumor cells. This anti-tumor immune function is carried out by lymphocytes, macrophages, and natural killer cells (4, 5). The activation of macrophages, B and T lymphocytes are essential steps in the initial regulation of the immune system, which is the defense mechanism of the body (6). Recently, immunotherapy has been used to induce cancer tissue destruction through the activation of cancer antigen-specific T helper (Th) and cytotoxic T (Tc) cells, macrophages, and natural killer (NK) cells (6, 7). The continued activation of immune cells results in the secretion of various cytokines during cell proliferation and differentiation, enabling the continuous amplification and control of immune functions. Therefore, recent studies have focused on discovering natural products and their immune-modulating ingredients that may serve as potential immune boosters, which can be used as ingredients in functional foods (1, 8).

Cyclophosphamide (Cy) exerts anti-tumor and immunomodulatory effects through immunosuppression, myelosuppression, and cytotoxicity (9, 10). Cy can cause a drastic change in the Th1/Th2 ratio bias, resulting in immunosuppression. The immunological effect of Cy reduced lymphocyte proliferation, including that of T cells, which was confirmed by a decrease in the levels of cytokines (tumor necrosis factor (TNF)-α, interferon (IFN)-γ, interleukin (IL)-2, and IL-12) produced by Th1 cells and cytokines (IL-4, IL-6, and IL-10) produced by Th2 cells (11, 12).

Since plants have beneficial pharmacological effects, low toxicity, and fewer side effects on human health, they have traditionally been used in oriental medicine. *Kalopanax pictus* Nakai Bark (KP) and *Nelumbo nucifera* Gaertner leaf (NN) have been shown to have various pharmacological activities, including anti-inflammatory (13–16), anti-nociceptive (14), anti-diabetic (15, 16), and anti-cancer (15–19) effects. The main components of KP and NN have been identified as liriodendrin and kalopanaxaponin (20, 21), and flavonoids and alkaloids (22, 23), respectively. These components are pharmacologically active in KP and NN, and are directly involved in therapeutic efficacy. Natural products are often blended to maximize the therapeutic effect. Although the anti-inflammatory effects of KP and NN extracts have been demonstrated *in vitro* and *in vivo* (13–16), the effects of KP and NN combination (KPNN) treatment on the immune response are yet to be elucidated. Therefore, we investigated the immune-enhancing effects and synergistic effect of KPNN in macrophages, splenocytes, and an immunosuppressed rat model.

MATERIALS AND METHODS

Preparation of Samples

Plant extracts were prepared and purified by Hanpoong Pharm & Foods Co., Ltd. (Jeonju, Jeonbuk, South Korea). Briefly, KP was extracted twice in 50% ethanol (v/v, HPS-3C) at 84–90°C or distilled water (HPS-3A) for 3 h. NN was extracted with 50% ethanol (v/v, HPS-3D) at 84–90°C or distilled water (HPS-3B) for 3 h. Each sample solution was separated through a 5-μm membrane filter, evaporated under reduced pressure at 60°C, and then vacuum-dried. The extract was lyophilized to produce a powder, and aliquots were stored at −80°C until use. KP and NN sample was extracted in water and 50% ethanol, respectively; HPS-3A: KP water extract, HPS-3C: KP ethanol extract, HPS-3B: NN water extract, HPS-3D: NN ethanol extract. The KPNN sample was extracted by mixing KP and NN in 50% ethanol at a ratio of 0.5:1 (KP:NN, HPS-3E), 1:1 (HPS-3F), 1:0.5 (HPS-3G). A screening test was performed using KP, NN, and KPNN extract to determine the optimal concentration and sample showing immune-enhancing effects. Cell viability analysis revealed that RAW 264.7 macrophages and splenocytes had the highest non-toxic concentrations of $\leq$ 500 and 100 μg/ml, respectively, in all samples (**Supplementary Figures 1, 2**). Therefore, subsequent *in vitro* experiments were performed at a concentration of $\leq$ 500 μg/ml. Cy-treated splenocytes viability was analyzed after treatment with the highest non-toxic concentration of the sample or Cy. As a result, HPS-3G (KP:NN = 1:0.5) sample showed the highest cell viability by Cy treatment. When considering cytotoxicity tests and cell viability tests of Cy-induced splenocytes were collected, HPS-3G samples were selected for this study (**Supplementary Figure 3**). For the animal study, 50, 100, and 200 mg of the tested KPNN (HPS-3G) extract/kg body weight was used. *Escherichia coli* lipopolysaccharide (LPS) and Cy were purchased from Sigma-Aldrich (St. Louis, MO, United States), and HemoHIM was purchased from Kolmar BNH Co., Ltd., (Sejong, South Korea).

Cell Culture

RAW 264.7 macrophage cell lines were purchased from the Korean Cell Line Bank (Seoul, South Korea) and grown in DMEM (Invitrogen, Carlsbad, CA, United States) culture medium supplemented with 10% fetal bovine serum (FBS) (Gibco BRL, Gaithersburg, MD, United States) with 1% penicillin and streptomycin (Invitrogen) at 37°C in a humidified incubator with 5% CO_2. Splenocytes were obtained by aseptically dissecting the Wistar rat spleens. The spleen was gently pressed with forceps and passed through a 70-μm cell strainer (SPL Life Sciences, Pocheon, Gyeonggi, South Korea). The cells were harvested and washed thrice in RPMI-1640 (Invitrogen) by centrifugation (80 × *g*, 3 min, 4°C). The cells were then treated with red blood cell lysis buffer (Sigma-Aldrich). Isolated splenocytes were maintained in RPMI-1640 media supplemented with 10% FBS (Gibco BRL) and 1% penicillin/streptomycin (Invitrogen) at 37°C in a humidified incubator with 5% CO_2.

Cell Viability Assay

For cell viability analysis, RAW 264.7 cells were seeded in 96-well plates (1×10^4 cells/90 μl/well) and treated with varying concentrations of KPNN or LPS (300 ng/ml) and incubated at 37°C and 5% CO_2 for 24 h. Additionally, to analyze the viability of Cy-treated splenocytes, the isolated splenocytes were aliquoted at 1×10^6 cells/90 μl/well in a 96-well plate. After incubation for 24 h, various KPNN concentrations were applied to the cells in the absence or presence of Cy (1.6 mg/ml). After incubation for 24 h, the WST-1 (10 μl; ITSBio, Inc., Seoul, South Korea) solution was added to the cell culture medium (100 μl) and incubated for 1 h. The absorbance values were then measured at 405 nm using a Multi-Detection Reader (Infinite 200, TECAN Group Ltd., Switzerland). The percentage of cell viability was calculated using the following equation: (mean OD of treated cells/mean OD of control cells) × 100.

Nitric Oxide Measurement

Nitric oxide (NO) production was determined as previously described (24). Briefly, after dispensing RAW 264.7 cells in a 48-well plate at a concentration of 8×10^4 cells/400 μl/well, KPNN (0, 30, 50, 100, 300 500, or 1,000 μg/ml) or LPS (300 ng/ml) was added and incubated for 24 h. The supernatant (100 μl) was transferred to another plate. Griess reagent (100 μl) was added, and the plate was incubated at room temperature for 5 min. The absorbance was measured using a microplate reader (TECAN Group Ltd.) at a wavelength of 540 nm. Absorbance was calculated and analyzed according to the standard curve of sodium nitrite.

Western Blotting Analysis

After dispensing the RAW 264.7 cells (1×10^6 cells/ml) in a 100 mm dish, the samples were treated and incubated for 24 h. Cells were then washed with ice-cold PBS and lysed with lysis buffer (PRO-PREP™ protein extraction solution, iNtRON, South Korea). After disrupting the cell line by vortexing, the lysates were precipitated at 14000 rpm for 10 min at 4°C using a centrifuge. The supernatant was quantified with the same amount of protein lysates using Bradford reagent (Bio-Rad, Hercules, CA, United States). Then, electrophoresis was conducted on a sodium dodecyl sulfate-polyacrylamide gel electrophoresis (SDS-PAGE) gel. The protein was then transferred to a polyvinylidene fluoride (PVDF) membrane and blocked with 5% skim milk solution for 1 h. The membranes were then incubated with primary antibodies overnight at 4°C. After washing the membranes with Tris-buffered saline containing Tween 20 (TBS-T), they were treated with secondary antibodies containing horseradish peroxidase (HRP) for 1 h and then washed with PBS-T. The washed membrane was treated with enhanced chemiluminescence (ECL) solution (EZ-Western Lumi Pico, DoGen, South Korea) and detected using a C-Digit western scanner (LI-COR, Lincoln, NE, United States). The following primary antibodies purchased from Cell Signaling Technology (Beverly, MA, United States) were used: anti-NF-kB p65, anti-phospho-NF-κB p65, anti-p44/42 MAPK (Erk1/2), anti-Phospho-p44/42 MAPK (Erk1/2) (Thr202/Tyr204). Anti-β-actin was purchased from Sigma-Aldrich.

Natural Killer Cell Activity Assay

Briefly, AR42J rat pancreatic tumor cells obtained from the American Type Culture Collection (ATCC, Manassas, VA, United States) were used as target cells for the NK cell activity assay. Control or KPNN-treated splenocytes were used as effector cells. Splenocytes were co-cultured with AR42J cells in 96-well plates at a 20:1 ratio of effector to target cells and incubated for 24 h. The viability of AR42J cells was assessed using the CytoTox detection kit (TaKaRa, Shiga, Japan) on a microplate reader. NK cell activity was calculated as the viability of AR42J cells compared to that of control cells.

Cytokine Measurement in Splenocytes

To analyze immune-related cytokine levels, the culture medium was treated with Cy (1.6 mg/ml) and KPNN (5, 10, 30, 50, 100 μg/ml) for 24 h. TNF-α, IL-6, and IFN-γ levels were detected using the Cytokine Activation Analysis Kits (R&D Systems Inc., Minneapolis, MN, United States), according to the manufacturer's instructions.

Animals and Experimental Design

Five-week-old specific pathogen-free (SPF) male Wistar rats (n = 60) were purchased from Orient Bio Inc., (Seongnam, Gyeonggi-do, South Korea) and adapted to the following conditions (12-h light/dark cycle; temperature, 22 ± 3°C; humidity, 50 ± 5%) for 7 days. The experiment was conducted using a standard diet and drinking water. The experiments were conducted after a week of acclimatization. A model for inducing immunosuppression was established by orally administering Cy (5 mg/kg). The 60 rats were divided into six groups of 10 animals each, after weighing each group: normal control group (normal), immunosuppression group (control), immunosuppression + KPNN 50 mg/kg group (KPNN 50), immunosuppression + KPNN 100 mg/kg group (KPNN 100), immunosuppression + 200 mg/kg group (KPNN 200), and immunosuppression + HemoHIM 1,000 mg/kg group (HemoHIM 1000). All drugs and vehicles were administered orally for 4 weeks. Body weight was measured once per week for clinical evaluation. All animal experiments were approved by the Institutional Animal Care and Use Committee of INVIVO Co., Ltd. (IV-RB-17-2105-11-01).

Complete Blood Cell (CBC) Count and Cytokine Analyses in Animal Models

Briefly, Wistar rats were orally administered KPNN (0, 50, 100, or 200 mg/kg/day) and Cy (5 mg/kg once per day) for 4 weeks. After the final administration of KPNN, whole blood was collected from the abdominal vena cava of the animals after inhalation anesthesia and divided into ethylenediaminetetraacetic acid (EDTA)-coated tubes (DB Caribe, Ltd., United States) and conical tubes for analysis. The number of total white blood cells (WBCs), lymphocytes, granulocytes, and the mid-range absolute

counts (Mid) collected in EDTA-coated tubes were analyzed using a Hemavet 950 counter (Drew Scientific Group, Dallas, TX, United States). For cytokine analysis, blood collected in a conical tube was coagulated at room temperature for 30 min and then separated in a centrifuge at 3000 rpm for 10 min to collect serum. The separated serum was analyzed for TNF-α, IL-6, and IFN-γ levels using an ELISA kit (R&D Systems).

Histological Analysis

After the animals were euthanized, the spleens were removed, weighed, and the extracted spleen tissue was cut, fixed in 10% formalin solution (trimming), fixed again with 10% formalin solution, embedded in paraffin, and cut into sections with a thickness of 4–7 μm. For hematoxylin-eosin staining, paraffin was removed from xylene and dehydrated, followed by staining with hematoxylin for 4 min and eosin for 2 min. The stained tissue preparations were observed and photographed using an optical microscope (BX50 F4; Olympus, Fukuoka, Japan).

Statistical Analysis

All experimental results were calculated as mean ± SEM using a statistical analysis program (SPSS ver.12.0, SPSS Inc., Chicago, IL, United States). Statistical analysis to evaluate the significant difference between each experimental group was performed using ANOVA (one-way analysis of variance test) and Duncan's multiple range tests. Each value represents the mean of at least three independent experiments for each group. Statistical significance was set at $p < 0.05$.

RESULTS

Effects of KPNN-Mediated Cell Proliferation and Nitric Oxide Production in RAW 264.7 Cells

To confirm the immune-enhancing effect of KPNN (HPS-3G) extracts on macrophages, toxic concentrations were first tested. The cell viability of the group treated with different KPNN concentrations was analyzed based on the control group to confirm the KPNN concentration that was toxic for macrophages. The viability of RAW 264.7 cells increased in the range of 30–300 μg/ml but decreased in a concentration-dependent manner from a concentration of 500 μg/ml or higher (**Figure 1A**). An experiment was conducted to analyze the amount of NO production in KPNN-treated RAW 264.7 cells. NO production was not notably different between the KPNN-treated and control groups but was increased in the LPS-treated group (**Figure 1B**).

Activation of ERK and NF-κB Proteins by KPNN in RAW 264.7 Cells

To investigate the mechanism of KPNN-mediated immune enhancement, activation of the extracellular-signal-regulated kinase (ERK) and nuclear factor-kappa B (NF-κB) pathways in response to KPNN was evaluated in RAW 264.7 cells by western blotting analysis. Our results showed that KPNN increased the phospho-NF-κB and phospho-ERK levels (**Figure 2A**). The expression of each protein was normalized, and the relative expression levels of the control group were analyzed. We confirmed that the p-ERK and p-NF-κB protein levels in the KPNN-treated group were higher than that of the LPS (300 ng/ml)-treated (positive control) group (**Figure 2B**).

Cell Viability Effect of KPNN on Cy-Induced Splenocytes

To confirm the cytotoxicity of KPNN against splenocytes, cells were incubated with various KPNN concentrations for 24 h. Cell viability was unaffected at KPNN concentrations of < 100 μg/ml (**Figure 3A**). Based on these results, 100 μg/ml was set as the optimal non-cytotoxic concentration, and cell viability was analyzed according to Cy (1.6 mg/ml) treatment at < 100 μg/ml KPNN. The analysis of splenocyte viability after treatment with KPNN or Cy revealed that the group treated with Cy alone showed a significant decrease in cell viability to 62.0 ± 2.4% compared to that of the untreated control group. However, the cell viability of the group co-treated with Cy and KPNN was 58–62% at all concentrations, similar to that of the group treated with Cy alone, and no significant difference was observed (**Figure 3B**).

Effects of KPNN on Natural Killer Cell Activity in Splenocytes

An NK cell activity assay was used to evaluate the effect of functional foods on non-specific cell-mediated immunity. Therefore, we examined the effect of KPNN on NK cell activity. Splenocyte cytotoxicity was tested in NK-sensitive tumor cells (AR42J cells). NK cell activity increased after treatment with various concentrations of KPNN (**Figure 4A**). As shown in **Figure 4B**, the activity of NK cells significantly increased after exposure to KPNN compared to that of the control group.

Effect of KPNN on Cytokine Expression in Cy-Treated Splenocytes

To determine the effect of KPNN on cytokine production in splenocytes by Cy treatment, the amounts of TNF-α, IL-6, and IFN-γ produced were analyzed. The cells were incubated with Cy (1.6 mg/ml) and KPNN (5, 10, 30, 50, and 100 μg/ml) for 24 h. KPNN increased cytokine levels, confirming that KPNN restored the decreased levels of TNF-α, IL-6, and IFN-γ in Cy-induced immune-reduced splenocytes (**Figure 5**).

Effects of KPNN on Thymus and Spleen Damage From Cy-Induced Immunosuppression Rats

To evaluate the effect of a 4-week regimen of KPNN feeding *in vivo*, 6-week-old Wistar rats were orally administered KPNN at three different concentrations (50, 100, or 200 mg/kg). Weekly changes in body weight, water, and food intake were monitored for animals and compared between the groups. The results confirmed that the body weight of the control group administered only Cy (5 mg/kg) was significantly lower than that of the normal control group. In contrast, the group administered various KPNN concentrations in the Cy-induced immunosuppression rat model

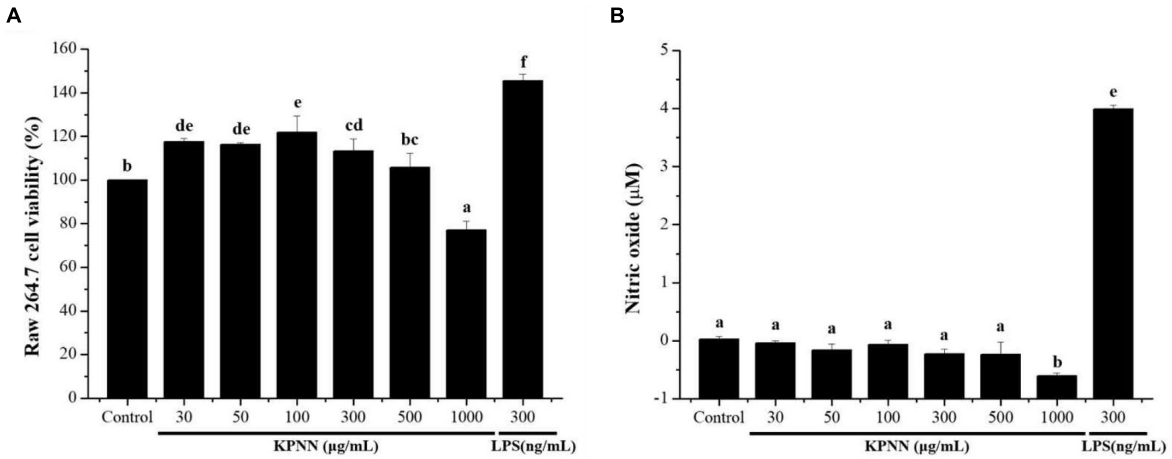

FIGURE 1 | Effect of the KPNN extract on cell survival rate and NO production by macrophages. **(A)** RAW 264.7 cells were seeded in 96-well plates (1×10^4 cells/90 μl/well) and treated with KPNN (0, 30, 50, 100, 300, 500, and 1,000 μg/ml) or LPS (300 ng/ml) and incubated at 37°C and 5% CO_2 for 24 h. Next, cell viability was measured using a WST-1 assay. **(B)** RAW 264.7, cells were dispensed in a 48-well plate (8×10^4 cells/400 μl/well) and treated with KPNN (0, 30, 50, 100, 300, 500, and 1,000 μg/ml) or LPS (300 ng/ml) for 24 h. NO concentrations in the culture supernatants were assessed using the Griess assay. Bars labeled with different superscripts are significantly different ($p < 0.05$ vs. control). The results are expressed as mean ± SEM of at least three independent experiments ($n = 3$).

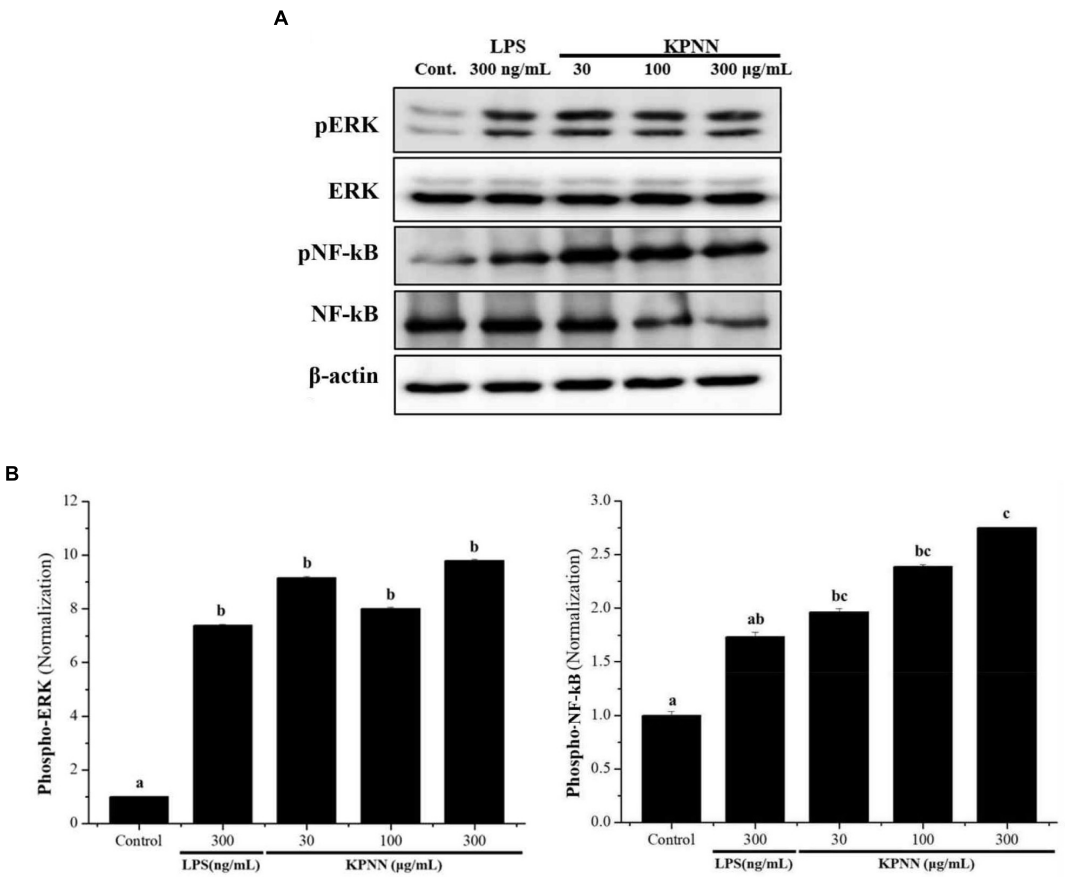

FIGURE 2 | Activation of ERK and NF-κB by KPNN in RAW 264.7 cells. **(A)** RAW 264.7 were aliquoted at 1×10^6 cells/ml in a 100 mm dish/well and treated with KPNN (0, 30, 100, 300 μg/ml) or LPS (300 ng/ml) and incubated for 24 h. The expression levels of phospho-ERK and phospho-NF-κB were examined by western blot analysis using anti-NF-κB p65, p-NF-κB p65, p44/42 MAPK (Erk1/2), and p-p44/42 MAPK (Erk1/2) antibodies. **(B)** Western blots were quantified using the Quantity One 4.6.6 software. Values are presented as mean ± SEM ($n = 3$). Bars labeled with different superscript numerals indicate $p < 0.05$.

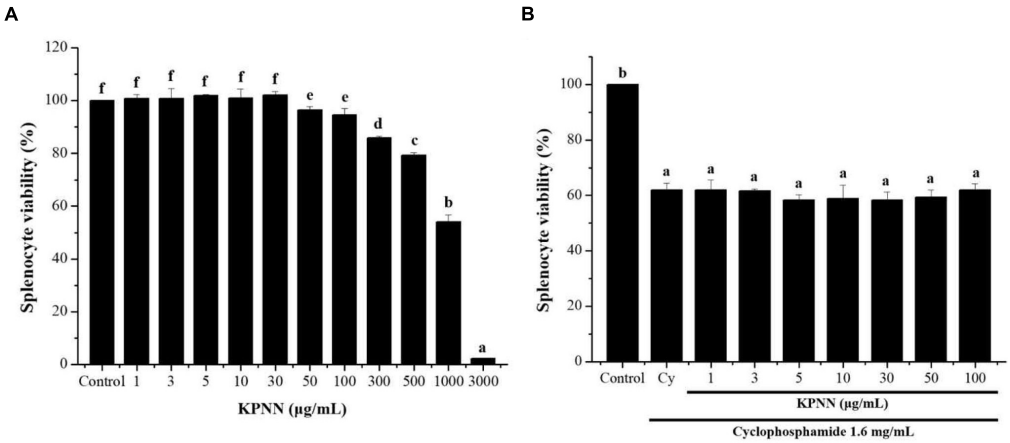

FIGURE 3 | Effects of KPNN on Cy-induced splenocytes. **(A)** Isolated splenocytes were seeded in 96-well plates (1×10^6 cells/90 μl/well) and treated with KPNN (0, 1, 3, 5, 10, 30, 50, 100, 300, 500, 1,000, and 3,000 μg/ml) for 24 h. Then, cell proliferation was determined using a WST-1 assay. **(B)** Splenocytes were seeded into 96-well plates, followed by treatment with KPNN (0, 1, 3, 5, 10, 30, 50, and 100 μg/ml) and Cy (1.6 mg/ml) for 24 h. Cell viability was measured using a WST-1 kit. Data are expressed as mean ± SEM of three independent experiments. $p < 0.05$ vs. control group ($n = 3$). Bars labeled with different superscript numerals indicate $p < 0.05$.

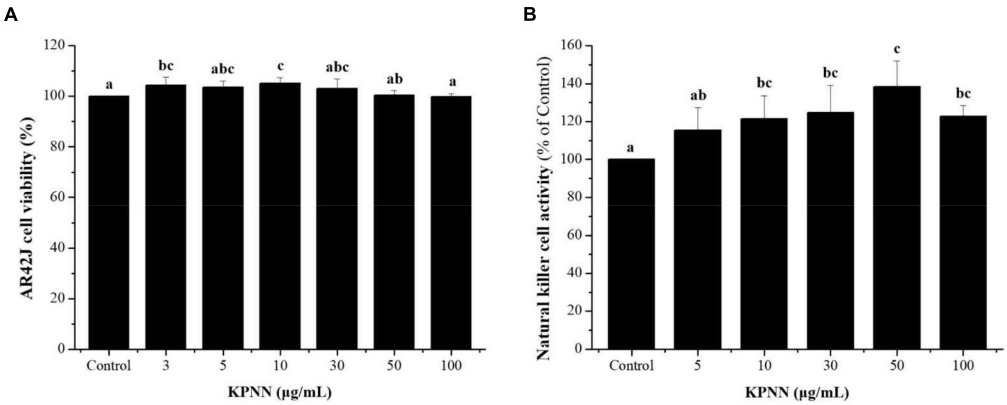

FIGURE 4 | Effects of KPNN on NK cell activity in the splenocytes. **(A)** Splenocytes were co-cultured with target cells (AR42J) in 96-well plates, followed by treatment with KPNN (0, 3, 5, 10, 30, 50, and 100 μg/ml), and incubated for 24 h in a 5% CO_2 incubator with an effector to target cell ratio of 20:1. **(B)** NK cell activity was calculated as the survival rate of AR42J cells compared to that of the control. Bars labeled with different superscripts indicate significantly different values ($p < 0.05$ vs. control). Data are presented as mean ± SEM ($n = 3$).

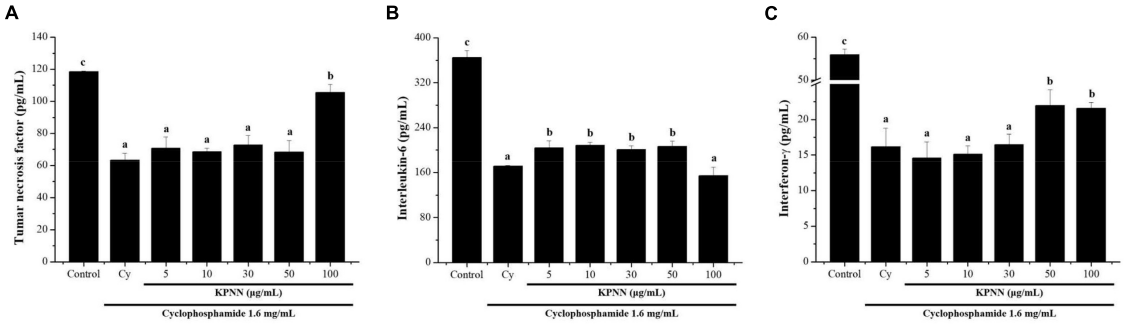

FIGURE 5 | Effects of KPNN on cytokine expression in Cy-treated splenocytes. To analyze the cytokine levels, splenocytes were seeded into a 96-well plate after incubation with Cy (1.6 mg/ml) and KPNN (0, 5, 10, 30, 50, 100 μg/ml) for 24 h in a 5% CO_2 atmosphere. After 24 h, **(A)** TNF-α, **(B)** IL-6, and **(C)** IFN-γ levels in the culture media were assayed using cytokine activation analysis kits. Data are reported as the mean ± SEM ($n = 3$). $p < 0.05$ vs. control. Bars labeled with different superscript numerals indicate $p < 0.05$.

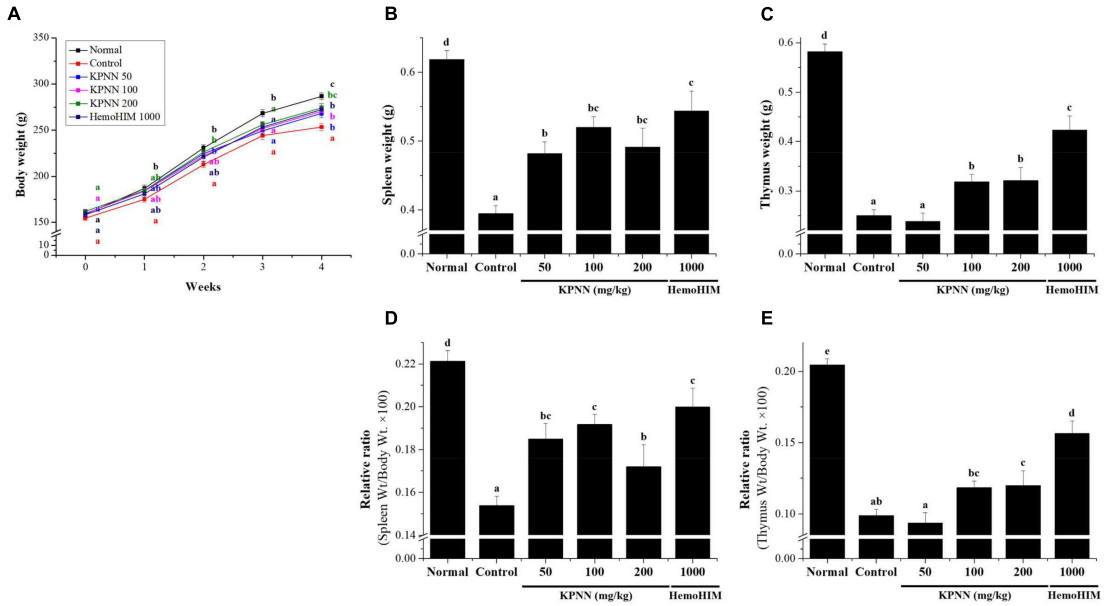

FIGURE 6 | Effects of KPNN on thymus and spleen damage in rats with Cy-induced immunosuppression. The 60 Wistar rats were divided into six groups of 10 animals each and were administered orally for 4 weeks: normal control group (Normal), immunosuppression group (Control), immunosuppression + KPNN 50 mg/kg group (KPNN 50), immunosuppression + KPNN 100 mg/kg group (KPNN 100), immunosuppression + 200 mg/kg group (KPNN 200), and immunosuppression + HemoHIM 1000 mg/kg group (HemoHIM 1000). **(A)** Body weights were measured once per week. The indices of **(B)** spleen and **(C)** relative ratio (weight/body weight × 100), **(D)** thymus, and **(E)** relative ratio (wt./body wt. × 100). Data are expressed as mean ± SEM of three independent experiments, $p < 0.05$ compared to the control group ($n = 10$). Bars labeled with different superscript numerals indicate $p < 0.05$.

showed significantly increased body weight compared to that of the control group. The rats in the KPNN 200 and HemoHIM (1,000 mg/kg, positive control) groups registered similar body weights (**Figure 6A**). To investigate the effect of KPNN on immune-related tissues in an immunosuppressed rat model, the weights of the spleen and thymus tissues were measured. The indices of representative immune organs, i.e., the spleen and thymus, were significantly reduced by oral administration of Cy (**Figures 6B,C**). However, these decreases in Cy-treated rats were significantly recovered by orally administering KPNN. These findings were similar in terms of relative ratio to body weight (**Figures 6D,E**).

Effects of KPNN on Immune Cell Number in Cy-Induced Immunosuppressed Rats

In this study, hematological analysis was performed to confirm the effect of KPNN on the blood immune cell content in immunocompromised rat models. The decreased number of immune cells, such as total white blood cells (WBCs), lymphocytes, mid-size cells (Mid), and granulocytes, in the Cy-induced immunosuppression model were increased in the KPNN-administered group (**Figure 7**).

Effect of KPNN on the Cytokine Level of Serum in Cy-Induced Immunosuppressed Rats

To confirm the immune-enhancing effect of KPNN, the serum cytokine content of each group was analyzed 4 weeks after sample administration. In the Cy-treated group, the immune-related cytokines TNF-α, IL-6, and IFN-γ were significantly reduced compared with those in the normal group. In contrast, decreased TNF-α levels in the control group were increased when KPNN ≥ 100 mg/kg was administered, and IL-6 levels were increased when KPNN 200 mg/kg was administered (**Figures 8A,B**). However, the IFN-γ levels were not significantly different from that in the control group at varying KPNN concentrations (**Figure 8C**).

Effects of KPNN on Spleen Damage in Cy-Induced Immunosuppressed Rats

We observed the splenic tissue lesions in each group under a microscope to determine the effect of KPNN on morphological changes in the Cy-treated spleens. The white pulp surrounding the central artery in the normal group and the lymph nodes at the edges were visibly demarcated from the red pulp (**Figure 9A**). However, atrophy of the white pulp and lymphoid depletion was observed in the control group (treated only with Cy), confirming Cy-induced immune suppression (**Figure 9B**). In the case of the KPNN-administered group, the marginal zone (MZ) region that separates the red and white pulp was not apparent in the KPNN 50 mg/kg group, but white pulp atrophy was better than that of the control group (**Figure 9C**). KPNN 100 mg/kg group had less white pulp atrophy and relatively minor damage (**Figure 9D**). This pattern was prominent in the KPNN 200 mg/kg group, where the marginal area around the red pulp was clearly visible, and there was no disruption of the white pulp (**Figure 9E**). In the

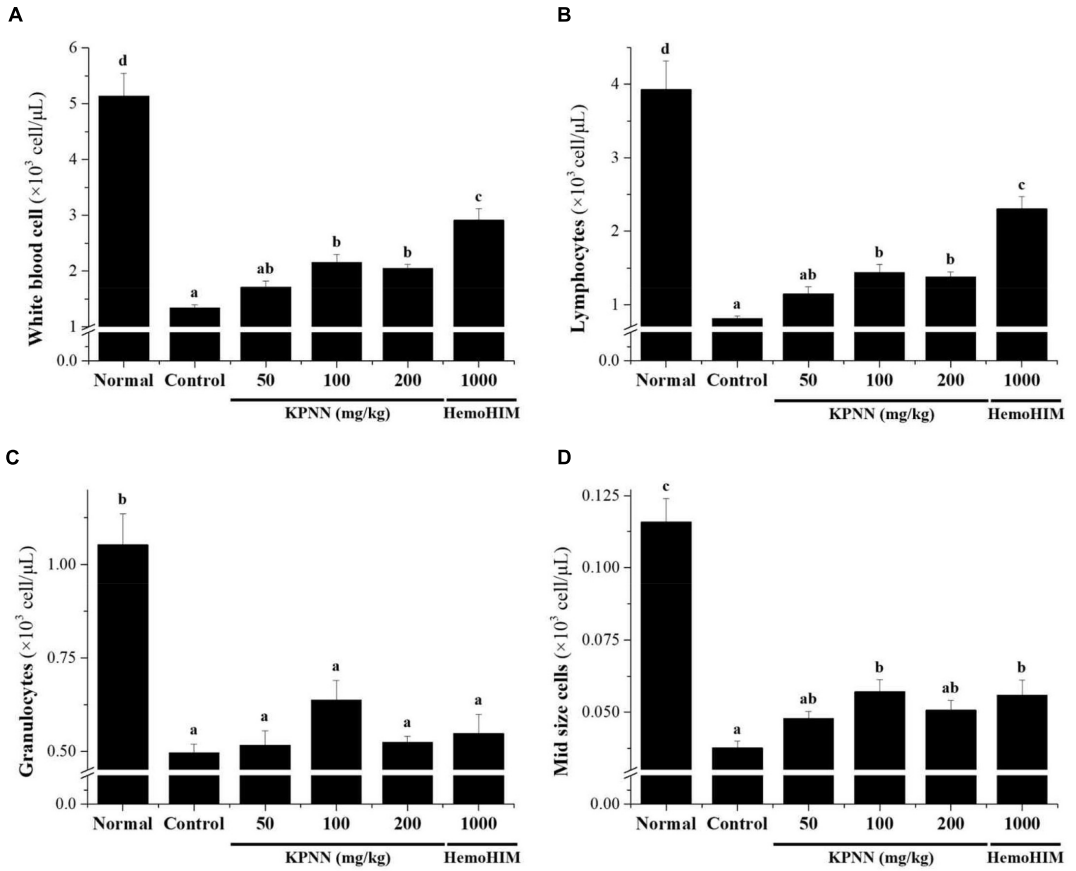

FIGURE 7 | Effects of KPNN on immune cell numbers in Cy. Wistar rats were treated with saline, cyclophosphamide (Cy; 5 mg/kg/day), oral KPNN (0, 50, 100, and 200 mg/kg/day), or oral HemoHIM (1,000 mg/kg/day) once daily for 4 weeks. Whole-blood samples were collected for analysis. The levels of **(A)** total WBCs, **(B)** lymphocytes, **(C)** granulocytes, and **(D)** mid-size cells in the blood samples were determined using a Hemavet 950 system. All data are expressed as mean ± SEM of three independent experiments, $p < 0.05$ vs. control group ($n = 10$). Bars labeled with different superscript numerals indicate $p < 0.05$.

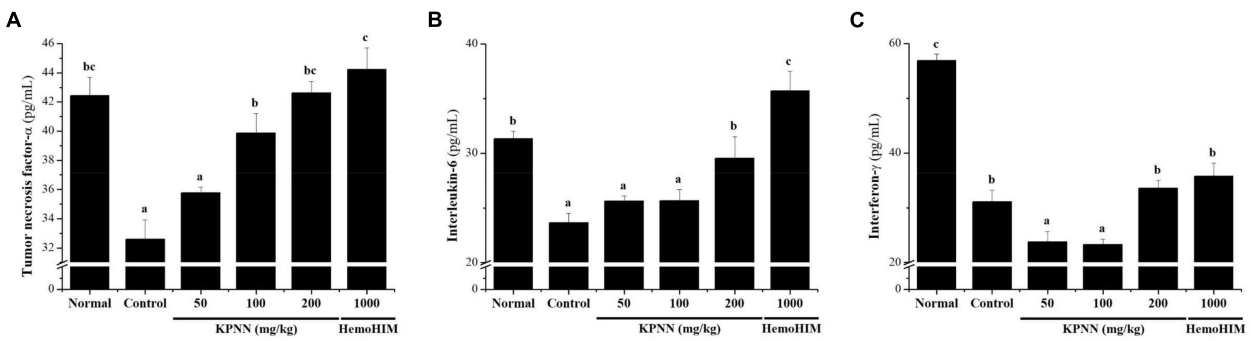

FIGURE 8 | Effect of KPNN on serum cytokine levels in rats with Cy-induced immunosuppression. Wistar rats were treated with saline, cyclophosphamide (Cy; 5 mg/kg/day), oral KPNN (0, 50, 100, and 200 mg/kg/day), or oral HemoHIM (1,000 mg/kg/day) once daily for 4 weeks. For cytokine analysis, blood collected in a conical tube was coagulated at room temperature for 30 min and then separated in a centrifuge at 3000 rpm for 10 min to collect serum. The separated serum was analyzed for **(A)** TNF-α, **(B)** IL-6, and **(C)** IFN-γ levels using an ELISA kit. The bar placed below the graph indicates significant differences at $p < 0.05$ ($n = 10$). Bars labeled with different superscript numerals indicate $p < 0.05$.

positive control group, tissue condensation did not appear, and it was significantly improved compared to that in the control group (**Figure 9F**). These results showed that KPNN stimulated innate and adaptive immunity by promoting immune-related cytokine production and improving the histopathological characteristics of Cy-induced spleen damage.

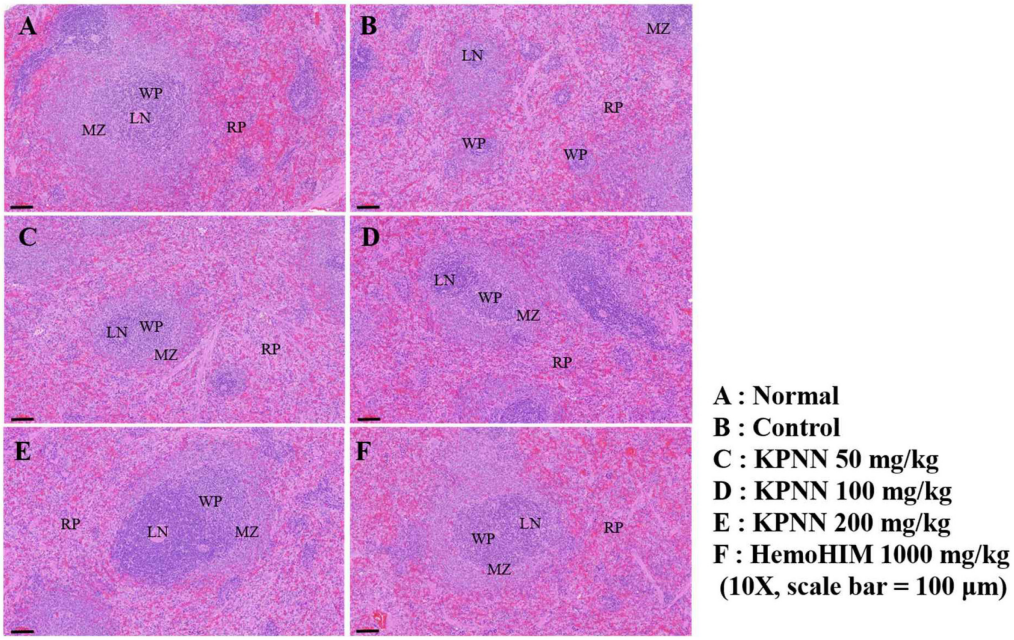

FIGURE 9 | Effects of KPNN on spleen damage in immunosuppressed rats. Wistar rats were treated with saline, cyclophosphamide (Cy; 5 mg/kg/day), oral KPNN (0, 50, 100, and 200 mg/kg/day), or oral HemoHIM (1,000 mg/kg/day) once daily for 4 weeks. Subsequently, damage to the spleen was analyzed histologically. Representative images of sectioned **(A)** normal (saline-treated), **(B)** control (only Cy-treated), and **(C–E)** KPNN-treated rats [treated with Cy and **(C)** KPNN 50 mg/kg, **(D)** KPNN 100 mg/kg, **(E)** KPNN 200 mg/kg, or **(F)** HemoHIM 1000 (HemoHIM 1,000 mg/kg)]. Scale bar = 100 μm. CV, central vein; LN, lymph nodule; MZ, marginal zone; RP, red pulp; WP, white pulp.

DISCUSSION

Immunity plays a vital role in maintaining homeostasis by inducing biological responses to effectively block external invasions (2, 3). Recently, research has been actively conducted to identify bioactive substances that can alleviate adverse effects on the immune function caused by various drugs used for anti-cancer treatment (1, 8, 25). Although KP or NN extracts as candidate substances are being studied extensively *in vitro* and *in vivo* (13, 15, 17, 19), the effect of KP and NN combination treatment on the immune response was not explored. Therefore, in this study, the immune-enhancing effects of KPNN were investigated using an immunosuppressed animal model. Our results suggest that KPNN extract promoted RAW 264.7 cell proliferation up to a concentration of 100 μg/ml and increased the levels of phospho-NF-κB and phospho-ERK proteins. Furthermore, the activity of NK cells was significantly increased after KPNN exposure. KPNN treatment protected splenocytes from Cy-induced cytotoxicity and increased the levels of immune-related serum cytokines, TNF-α, IL-6, and IFN-γ. Administration of KPNN extract to a Cy-treated immunosuppressed rat model significantly increased body weight compared to that in the control group. The damages in the representative immune organs, such as the spleen and thymus, were significantly alleviated. Furthermore, oral administration of KPNN increased total WBCs, lymphocyte, Mid, and granulocyte counts, as well as the immunity-related serum cytokines, TNF-α and IL-6, and restored normal splenic histology. These results suggest that KPNN restores the immunosuppressive response induced by Cy.

Cy, an alkylating agent with anti-cancer and immunosuppressive properties, has been widely used for immunosuppression in leukemia, rheumatoid arthritis, lymphoma, multiple myeloma, and bone marrow transplantation. However, the non-selective toxicity of Cy renders it toxic to normal cells, thereby causing bone marrow failure, which exacerbates anemia symptoms along with thrombocytopenia, and physiological phenomena, such as poor body growth and decreased immune function (26, 27). Thus, there is an increasing demand to identify and develop bioactive substances capable of lowering the side effects and toxicity of immunosuppressive drugs with non-selective toxicity (28–30).

Splenocytes consist of various cell types with different immune functions, including macrophages, dendritic cells, and T- and B-lymphocytes (31). Macrophages play important roles in both innate and adaptive immune responses. LPS-induced activation of macrophages produces pro-inflammatory cytokines (IL-1, TNF-α, IL-6, and IFN-γ), leading to the activation of phospholipase A2, which produces lipid metabolites of arachidonic acid, such as prostaglandins, and NO. Macrophages also induce MAPK-dependent phosphorylation, thereby activating multiple transcription factors (32–35). LPS upregulates TNF-α and iNOS expression by activating multiple transcription factors and inducing MAPK-dependent phosphorylation. NF-κB is also a major activator of TNF-α production by macrophages (35). Stimulation of splenocyte viability may consequently

increase the secretion of cytokines, potentially explaining the observed immune-enhancing and anti-cancer capacity (36). In this study, KPNN-treated RAW 264.7 cells showed increased cell viability in the range of 30–100 μg/ml KPNN concentration compared to that in the control group; however, the NO levels were not significantly altered. Despite the unaltered NO production, these findings suggest that KPNN promotes non-toxic and immune-enhancing effects in macrophages. In contrast, p-ERK and p-NF-κB protein levels in the KPNN-treated group were higher than those in the control and positive control groups. NF-κB and MAPK signaling play essential roles in immune responses (37, 38). A previous study reported that Red *Platycodon grandiflorus* root extract could enhance immunity by increasing the NF-κB phosphorylation level as well as the p38 MAPK-induced NF-κB activation in RAW 264.7 cells (39). KP or herbal mixture including KP showed anti-inflammatory effects by down-regulating IκBα, NF-κB, and JNK/p38 MAP kinase signaling pathways (13, 14, 40–43). In addition, NN exerts anti-inflammatory effects on LPS-stimulated RAW 264.7 macrophages through inhibition of NF-κB and MAPK pathways (44–48). Similar to a previous study (35, 40–48), our results showed that KPNN increased the p-NF-κB and p-ERK in RAW 264.7 cells. These findings are thought to be because of the positive role of KPNN in activating cytokines in Th1 cells, stimulating immune factors in the body, and increasing the activity of NK cells (49). However, downstream signal pathway of these proteins and further studies are required to identify the precise immunomodulatory mechanisms. Collectively, these results suggest that KPNN could induce immunostimulatory effects by regulating ERK and NF-κB signaling in macrophages.

In previous studies, Cy-induced immunosuppression in splenocytes reduced cell proliferation and cytokine levels and suppressed splenic NK cell activity (29, 50). NK cells can target and kill foreign and abnormal cells and play an important role in the early immune response. It is also activated by cytokine and chemokine stimulation and plays a pivotal role in tumor growth, metastasis regulation, and virus clearance (51). Therefore, NK cell activity is a valuable parameter to evaluate the cellular immune response of the host (52). As in previous reports, our results showed that the KPNN-treated group promoted the activity of NK cells and increased the production of cytokines, TNF-α, IL-6, and IFN-γ, in Cy-induced immunosuppressed splenocytes. NK cells were activated by IFN- or macrophage-derived cytokines. Only the infected cells selectively induced apoptosis by recognizing changes in MHC class expression and blocking the activation of uninfected cells (53). KPNN might play an effective role in activating NK cells and increasing cytokine production to remove cells infected by viruses and bacteria. These results suggest that KPNN modulates NK cell activity to improve cell-mediated immune responses.

Cy administration disrupts immune homeostasis in the body by damaging the spleen and thymus, which are representative immune organs that elicit immune responses (54). *In vitro* and *in vivo*, Cy-induced immunosuppression significantly reduced blood cell counts, suppressed the activity of splenic NK cells and Tc cells, and decreased cytokine (IL-2, IFN, and IL-10) levels (55, 56). In this study, as in a previous report (57), the spleen and thymus weights were reduced by Cy treatment, and the decreased indices were recovered upon KPNN treatment. Notably, in the high-dose KPNN group, body weight and spleen weight were restored to that in the HemoHIM (positive control) group. Blood, one of the most important indicators of immune function, defends the body in various ways, such as clotting during bleeding and phagocytosis during bacterial invasion (58). Additionally, immune cells, such as T and B lymphocytes, monocytes, and macrophages, play an important role in regulating the immune response (59). The contents of total leukocytes, lymphocytes, granulocytes, and intermediate cells in the control group were significantly reduced in a Cy dose-dependent manner compared to that in the normal group. In this study, as in a previous report (29), KPNN administration increased the number of total leukocytes, lymphocytes, and mid-size cells, compared to that in the control group. KPNN extract could act on blood cells that perform immune functions in the body, thereby reducing the Cy toxicity and exhibiting an immune-enhancing effect. Collectively, these findings suggest that KPNN enhances immunostimulatory activity by protecting against Cy-induced immune cell damage.

Cytokines perform crucial functions, including lymphocyte differentiation, inflammation regulation, cell survival, apoptosis, and immune responses (60). Among the diverse immune cells, T lymphocytes are essential regulatory cells in the adaptive immune system (61). The different cytokines secreted by T cell subtypes, Th1 and Th2, are important determinants of cell function. Th1 and Th2 cells are mainly involved in cell-mediated and humoral responses, respectively, and promote the secretion of IL-2, TNF-α, and IFN-γ, and IL-4, IL-6, and IL-10, respectively (11, 12, 35). TNF-α is produced by T cells, B cells, NK cells, and macrophages and regulates inflammation and host defense by inhibiting bacterial infection and acute stress (62). IFN-γ promotes Th1 cell differentiation and stimulates B cells to promote Ig production, leading to antibody immunoreactivity (35). Our study on the mouse RAW 264.7 macrophages suggested that KPNN might be involved in the production of macrophage-associated cytokines (TNF-α, IFN-γ, IL-1β, IL-6, and IL-12) *via* MAPK and NF-κB signaling. TLR4 is one of the most widely studied receptors for immune activity, mainly recognizing LPS, lipoic acid, and polysaccharides (35, 63). CLM (*ceriporia lacerata* mycelia) plays an immunostimulatory role in macrophages *via* TLR4-induced TNF-α, IL-1β, and IL-6 production (35). In previous reports, KP treatment inhibited LPS- or TNBS-induced TNF-α and IL-6 expression and production *in vitro* and *in vivo* (40, 42, 43). *In vitro* and *in vivo* studies revealed that NN reduced inflammation through downregulated proinflammatory cytokines TNF-α, IL-6, IL-1β, and IFN-γ in LPS- and DSS-induced inflammation model (44–46). Our results showed that KPNN restored the decreased levels of TNF-α, IL-6, and IFN-γ in a Cy-induced immunosuppressed splenocyte model. Additionally, the reduced TNF-α and IL-6 levels in the Cy-induced immunosuppression rat model were ameliorated by KPNN. However, further studies are required to precisely determine the immune-enhancing effects of KPNN. Collectively, these results suggest that KPNN may play a role in enhancing humoral and cell-mediated immune responses.

The spleen tissue lesions observed in the Cy-treated groups, the collapse of white pulp, and cell coagulation of red pulp observed in the control group tended to improve gradually in the KPNN-treated group. Notably, in the high-concentration KPNN-administered group, the white pulp was evenly distributed around the central vein, and the borders of the margins were visibly separated. These observations suggested that the damage to spleen tissue caused by the immunosuppressed substances was significantly reduced by KPNN treatment. Therefore, KPNN treatment can restore Cy-induced atrophy in the spleen.

CONCLUSION

In conclusion, combined treatment with KP and NN extracts increased cell viability, the levels of phospho-NF-κB and phospho-ERK proteins in macrophages, NK cell activity, and cytokine production in splenocytes. *In vivo* studies, KPNN extract was shown to strengthen immunity by increasing body weight, tissue weight, immune cells, and the cytokine content in the blood and reducing Cy-induced damage to the spleen. Therefore, these findings suggest that KPNN treatment effectively enhances immunity and may help develop therapeutic strategies or functional products.

DATA AVAILABILITY STATEMENT

The original contributions presented in the study are included in the article/**Supplementary Material**, further inquiries can be directed to the corresponding author.

ETHICS STATEMENT

The animal study was reviewed and approved by the Institutional Animal Care and Use Committee of INVIVO Co., Ltd.

AUTHOR CONTRIBUTIONS

YP, HL, DS, DK, JY, HY, MK, and JB: conceptualization and validation. YP, HL, DS, DK, JY, and JB: methodology and formal analysis. YP, DS, DK, JY, and JB: investigation and visualization. YP, HY, MK, and JB: resources and data curation. JB: writing – original draft and reviewing and editing. All authors contributed to the article and approved the final manuscript.

FUNDING

This work was supported by the "Food Functionality Evaluation Program" under the Ministry of Agriculture, Food, and Rural Affairs and the "The Research Program" of the Korea Food Research Institute.

SUPPLEMENTARY MATERIAL

The Supplementary Material for this article can be found online at: https://www.frontiersin.org/articles/10.3389/fnut.2022.898417/full#supplementary-material

REFERENCES

1. Bassaganya-Riera J, Berry EM, Blaak EE, Burlingame B, le Coutre J, van Eden W, et al. Goals in nutrition science 2020-2025. *Front Nutr.* (2021) 7:606378. doi: 10.3389/fnut.2020.606378
2. Haddad PS, Azar GA, Groom S, Boivin M. Natural health products, modulation of immune function and prevention of chronic diseases. *Evid Based Complement Altern Med.* (2005) 2:513–20. doi: 10.1093/ecam/neh125
3. Parkin J, Cohen B. An overview of the immune system. *Lancet.* (2001) 357:1777–89. doi: 10.1016/S0140-6736(00)04904-7
4. Gonzalez H, Hagerling C, Werb Z. Roles of the immune system in cancer: from tumor initiation to metastatic progression. *Genes Dev.* (2018) 32:1267–84. doi: 10.1101/gad.314617.118
5. Khalil DN, Smith EL, Brentjens RJ, Wolchok JD. The future of cancer treatment: immunomodulation, CARs and combination immunotherapy. *Nat Rev Clin Oncol.* (2016) 13:273–90. doi: 10.1038/nrclinonc.2016.25
6. Marshall JS, Warrington R, Watson W, Kim HL. Allergy, asthma, and clinical immunology : official journal of the Canadian society of allergy and clinical immunology. *Allergy Asthma Clin Immunol.* (2018) 14(Suppl. 2):49. doi: 10.1186/s13223-018-0278-1
7. Waldman AD, Fritz JM, Lenardo MJ. A guide to cancer immunotherapy: from T cell basic science to clinical practice. *Nat Rev Immunol.* (2020) 20:651–68. doi: 10.1038/s41577-020-0306-5
8. Talmadge JE. Natural product derived immune-regulatory agents. *Int Immunopharmacol.* (2016) 37:5–15. doi: 10.1016/j.intimp.2016.02.025
9. Tripathi DN, Jena GB. Intervention of astaxanthin against cyclophosphamide-induced oxidative stress and DNA damage: a study in mice. *Chem Biol Interact.* (2009) 180:398–406. doi: 10.1016/j.cbi.2009.03.017
10. Pass GJ, Carrie D, Boylan M, Lorimore S, Wright E, Houston B, et al. Role of hepatic cytochrome p450s in the pharmacokinetics and toxicity of cyclophosphamide: studies with the hepatic cytochrome p450 reductase null mouse. *Cancer Res.* (2005) 65:4211–7. doi: 10.1158/0008-5472
11. Zhou Y, Chen X, Yi R, Li G, Sun P, Qian Y, et al. Immunomodulatory effect of tremella polysaccharides against cyclophosphamide-induced immunosuppression in mice. *Molecules.* (2018) 23:239. doi: 10.3390/molecules23020239
12. Yu Q, Nie SP, Wang JQ, Liu XZ, Yin PF, Huang DF, et al. Chemoprotective effects of *Ganoderma atrum* polysaccharide in cyclophosphamide-induced mice. *Int J Biol Macromol.* (2014) 64:395–401. doi: 10.1016/j.ijbiomac.2013.12.029
13. Rahman MM, Kim HK, Kim SE, Kim MJ, Kim DH, Lee HS. Chondroprotective effects of a standardized extract (KBH-JP-040) from *Kalopanax pictus*, *Hericium erinaceus*, and *Astragalus membranaceus* in experimentally induced in vitro and in vivo osteoarthritis models. *Nutrients.* (2018) 10:356. doi: 10.3390/nu10030356
14. Kim IT, Park YM, Shin KM, Ha J, Choi J, Jung HJ, et al. Anti-inflammatory and anti-nociceptive effects of the extract from *Kalopanax pictus*, *Pueraria thunbergiana* and *Rhus verniciflua*. *J Ethnopharmacol.* (2004) 94:165–73. doi: 10.1016/j.jep.2004.05.015
15. Paudel KR, Panth N. Phytochemical profile and biological activity of *Nelumbo nucifera*. *Evid Based Complement Altern Med.* (2015) 2015:789124. doi: 10.1155/2015/789124
16. Chen G, Zhu M, Guo M. Research advances in traditional and modern use of *Nelumbo nucifera*: phytochemicals, health promoting activities and beyond. *Crit Rev Food Sci Nutr.* (2019) 59:S189–209. doi: 10.1080/10408398.2018.1553846

17. Hwang YS, Park KK, Chung WY. Kalopanaxsaponin A inhibits the invasion of human oral squamous cell carcinoma by reducing metalloproteinase-9 mRNA stability and protein traffi cking. *Biol Pharm Bull.* (2012) 35:289–300. doi: 10.1248/bpb.35.289
18. Park SK, Hwang YS, Park KK, Park HJ, Seo JY, Chung WY. Kalopanaxsaponin A inhibits PMA-induced invasion by reducing matrix metalloproteinase-9 *via* PI3K/Akt- and PKC-δ mediated signaling in MCF-7 human breast cancer cells. *Carcinogenesis.* (2009) 30:1225–33. doi: 10.1093/carcin/bgp111
19. Bishayee A, Patel PA, Sharma P, Thoutireddy S, Das N. Lotus (*Nelumbo nucifera* Gaertn.) and its bioactive phytocompounds: a tribute to cancer prevention and intervention. *Cancers (Basel).* (2022) 14:529. doi: 10.3390/cancers14030529
20. Sohn YA, Hwang SA, Lee SY, Hwang IY, Kim SW, Kim SY, et al. Protective effect of liriodendrin isolated from *Kalopanax pictus* against gastric injury. *Biomol Ther.* (2015) 23:53–9. doi: 10.4062/biomolther.2014.103
21. Hyun KT, Kim JS. The pharmacology and clinical properties of *Kalopanax pictus*. *J Med Plants Res.* (2009) 3:613–20.
22. Zhu MZ, Wu W, Jiao LL, Yang PF, Guo MQ. Analysis of favonoids in lotus (*Nelumbo nucifera*) leaves and their antioxidant activity using macroporous resin chromatography coupled with LC-MS/MS and antioxidant biochemical assays. *Molecules.* (2015) 20:10553–65. doi: 10.3390/molecules200610553
23. Guo Y, Chen X, Qi J, Yu B. Simultaneous qualitative and quantitative analysis of favonoids and alkaloids from the leaves of *Nelumbo nucifera* Gaertn. Using high-performance liquid chromatography with quadrupole time-of-fight mass spectrometry. *J Sep Sci.* (2016) 39:2499–507. doi: 10.1002/jssc.201501315
24. Park YM, Noh EM, Lee HY, Shin DY, Lee YH, Kang YG, et al. Anti-diabetic effects of *Protaetia brevitarsis* in pancreatic islets and a murine diabetic model. *Eur Rev Med Pharmacol Sci.* (2021) 25:7508–15. doi: 10.26355/eurrev_202112_27450
25. Artym J, Zimecki M, Paprocka M, Kruzel ML. Orally administered lactoferrin restores humoral immune response in immunocompromised mice. *Immunol Lett.* (2003) 89:9–15. doi: 10.1016/s0165-2478(03)00102-0
26. Wang H, Wang M, Chen J, Tang Y, Dou J, Yu J, et al. A polysaccharide from *Strongylocentrotus nudus* eggs protects against myelosuppression and immunosuppression in cyclophosphamide-treated mice. *Int Immunopharmacol.* (2011) 11:1946–53. doi: 10.1016/j.intimp.2011.06.006
27. Ogino MH, Tadi P. Cyclophosphamide. In: *StatPearls [Internet]*. Treasure Island, FL: StatPearls Publishing (2021). Available online at: https://www.ncbi.nlm.nih.gov/books/NBK553087 (accessed September 29, 2021).
28. Abdelzaher WY, Bahaa HA, Elkhateeb R, Atta M, Fawzy MA, Ahmed AF, et al. Role of JNK, ERK, and p38 MAPK signaling pathway in protective effect of sildenafil in cyclophosphamide-induced placental injury in rats. *Life Sci.* (2022) 293:120354. doi: 10.1016/j.lfs.2022.120354
29. Noh EM, Kim JM, Lee HY, Song HK, Joung SO, Yang HJ, et al. Immuno-enhancement effects of *Platycodon grandiflorum* extracts in splenocytes and a cyclophosphamide-induced immunosuppressed rat model. *BMC Complement Altern Med.* (2019) 19:322. doi: 10.1186/s12906-019-2724-0
30. Artym J, Zimecki M, Kruzel ML. Effects of lactoferrin on IL-6 production by peritoneal and alveolar cells in cyclophosphamide-treated mice. *J Chemother.* (2004) 16:187–92. doi: 10.1179/joc.2004.16.2.187
31. Klimp AH, de Vries EG, Scherphof GL, Daemen T. A potential role of macrophage activation in the treatment of cancer. *Crit Rev Oncol Hematol.* (2002) 44:143–61. doi: 10.1016/s1040-8428(01)00203-7
32. McAleer JP, Vella AT. Understanding how lipopolysaccharide impacts CD4 T-cell immunity. *Crit Rev Immunol.* (2008) 28:281–99. doi: 10.1615/critrevimmunol.v28.i4.20
33. Mburu S, Marnewick JL, Abayomi A, Ipp H. Modulation of LPS-induced CD4+ T-cell activation and apoptosis by antioxidants in untreated asymptomatic HIV infected participants: an in vitro study. *Clin Dev Immunol.* (2013) 2013:631063. doi: 10.1155/2013/631063
34. Park HJ, Lee KT, Jung WT, Choi JW, Kadota S. Protective effects of syringin isolated from *Kalopanax pictus* on galactosamine induced hepatotoxicity. *J Nat Med.* (1999) 53:113–7.
35. Hwang YP, Lee GH, Pham TH, Kim MY, Kim CY, Lee SY, et al. Immune-enhancing effect of submerged culture of *Ceriporia lacerata* mycelia on cyclophosphamide-induced immunosuppressed mice and the underlying mechanisms in macrophages. *Int J Mol Sci.* (2022) 23:597. doi: 10.3390/ijms23020597
36. Conniot J, Silva JM, Fernandes JG, Silva LC, Gaspar R, Brocchini S, et al. Cancer immunotherapy: nanodelivery approaches for immune cell targeting and tracking. *Front Chem.* (2014) 2:105. doi: 10.3389/fchem.2014.00105
37. Kim YS, Kim EK, Nawarathna W, Dong X, Shin WB, Park JS, et al. Immune-stimulatory effects of *Althaea rosea* flower extracts through the MAPK signaling pathway in RAW264.7 cells. *Molecules.* (2017) 22:679. doi: 10.3390/molecules22050679
38. Hayden MS, West AP, Ghosh S. NF-kappaB and the immune response. *Oncogene.* (2006) 25:6758–80. doi: 10.1038/sj.onc.1209943
39. Park EJ, Lee YS, Kim SM, Juna AJ, Yoo JH, Lee SH. Immune-enhancing effects of red *Platycodon grandiflorus* root extract *via* p38 MAPK-mediated NF-κB activation. *Appl Sci.* (2020) 10:5457. doi: 10.3390/app10165457
40. Jeong YH, Hyun JW, Kim Van Le T, Kim DH, Kim HS. Kalopanaxsaponin A exerts anti-inflammatory effects in lipopolysaccharide-stimulated microglia *via* inhibition of JNK and NF-κB/AP-1 pathways. *Biomol Ther (Seoul).* (2013) 21:332–7. doi: 10.4062/biomolther.2013.069
41. Joh EH, Jeong JJ, Kim DH. Kalopanaxsaponin B inhibits LPS-induced inflammation by inhibiting IRAK1 kinase. *Cell Immunol.* (2012) 279:103–8. doi: 10.1016/j.cellimm.2012.10.001
42. Joh EH, Kim DH. Kalopanaxsaponin A ameliorates experimental colitis in mice by inhibiting IRAK-1 activation in the NF-κB and MAPK pathways. *Br J Pharmacol.* (2011) 162:1731–42. doi: 10.1111/j.1476-5381.2010.01195.x
43. Jeong JJ, Jang SE, Joh EH, Han MJ, Kim DH. Kalopanaxsaponin B ameliorates TNBS-induced colitis in mice. *Biomol Ther (Seoul).* (2012) 20:457–62. doi: 10.4062/biomolther.2012.20.5.457
44. Liu SH, Lu TH, Su CC, Lay IS, Lin HY, Fang KM, et al. Lotus leaf (*Nelumbo nucifera*) and its active constituents prevent inflammatory responses in macrophages *via* JNK/NF-κB signaling pathway. *Am J Chin Med.* (2014) 42:869–89. doi: 10.1142/S0192415X14500554
45. Li C, He Y, Yang Y, Gou Y, Li S, Wang R, et al. Antioxidant and inflammatory effects of *Nelumbo nucifera* Gaertn leaves. *Oxid Med Cell Longev.* (2021) 2021:8375961. doi: 10.1155/2021/8375961
46. Min X, Guo Y, Zhou Y, Chen X. Protection against dextran sulfate sodium-induced ulcerative colitis in mice by neferine, a natural product from *Nelumbo nucifera* Gaertn. *Cell J.* (2021) 22:523–31. doi: 10.22074/cellj.2021.6918
47. Park E, Kim GD, Go MS, Kwon D, Jung IK, Auh JH, et al. Anti-inflammatory effects of *Nelumbo* leaf extracts and identification of their metabolites. *Nutr Res Pract.* (2017) 11:265–74. doi: 10.4162/nrp.2017.11.4.265
48. Moon SW, Ahn CB, Oh Y, Je JY. Lotus (*Nelumbo nucifera*) seed protein isolate exerts anti-inflammatory and antioxidant effects in LPS-stimulated RAW264.7 macrophages *via* inhibiting NF-κB and MAPK pathways, and upregulating catalase activity. *Int J Biol Macromol.* (2019) 134:791–7. doi: 10.1016/j.ijbiomac.2019.05.094
49. Caamano J, Hunter CA. NF-κB family of transcription factors: central regulators of innate and adaptive immune functions. *Clin Microbiol Rev.* (2002) 15:414–29. doi: 10.1128/CMR.15.3.414-429.2002
50. Han NR, Kim KC, Kim JS, Ko SG, Park HJ, Moon PD. The immune-enhancing effects of a mixture of *Astragalus membranaceus* (Fisch.) Bunge, *Angelica gigas* Nakai, and *Trichosanthes Kirilowii* (Maxim.) or its active constituent nodakenin. *J Ethnopharmacol.* (2022) 285:114893. doi: 10.1016/j.jep.2021.114893
51. Kos FJ, Engleman EG. Immune regulation: a critical link between NK cells and CTLs. *Immunol Today.* (1996) 17:174–6. doi: 10.1016/0167-5699(96)80616-5
52. Elemans M, Thiébaut R, Kaur A, Asquith B. Quantification of the relative importance of CTL, B cell, NK cell, and target cell limitation in the control of primary SIV-infection. *PLoS Comput Biol.* (2011) 7:e1001103. doi: 10.1371/journal.pcbi.1001103
53. Dokun AO, Kim S, Smith HR, Kang HS, Chu DT, Yokoyama WM. Specific and nonspecific NK cell activation during virus infection. *Nat Immunol.* (2001) 2:951–6. doi: 10.1038/ni714
54. Tanahashi T, Sekiguchi N, Matsuda K, Matsumoto A, Ito T, Nakazawa H, et al. A screening method with lymphocyte percentage and proportion of granular lymphocytes in the peripheral blood for large granular lymphocyte (LGL) leukemia. *Int J Hematol.* (2017) 105:87–91. doi: 10.1007/s12185-016-2092-1
55. Huang GC, Wu LS, Chen LG, Yang LL, Wang CC. Immuno-enhancement effects of Huang Qi Liu Yi Tang in a murine model of cyclophosphamide-induced leucopenia. *J Ethnopharmacol.* (2007) 109:229–35. doi: 10.1016/j.jep.2006.07.023

56. Hu TJ, Shuai XH, Chen JR, Wei YY, Zheng RL. Protective effect of a *Potentilla anserine* polysaccharide on oxidative damages in mice. *Int J Biol Macromol.* (2009) 45:279–83. doi: 10.1016/j.ijbiomac.2009.06.011
57. Cui HL, Chen Y, Wang SS, Kai GQ, Fang YM. Isolation, partial characterisation and immunomodulatory activities of polysaccharide from Morchella esculenta. *J Sci Food Agric.* (2011) 91:2180–5. doi: 10.1002/jsfa.4436
58. Gandhi GR, Neta MTSL, Sathiyabama RG, Quintans JSS, de Oliveira E Silva AM, Araújo AAS, et al. Flavonoids as Th1/Th2 cytokines immunomodulators: a systematic review of studies on animal models. *Phytomedicine.* (2018) 44:74–84. doi: 10.1016/j.phymed.2018.03.057
59. Boyman O, Sprent J. The role of interleukin-2 during homeostasis and activation of the immune system. *Nat Rev Immunol.* (2012) 12:180–90. doi: 10.1038/nri3156
60. Lacy P, Stow JL. Cytokine release from innate immune cells: association with diverse membrane trafficking pathways. *Blood.* (2011) 118:9–18. doi: 10.1182/blood-2010-08-265892
61. Constant SL, Bottomly K. Induction of Th1 and Th2 CD4+ T cell responses: the alternative approaches. *Annu Rev Immunol.* (1997) 15:297–322. doi: 10.1146/annurev.immunol.15.1.297
62. Giai C, Gonzalez C, Ledo C, Garofalo A, Di Genaro MS, Sordelli DO, et al. Shedding of tumor necrosis factor receptor 1 induced by protein A decreases tumor necrosis factor alpha availability and inflammation during systemic *Staphylococcus aureus* infection. *Infect Immun.* (2013) 81:4200–7.
63. Pan G, Xie Z, Huang S, Tai Y, Cai Q, Jiang W, et al. Immune-enhancing effects of polysaccharides extracted from *Lilium lancifolium* Thunb. *Int Immunopharmacol.* (2017) 52:119–26. doi: 10.1016/j.intimp.2017.08.030

Conflict of Interest: YP, HL, and DS were employed by INVIVO Co., Ltd. DK and JY were employed by Hanpoong Pharm & Foods Co., Ltd.

The remaining authors declare that the research was conducted in the absence of any commercial or financial relationships that could be construed as a potential conflict of interest.

Publisher's Note: All claims expressed in this article are solely those of the authors and do not necessarily represent those of their affiliated organizations, or those of the publisher, the editors and the reviewers. Any product that may be evaluated in this article, or claim that may be made by its manufacturer, is not guaranteed or endorsed by the publisher.

Copyright © 2022 Park, Lee, Shin, Kim, Yoo, Yang, Kim and Bae. This is an open-access article distributed under the terms of the Creative Commons Attribution License (CC BY). The use, distribution or reproduction in other forums is permitted, provided the original author(s) and the copyright owner(s) are credited and that the original publication in this journal is cited, in accordance with accepted academic practice. No use, distribution or reproduction is permitted which does not comply with these terms.

frontiers | Frontiers in Immunology

ORIGINAL RESEARCH
published: 19 May 2022
doi: 10.3389/fimmu.2022.916618

Effects of Fucoidan Isolated From *Laminaria japonica* on Immune Response and Gut Microbiota in Cyclophosphamide-Treated Mice

Yunping Tang[1], Qiuyan Pu[1], Qiaoling Zhao[2], Yafeng Zhou[1], Xiaoxia Jiang[1] and Tao Han[3]**

[1] Zhejiang Provincial Engineering Technology Research Center of Marine Biomedical Products, School of Food and Pharmacy, Zhejiang Ocean University, Zhoushan, China, [2] Zhoushan Institute for Food and Drug Control, Zhoushan, China, [3] Department of Aquaculture, Zhejiang Ocean University, Zhoushan, China

OPEN ACCESS

Edited by:
Bin Du,
Hebei Normal University of Science and Technology, China

Reviewed by:
Fei Peng,
Hebei Normal University of Science and Technology, China
Xiaoting Fu,
Ocean University of China, China

***Correspondence:**
Yunping Tang
tangyunping1985@163.com
Tao Han
goodhantao@gmail.com

Specialty section:
This article was submitted to Nutritional Immunology, a section of the journal Frontiers in Immunology

Received: *09 April 2022*
Accepted: *25 April 2022*
Published: *19 May 2022*

Citation:
Tang Y, Pu Q, Zhao Q, Zhou Y, Jiang X and Han T (2022) Effects of Fucoidan Isolated From Laminaria japonica on Immune Response and Gut Microbiota in Cyclophosphamide-Treated Mice. Front. Immunol. 13:916618. doi: 10.3389/fimmu.2022.916618

The effects of *Laminaria japonica* fucoidan (LF) on immune regulation and intestinal microflora in cyclophosphamide (CTX)-treated mice were investigated in this work. Results indicated that LF significantly enhanced the spleen and thymus indices, promoted spleen lymphocyte and peritoneal macrophages proliferation, and increased the immune-related cytokines production in serum. Moreover, LF could regulate intestinal flora composition, increasing the abundance of *Lactobacillaceae* and *Alistipes*, and inhibiting *Erysipelotrichia*, *Turicibacter*, *Romboutsia*, *Peptostreptococcaceae*, and *Faecalibaculum*. These results were positively correlated with immune characteristics. Overall, LF could be useful as a new potential strategy to mitigate CTX immunosuppression and intestinal microbiota disorders.

Keywords: fucoidan, cyclophosphamide, immunosuppression, immunomodulatory, gut microbiota

INTRODUCTION

The immune system comprises immune organs, cells, and immune-reactive substances, which play vital roles in the host's defense against foreign pathogens and microorganisms (1–3). The interaction between the natural and specific immune systems is necessary to maintain host health, and therefore, infections and various diseases will occur when the immune system is dysfunctional or impaired (4). Cyclophosphamide (CTX) is a potent immunosuppressant widely used in treating several immune diseases and malignant tumors (5, 6). However, numerous studies indicated that CTX could disrupt the DNA structure and immune cells and reduce normal lymphocytes and macrophages, thereby inhibiting cellular and humoral immune responses (7, 8). On the other hand, long-term or high doses usage of CTX (80 or 100 mg/kg body weight (BW)) can cause intestinal injury and intestinal microbiota disruption (9–11). Therefore, it is essential to discover effective immunomodulators to reduce the CTX side effects.

Recently, numerous natural polysaccharides have attracted more attention due to their various physiological activities without side effects (12–15). Polysaccharides have been developed as novel immunomodulators, enhancing host immunity and preserving intestinal health (16–18). It has been described that sulfated yam polysaccharide possesses stronger immunomodulatory activity to modulate gut microbiota structure in CTX-treated mice (11). Mulberry leaf polysaccharide has immunomodulatory activity by restoring the injured intestinal barrier and gut microbiota composition in CTX-treated mice (16). At the same time, one report indicated that *Millettia Speciosa Champ* polysaccharide modulates gut health and ameliorates immunosuppression and intestinal injury in CTX-treated mice (17). Considering all these studies, polysaccharides have the potential to be used as an effective immunomodulator to enhance immune function and regulate intestinal flora.

Due to the exploitation and utilization of marine resources, marine natural products have become a research hotspot (19, 20). Fucoidan, a sulfated polysaccharide, has numerous biological activities, including antitumor, antioxidant, anti-inflammatory, immunoregulatory, among others (21–24). *Kjellmaniella crassifolia* or *Undaria pinnatifida* fucoidan could stimulate RAW264.7 cell proliferation *in vitro* and induce a significant immune enhancement *in vivo* (22). Hwang et al. (23) indicated that low-molecular-weight fucoidan from *Laminaria japonica* could enhance the innate and adaptive immune responses and protects against *Mycoplasma pneumoniae* antigen stimulation. Sun et al. (24) indicated that low-molecular-weight fucoidan from *Laminaria japonica* could play an antiviral role by improving the quality of immune organs, improving immune cell phagocytosis and humoral immunity. Nevertheless, there is still a lack of systematic studies regarding the link between the immune regulation function of *Laminaria japonica* fucoidan and intestinal flora.

In our previous studies, we discovered that *Laminaria japonica* fucoidan (LF) could effectively ameliorate CTX-induced liver and kidney injury (25). Herein, the immunomodulatory function of LF was investigated using immunosuppressed mice. In addition, the link between immunomodulatory function and gut microbiota was also evaluated. This systematic research could provide insights into the link between immune regulation function and intestinal flora, and also provided a better understanding of the LF applicability.

MATERIALS AND METHODS

Materials and Reagents

LF, with an average molecular weight of 250 kDa, is composed of mannose, rhamnose, galactose, xylose, and fucose in a molar ratio of 2.04: 0.58: 1.04: 3.91: 12.43, respectively (25). CTX was supplied by Hengrui Medicine (Lianyungang, China). Concanavalin A (ConA) and lipopolysaccharide (LPS) were purchased from Sigma-Aldrich (Sigma-Aldrich, USA). Tumor necrosis factor (TNF)-α, interleukin (IL)-6, and IL-1β ELISA kits were purchased from Boster (Wuhan, China). Immunoglobulin G (IgG) ELISA kit was purchased from Solarbio (Beijing, China).

Animals and Design

Male ICR mice (18-22 g, 6-8 weeks) were purchased from the Zhejiang Academy of Medical Sciences. All mice were maintained in a breeding environment (23 ± 2°C, 60% ± 5 humidity) on a 12 h light/12 h dark cycle. After 7 days of adaptive feeding, mice were randomly divided into 4 groups (n = 8 per group) as follows: control (only treated with a saline solution), model (mice treated with 80 mg/kg BW CTX), 20 LF (mice treated with 20 mg/kg BW LF), and 40 LF (mice treated with 40 mg/kg BW LF). The control group received gavages with saline solution for 19 days (once daily), while the remaining three groups were firstly injected with CTX (80 mg/kg BW) for 5 days (once daily) and then saline solution or 20 and 40 mg/kg BW of LF for another 14 consecutive days (once daily) were received by gavage.

Spleen and Thymus Indices Determination

The spleen and thymus indices were calculated as follows:

$$\text{spleen or thymus indices (mg/g)} = \text{spleen or thymus weight (mg)}/\text{body weight (g)}$$

Splenic Lymphocyte Proliferation Assay

Splenic lymphocyte was prepared according to Han and collaborators (26). Briefly, the mouse spleen was grinding, and splenic lymphocytes were collected. Next, erythrocyte lysis buffer was added to lyse the red blood cells, and the supernatant was collected by centrifugation (at 1500 × g, 5 min). After removing adherent cells, the cells were incubated in a 6-well plate for 6 h, and the suspended cells were collected as splenic lymphocytes. Then, the cells (1×10^6 cells/mL) were seeded in 96-well plates (final volume of 100 μL). Then, ten microliters of ConA (5 μg/mL) or LPS (1 μg/mL) were added and incubated for 72 h at 37°C with 5% CO_2. Next, the MTT solution (10 μL, 5 mg/mL) was added, and the absorbance at 490 nm was detected on a microplate reader (Molecular Devices, CA, USA).

Macrophages Proliferation Assay

The mice were intraperitoneally injected with 5 mL sterile saline solution, and the abdomen was gently pressed for 2 min. After, the abdominal wall was cut open with sterilized scissors, and the abdominal fluid was sucked into a centrifuge tube with a sterile straw. The cell suspension was centrifuged (2000 rpm, 10 min) and resuspended with DMEM medium. The supernatant was discarded to obtain purified macrophages after incubation at 37°C with 5% CO_2 for 4 h. After this, the cells (1×10^4 cells/mL) were seeded in a 96-well plate (final volume of 200 μL). After 24 h at 37°C with 5% CO_2, an MTT solution (10 μL, 5 mg/mL) was added, and the absorbance at 490 nm was detected on a microplate reader.

Phagocytic Activity of Peritoneal Macrophages

The macrophages (1×10^4 cells/mL) were seeded in a 96-well plate (final volume of 200 μL). After 36 h, the medium was discarded, and a neutral red solution (0.1%) was added. After 3 h incubation, the excess neutral red was removed by washing twice with 0.1 M PBS, and lysis solutions (200 μL) were added and shaken for 10 min at 25°C. The absorbance at 540 nm was detected on a microplate reader.

Serum Cytokines and IgG Content Analysis

The blood was collected from eyeball extirpation, and serum was acquired by centrifugation (6000 × g, 3 min, 4°C) of the blood. The serum levels of TNF-α, IL-6, IL-1β, and IgG were determined using Boster's ELISA kits.

Histological Analysis

The spleen and thymus cross-sections were fixed (4% paraformaldehyde) and embedded in paraffin (10%). The hematoxylin-eosin (HE) staining was performed as in previous studies (20, 27). Micrographs were taken using a light microscope CX31 (Olympus, Japan).

Oxidative Stress Index Analysis

The spleen was ground in saline, and the supernatant was collected by centrifugation. Malondialdehyde (MDA), glutathione peroxidase (GSH-Px), superoxide dismutase (SOD), and catalase (CAT) levels in spleen tissues were measured using Jiancheng's commercial kits (Nanjing, China).

Fecal Microbiota Analysis

The genomic DNA of mice feces was extracted, and 338F and 806R primers were used to amplify the V3-V4 region of bacterial 16S rRNA as previously described (27, 28). The MiSeq library was constructed by adding the Illumina official connector sequences to the target area of the PCR products (Shanghai Origingene Bio-pharm Technology Co.Ltd., China). Then, the Illumina Novaseq6000 platform (Illumina, San Diego, USA) was applied for paired sequencing, and the paired-end reads were chosen according to the overlapping relationship. Operational taxonomic units (OTUs) clustering analysis and taxonomic analysis were performed to analyze the diversity indices and community structure at different taxonomic levels, respectively.

Correlation Between Key Microbes and Immunity-Related Parameters

The correlation heatmap analysis was used to calculate the Spearman rank correlation coefficient between the intestinal key microbial species and basic immunity-related parameters (29). In addition, the microorganisms expressing the highest correlation with LF to enhance the CTX-induced immunosuppression were screened out.

Statistical Analysis

Results are expressed as the mean ± standard deviation (SD). Data analysis was performed using SPSS 24.0 (SPSS Inc., Chicago, IL, USA). $P < 0.05$ was considered statistically significant.

RESULTS

Effect of LF on Spleen and Thymus Indices

In the model group, the spleen and thymus indices were significantly decreased compared to the control group (**Figure 1A**). However, when treated with LF, the spleen and thymus indices showed a significant increase compared to the model ($P < 0.05$ or $P < 0.01$), suggesting that LF treatment could effectively alleviate the CTX-induced atrophy of the spleen and thymus.

Effect of LF on Splenic Lymphocyte Proliferation

When treated with ConA or LPS, spleen lymphocytes were induced into T and B lymphocytes, respectively (30, 31). Compared to the control, the proliferation of T and B lymphocytes was significantly reduced ($P < 0.01$) in the model, suggesting that CTX could modulate and reduce the cellular immune response (**Figure 1B**). On the other hand, when treated with both LF treatments, the proliferation indices were significantly enhanced compared with the model ($P < 0.01$), suggesting that LF could improve cellular immune response by promoting spleen lymphocytes proliferation. Compared to the model, the macrophages' relative proliferation rate and the phagocytic index were significantly increased in the 20 LF and 40 LF groups (**Figures 1C, D**, $P < 0.01$), suggesting that LF could promote the macrophages' proliferation and overcome the immunosuppressed activity induced by CTX.

Serum Cytokines and IgG Content Analysis

Compared to the control, the IL-6, IL-1β, TNF-α, and IgG levels in the model group were significantly decreased (**Figure 2**, $P < 0.01$), suggesting that CTX inhibited the immune regulation system of mice. However, after treatment with LF, these levels in the 20 LF and 40 LF groups were significantly restored compared to the model ($P < 0.01$), suggesting that LF could improve mice immunosuppression *via* enhancing the cytokines and IgG production.

Histological Analysis

To observe the effect of LF on the immune organs, HE staining was applied to detect alterations in the spleen and thymus (**Figure 3A**). The splenic vesicles in the control group remained structurally intact, and a clear demarcation line between the red and white marrow was observed. The splenic cords in the red marrow were connected as a whole, and the blood cells around the exterior of the splenic vesicles were surrounded orderly (**Figure 3A**). However, there were no clearly formed splenic vesicles in the spleen in the model group, and the white and red medullae were partially mixed. The thinning of the lymphatic sheath around the small central artery implies that CTX could damage the spleen immune cells, resulting in spleen atrophy. When treated with 20 mg/kg LF, the general structure of the splenic vesicles could be observed, but the boundary among the red and white medulla remained

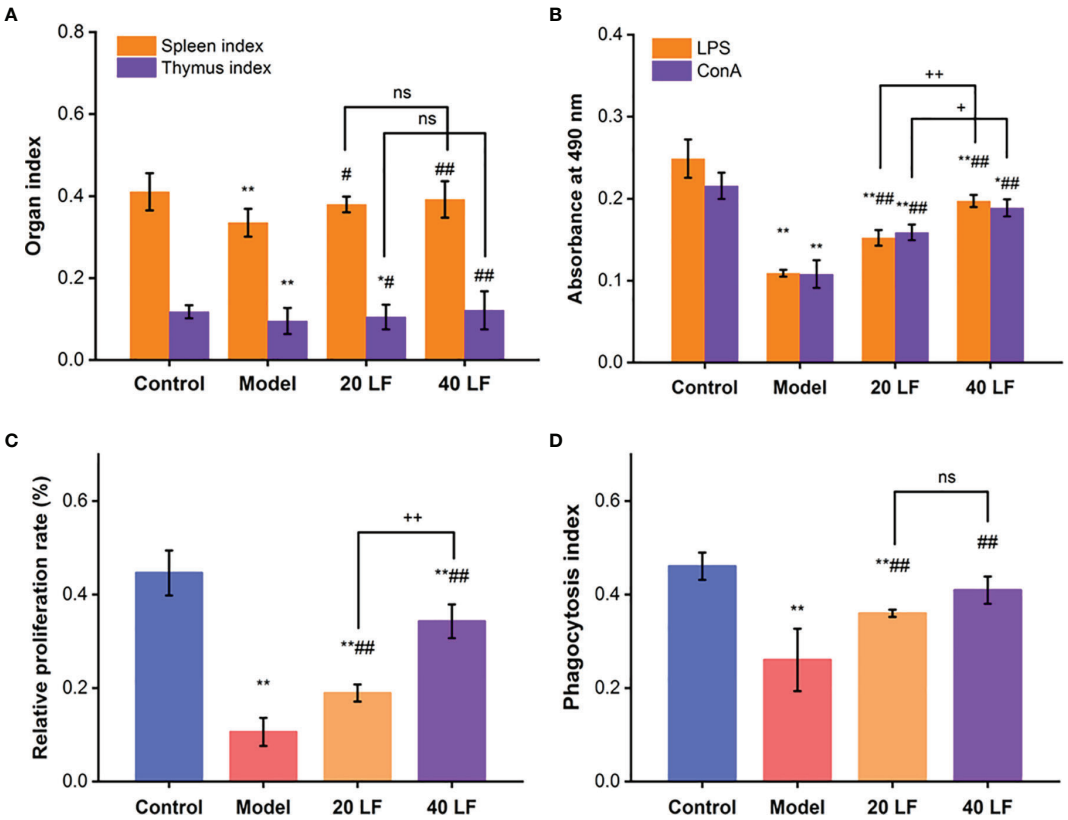

FIGURE 1 | Immune organ indexes of spleen and thymus **(A)**, splenic lymphocytes proliferation **(B)**, peritoneal macrophage proliferation **(C)**, and the phagocytic **(D)** index, (n = 8). $^{*}P < 0.05$, $^{**}P < 0.01$ *vs* control; $^{\#}P < 0.05$, $^{\#\#}P < 0.01$ *vs* model, $^{+}P < 0.05$, $^{++}P < 0.01$ compared between 20 LF and 40 LF, and ns means no significant difference.

unclear. Moreover, after treatment with 40 LF, the red and white medulla could be observed, and the marginal area of the white medulla was widened. Overall, the morphology of the spleen in the LF group gradually returned to a similar shape found in the control, suggesting that LF could restore the spleen injury caused by CTX.

Moreover, the cortical and medullary structures of the control were clear and distinct, and evident thymus vesicles could be observed in the medulla (**Figure 3B**). However, when treated with CTX, the structure of the cortex and medulla in the model group was diffused, and few and not evident thymus vesicles were observed in the visual field. On the other hand, there was a clear distinction between the cortex and medulla when treated with LF, mainly in the 40 LF group. Furthermore, the morphology was similar to the control, suggesting that LF could restore the thymus injury caused by CTX.

Oxidative Stress Index Analysis

The MDA levels and the activities of GSH-Px, SOD, and CAT were also assessed in the spleen. Compared to the control, the MDA contents were significantly increased, and the GSH-Px, SOD, and CAT activities were significantly decreased in the model (**Figure 4**) ($P < 0.01$). After being treated with LF, the MDA contents were significantly reduced ($P < 0.01$), and the GSH-Px, SOD, and CAT activities were significantly increased compared to the model group ($P < 0.01$). These results suggest that LF could improve CTX-induced oxidative stress in the spleen tissues.

Diversity Analysis of the Intestinal Flora

To investigate the LF effect on intestinal microflora composition in mice, a 16S rRNA sequencing was performed. The Venn diagram showed common and unique OTUs between different samples (**Figure 5A**), and 803 OTUs in all samples were identified. Additionally, 640 shared OTUs in the four groups, accounting for 79.70% of the total OTUs, indicating that the bacterial compositions of all groups were similar. Non-metric multi-dimensional scaling (NMDS) analysis can reflect the relationship between microbial communities of different samples. As shown in **Figure 5B**, there are significant differences in the microbial community structure between the control and the model group, while the microorganisms of the 20 LF and 40 LF groups are relatively similar to those of the control group. In addition, the alpha diversity change (Shannon and

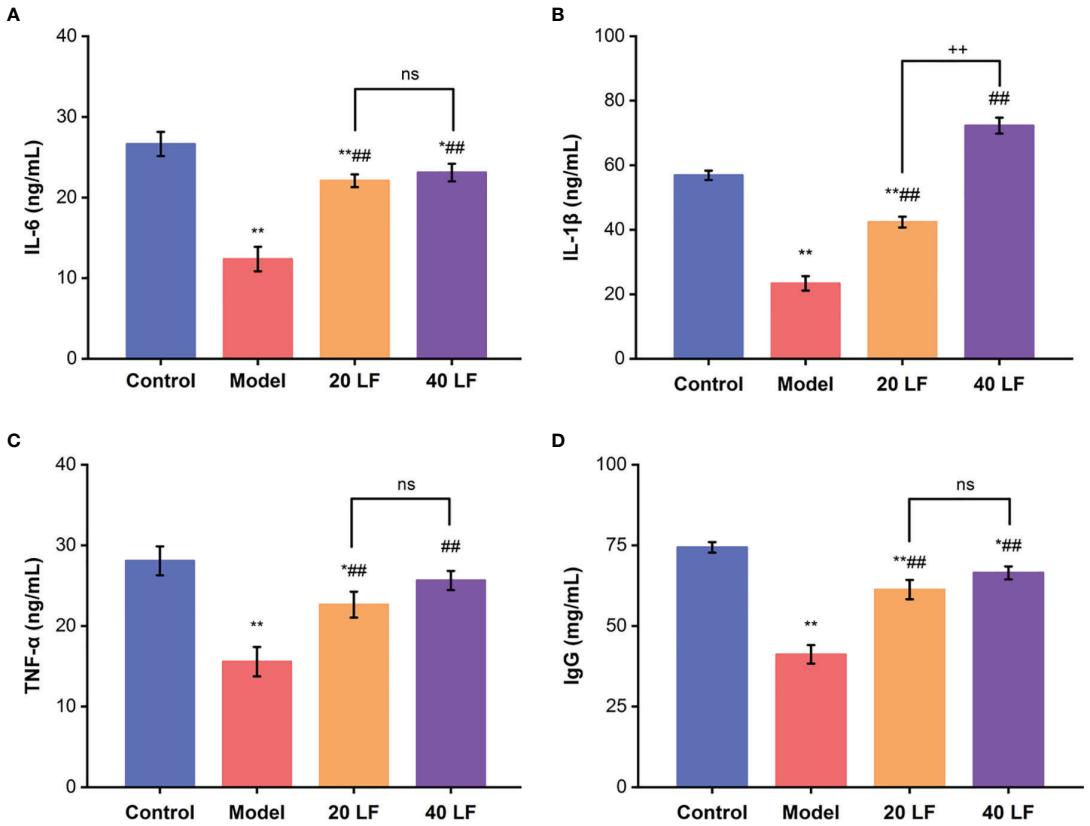

FIGURE 2 | Effects of LF on the serum levels of IL-6 **(A)**, IL-1β **(B)**, TNF-α **(C)**, and IgG **(D)**, (n = 8). $^{*}P < 0.05$, $^{**}P < 0.01$ *vs* control; $^{\#\#}P < 0.01$ *vs* model, $^{++}P < 0.01$ compared between 20 LF and 40 LF, and ns means no significant difference.

Chao indices) was shown in **Figures 5C, D**. Except for the Chao index of the 40 LF group, the results of alpha diversity were significantly different from the CTX group after different doses of LF intervention ($P < 0.05$), indicating that LF could reverse the changes in the abundance and diversity of fecal bacteria caused by CTX.

Principal coordinates analysis (PCOA) and cluster tree analysis were performed to analyze the similarity of microbial communities

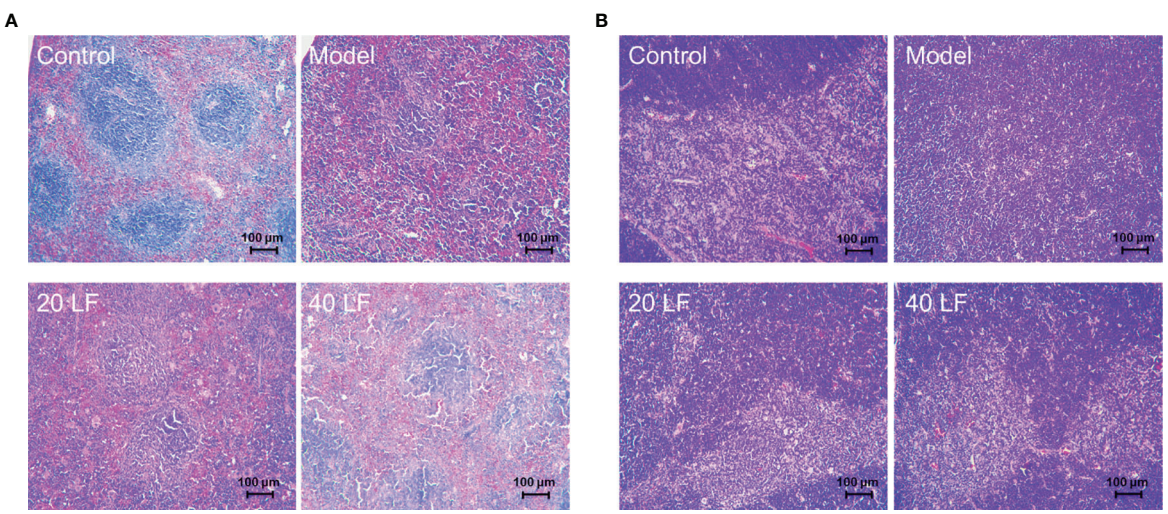

FIGURE 3 | Histomorphology of spleen **(A)** and thymus **(B)** in mice (×100).

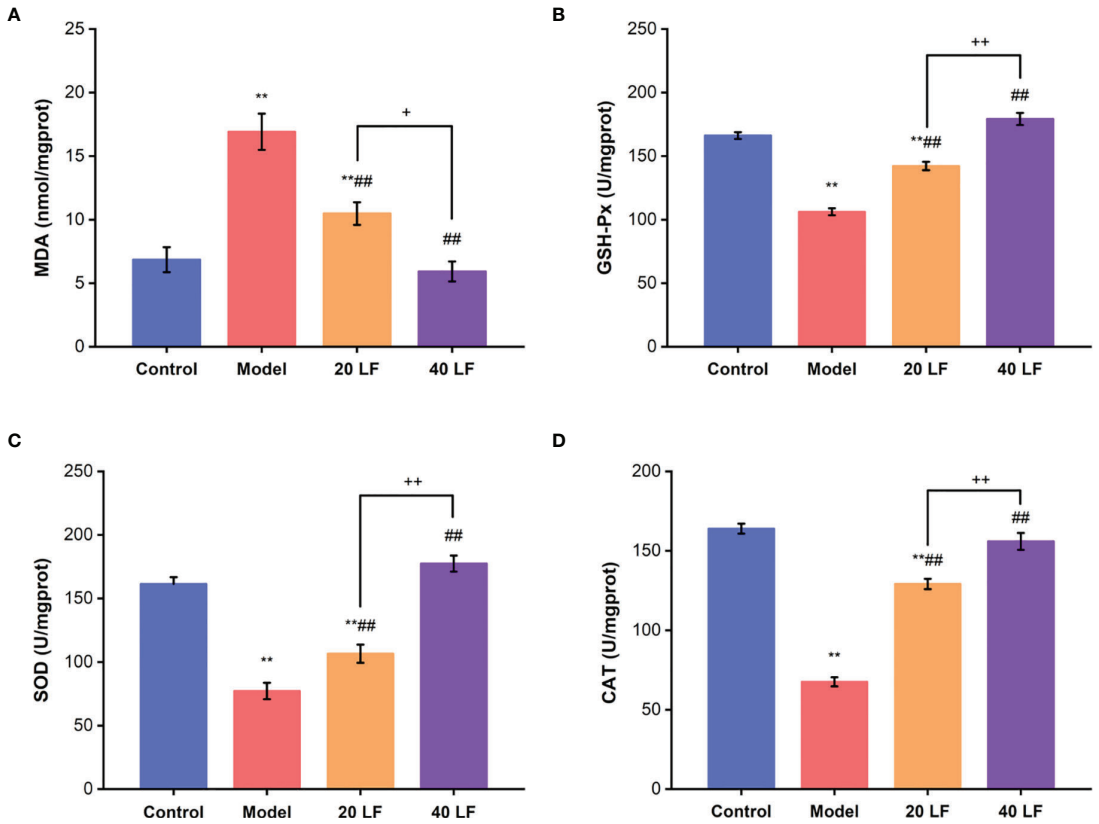

FIGURE 4 | Effects of LF on the MDA levels **(A)**, GSH-Px, SOD, and CAT activities GSH-Px **(B)**, SOD **(C)**, and CAT **(D)** of the spleen (n = 8). $^{**}P < 0.01$ *vs* control; $^{\#\#}P < 0.01$ *vs* model, $^{*}P < 0.05$, $^{++}P < 0.01$ compared between 20 LF and 40 LF.

among different groups. The PCOA results suggested that CTX and LF intervention significantly affected the intestinal flora composition (**Figure 5E**). Furthermore, the distance between the 40 LF and control groups was smaller than that between the control and model groups, suggesting that the intervention of LF could cause a shift in gut flora composition. In addition, the cluster analysis results based on bray curtis distance were consistent with the PCOA results (**Figure 5F**), suggesting that CTX and LF could effectively influence the intestinal flora composition. In addition, the intestinal flora of the LF group was more similar to the control.

Analysis of Community Differences of Intestinal Flora

To identify specific taxa associated with LF, we assessed the relative abundance of species at phylum and family levels. The mouse intestinal flora comprises Firmicutes, Bacteroidetes, and Proteobacteria, together accounting for over 90% (**Figure 6A**). The differences in the relative abundance of these three major bacteria were further analyzed (**Figure 6B**). It was observed that CTX treatment significantly decreased the abundance of Firmicutes and significantly increased the abundance of Proteobacteria ($P < 0.05$). After LF treatment, the changes of relative abundance of the three phyla were reversed, but only changes of Proteobacteria abundance in the 20 LF group were significantly different. The gut flora varied significantly at the family level (**Figure 6C**), where the top 10 species with relative abundance were *Lactobacillaceae*, *Lachnospiraceae*, *Bacteroidales*_S24-7_group, *Ruminococcaceae*, *Rikenellaceae*, *Porphyromonadaceae*, *Enterobacteriaceae*, *Helicobacteraceae*, *Bacteroidaceae*, and *Peptostreptococcaceae* (**Table 1**). CTX significantly altered the relative abundance of *Lactobacillaceae*, *Bacteroidales*_S24-7_group, and *Peptostreptococcaceae* compared to the control, and LF treatment at different doses reversed these changes caused by CTX (**Figure 6D**, $P < 0.01$).

LEfSe Analysis of Intestinal Flora in Mice

LEfSe was performed to identify taxa with significant differences in abundance, while linear discriminant analysis (LDA) was performed to estimate the influence of the abundance of each component on the differential effect. From the Lefse results (**Figure 7**), it was observed that the CTX treatment mainly suppressed the relative abundance of *Lactobacillales*, *Bacilli*, *Enterobacteriales*, and *Gammaproteobacteria*, and promoted the relative abundance of *Family*_XIII_UCG_001,

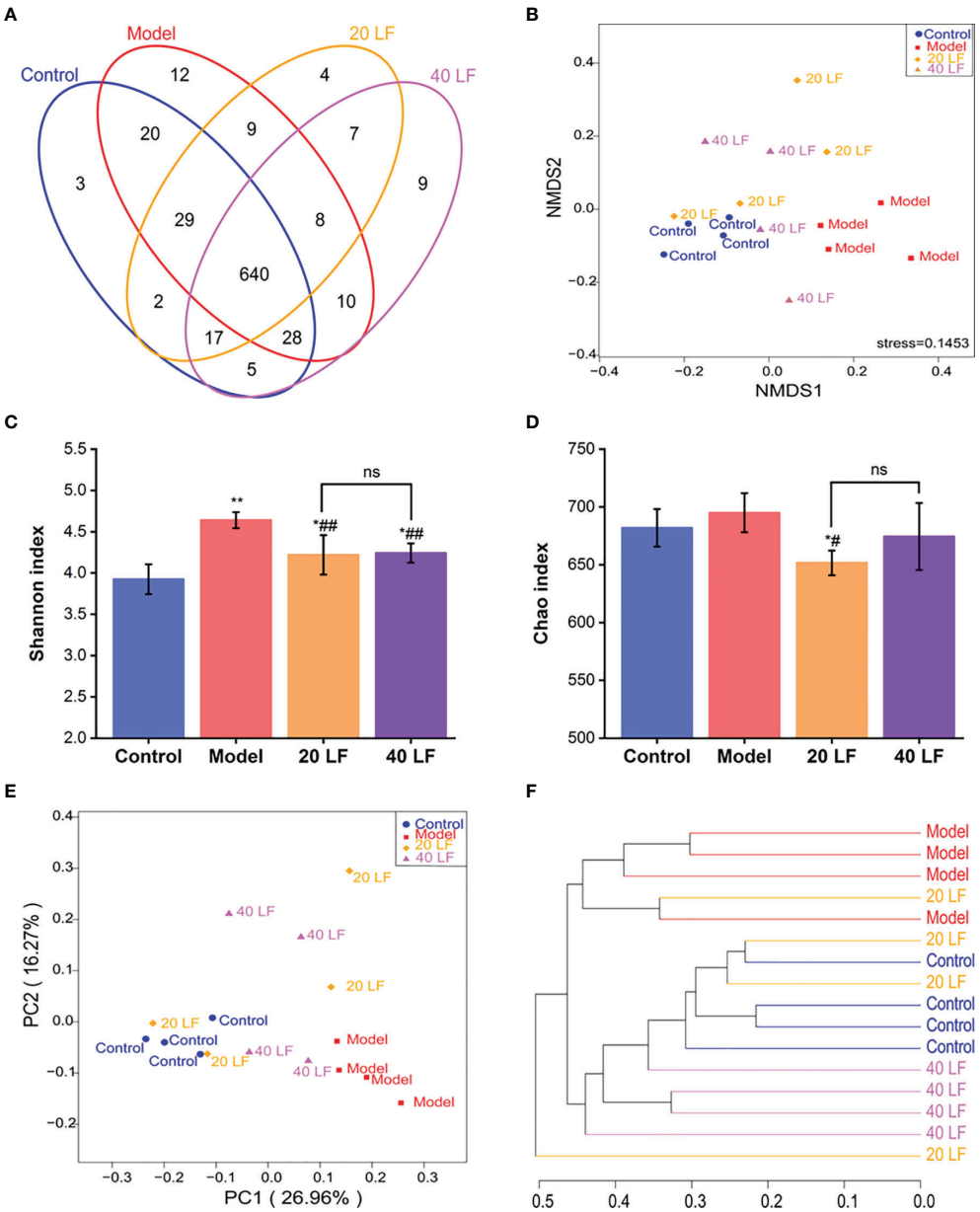

FIGURE 5 | Effects of LF treatment on the gut microbiota composition of the CTX-induced mice (n = 4). **(A)** Venn diagrams. **(B)** Non-metric multi-dimensional scaling (NMDS) analysis. **(C)** Shannon indices. **(D)** Chao indices. **(E)** Principal coordinates analysis. **(F)** Cluster tree analysis based on the unweighted UniFrac at the genus level. $^{*}P < 0.05$, $^{**}P < 0.01$ *vs* control; $^{\#}P < 0.05$, $^{\#\#}P < 0.01$ *vs* model, and ns means no significant difference.

*Eubacterium*_brachy_group, *Blautia*, *Lachnoclostridium*, *Romboutsia*, *Peptostreptococcaceae*, *Anaerotruncus*, *Ruminococcaceae*_UCG_010, *Faecalibaculum*, *Turicibacter*, *Erysipelotrichia*, *Helicobacteraceae*, *Campylobacterales*, and *Epsilonproteobacteria*. Compared to the model, 40 LF treatment significantly suppressed the relative abundance of the CTX-stimulated microorganisms, especially the relative abundance of *Erysipelotrichia*-related groups, and promoted the relative abundance of *Alistipes*, *Gastranaerophilales*, *Cyanobacteria*, and *Streptococcus*.

Correlation Between Key Microbes and Host Parameters

The correlation heatmap analysis was used to calculate the Spearman rank correlation coefficient between the intestinal key microbial species and host parameters. In addition, the key microorganisms expressing the highest correlation with LF to enhance the CTX-induced immunosuppression were screened out. As depicted in **Figure 8**, 5 types of microbes (*Romboutsia*, *Peptostreptococcaceae*, *Faecalibaculum*, *Turicibacter*, and *Erysipelotrichia*) presented a significant negative correlation with the CAT, SOD, and GSH-Px

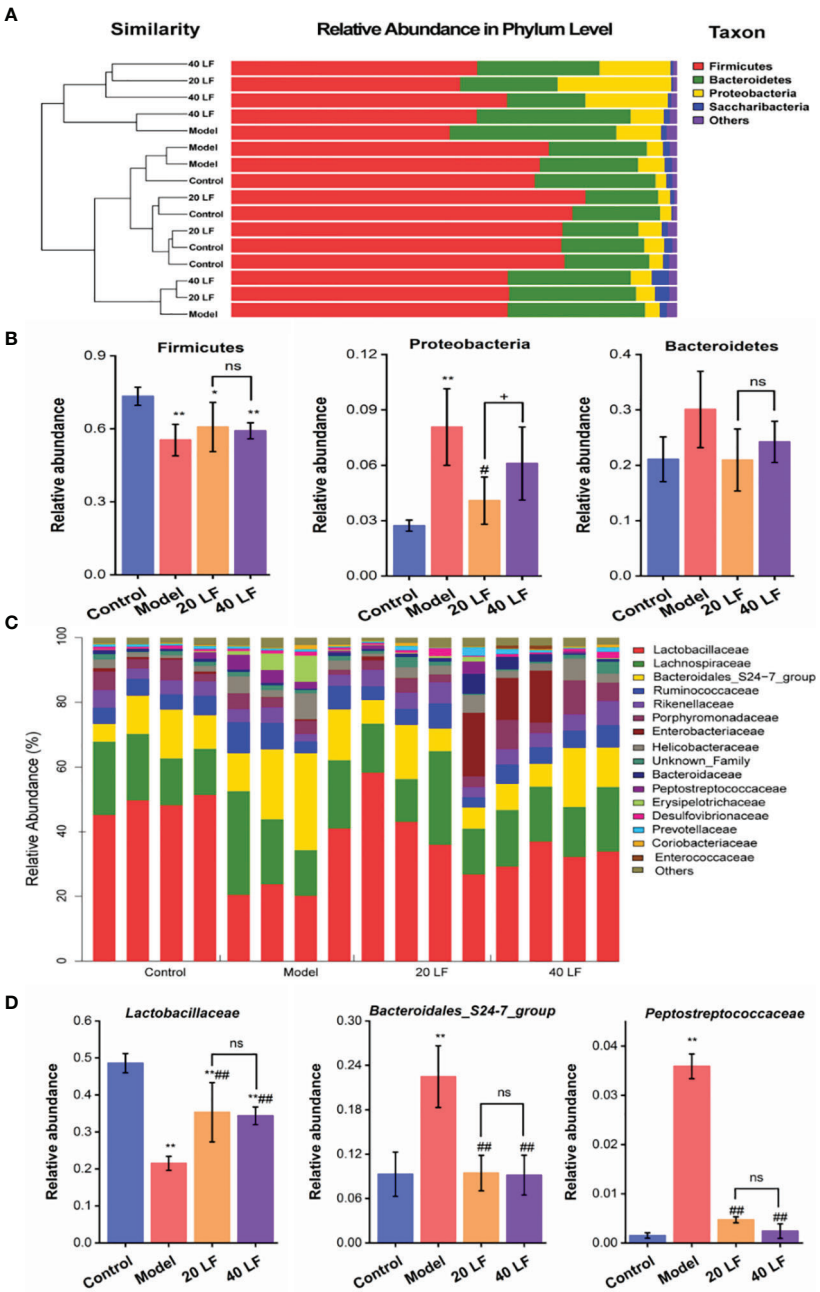

FIGURE 6 | Comparisons of the gut microbiota at phylum and family taxonomic levels (n = 4). **(A)** Gut microbiota composition at the phylum level. **(B)** Relative abundance of the gut microbiota at the phylum level. **(C)** Gut microbiota composition at the family level. **(D)** Relative abundance of the gut microbiota at the family level. $^{*}P < 0.05$, $^{**}P < 0.01$ *vs* control; $^{\#}P < 0.05$, $^{\#\#}P < 0.01$ model, $^{+}P < 0.05$ compared between 20 LF and 40 LF, and ns means no significant difference.

activities, pro-inflammatory cytokine levels (IL-1β and TNF-α), while also being positively correlated with the MDA content ($P < 0.05$). These bacteria were the key species of intestinal microbiota in the model group and were also inhibited by LF. In contrast, 3 types of key microorganisms (*Lactobacillaceae*, *Bacilli*, and *Lactobacillus*) presented a positively correlated with pro-inflammatory cytokine levels (IL-6 and TNF-α), IgG, CAT activity. Moreover, the LF group was also enriched with *Alistipes*, presenting a significant negative correlation with MDA levels and positively correlated with SOD and GSH-Px activities.

TABLE 1 | Changes of intestinal microorganisms in the top 10 relative abundance at the family level (n = 4).

Microorganisms	Control	Model	20 LF	40 LF
Lactobacillaceae	0.486 ± 0.026	0.215 ± 0.019 **	0.353 ± 0.080 **##	0.344 ± 0.024 **##
Lachnospiraceae	0.164 ± 0.036	0.285 ± 0.049 **	0.179 ± 0.074	0.175 ± 0.019
Bacteroidales_S24-7_group	0.093 ± 0.030	0.225 ± 0.042 *	0.094 ± 0.024 ##	0.092 ± 0.027 ##
Ruminococcaceae	0.052 ± 0.006	0.083 ± 0.012 **	0.050 ± 0.020	0.058 ± 0.008
Porphyromonadaceae	0.050 ± 0.018	0.029 ± 0.013	0.035 ± 0.007	0.072 ± 0.033 #
Rikenellaceae	0.044 ± 0.009	0.029 ± 0.008	0.050 ± 0.014	0.054 ± 0.014
Helicobacteraceae	0.017 ± 0.007	0.053 ± 0.026 *	0.031 ± 0.019	0.035 ± 0.022
Bacteroidaceae	0.008 ± 0.002	0.004 ± 0.003	0.021 ± 0.027	0.017 ± 0.016
Enterobacteriaceae	0.007 ± 0.002	0.001 ± 0.0006 *	0.053 ± 0.007	0.043 ± 0.074
Peptostreptococcaceae	0.0015 ± 0.0008	0.0359 ± 0.0025 **	0.0047 ± 0.0006 ##	0.0024 ± 0.0015 ##

*$P < 0.05$, **$P < 0.01$ vs the Control, #$P < 0.05$, ##$P < 0.01$ vs model.

DISCUSSION

CTX is an effective immunosuppressant, widely applied as a vital drug in cancer treatment and both blood and bone marrow transplants (5). However, CTX treatment can induce immunosuppression and intestinal flora dysfunction (32, 33). Polysaccharides could be used to alleviate the CTX-induced immunosuppression and intestinal dysbacteriosis (16, 17).

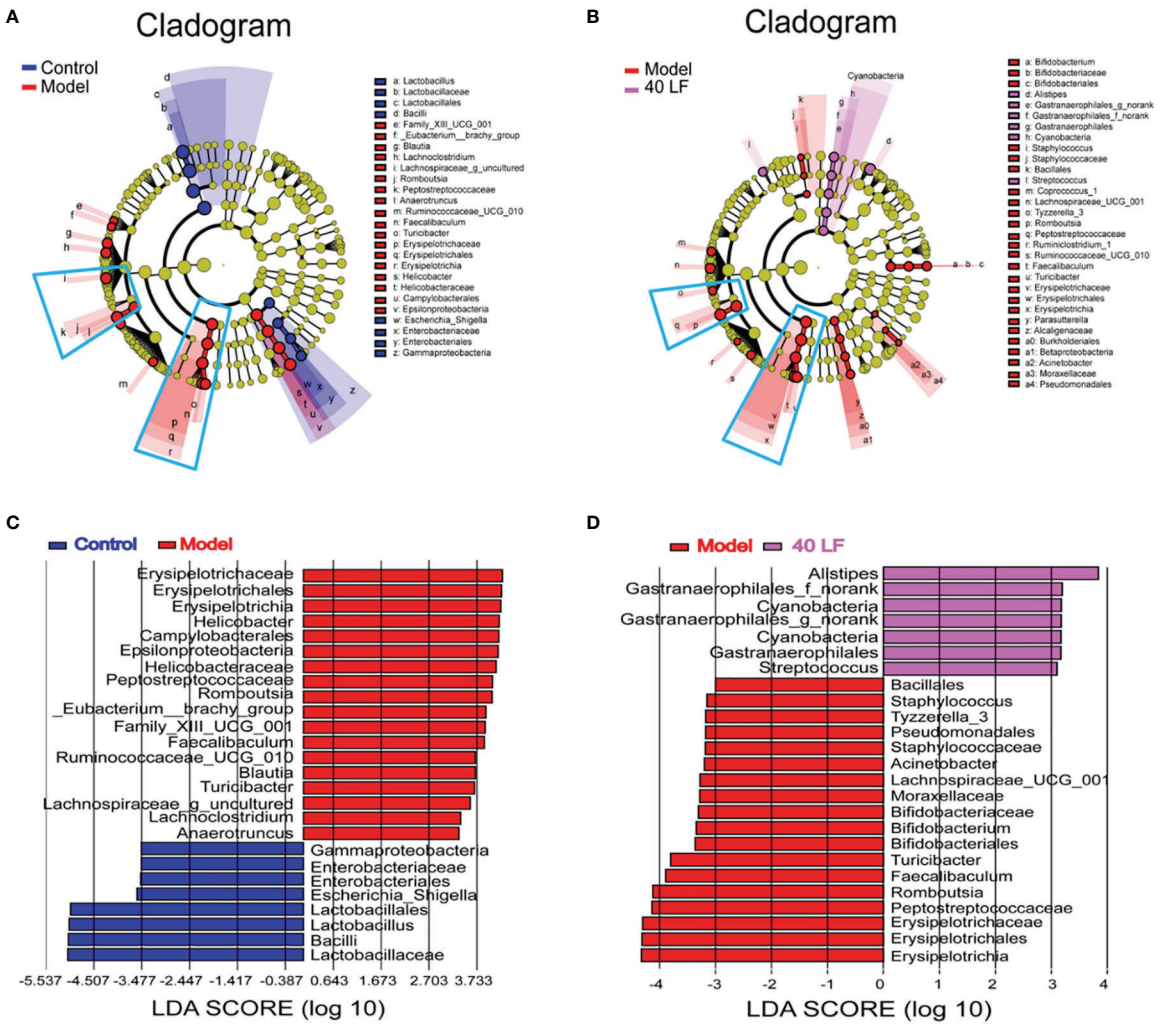

FIGURE 7 | The LEfSe and Spearman correlation analyses of the fecal microbes of the different mice groups (n = 4). **(A)** LEfSe analysis showing the key differential microbes of the CTX-induced mice. **(B)** LEfSe analysis showing the key differential microbes of the CTX-induced immunosuppressed mice subjected to the 40 LF intervention. **(C)** The LDA score between the control and the model groups. **(D)** The LDA score between the model and the 40-LF treated groups.

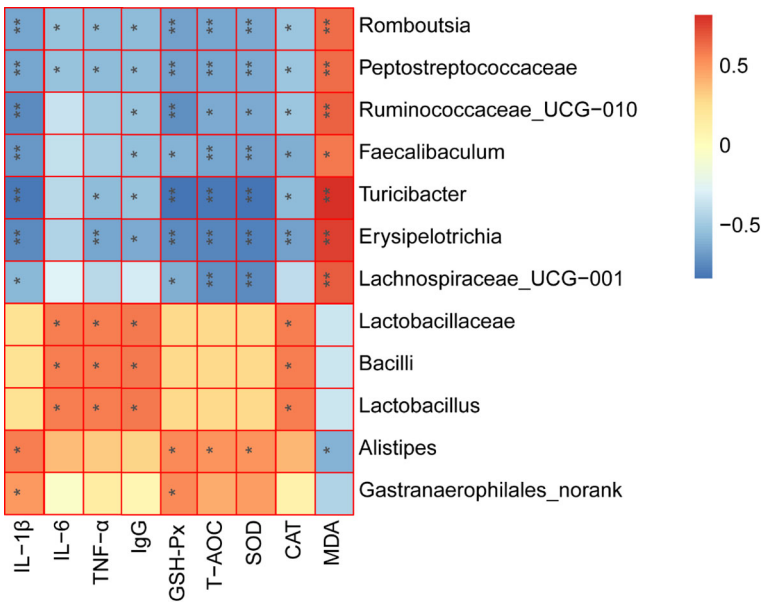

FIGURE 8 | Spearman correlation analysis between the key microbial communities and immune-related biochemistry parameters. *$P < 0.05$, **$P < 0.01$.

Forexample, Mulberry leaf-derived polysaccharide has the potential to modulate the immune response and gut microbiota composition in immunosuppressed mice (16). Millettia Speciosa Champ roots polysaccharides could modulate gut health and ameliorate CTX-induced intestinal injury and immunosuppression (17). In this work, immunosuppression was induced in mice to investigate the possible positive effects of LF treatment on such immunosuppression, as well as the intestinal flora dysfunction caused by CTX.

The ability of the spleen to induce lymphocytic proliferation is an important index of the body's immune response (26). As another important immune cell, macrophages exist in various cellular tissues and, together with neutrophils, constitute the first line of the body's immune defense, playing vital roles in non-specific and specific immunity (30). Macrophages are phagocytes derived from monocytes and play key roles in natural and specific immune systems (31). Activated macrophages can actively phagocytose and remove foreign antigens or directly kill pathogenic microorganisms. In this study, CTX significantly decreased the mice's T and B lymphocyte proliferation, suggesting an impaired cellular immune response, consistent with previous studies (26, 34). However, LF (20 mg/kg or 40 mg/kg) treatment could significantly promote the T and B lymphocytes proliferation. Moreover, the proliferative capacity and phagocytosis indices of peritoneal macrophages were also significantly increased after LF treatment. These results showed that LF treatment ameliorated the CTX injury to immune cells and enhanced the immune response of mice.

Cytokines are soluble extracellular polypeptides or glycoproteins indispensable in the immune response (29, 32). Immunoglobulins, secreted by B cells, are an important part of the immune response (29). CTX could decrease the serum levels of cytokines or immunoglobulins, causing a decrease in immunity (29, 31). Our results indicated that the IL-6, IL-1β, TNF-α, and IgG serum levels were decreased in the model group, which was consistent with previous studies (29, 31). However, after treatment with LF, both cytokines (IL-6, IL-1β, TNF-α) and IgG serum levels were significantly increased compared with the model, indicating that LF could promote IL-6, IL-1β, TNF-α, and IgG serum levels to improve immune function, consistent with the previous studies (23). The spleen and thymus are two important immune organs (35). In this work, the spleen and thymus indices were decreased significantly after CTX treatment, and HE staining results also indicated that CTX could induce apoptosis of the spleen and thymus, but LF treatment could reverse these adverse effects, suggesting that LF had a rescue effect. Sun et al. (24) that low-molecular-weight fucoidan from *Laminaria japonica* could increase the thymus and spleen index in the virus-infected mice, and our results were consistent with their studies. Furthermore, previous studies have shown a correlation between immune ecology and oxidative stress, and immune organ damage is closely related to oxidative stress (29, 36). Moreover, the dynamic balance between the oxidative and antioxidant states of the body plays a vital role in safeguarding the organism's health (30, 37). Polysaccharides have strong antioxidant properties and can ameliorate the CTX-induced low immunity by alleviating oxidative stress damage (30, 38). In this work, the spleen levels of GSH-Px, CAT, and SOD were significantly decreased, and MDA levels were significantly increased in the model group, consistent with previous studies (38). While GSH-Px, CAT, and SOD levels were significantly enhanced after LF treatment, MDA levels were

significantly reduced. These results suggested that LF could ameliorate the CTX-induced oxidative stress, consistent with our previous studies (25).

Gut flora plays key roles in shaping the immune system (39). CTX could modulate the intestinal flora composition, while polysaccharides also can modulate intestinal flora composition after CTX treatment, thus regulating the host's immunity (11, 29). In this work, after CTX treatment, the relative abundances of *Lactobacillaceae*, *Porphyromonadaceae*, *Rikenellaceae*, *Bacteroidaceae*, and *Enterobacteriaceae* were decreased, and the relative abundances of *Bacteroidales_S24-7_group*, *Ruminococcaceae, Lachnospiraceae*, *Helicobacteraceae*, and *Peptostreptococcaceae* were significantly increased. These results are in agreement with the work performed by Ding and collaborators (40). However, LF can reverse the CTX-induced changes in the abundance of bacteria at the family level. A comprehensive analysis of Lefse and community composition found that LF treatment significantly reversed the intestinal flora disturbance caused by CTX by significantly inhibiting the relative abundance of *Erysipelotrichia*, *Peptostreptococcaceae*, *Faecalibaculum*, *Turicibacter*, *Romboutsia*, and *Helicobacteraceae*. The relative abundance of *Erysipelotrichia* related groups, and beneficial strains, including *Lactobacillaceae*, *Alistipes*, *Gastranaerophilales*, *Cyanobacteria*, and *Streptococcus*, increased significantly. Further, the Spearman rank correlation coefficient was used to calculate the association between the intestinal key microbial species and host parameters. The results showed that 5 types of key microorganisms (*Romboutsia*, *Peptostreptococcaceae*, *Faecalibaculum*, *Turicibacter*, and *Erysipelotrichi*) were negatively correlated with immune characteristics, and 4 types of key microorganisms (*Lactobacillaceae*, *Bacilli*, *Lactobacillus*, and *Alistipes*) were positively correlated with immune characteristics.

CONCLUSION

In summary, LF enhanced the immune response by enhancing the secretion of cytokines and IgG, alleviating spleen and thymus injury in CTX-treated mice. In addition, LF could also regulate the intestinal flora disorder caused by CTX. These findings indicated that LF has the potential to be used as an immunoregulatory adjuvant or functional food additive to ameliorate CTX-induced immunosuppression.

DATA AVAILABILITY STATEMENT

The datasets presented in this study can be found in online repositories. The names of the repository/repositories and accession number(s) can be found below: https://www.ncbi.nlm.nih.gov/genbank/, PRJNA830087.

ETHICS STATEMENT

The animal study was reviewed and approved by Animal Ethics Committee of Zhejiang Ocean University.

AUTHOR CONTRIBUTIONS

YT and TH conceived the study and designed the project. YT, QP, QZ, YZ, and XJ performed the experiment and analyzed the data. YT drafted the manuscript. YT and TH revised the manuscript and supervised the whole study. All authors contributed to the article and approved the submitted version.

FUNDING

This work was financially supported by the Zhoushan Science and Technology Project (No.2022C41004), and the National Natural Science Foundation of China (No. 41806153).

REFERENCES

1. Chen XH, Wang SS, Chen GJ, Wang ZR, Kan JQ. The Immunomodulatory Effects of *Carapax Trionycisultrafine* Powder on Cyclophosphamide-Induced Immunosuppression in Balb/c Mice. *J Sci Food Agri* (2021) 101(5):2014–26. doi: 10.1002/jsfa.10819
2. Berkoz M, Yalin S, Ozkan-Yilmaz F, Ozluer-Hunt A, Krosniak M, Francik R, et al. Protective Effect of Myricetin, Apigenin, and Hesperidin Pretreatments on Cyclophosphamide-Induced Immunosuppression. *Immunopharmacol Immunotoxicol* (2021) 43(3):353–69. doi: 10.1080/08923973.2021.1916525
3. Lv L, Mu D, Du Y, Yan R, Jiang H. Mechanism of the Immunomodulatory Effect of the Combination of Live Bifidobacterium, Lactobacillus, Enterococcus, and Bacillus on Immunocompromised Rats. *Front Immunol* (2021) 12:694344. doi: 10.3389/fimmu.2021.694344
4. Parkin J, Cohen B. An Overview of the Immune System. *Lancet* (2001) 357 (9270):1777–89. doi: 10.1016/S0140-6736(00)04904-7
5. Ahlmann M, Hempel G. The Effect of Cyclophosphamide on the Immune System: Implications for Clinical Cancer Therapy. *Cancer Chemother Pharmacol* (2016) 78(4):661–71. doi: 10.1007/s00280-016-3152-1
6. Li CP, Duan SS, Li YP, Pan X, Han LR. Polysaccharides in Natural Products That Repair the Damage to Intestinal Mucosa Caused by Cyclophosphamide and Their Mechanisms: A Review. *Carbohydr Polym* (2021) 261:117876. doi: 10.1016/j.carbpol.2021.117876
7. Deng J, Zhong YF, Wu YP, Luo Z, Sun YM, Wang GE, et al. Carnosine Attenuates Cyclophosphamide-Induced Bone Marrow Suppression by Reducing Oxidative DNA Damage. *Redox Biol* (2018) 14:1–6. doi: 10.1016/j.redox.2017.08.003
8. Yu Y, Mo SR, Shen MY, Chen Y, Yu Q, Li ZD, et al. Sulfated Modification Enhances the Immunomodulatory Effect of Cyclocarya Paliurus Polysaccharide on Cyclophosphamide-Induced Immunosuppressed Mice Through MyD88-Dependent MAPK/NF-Kappa B and PI3K-Akt Signaling Pathways. *Food Res Int* (2021) 150(Pt A):110756. doi: 10.1016/j.foodres.2021.110756
9. Liu T, Wu Y, Wang L, Pang X, Zhao L, Yuan H, et al. A More Robust Gut Microbiota in Calorie-Restricted Mice Is Associated With Attenuated Intestinal Injury Caused by the Chemotherapy Drug Cyclophosphamide. *mBio* (2019) 10(2):02903–18. doi: 10.1128/mBio.02903-18
10. Shi H, Chang Y, Gao Y, Wang X, Chen X, Wang Y, et al. Dietary Fucoidan of *Acaudina Molpadioides* Alters Gut Microbiota and Mitigates Intestinal

Mucosal Injury Induced by Cyclophosphamide. *Food Funct* (2017) 8(9):3383–93. doi: 10.1039/C7FO00932A
11. Huang R, Xie J, Liu X, Shen M. Sulfated Modification Enhances the Modulatory Effect of Yam Polysaccharide on Gut Microbiota in Cyclophosphamide-Treated Mice. *Food Res Int* (2021) 145:110393. doi: 10.1016/j.foodres.2021.110393
12. Chu Q, Zhang Y, Chen W, Jia R, Yu X, Wang Y, et al. Apios Americana Medik Flowers Polysaccharide (AFP) Alleviate Cyclophosphamide-Induced Immunosuppression in ICR Mice. *Int J Biol Macromol* (2020) 144:829–36. doi: 10.1016/j.ijbiomac.2019.10.035
13. Jie D, Gao T, Shan Z, Song J, Zhang M, Kurskaya O, et al. Immunostimulating Effect of Polysaccharides Isolated From Ma-Nuo-Xi Decoction in Cyclophosphamide-Immunosuppressed Mice. *Int J Biol Macromol* (2020) 146:45–52. doi: 10.1016/j.ijbiomac.2019.12.042
14. Li C, Duan S, Li Y, Pan X, Han L. Polysaccharides in Natural Products That Repair the Damage to Intestinal Mucosa Caused by Cyclophosphamide and Their Mechanisms: A Review. *Carbohydr Polym* (2021) 261:117876. doi: 10.1016/j.carbpol.2021.117876
15. Shu G, Xu D, Zhao J, Yin L, Lin J, Fu H, et al. Protective Effect of *Polygonatum Sibiricum* Polysaccharide on Cyclophosphamide-Induced Immunosuppression in Chickens. *Res Vet Sci* (2021) 135:96–105. doi: 10.1016/j.rvsc.2020.12.025
16. Chen X, Cai B, Wang J, Sheng Z, Yang H, Wang D, et al. Mulberry Leaf-Derived Polysaccharide Modulates the Immune Response and Gut Microbiota Composition in Immunosuppressed Mice. *J Funct Food* (2021) 83(25):104545. doi: 10.1016/j.jff.2021.104545
17. Chen X, Sun W, Xu B, Wu E, Cui Y, Hao K, et al. Polysaccharides From the Roots of Millettia Speciosa Champ Modulate Gut Health and Ameliorate Cyclophosphamide-Induced Intestinal Injury and Immunosuppression. *Front Immunol* (2021) 12:766296. doi: 10.3389/fimmu.2021.766296
18. Huang W, Tan H, Nie S. Beneficial Effects of Seaweed-Derived Dietary Fiber: Highlights of the Sulfated Polysaccharides. *Food Chem* (2022) 373(Pt B):131608. doi: 10.1016/j.foodchem.2021.131608
19. Chen Y, Jin H, Yang F, Jin S, Liu C, Zhang L, et al. Physicochemical, Antioxidant Properties of Giant Croaker (*Nibea Japonica*) Swim Bladders Collagen and Wound Healing Evaluation. *Int J Biol Macromol* (2019) 138:483–91. doi: 10.1016/j.ijbiomac.2019.07.111
20. Yu FM, He K, Dong XZ, Zhang ZW, Wang FL, Tang YP, et al. Immunomodulatory Activity of Low Molecular-Weight Peptides From *Nibea Japonica* Skin in Cyclophosphamide-Induced Immunosuppressed Mice. *J Funct Food* (2020) 68:103888. doi: 10.1016/j.jff.2020.103888
21. Li HY, Yi YL, Guo S, Zhang F, Yan H, Zhan ZL, et al. Isolation, Structural Characterization and Bioactivities of Polysaccharides From *Laminaria Japonica*: A Review. *Food Chem* (2021) 370:131010. doi: 10.1016/j.foodchem.2021.131010
22. Peng Y, Song Y, Wang Q, Hu Y, He Y, Ren D, et al. *In Vitro* and *In Vivo* Immunomodulatory Effects of Fucoidan Compound Agents. *Int J Biol Macromol* (2019) 127:48–56. doi: 10.1016/j.ijbiomac.2018.12.197
23. Hwang PA, Lin HTV, Lin HY, Lo SK. Dietary Supplementation With Low-Molecular-Weight Fucoidan Enhances Innate and Adaptive Immune Responses and Protects Against *Mycoplasma Pneumoniae* Antigen Stimulation. *Mar Drugs* (2019) 17(3):175. doi: 10.3390/md17030175
24. Sun TH, Zhang XH, Miao Y, Zhou Y, Shi J, Yan MX, et al. Studies on Antiviral and Immuno-Regulation Activity of Low Molecular Weight Fucoidan From. *Laminaria Japonic J Ocean U China* (2018) 17(3):705–11. doi: 10.1007/s11802-018-3794-1
25. Tian SS, Jiang XX, Tang YP, Han T. *Laminaria Japonica* Fucoidan Ameliorates Cyclophosphamide-Induced Liver and Kidney Injury Possibly by Regulating Nrf2/HO-1 and TLR4/NF-Kappa B Signaling Pathways. *J Sci Food Agr* (2021) 102(6):2604–12. doi: 10.1002/jsfa.11602
26. Han L, Lei H, Tian Z, Wang X, Cheng D, Wang C. The Immunomodulatory Activity and Mechanism of Docosahexenoic Acid (DHA) on Immunosuppressive Mice Models. *Food Funct* (2018) 9(6):3254–63. doi: 10.1039/C8FO00269J
27. Zhou YF, Tian SS, Qian L, Jiang S, Tang YP, Han T. DHA-Enriched Phosphatidylserine Ameliorates Non-Alcoholic Fatty Liver Disease and Intestinal Dysbacteriosis in Mice Induced by a High-Fat Diet. *Food Funct* (2021) 12(9):4021–33. doi: 10.1039/D0FO03471A
28. Liu ZB, Chen Q, Zhang C, Ni L. Comparative Study of the Anti-Obesity and Gut Microbiota Modulation Effects of Green Tea Phenolics and Their Oxidation Products in High-Fat-Induced Obese Mice. *Food Chem* (2022) 367:130735. doi: 10.1016/j.foodchem.2021.130735
29. Zhao Y, Yan Y, Zhou W, Chen D, Huang K, Yu S, et al. Effects of Polysaccharides From Bee Collected Pollen of Chinese Wolfberry on Immune Response and Gut Microbiota Composition in Cyclophosphamide-Treated Mice. *J Funct Food* (2020) 72(3):104057. doi: 10.1016/j.jff.2020.104057
30. Xia XW, Hao H, Zhang XY, Wong IN, Chung SK, Chen ZX, et al. Immunomodulatory Sulfated Polysaccharides From *Caulerpa Racemosa* Var. Peltata Induces Metabolic Shifts in NF-KB Signaling Pathway in RAW 264.7 Macrophages. *Int J Biol Macromol* (2021) 182:321–32. doi: 10.1016/j.ijbiomac.2021.04.025
31. Yu F, Zhang Z, Ye S, Hong X, Jin H, Huang F, et al. Immunoenhancement Effects of Pentadecapeptide Derived From *Cyclina Sinensis* on Immune-Deficient Mice Induced by Cyclophosphamide. *J Funct Food* (2019) 60 (1):103408. doi: 10.1016/j.jff.2019.06.010
32. Zhu G, Jiang Y, Yao Y, Wu N, Luo J, Hu M, et al. Ovotransferrin Ameliorates the Dysbiosis of Immunomodulatory Function and Intestinal Microbiota Induced by Cyclophosphamide. *Food Funct* (2019) 10(2):1109–22. doi: 10.1039/C8FO02312C
33. Zhao S, Peng X, Zhou Q, Huang Y, Rao X, Tu J, et al. *Bacillus Coagulans* 13002 and Fructo-Oligosaccharides Improve the Immunity of Mice With Immunosuppression Induced by Cyclophosphamide Through Modulating Intestinal-Derived and Fecal Microbiota. *Food Res Int* (2021) 140:109793. doi: 10.1016/j.foodres.2020.109793
34. Liu Y, Wu X, Wang Y, Jin W, Guo Y. The Immunoenhancement Effects of Starfish *Asterias Rollestoni* Polysaccharides in Macrophages and Cyclophosphamide-Induced Immunosuppression Mouse Models. *Food Funct* (2020) 11(12):10700–8. doi: 10.1039/D0FO01488E
35. Ma T, Li C, Zhao F, Cao J, Zhang X, Shen X. Effects of Co-Fermented Collagen Peptide-Jackfruit Juice on the Immune Response and Gut Microbiota in Immunosuppressed Mice. *Food Chem* (2021) 365:130487. doi: 10.1016/j.foodchem.2021.130487
36. Shi J, Zhang Q, Zhao X-H, Wang L. The Impact of Caseinate Oligochitosan-Glycation by Transglutaminase on Amino Acid Compositions and Immune-Promoting Activity in BALB/c Mice of the Tryptic Caseinate Hydrolysate. *Food Chem* (2021) 350:129302. doi: 10.1016/j.foodchem.2021.129302
37. Jiang S, Zhang Z, Huang F, Yang Z, Yu F, Tang Y, et al. Protective Effect of Low Molecular Weight Peptides From *Solenocera Crassicornis* Head Against Cyclophosphamide-Induced Nephrotoxicity in Mice *via* the Keap1/Nrf2 Pathway. *Antioxidants* (2020) 9(8):745. doi: 10.3390/antiox9080745
38. Han L, Meng M, Guo M, Cheng D, Shi L, Wang X, et al. Immunomodulatory Activity of a Water-Soluble Polysaccharide Obtained From Highland Barley on Immunosuppressive Mice Models. *Food Funct* (2019) 10(1):304–14. doi: 10.1039/C8FO01991F
39. Geuking MB, Koller Y, Rupp S, McCoy KD. The Interplay Between the Gut Microbiota and the Immune System. *Gut Microbes* (2014) 5(3):411–8. doi: 10.4161/gmic.29330
40. Ding Y, Yan YM, Chen D, Ran LW, Mi J, Lu L, et al. Modulating Effects of Polysaccharides From the Fruits of *Lycium Barbarum* on the Immune Response and Gut Microbiota in Cyclophosphamide-Treated Mice. *Food Funct* (2019) 10(6):3671–83. doi: 10.1039/C9FO00638A

Conflict of Interest: The authors declare that the research was conducted in the absence of any commercial or financial relationships that could be construed as a potential conflict of interest.

Publisher's Note: All claims expressed in this article are solely those of the authors and do not necessarily represent those of their affiliated organizations, or those of the publisher, the editors and the reviewers. Any product that may be evaluated in this article, or claim that may be made by its manufacturer, is not guaranteed or endorsed by the publisher.

Copyright © 2022 Tang, Pu, Zhao, Zhou, Jiang and Han. This is an open-access article distributed under the terms of the Creative Commons Attribution License (CC BY). The use, distribution or reproduction in other forums is permitted, provided the original author(s) and the copyright owner(s) are credited and that the original publication in this journal is cited, in accordance with accepted academic practice. No use, distribution or reproduction is permitted which does not comply with these terms.

frontiers | Frontiers in Nutrition

ORIGINAL RESEARCH
published: 15 June 2022
doi: 10.3389/fnut.2022.922569

Structure Characterization, Immunological Activity, and Mechanism of a Polysaccharide From the Rhizome of *Menispermum dauricum* DC

Pei Yang[1†], *Juan Jin*[1†], *Yan Ma*[1], *Fengshan Wang*[2], *Yaying Li*[3], *Baoguo Duan*[4], *Yongqing Zhang*[1*] *and Yuhong Liu*[1*]

[1] School of Pharmaceutical Sciences, Collaborative Innovation Center for Quality Control and Construction of the Whole Industrial Chain of Traditional Chinese Medicine, Shandong University of Traditional Chinese Medicine, Jinan, China, [2] National Medical Products Administration Key Laboratory for Quality Research and Evaluation of Carbohydrate-Based Medicine, Jinan, China, [3] Experimental Center, Shandong University of Traditional Chinese Medicine, Jinan, China, [4] Sishui Siheyuan Culture and Tourism Development Company, Ltd., Sisui, China

OPEN ACCESS

Edited by:
Bin Du,
Hebei Normal University of Science and Technology, China

Reviewed by:
Radjassegarin Arumugam,
A. V. C. College, India
Ding-Tao Wu,
Chengdu University, China

***Correspondence:**
Yuhong Liu
yhliu@sdutcm.edu.cn
Yongqing Zhang
zyq622003@126.com

[†] These authors have contributed equally to this work

Specialty section:
This article was submitted to Nutritional Immunology, a section of the journal Frontiers in Nutrition

Received: 18 April 2022
Accepted: 12 May 2022
Published: 15 June 2022

Citation:
Yang P, Jin J, Ma Y, Wang F, Li Y, Duan B, Zhang Y and Liu Y (2022) Structure Characterization, Immunological Activity, and Mechanism of a Polysaccharide From the Rhizome of Menispermum dauricum DC. Front. Nutr. 9:922569. doi: 10.3389/fnut.2022.922569

The purpose of this study was to investigate the structural characterization and immunological activity *in vitro* and *in vivo* of a polysaccharide from the rhizome of *Menispermum dauricum*. A new polysaccharide named MDP was isolated from the rhizome of *Menispermum dauricum* by hot water extraction, ethanol precipitation, anion-exchange, and gel-filtration chromatography. MDP was homogeneous and had a molecular weight of 6.16×10^3 Da, and it was an α-D-glucan containing a (1→ 6)-linked backbone, with a glucosyl residue at the C-3 position along the main chain. MDP exhibited immunological activity *in vitro*, which could significantly promote the proliferation and phagocytosis of RAW264.7 cells and the release of TNF-α and IL-6 factors. For immunological activity *in vivo*. MDP could significantly increase the thymus and spleen indices, enhance the macrophage function, increase the level of cytokine (IL-6 and TNF-α) and immunoglobulin IgM in the serum and regulate T lymphocyte subsets. Furthermore, MDP elevated the expression of the critical nodes in the TLR4-MyD88 signaling pathways *in vivo*. These results support the concept that MDP may exhibit immunological activity through TLR4-MyD88 signaling pathway in *vivo*.

Keywords: ***Menispermum dauricum*** **DC, polysaccharide, structure characterization, immunological activity, TLR4**

INTRODUCTION

The immune system is an essential defense system which can defend against foreign invasion. It has the capacity to cooperate with other body systems to sustain the stability and physiological balance of the body (1, 2). Immunosuppression is the inhibition of the immune response, which can bring about a variety of diseases such as urinary tract infection, meningitis, and sepsis (1, 2). Therefore, maintaining the normal state of the immune system to reduce immunosuppression is significant in preventing the occurrence of various diseases.

The traditional treatment of immunosuppression has so far been mainly chemical drugs. The immunopotentiators commonly used in clinical practice currently include levamisole, isoprinosine, interferon, interleukin, BCG, etc. Among them, levamisole and isoprinosine are chemically synthesized drugs; interferon, interleukin and BCG are originated from microorganisms (3). However, these drugs are generally accompanied by many side effects, such as nausea, vomiting, abdominal pain and other gastrointestinal reactions; some drugs may lead to anaphylactic shock and even death, take BCG, for example (4). Due to the drawbacks of pharmaceutical therapy, the interest of researchers in the active ingredients of natural origin had remarkably increased throughout the past decades, especially for polysaccharide components of various traditional Asian medicines. Many pharmacological effects of polysaccharides have been recently discovered, including liver protection, resistance to oxidation and aging, and anticancer properties. Polysaccharides obtained from various traditional medicinal plants also had been proven to exert profound effects on the immune system *in vivo* and *in vitro* through their capacity to modulate immune function, including cytokine/chemokine production, reactive oxygen species (ROS) production, and cell proliferation. It has promising possibilities as an immunomodulator having no significant side effects (5).

The rhizome of *Menispermum dauricum DC* (Menispermaceae), called Bei Dou Gen in Chinese, is a traditional Chinese medicinal herb that has been used widely in clinical practice for treating rheumatic arthralgia, dysentery, colitis, and sore throats (6). Alkaloids are the main chemical components of the rhizome of *M. dauricum* and possess various bioactivities, including antiarrhythmic, antitumor and cardiovascular effects (7–9). Moreover, the injection of total alkaloids has been applied clinically for a long time to treat chronic tracheitis, throat sores and arthralgia (10). Nevertheless, the polysaccharides from the rhizome of *M. dauricum* have received little attention. Only a few researchers reported its preparation, antitumor (11, 12), and anti-mutagenic (13) activities. Unfortunately, there was no research on the structure and the immunological activity of the polysaccharide of the rhizome of *M. dauricum*, which greatly limits its further development and utilization. Thus, an in-depth study of the immunological activity and structural characterization of polysaccharides from the rhizome of *M. dauricum* requires thorough studies.

In the present research, isolation of the novel polysaccharide (MDP) was conducted from the rhizome of *M. dauricum* and its structural characterization was performed. Furthermore, the immunological effects and potential mechanism of action of MDP were carried out.

MATERIALS AND METHODS

Materials and Chemicals

Shandong Baiweitang Chinese Herbal Pieces Co., Ltd. (Jinan, Shandong Province, China) supplied the rhizome of *M. dauricum* (No. 181201). The voucher sample of rhizome of *M. dauricum* was deposited in the School of Pharmaceutical Sciences of Shandong University of Traditional Chinese Medicine, Jinan, China.

Chemicals: Yuanye Biological Co., Ltd. (Shanghai, China) supplied the DEAE-cellulose-52. GE Healthcare Life Sciences (Piscataway, NJ, USA) supplied Sephadex G-50 and Sephacryl S-100. Guoyao Group Co., Ltd. (Beijing, China) supplied galactose and glucose. Macklin Biochemical Technology Co., Ltd. (Shanghai, China) supplied arabinose and xylose. The purchase of DMEM was achieved from GIBCO (USA) with supplementing of 1% streptomycin, 10% FBS, and 1% penicillin. Sigma-Aldrich (St. Louis, MO, USA) supplied LPS. Enzyme-linked Biotechnology Co., Ltd. (Shanghai, China) supplied ELISA kits, which were used in the NO, TNF-α, IL-6, and IgM tests. Injectable levamisole (LMS) was purchased from Yuanye Biological Co., Ltd. (Shanghai, China). Injectable cyclophosphamide (CTX) was purchased from Jiangsu Hengrui Medicine Co. (Lianyungang, Jiangsu, China). Antibodies against MyD88, NFκB, and JNK were purchased from ABclonal (Wuhan, China) and other antibodies were obtained from Cell Signaling Technology (Beverly, MA, USA).

Extraction and Purification of Polysaccharide

The extraction of crude polysaccharides from the rhizome of *M. dauricum* was conducted with distilled water every 3 h at a temperature of 87°C at a ratio of 20:1 (w/w). The aqueous extract was concentrated under vacuum after three rounds of extraction. Subsequently, four times the volume of ethanol was added for the purpose of precipitating the polysaccharide, and the mixture was allowed to stand at 4°C overnight (14). The precipitate was collected and deproteinized by means of the TCA-n-butanol method (15) and then subjected to freeze-drying so as to yield a crude polysaccharide fraction (CMDP).

The CMDP was purified with the DEAE-52 cellulose column (5.5 × 30 cm) and eluted using distilled water as well as 0.1 M, 0.2 M, 0.3 M, and 0.5 M NaCl. The fraction eluted using 0.2 M NaCl was found to have the highest polysaccharides yield. As a result, it was collected and dialyzed to remove NaCl and then further purified by Sephacryl S-100 column (1.75 × 66 cm) and Sephadex G-50 column (1.75 × 66 cm) eluted with deionized water. The solution obtained after elution was then collected based on the phenol-sulfuric acid approach, and the major fraction was collected and lyophilized for the purpose of acquiring a white purified polysaccharide (MDP).

Determination of Total Carbohydrate and Protein

The determination of the contents of total carbohydrates and proteins was performed by performing a phenol-sulfuric acid test (16) as well as a Folin–phenol test (17), respectively.

Analysis of the Molecular Weight

The estimations for the homogeneity and average molecular weight of MDP were performed with the aid of the Agilent 1200 system (Agilent Technologies, Palo Alto, CA, USA) utilizing the high-performance gel permeation chromatography (HPGPC) coupled with PL aquagel-OH MIXED-M gel column (7.5 ×

300 mm, Agilent, Palo Alto, CA, USA) as well as refractive index detector (RID, Agilent Technologies, Palo Alto, CA, USA). The column was subjected to an elution at a flow rate of 1 mL/min with the use of a 0.1 mol/L $NaNO_3$. Dextrans having different molecular weights (Sigma, USA) were utilized as the standard for molecular weight determination (18).

Structure Characterization

Analysis of the Monosaccharide Composition

An analysis of the MDP monosaccharide composition was conducted by means of thin-layer chromatography (TLC) and GC-MS (Agilent Technologies, USA) coupled with an HP-5 capillary column (30 m×250 μm i.d., 0.25 μm film thickness). MDP (10 mg) was added to 6 mL of 2 mol/L trifluoroacetic acid (TFA) and hydrolyzed at 110°C for 3 h. Through concentrating under reduced pressure, the mixture was classified into two parts after removing TFA. TLC was used to analyze one part of the hydrolysate to determine whether the sample was hydrolyzed completely and contained uronic acid. Monosaccharide standards and hydrolyzed MDP were acetylated through the addition of acetic anhydride and pyridine, after which analysis was performed by GC-MS. The temperature program was 170°C for 3 min, 170–178°C at a rate of 0.5°C/min for 3 min, and then increased to 210°C for 5 min at a rate of 2°C/min.

Methylation Analysis

Methylation of polysaccharides was carried out in accordance with Need's method with some adjustments (19). After methylation, hydrolysis, reduction, and acetylation, which are the basic steps of methylation, the polysaccharide samples were subjected to GC-MS analysis. The dried MDP (10 mg) was dissolved with the use of 3 mL of dimethyl sulfoxide and stirred at room temperature until the polysaccharide sample was dissolved entirely. Sodium hydroxide (60 mg) was added and ground into a fine powder, and then the mixture was stirred for 1 h at room temperature. After the reaction, 2.5 mL of CH_3I was gradually dropped into the sample under a nitrogen environment, and the reaction was continued at 20°C for 1 h while avoiding light. For the purpose of terminating the reaction, 2 mL of distilled water was then added. Three extractions of the methylated polysaccharides were performed with 5 ml of chloroform, and the chloroform extract was collected and then extracted with deionized water 4 times to remove water-soluble impurities in the chloroform extract. This methylation procedure was carried out 4 times, and confirmation of the full methylation was established based on the absence of hydroxyl peaks in the IR spectrum.

Depolymerization of the dried permethylated product was performed at 100°C with 90% HCOOH for 6 h and further hydrolyzed for 3 h with the use of 2 M TFA at 110°C. Reducting of the residues was conducted with $NaBH_4$, followed by acetylation with the use of the acetic anhydride. Lastly, redissolving of the methylated alditol acetates were achieved in $CHCl_3$, followed by GC-MS analysis. The GC temperature program was 170°C for 3 min, 170–178°C for 3 min at a rate of 0.5°C/min, and increased to 210°C for 5 min at a rate of 2°C/min. These alditol derivatives were obtained by GC-MS database and published literature combined with the relative retention times on GC-MS, and the assessment of the molar ratios was completed according to the response factors and the peak areas.

Periodate Oxidation and Smith Degradation

The reported approach was used in treating the MDP sample (20). In short, MDP was dissolved in 15 mmol/L sodium periodate and kept in darkness at room temperature. Monitoring of $NaIO_4$ consumption was performed with the aid of a UV-2550 spectrophotometer every 12 h at 223 nm until the absorption value observed became stable. After the completion of the oxidation reaction, excess $NaIO_4$ was removed through the addition of ethylene glycol. Determination for the production of formic acid was performed by titration with 0.01 M NaOH. The reaction solution was then dialyzed for 48 h (MW cutoff: 500 Da) and the addition of 50 mg of $NaBH_4$ was done to reduce and dialyze again. Next, 2 M TFA was added to hydrolyze the polysaccharide solution. After complete hydrolysis, methanol was added under a reduced pressure to remove the acid by evaporation. Lastly, by performing GC-MS analysis, we investigated the acetylated product.

Analysis for FT-IR and UV Spectroscopy

MDP was ground with the use of KBr powder, after which it was pressed into pellets. Then, FT-IR analysis was conducted on Fourier transform infrared (FT-IR, PerkinElmer Co., Ltd., USA) instrument in the 4,000–400 cm^{-1} region. We recorded the UV spectra of MDP in a 200–400 nm wavelength range with the aid of a UV-2800 UV-visible spectrophotometer (Shimadzu Inc., Japan).

NMR Spectroscopy Analysis

A total of 20 mg MDP fraction that was already dried was kept over P_2O_5 under vacuum for several days, followed by dissolving in 0.5 mL of D_2O. The ^1H-^{13}C HSQC, HMBC, ^1H NMR, ^{13}C NMR, and ^1H-^1H COSY spectra were observed using a Bruker AV-600 spectrometer (Germany) at 28°C.

Immunological Activity *in vitro*

Cell Culture

We acquired RAW264.7 cells from Beina Chuanglian Biotechnology Co., Ltd. (Beijing, China). The cells were subjected to incubation in DMEM supplemented with penicillin (100 units/mL), 10% FBS, and streptomycin sulfate (100 μg/mL) at a temperature of 37°C in a humidified 5% CO_2 incubator atmosphere.

Cell Viability Test

The impact of MDP at different concentrations on RAW264.7 cell viability was explored by performing the MTT assay *in vitro*. In short, RAW264.7 cells were seeded at a density of 1 × 10^4 cells/well into 96-well microplates. After the cells were subjected to incubation at 37°C for 24 h with 5% CO_2, then incubated for 24 h with MDP samples (0, 10, 50, 100, 200, and 400 μg/mL) or LPS (1 μg/mL, positive control) additionally. After incubation, an addition of 20 μL of the MTT solution (5 mg/mL) was added to each well and then incubated again at 37°C for an additional 4 h in the medium. Afterward, each

well was subjected to treatment with 150 μL of DMSO for the purpose of dissolving formazan crystals after careful aspiration of the medium. Finally, we utilized a microplate reader (BioTek Instruments Inc., Winooski, VT, USA) with the purpose of detecting the absorbance at 570 nm.

$$\text{Cell viability \%} = (OD_{\text{treatment group}})/(OD_{\text{control group}}) \times 100\%.$$

NO, TNF-α, and IL-6 Measurement

After incubation of RAW264.7 cells for 24 h with polysaccharide samples as shown above, determination of the expression levels of NO, TNF-α, and IL-6 in the culture supernatants was performed with the aid of the enzyme-linked immunosorbent assay (ELISA) kits (ML BIO Biotechnology, Shanghai, China). Assays were conducted following the instructions provided by the manufacturer, and cytokine concentrations were computed based on the standard curves.

Phagocytic Activity Determination

An analysis of the phagocytic activity was performed through flow cytometry. RAW264.7 macrophages were cultured in an incubator at a density of 1×10^5 cells/well in a 24-well plate for 24 h. Subsequently, cells were subjected to incubation for 24 h with MDP (50, 100, 200, and 400 μg/mL) or LPS (1 μg/mL), after which the medium was changed with 1 mL PBS comprising 100 μL FITC-dextran (1 mg/mL). The plate was then allowed to be incubated in an incubator for an additional 30 min. Afterward, phagocytosis was halted through the addition of 2 mL of ice-cold PBS, after which cold PBS was utilized for the purpose of washing the cells 3 times (21). Flow cytometry was used in analyzing the phagocytic activity (Beckman, Sanjose, CA, USA) using Flow Jo software.

Measurement of Reactive Oxygen Species (ROS)

RAW 264.7 cells (1×10^5 cells/mL) were subjected to seeding in a 6-well flat-bottom plate and incubation for 24 h. Each well was cultured with the aid of several concentrations of MDP solutions (50, 100, 200, and 400 μg/mL). The positive control group was treated with 50 μg/mL Rosup provided in the kit for 30 min. Next, the cells were exposed for an additional 30 min to DCFH-DA (10 μM), after which they were washed 3 times with PBS. Finally, flow cytometry was utilized in measuring fluorescence.

Immunological Activity *in vivo*

Animal Treatment and Experimental Design

SPF Male BALB/c mice (18–22 g) were procured from Weitonglihua Laboratory Animal Technology Co., Ltd. (Beijing, China). The animals were provided with water and mouse chow *ad libitum*, and were housed in a rodent facility at 22 ± 1°C with a 12 h light-dark cycle for acclimatization. After 5 days environmental adaptation period, mice were randomly divided into five groups: the control group, CTX model group, the positive group (CTX+LMS), the low and high doses of MDP groups (CTX+MDP-L and CTX+MDP-H). MDP groups were treated with MDP (100, 200 mg/kg, i.g.) once daily on a continuous basis for 14 days. All experiments used 12 mice per group. The positive group was given LMS at a dose of 10 mg/kg (i.p.) at the same frequency. While only saline was given to the control and CTX groups. On the 10–12th days, CTX (80 mg/kg, i.p.) was given to all the groups with the exception of the control group to induce the state of immunosuppression.

Phagocytosis of Mononuclear

Mice were given a tail vein injection of diluted India ink (100 μL/10 g). Blood samples were collected from the retroorbital vein at 2 min (t_1) and 10 min (t_2), and 20 μL of blood samples were mixed with 2 mL of 0.1% sodium carbonate solution. The absorbance was measured by UV-Vis spectrophotometer at 675 nm, where OD_1 was the absorbance at t_1 and OD_2 was the t_2. The phagocytic index was calculated as the following formula:

$$\begin{aligned} K &= (\lg OD_1 - \lg OD_2)/(t_2 - t_1) \\ \text{Phagocytic index } \alpha &= \sqrt[3]{K} \times A/(B + C) \end{aligned} \quad (1)$$

Where A is the body weight, B is the liver weight and C is the spleen weight.

Spleen and Thymus Indices

Twenty-four hours after the last dose, mice were weighed and sacrificed. The spleen and thymus were removed and weighed. The spleen and thymus indices were calculated according to the following formula: thymus or spleen index (mg/g) = (weight of thymus or spleen/body weight).

Measurements of IgM, IL-6, and TNF-α in Serum

Serum levels of IgM, IL-6, and TNF-α were determined by colorimetry. The colorimetry was read with an enzymatic reader using the mouse ELISA kit according to the instructions.

Histochemical Examinations of Spleen

The Hematoxylin and eosin (HE) staining of the spleen tissues were performed to assess the histopathological condition and photographed under the microscope.

Immunohistochemistry of Spleen

Positioning of CD4 and CD8 was visualized by immunohistochemical staining as previously described (22). Histological sections (4 μm) were prepared from formalin-fixed, paraffin-embedded tissues. After deparaffinization and rehydration for antigen retrieval, slides were heated in 10 mM citrate buffer (pH 6.0) in a microwave oven and cooled to room temperature.

Western Blot Assay

Spleen tissue stored at −80°C was centrifuged (12,000 *g*, 20 min, 4°C) after homogenization in an ice bath with lysis buffer for 5 min. BCA assay was used to determine the protein content. The proteins denatured were separated with loading onto 10% SDS-PAGE by electrophoresis and transferred to PVDF membranes. 10% skim milk (made in TBS that contains 0.1% Tween 20) was utilized to block the membrane at room temperature for 4 h. The membranes were incubated with primary antibodies against TLR4 (1:1000), MyD88 (1:1500), p-NFκB (1:1000), NFκB (1:1500), p-JNK (1:2000), JNK (1:1500),

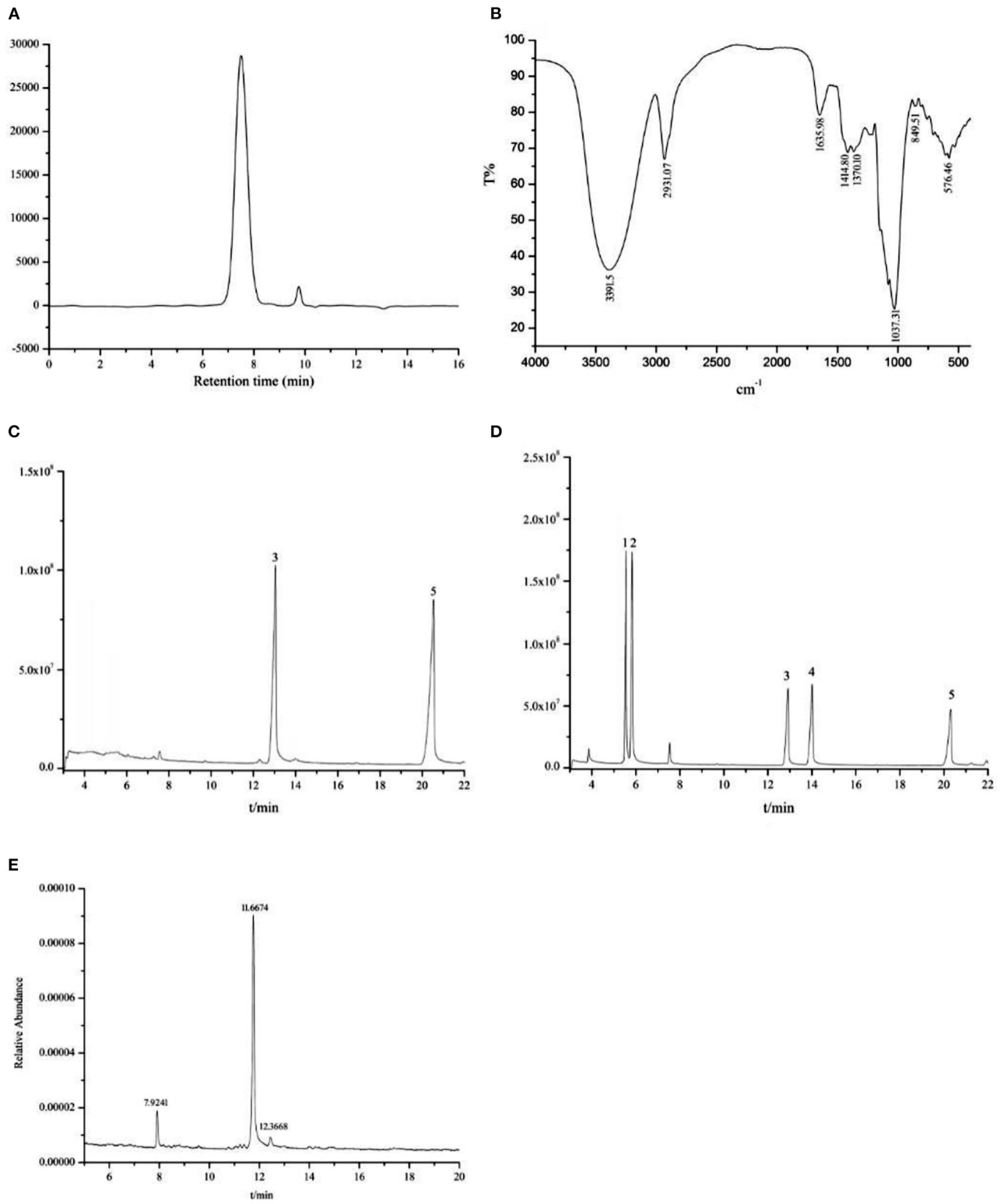

FIGURE 1 | The physicochemical properties and structure characterization of MDP. **(A)** HPGPC chromatogram of MDP; **(B)** FT-IR of MDP. **(C)** GC-MS study of the monosaccharide composition of MDP; **(D)** GC-MS analysis of mixed standards. (1) Ara; (2) Xyl; (3) Glc; (4) Gal; (5) internal standard; **(E)** GC-MS analysis of the MDP methylation product.

TABLE 1 | GC–MS data of alditol acetate derivatives from the methylated product of MDP.

Methylated sugars (as alditol acetates)	Linkage type	Molar ratio	Mass fragments (m/z)
2,3,4,6-O-Me_4-Glc	Glcp-(1→	2.24	43; 71; 87; 101; 117; 129; 145; 161; 205
2,3,4-O-Me_3-Glc	→ 6)-Glcp-(1→	31.27	43; 87; 113; 117; 129; 161; 173; 189; 233
2,4-O-Me_2-Glc	→ 3,6)-Glcp-(1→	1.00	43; 87; 99; 101; 117; 129; 189; 233

p-ERK (1:1500), ERK (1:1500), p-P38 (1:1000), P38 (1:750) according to the manufacturer's instructions. After being washed 3 times with TBST, the membranes were incubated with the secondary antibody (1:5000) at room temperature for 1 h. The signal was detected with an ECL chemiluminescence detection kit (Millipore, Massachusetts, USA) and quantified by Amersham Imager 600 Chemiluminescence imaging system (GE, Boston, USA).

Statistical Analysis

All data obtained were expressed as mean ± standard deviation (SD). One-way method of variance (ANOVA) was used to determine the statistical significance of different groups. The SPSS 20.0 software was used for all statistical analyses, $^*P < 0.05$ was regarded as statistically significant.

RESULTS AND DISCUSSION

Extraction and Purification of MDP

CMDP was acquired from the rhizome of *M. dauricum* with a yield of 3.00 ± 0.14% (w/w), after a number of processing steps, which include hot water extraction, ethanol precipitation, and deproteinization by the TCA-n-butanol method. CMDP was purified through DEAE-cellulose with 0.2 M NaCl solution as the eluent and then further purified by Sephacryl S-100 and Sephadex G-50 chromatography with deionized water for the purpose of obtaining a purified polysaccharide (MDP), the yield of MDP was 0.72 ± 0.05%. The results showed that MDP is predominantly composed of polysaccharides (95.32%) with almost no protein (0.38%).

Physicochemical Properties of MDP

The appearance of MDP was a white powder. Monitoring UV absorption at 280 or 260 nm revealed that there were hardly any proteins or nucleic acids. The HPGPC elution profile of MDP (**Figure 1A**) displayed a single symmetrical and narrow peak, suggesting that it was a homogeneous polysaccharide. According to the calibration curve of the dextran standard ($y = -0.7982x + 9.753$, $r = 0.9992$) obtained by Agilent GPC software, the molecular weight of MDP was $\sim 6.16 \times 10^3$ Da. The FT-IR spectrum of MDP (**Figure 1B**) revealed that the absorption was highly significant at 3,391.5 cm^{-1}, which attributed to the angular vibration and stretching vibration of the O-H linkage of the polysaccharide. The signal at 2,931.07 cm^{-1} contributed to the stretching vibration of C-H in the sugar ring. The presence of α-configuration glycosidic bonds in MDP was confirmed by a characteristic absorption at 849.51 cm^{-1}.

Structural Characterization of MDP

TLC (**Supplementary Figure 1**) and GC-MS analysis (**Figures 1C,D**) suggested that MDP did not contain uronic acid and consisted only of glucose.

The completely methylated MDP product was hydrolyzed with acid, transformed into alditol acetate, and subjected to a GC–MS analysis (**Figure 1E**). Three main peaks were observed with retention times of 7.9421, 11.6674, and 12.3668, and the three kinds of derivatives were identified as 1,5-di-O-acetyl-2,3,4,6-tetra-O-methyl-glucitol, 1,5,6-tri-O-acetyl-2,3,4-tri-O-methyl-glucitol, and 1,3,5,6-tetra-O-acetyl-2,4-di-O-methyl-glucitol. The results revealed that MDP was composed of (1→ 6)-linked, (1→ 3, 6)-linked, and terminal glucosyl residues in a molar ratio of 31.27:1.00:2.24 (**Table 1**), indicating that MDP has a backbone consisting of (1→ 6)-linked glucosyl residues, with a single glucose branch at the C-3 position and one terminal glucosyl residue at the non-reducing end together with the main chain.

The periodate oxidation concerning MDP led to a consumption of 2.04 mol of periodate and output of a formic acid of 1.03 mol per sugar residue, suggesting the presence of 1→ or 1→ 6 linkages. The degradation products following Smith degradation of the oxidized product were subjected to GC-MS analysis. Glycerol was mainly found, suggesting a large amount of 1→ , 1→ 6, or 1→ 2 linkages. The periodate that was consumed was about twice the formic acid obtained, suggesting that there was no 1→ 2 linkage. These findings were in good agreement with multiple studies regarding MDP methylation.

The sugar residues were assigned by applying 1D (^{1}H NMR and ^{13}C NMR) and 2D (^{1}H–^{1}H COSY, ^{1}H–^{13}C HSQC, and HMBC) NMR spectra. As most sets of signals overlap, there was a challenge in the identification of non-anomeric proton signals in the MDP ^{1}H NMR spectrum (**Figure 2A**). However, there was a presence of three anomeric proton signals in the ^{1}H-^{1}H COSY correlations (**Figure 3A**), confirming the presence of three anomeric protons at δ 4.97, 5.23, and 5.29, which were allocated to H-1 of (1→ 3,6)-linked (A), (1→)-linked (B), and (1→ 6)-linked (C) glucosyl residues (**Figure 4**), respectively. The sugar residues A, B and C were all α-configuration units according to the chemical shifts for the anomeric protons as well as the published literature comparison (23).

Three anomeric signals at δ 99.52, 99.81, and 103.25 were included in the ^{13}C NMR spectrum (**Figure 2B**) and they were assigned to C-1 of (1→ 6)-linked (C), (1→)-linked (B), and (1→ 3,6)-linked (A) glucosyl residues. The C-3 signal of (1→ 3,6)-linked glucosyl residues and the C-6 of (1→ 3,6)-linked, (1→ 6)-linked glucosyl residues underwent a downfield shift caused by the glycosylation effect. The signal at δ 81.09 was assigned to C-3 of (1→ 3,6)-linked glucosyl residues, and the signals at δ 71.40 and 71.47 were assigned to O-substituted C-6 of (1→ 3,6)-linked and (1→ 6)-linked glucosyl residues, respectively.

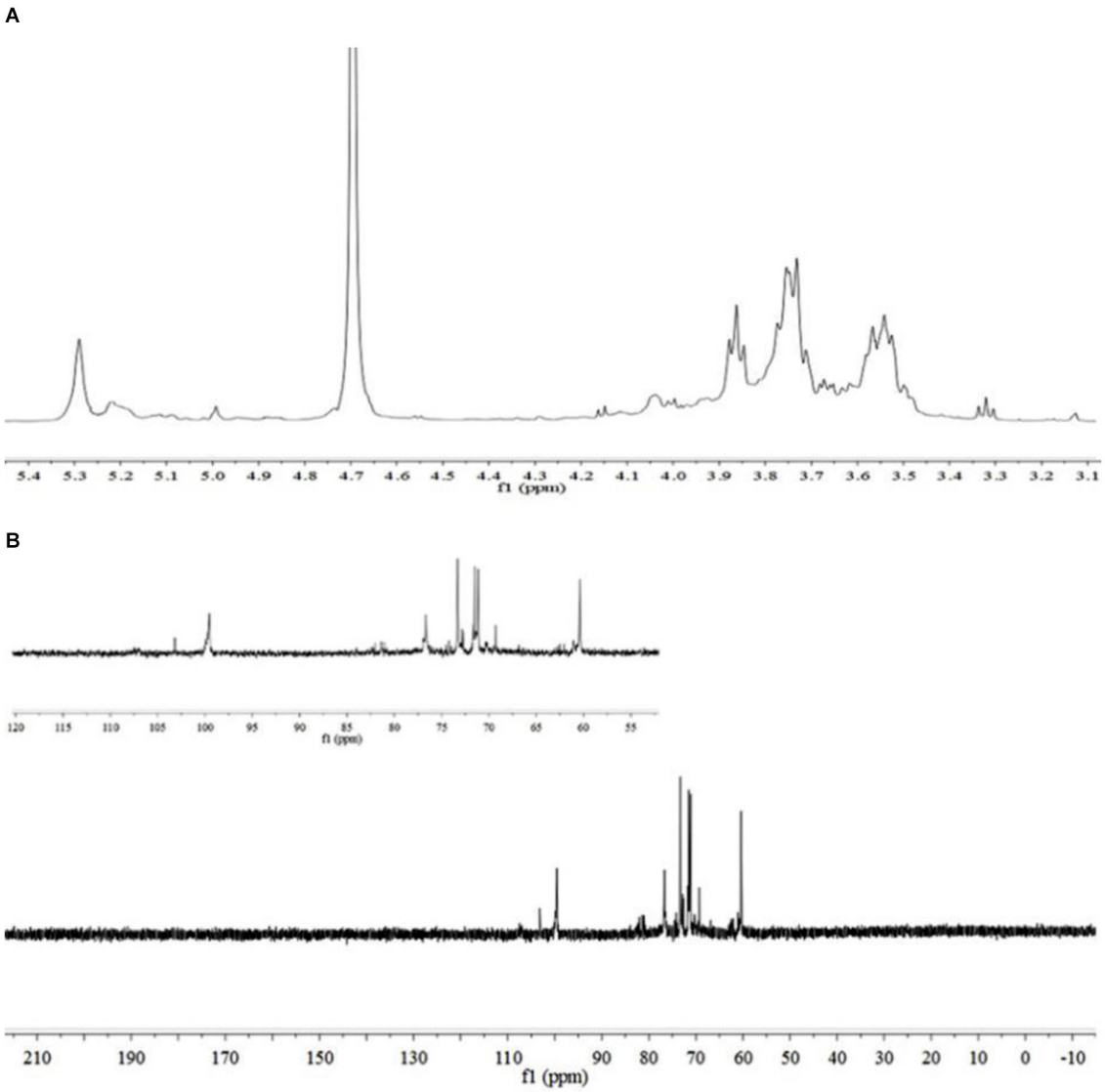

FIGURE 2 | NMR spectra of MDP. **(A)** ^{1}H NMR spectrum of MDP and **(B)** ^{13}C NMR spectrum of MDP.

The identification of three groups with related signals was achieved from the COSY spectrum (**Figure 3A**): H-1/H-2 at δ 4.97/4.00, H-2/H-3 at δ 4.00/4.03, H-3/H-4 at δ 4.03/3.92, H-4/H-5 at δ 3.92/3.72, H-5/H-6a, H-6b at δ 3.72/3.52, 3.73; H-1/H-2 at δ 5.23/3.53, H-2/H-3 at δ 3.53/3.60, H-3/H-4 at δ 3.60/3.31, H-4/H-5 at δ 3.31/3.52, H-5/H-6a, H-6b at δ 3.52/3.66, 3.77; H-1/H-2 at δ 5.29/3.52, H-2/H-3 at δ 3.52/3.85, H-3/H-4 at δ 3.85/3.75, H-4/H-5 at δ 3.75/3.55, and H-5/H-6a, H-6b at δ 3.55/3.52, 3.73.

The ^{1}H-^{13}C HMQC (**Figure 3B**) spectrum of MDP suggested data on the relationship of ^{13}C and its linked ^{1}H: H-1/C-1 at δ 4.97/103.25, H-2/C-2 at δ 4.00/70.25, H-3/C-3 at δ 4.03/81.09, H-4/C-4 at δ 3.92/70.11, H-5/C-5 at δ 3.72/76.37 and H-6a, H-6b/C-6 at δ 3.52, 3.73/71.40 for (1→ 3,6)-linked glucosyl residue; H-1/C-1 at δ 5.23/99.81, H-2/C-2 at δ 3.53/70.28, H-3/C-3 at δ 3.60/73.19, H-4/C-4 at δ 3.31/69.20, H-5/C-5 at δ 3.52/73.12 and H-6a, H-6b/C-6 at δ 3.66, 3.77/60.36 for (1→)-linked glucosyl residue; H-1/C-1 at δ 5.29/99.52, H-2/C-2 at δ 3.52/71.47, H-3/C-3 at δ 3.85/73.55, H-4/C-4 at δ 3.75/71.00, H-5/C-5 at δ 3.55/76.86, and H-6a, H-6b/C-6 at δ 3.52, 3.73/71.47 for (1→ 6)-linked glucosyl residue.

To deduce glycosidic bonds between sugar residues in MDP, long-range proton-carbon correlations were determined using ^{1}H-^{13}C HMBC (**Figure 3C**). In the anomeric region of the HMBC spectrum, associations from H-1 (δ 4.97) of the (1→ 3,6)-linked glucosyl residue to C-6 (δ 71.47) of the (1→ 6)-linked glucosyl residue and from H-1 (δ 5.23) of the (1→)-linked glucosyl residue to C-3 (δ 81.09) of the (1→ 3,6)-linked glucosyl residue were found. MDP had a (1→ 6)-linked backbone, and a (1→)-linked glucosyl residue was connected to the C-3 of the main chain according

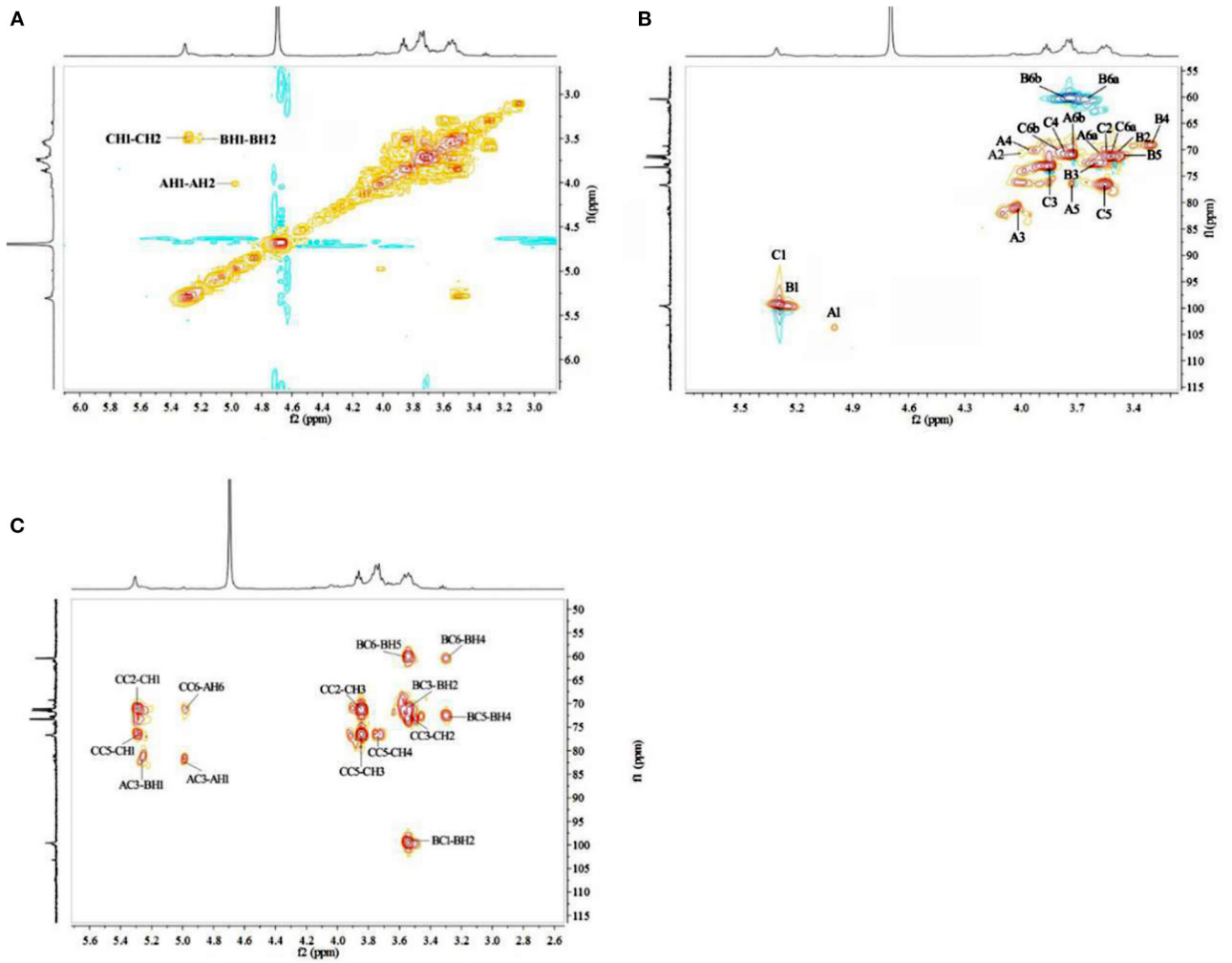

FIGURE 3 | 2D-NMR spectra of MDP. **(A)** ^{1}H–^{1}H COSY spectrum of MDP, **(B)** ^{1}H–^{13}C HSQC spectrum of MDP, and **(C)** ^{1}H–^{13}C HMBC spectrum of MDP.

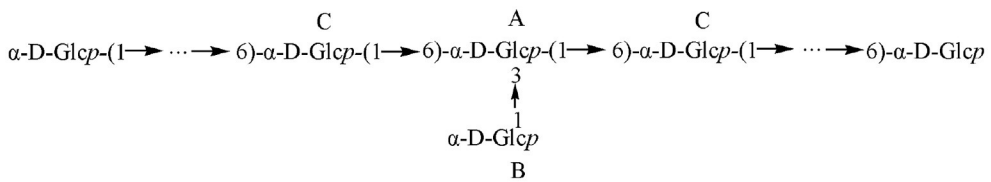

FIGURE 4 | Schematic of the structure of MDP.

to this finding. The entire structural features of MDP were obtained from the above results, and the proton and carbon chemical shifts of different glucose residues are displayed in **Table 2**.

On the above basis of the results, it can be concluded as follows: MDP is an α-D-glucan that has a (1→ 6)-linked backbone, with a single glucose branch at the C-3 position in the main chain. The predicted structure is shown in **Figure 4**.

Immunological Activities of MDP *in vitro*

Effect of MDP on RAW264.7 Cell Viability

In the innate immune system, Macrophages are the key cells. Furthermore, they are the primary cells underlying host inflammatory and other immune processes. A number of polysaccharides have been proven to promote activity and proliferation of RAW264.7 cells (24). Therefore, we assessed the influence of MDP on RAW264.7 cell

TABLE 2 | ^{1}H and ^{13}C NMR chemical shifts of polysaccharide MDP in D_2O.

Linkage type	H-1/C-1	H-2/C-2	H-3/C-3	H-4/C-4	H-5/C-5	H-6/C-6
→ 3,6)-Glcp-(1→	4.97/103.25	4.00/70.25	4.03/81.09	3.92/70.11	3.72/76.37	3.52,3.73/71.40
Glcp-(1→	5.23/99.81	3.53/70.28	3.60/73.19	3.31/69.20	3.52/73.12	3.66,3.77/60.36
→ 6)-Glcp-(1→	5.29/99.52	3.52/71.47	3.85/73.55	3.75/71.00	3.55/76.86	3.52,3.73/71.47

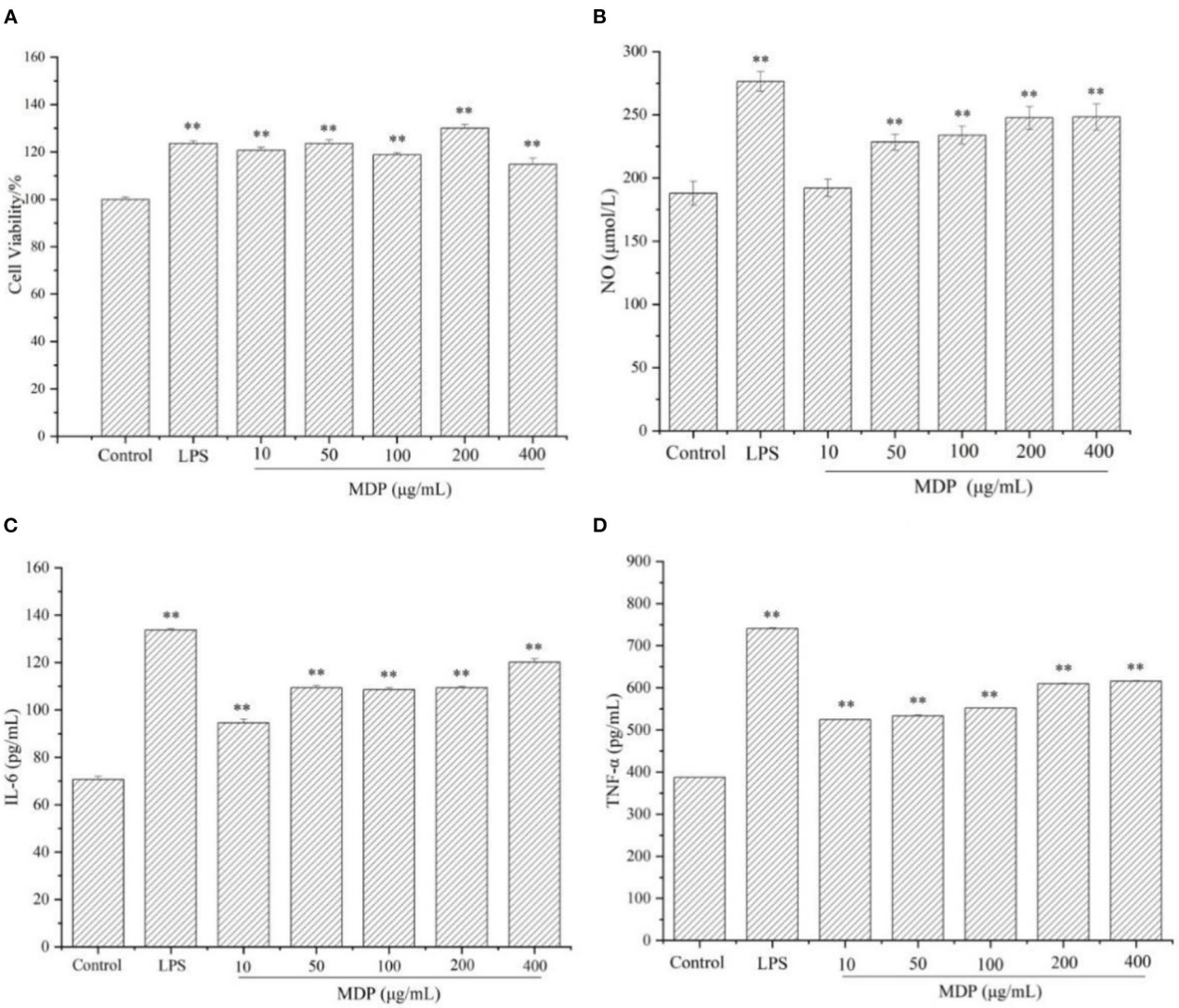

FIGURE 5 | The immunological activities of MDP *in vitro*. **(A)** Effects of MDP on the viability of RAW264.7 cells. **(B)** Effect of MDP on the secretion of NO in RAW264.7 cells. **(C)** Effect of MDP on the secretion of the cytokine IL-6 in RAW264.7 cells. **(D)** Effect of MDP on the secretion of the cytokine TNF-α in RAW264.7 cells. The values are presented as the mean ± SD, $n = 3$. $^{**}P < 0.01$ vs. control group.

viability, and the findings were presented in **Figure 5A**. The cell viability levels of different groups were 120.66, 123.64, 118.76, 130.02, and 114.73%, respectively, at dosages of 10, 50, 100, 200, and 400 μg/mL, ($P > 0.05$), which showed that MDP could remarkably enhance RAW264.7 proliferation.

Effect of MDP on the Secretion of NO, TNF-α, and IL-6 in RAW264.7 Cells

Macrophages are the most crucial immune defense-related cells in the body. After activation, they can generate a variety of cytokines and chemokines. The release of a series of biological factors (NO, TNF-α, IL-6, and etc.) is a fundamental mechanism

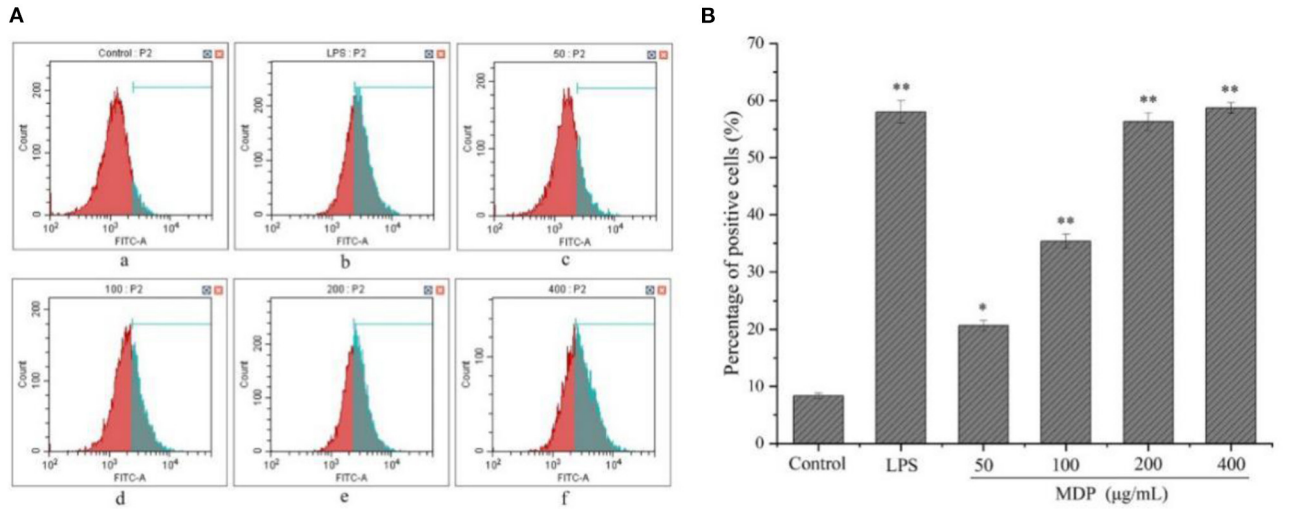

FIGURE 6 | Impacts exerted by MDP on the RAW264.7 cells' phagocytic activity. **(A)** Assessment for the phagocytic activity was performed through the use of the flow cytometry (a) Control group; (b) 1 μg/mL LPS; (c) 50 μg/mL MDP; (d) 100 μg/mL MDP; (e) 200 μg/mL MDP; (f) 400 μg/mL MDP. **(B)** Quantitative analysis of the RAW264.7 cells' phagocytic activity. The values are reported as the mean ± SD, $n = 3$. $^{*}P < 0.05$ or $^{**}P < 0.01$ vs. control group.

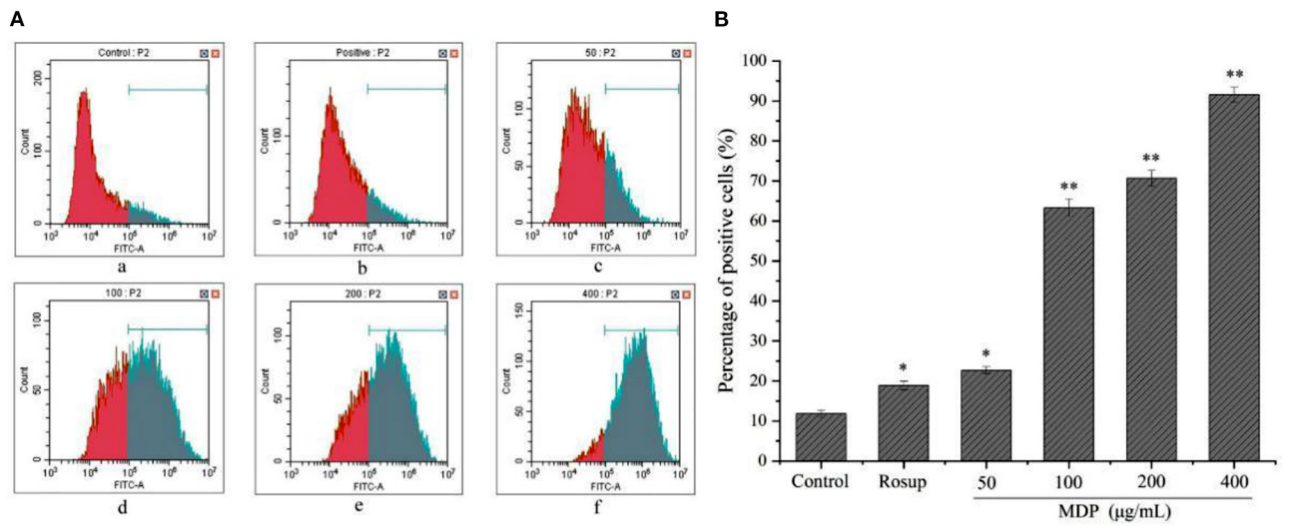

FIGURE 7 | Effect of MDP on the production of ROS in RAW264.7 cells. **(A)** The production of ROS was examined by flow cytometry (a) Control group; (b) 50 μg/mL Rosup; (c) 50 μg/mL MDP; (d) 100 μg/mL MDP; (e) 200 μg/mL MDP; (f) 400 μg/mL MDP. **(B)** Quantitative analysis of the ROS production in RAW264.7 cells. The values are reported as the mean ± SD, $n = 3$. $^{*}P < 0.05$ or $^{**}P < 0.01$ vs. control group.

of immunomodulators (25). As a type of essential molecule generated by macrophages, NO exerts a crucial role in apoptosis regulation and host defense against tumor cells and pathogens. Moreover, NO might also enhance the phagocytosis as well as the lysis of macrophages. As a result, the capacity of releasing NO by macrophages indicates the impacts of polysaccharides on immune function. The primary active molecules in organisms, including IL-6 and TNF-α, play crucial functions in the process of inflammation, cancer, and immune diseases (26). When the host is invaded by exogenous pathogen threats, activated macrophages generate IL-6 and TNF-α to mediate the immune system (27). The results were displayed in **Figure 5**. After MDP administration, there was a remarkable elevation in the expression of NO (**Figure 5B**), IL-6 (**Figure 5C**), and TNF-α (**Figure 5D**) levels. These results suggested that MDP has significant immunomodulatory activities *via* the mechanism of increasing the release of NO and cytokines (IL-6, TNF-α) in RAW264.7 cells.

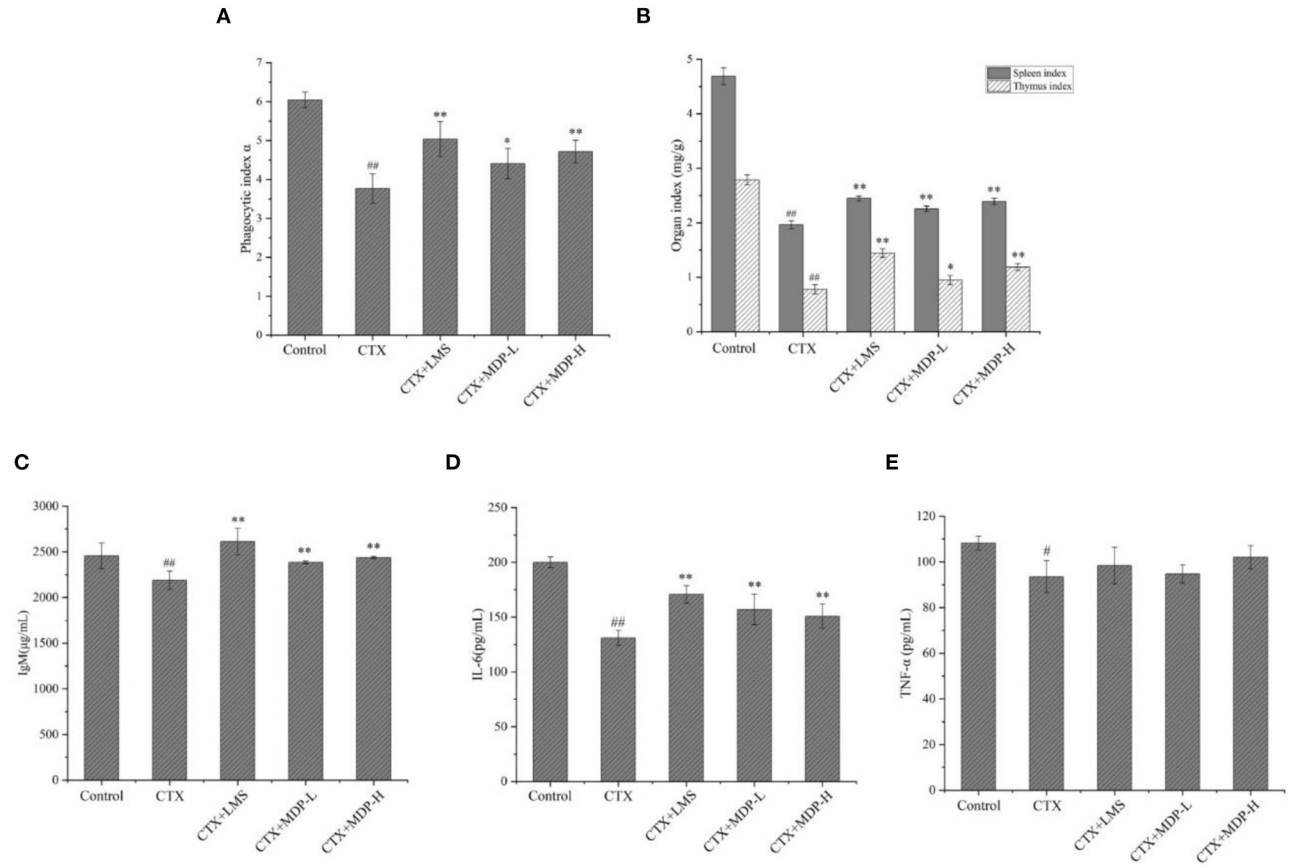

FIGURE 8 | The immunological activities of MDP in *vivo*. **(A)** Effect of MDP on the phagocytic index α. **(B)** Effect of MDP on the spleen and thymus indices in mice induced by CTX. **(C)** Effect of MDP on the secretion of IgM in serum of mice induced by CTX. **(D)** Effect of MDP on the secretion of IL-6 in serum of mice induced by CTX. **(E)** Effect of MDP on the secretion of TNF-α in serum of mice induced by CTX. Values are given as means ± S.D [$n = 3$ of **(A,C–E)** and $n = 12$ of **(B)**]. $^{\#}P < 0.05$, $^{\#\#}P < 0.01$ vs. control group; $^{*}P < 0.05$, $^{**}P < 0.01$ vs. CTX group.

Effect of MDP on the Phagocytic Activity of RAW264.7 Cells

Macrophages have the ability to swallow big foreign particles and multiple organelles or macromolecules in the cells, thus exerting a critical role in resisting infection and maintaining normal physiological functions. The phagocytic ability of FITC-dextran in RAW264.7 cells was performed with the aid of flow cytometry (**Figure 6**). In comparison to the control group, 50–400 μg/mL MDP treatment improved the RAW264.7 cells' phagocytic capacity in a dose-dependent way, the percentages of positive cells in MDP-induced RAW264.7 cells (50, 100, 200, and 400 μg/mL) were 20.65, 35.33, 56.28, and 58.69%, respectively. These results revealed that MDP has significant immunomodulatory activity by moderately improving the phagocytic ability of the large molecules in RAW264.7 cells.

Effect of MDP on the Production of ROS in RAW264.7 Cells

ROS plays a role in the production of multiple inflammatory factors or capacity enhancement of cells to phagocytose, eliminating bacteria as well as other foreign materials (28). Thus, the concentration of intracellular ROS is a viable biomarker for indicating the immuno-stimulating impact of samples in RAW264.7 cells. As demonstrated in **Figure 7**, the intensity of DCF fluorescence enhanced gradually with the increase of the dosage of MDP. In other words, the generation amount of ROS was elevated significantly in a dose-dependent way in comparison to the control group, indicating that MDP might improve the immune ability by stimulating the production of ROS.

Immunological Activities of MDP *in vivo*

Effect of MDP on the Phagocytosis of Mononuclear Macrophages

The carbon clearance tests can reflect the monocytes' phagocytic function. The removal rate of carbon particles was found to be related to the enhancement of phagocytosis (1). The phagocytic ability of mononuclear macrophages is usually denoted by the phagocytic index α. As shown in **Figure 8A**, it was observed that the phagocytic index α was markedly decreased in the model group compared with the control group ($P < 0.01$). MDP were effective in increasing the phagocytic index α in CTX-treated mice in a dose-dependent manner, and the phagocytic activities

TABLE 3 | Effect of MDP on the body weight in mice induced by CTX.

Groups	Final bodyweight	Increase of bodyweight
Control	22.42 ± 0.47	3.18 ± 0.44
CTX	17.92 ± 1.03##	−1.63 ± 0.74
CTX+LMS	19.93 ± 0.38**	−1.00 ± 0.41
CTX+MDP-L	18.94 ± 0.51*	−0.83 ± 0.31
CTX+MDP-H	19.10 ± 0.41*	−0.12 ± 0.36

Values are given as means ± S.D (n = 12).
##P < 0.01 vs. control group.
**P < 0.05, **P < 0.01 vs. CTX group.*

were nearly reinstated to the control levels at a dose of 200 mg/kg, demonstrating that MDP capable of improving the macrophage function in CTX-induced mice.

Effect of MDP on the Bodyweight, Spleen, and Thymus Indices

Body weight is an indicator of the growth status of mice, while thymus and spleen are the major organs of immunity, so they can be a reflection of the immunity functions of mice induced by CTX. The effect of MDP on the bodyweight of mice was presented in **Table 3**. CTX was found to cause a marked reduction in bodyweight to just 17.92 g compared to the control value of 22.42 g, which indicated that the immunosuppressive modeling was built successfully. Bodyweight was significantly restored when mice were treated with MDP, indicating that MDP could alleviate the weight loss caused by CTX. The spleen and thymus indices were shown in **Figure 8B**. Compared with the control group, CTX-treatment mice had much lower thymus and spleen indices, reflecting the worse immune activity. The thymic and splenic indices were ameliorated in LMS than in model groups, and MDP also increased the splenic and thymic indexes in CTX-induced BALB/c mice, which suggested that MDP could reverse the immune organ atrophy induced by CTX.

Effect of MDP on Cytokines and Immunoglobulin in Serum

Immuneglobulin (Ig) and cytokines are both engaged in immune response and regulation. Thus, we measured the releases of IgM, IL-6 and TNF-α in serum by ELISA according to the manufacturer's protocols. The results were shown in **Figures 8C–E**, the serum levels of IgM, IL-6 and TNF-α in the model group reduced significantly compared to the control group ($P < 0.01$). However, the addition of MDP resulted in an increase of IgM and IL-6 in immunosuppressive mice. MDP also increased the levels of TNF-α, but there was no significant difference. These results suggested that MDP could enhance the cytokine and immunoglobulin levels in serum of mice dramatically.

Effect of MDP on the Histological Morphology of Spleen

As shown in **Figure 9**, clear demarcation between the white and the red pulp was observed in the spleen of the control group, and the spleen cells were dense and arranged in good order with a clear nucleus. In contrast, in the CTX group, no visible demarcation was observed between the spleen white and red pulp. What' more, CTX group displayed the small splenic corpuscle with irregular shape and discrete lymphocyte arrangement. After the intervention of MDP, the area of splenic corpuscle increased, and the dividing line became obvious. This result showed that MDP could repair the damage of CTX on the spleen through protecting the splenic corpuscle and recovering lymphocyte quantity.

Effect of MDP on the $CD4^+$ and $CD8^+$ T Lymphocytes of Spleen

To investigate the effects of MDP on cellular immunity, $CD4^+$ and $CD8^+$ T lymphocyte levels were determined by immunohistochemistry. The percentages of splenic $CD4^+$ T lymphocytes (**Figure 10A**) were significantly higher in the MDP-treated groups than in the CTX group. Compared with the CTX group, the increases in $CD8^+$ T lymphocytes (**Figure 10B**) in the MDP-treated groups were not statistically significant. The $CD4^+/CD8^+$ (**Figure 10C**) of the MDP-treated groups also led to a significant increase when compared with the CTX group, indicating that MDP improved immune function by regulating T lymphocyte subsets.

Effect of MDP on the TLR4-MyD88 Pathways *in vivo*

TLR4, a canonical receptor for LPS, is known to recognize a variety of natural polysaccharides. TLR4 has two distinct downstream signaling pathways, including MyD88- and TRIF-dependent signaling pathways. Subsequent activation of MAPK/NF-κB signaling pathway by MyD88-dependent pathway induces the secretion of effector cytokines (29). To further verify whether TLR4-MyD88 mediates the immunomodulatory effects of MDP, we measured the effect of MDP on the protein expression levels of key nodes in the TLR4-MyD88 signaling pathway in the CTX-treated mice. The results showed MDP significantly elevated the protein expression (**Figure 11**) of TLR4, MyD88, p-NFκB, and p-JNK. The results demonstrated that MDP activates MyD88-dependent signaling pathways through TLR4 to promotes immune activity (**Figure 12**).

DISCUSSION

According to the findings of the present research, MDP presented significant immunomodulatory activity as a plant-originated polysaccharide. In recent years, more and more glucans with immunomodulatory activity have been reported. Bao et al. (30) found that branched (1→ 3)-α-d-Glc*p* isolated from *Ganoderma lucidum* spores may boost both *in vitro* and *in vivo* lymphocyte proliferation as well as antibody production. Yang et al. (31) extracted a polysaccharide called NGP from ginger that had a main chain of 1,4-linked α-D-Glc*p* and α-D-Glc*p* residues branched at the C-6 position. NGP could boost macrophage proliferation significantly without cytotoxicity and promote immune substances production (NO, TNF-α, IL-1β, and IL-6). Nair et al. (32) revealed that α-glucan containing a (1→ 4) linked backbone and (1→ 6)

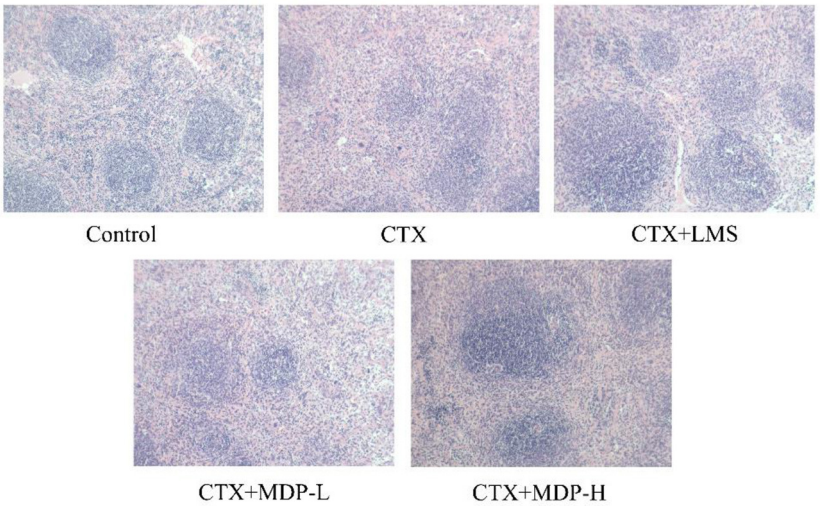

FIGURE 9 | Effect of MDP on the histological morphology of spleen in mice induced by CTX.

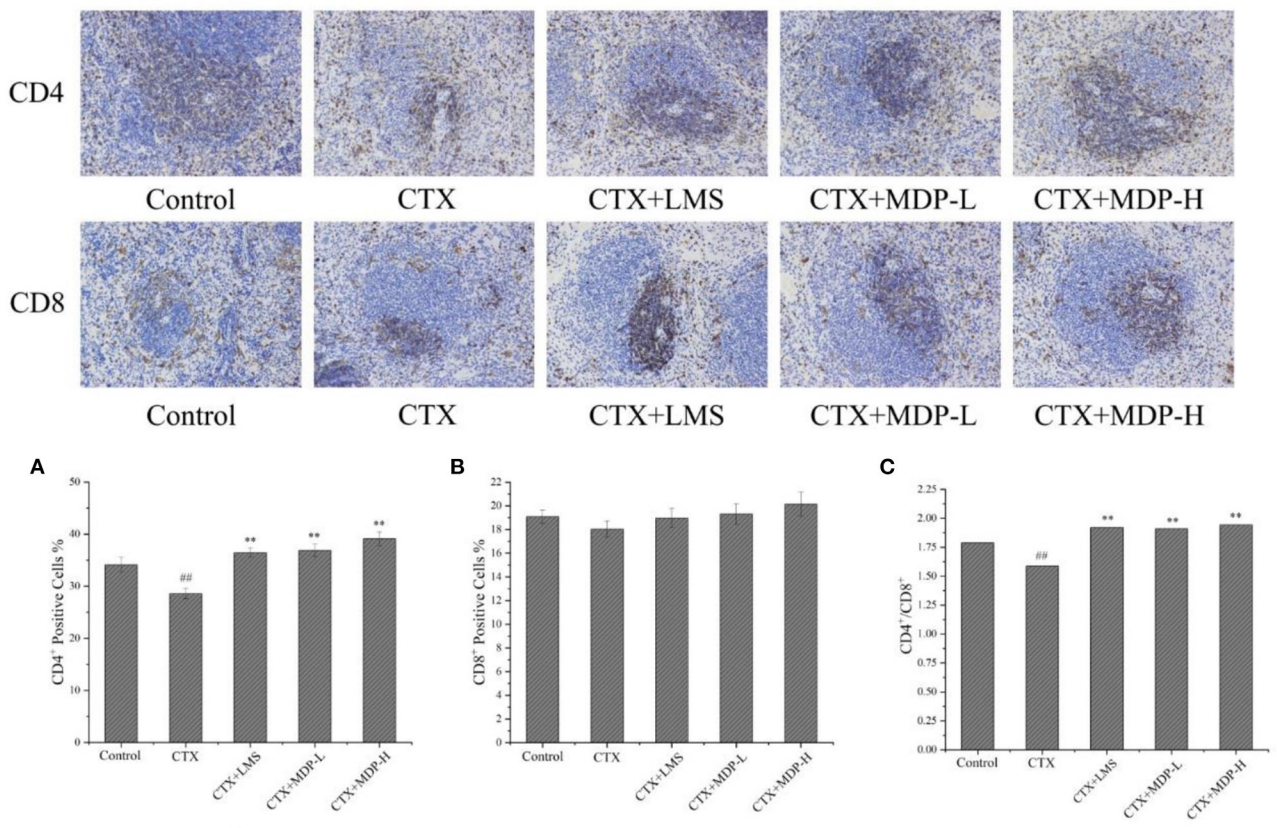

FIGURE 10 | Effect of MDP on the T lymphocyte of spleen. **(A)** Quantitative analysis of the effect of MDP on the $CD4^+$ T lymphocyte of spleen. **(B)** Quantitative analysis of the effect of MDP on the CD4+ T lymphocyte of the spleen. **(C)** Effect of MDP on the $CD4^+/CD8^+$ of the spleen. Values are given as means ± S.D ($n = 3$). $\#\#P < 0.01$ vs. control group; $^{**}P < 0.01$ vs. CTX group.

linked branches from *Tinospora cordifolia* presented distinctive immune-stimulating characteristics. Many polysaccharides containing (1→ 6)-α-D-glucan have great immunological activity. Zhao et al. (33) reported that (1→ 6)-α-D-glucan

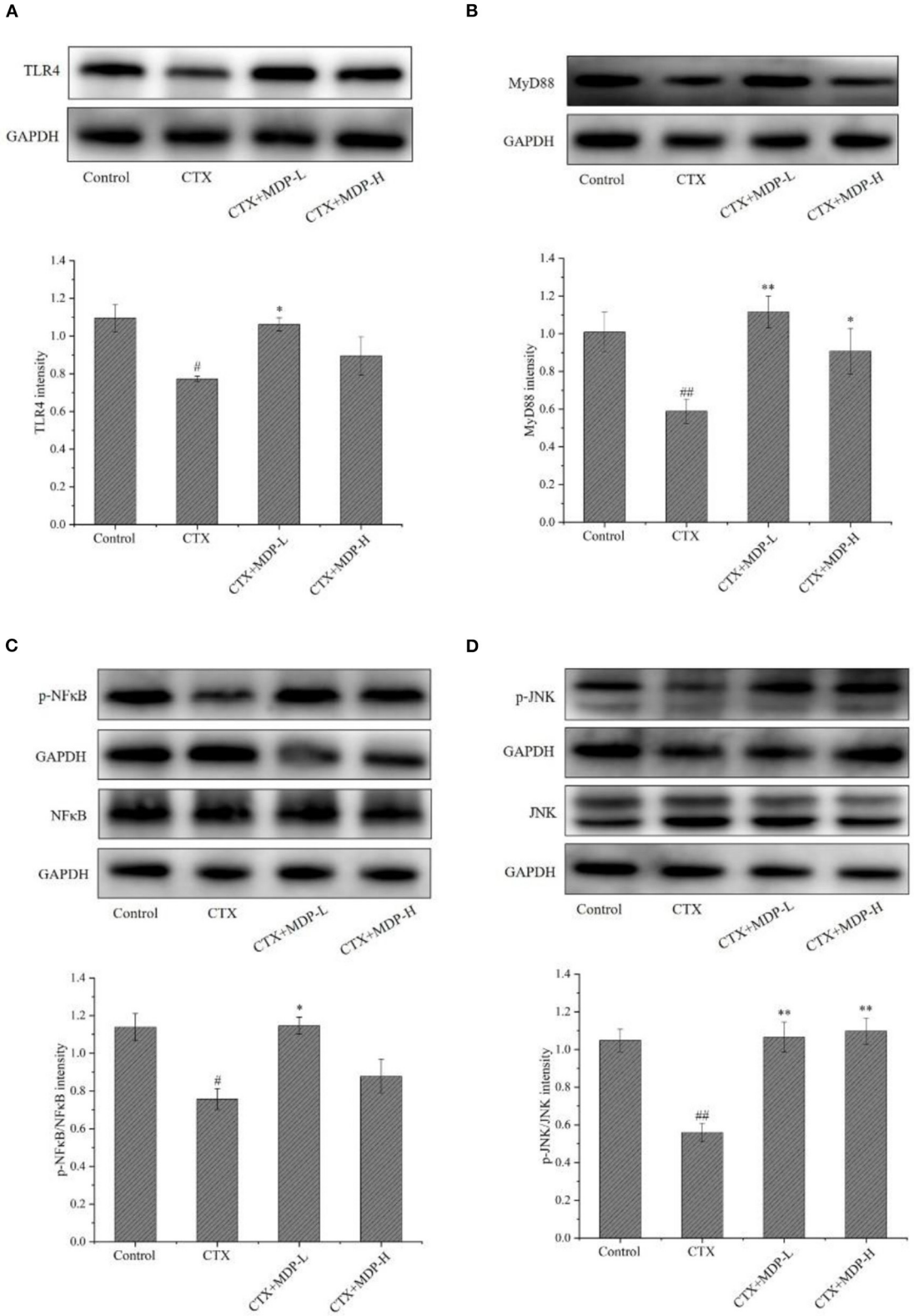

FIGURE 11 | Effect of MDP on the TLR4-MyD88 pathways *in vivo*. **(A)** The protein expressions of TLR4. **(B)** The protein expressions of MyD88. **(C)** The protein expressions of p-NFκB. **(D)** The protein expressions of p-JNK. Values are given as means ± S.D ($n = 3$). $^{\#}P < 0.05$, $^{\#\#}P < 0.01$ vs. control group; $^{*}P < 0.05$, $^{**}P < 0.01$ vs. CTX group.

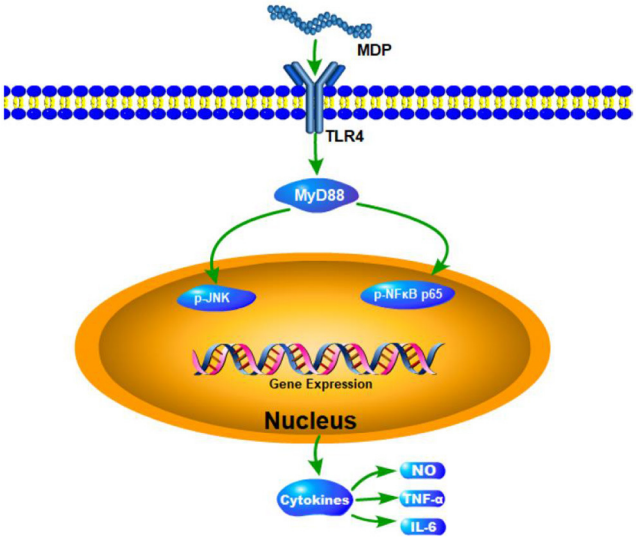

FIGURE 12 | The proposed mechanism underlying the immunological effects of MDP.

from the *Ipomoea batatas* root could contribute to an improvement in the immune system and be considered as a biological response modifier. Yang et al. (34) extracted an α-(1→ 6)-D-glucan from banana, its immunostimulatory activities had similarities to a clinical immunostimulatory drug known as β-(1→ 3)-D-glucan. Similarly, in our study, MDP could also activate macrophages to promote immune activity, which may be related to the inclusion of α-(1→ 6)-D-glucan.

In summary, a new water-soluble polysaccharide called MDP containing a molecular weight of 6.16×10^3 Da was acquired in the present research with the use of DEAE-52 cellulose, Sephacryl S-100, and Sephadex G-50 column chromatography. MDP is an α-D-glucan, which has a (1→ 6)-linked backbone branched at the C-3 position with a glucosyl residue. MDP could remarkably enhance the proliferation, phagocytosis, and release of ROS, NO, TNF-α, and IL-6 factors in RAW264.7 cells. For immunological activity *in vivo*, MDP could significantly increase the thymus and spleen indices, enhance the macrophage function, increase the level of cytokine (IL-6 and TNF-α) and immunoglobulin (IgM) in the serum and regulate T lymphocyte subsets. Furthermore, MDP elevated the expression of the critical nodes in the TLR4-MyD88 signaling pathways *in vivo*. The results indicate that MDP has the capacity of becoming an immunomodulator and could further be applied in the pharmaceutical as well as functional food industries.

DATA AVAILABILITY STATEMENT

The raw data supporting the conclusions of this article will be made available by the authors, without undue reservation.

ETHICS STATEMENT

The animal study was reviewed and approved by Shandong University of Traditional Chinese Medicine Welfare Ethics Review Committee.

AUTHOR CONTRIBUTIONS

PY: conceptualization, methodology, formal analysis, investigation, and writing-original draft. JJ: conceptualization, methodology, formal analysis, investigation, and data curation. FW: resources and validation. YLi: conceptualization and methodology. YM: validation and writing-review and editing. BD: project administration. YZ: supervision, project administration, validation, and visualization. YLiu: supervision, project administration, validation, and writing—review and editing. All authors contributed to the article and approved the submitted version.

FUNDING

We received support in the form of grants from the National Natural Science Foundation of China (81973218), Natural Science Foundation of Shandong Province (ZR2019MH082), Taishan Industry Leading Talents Project (tscy20200410), Technology Development Program of TCM of Shandong Province (2019-0024), Open Projects Fund of NMPA Key Laboratory for Quality Research and Evaluation of Carbohydrate-Based Medicine (No. 2021QRECM02), Shandong Key Laboratory of Carbohydrate Chemistry and Glycobiology, Shandong University (2021CCG05), and Scientific Foundation of Shandong University of Traditional Chinese Medicine (2018zk15).

ACKNOWLEDGMENTS

The authors gratefully acknowledge the Experimental Center, Shandong University of Traditional Chinese Medicine, Jinan, China.

SUPPLEMENTARY MATERIAL

The Supplementary Material for this article can be found online at: https://www.frontiersin.org/articles/10.3389/fnut.2022.922569/full#supplementary-material

REFERENCES

1. Chu Q, Zhang Y, Chen W, Jia R, Yu X, Wang Y, et al. Apios americana Medik flowers polysaccharide (AFP) alleviate Cyclophosphamide-induced immunosuppression in ICR mice. *Int J Biol Macromol.* (2020) 144:829–36. doi: 10.1016/j.ijbiomac.2019.10.035

2. Horvat TZ, Adel NG, Dang TO, Momtaz P, Postow MA, Callahan MK, et al. Immune-related adverse events, need for systemic immunosuppression, and effects on survival and time to treatment failure in patients with melanoma treated with ipilimumab at memorial sloan kettering cancer center. *J Clin Oncol.* (2015) 33:3193–8. doi: 10.1200/JCO.2015.60.8448

3. Hu Z, Ott PA, Wu CJ. Towards personalized, tumour-specific, therapeutic vaccines for cancer. *Nat Rev Immunol.* (2018) 18:168–82. doi: 10.1038/nri.2017.131
4. Savard J, Ivers H, Savard MH, Morin CM. Cancer treatments and their side effects are associated with aggravation of insomnia: results of a longitudinal study. *Cancer.* (2015) 121:29244. doi: 10.1002/cncr.29244
5. Chen Y, Tang J, Wang X, Sun F, Liang S. An immunostimulatory polysaccharide (SCP-IIa) from the fruit of *Schisandra chinensis* (Turcz). *Baill Int J Biol Macromol.* (2012) 50:844–8. doi: 10.1016/j.ijbiomac.2011.11.015
6. Anon. *Dictionary of Traditional Chinese Medicine*. Shanghai: Shanghai Sci. Tech. Pub. (1977). p. 2612–4.
7. Yu YY, Shao J, Chen F, Zhang TT, Wei JX, Li LZ, et al. Study on oxoisoaporphine alkaloids from rhizome of *Menispermum dauricum* and their anti-myocardial ischemia activities. *J Log Uni PAP.* (2019) 28:1–6. doi: 10.16548/j.2095-3720.2019.11.001
8. Wu D, Du JK, Zhang Y, Su YM, Zhang HF. Anti-tumor effects of phenolic alkaloids of *menispermum dauricum* on gastric cancer *in vivo* and *in vitro*. *J Cancer Res Ther.* (2018) 2018:14. doi: 10.4103/0973-1482.184521
9. Zhou YL, Zhao X, Li SX, Lv HM, Wang AL, Zhang Y. Alkaloids from rhizome of *Menispermum dauricum* and Their anti-inflammatory activity. *Mod Chin Med.* (2018) 20:163–8. doi: 10.13313/j.issn.1673-4890.20170831005
10. Chen JY, Xie YF, Zhou TX, Qin GW. Chemical constituents of *Menispermum dauricum*. *Chin J Nat Med.* (2012) 10:292–4. doi: 10.3724/SP.J.1009.2012.00292
11. Lin M, Xia BR, Yang M. Anti-ovarian cancer potential of two acidic polysaccharides from the rhizoma of *Menispermum dauricum*. *Carbohydr Polym.* (2012) 92:2212–7. doi: 10.1016/j.carbpol.2012.12.013
12. Lin M, Xia BR, Yang M. Characterization and antitumor activities of a polysaccharide from the rhizoma of *Menispermum dauricum*. *Int J Biol Macromol.* (2013) 53:72–6. doi: 10.1016/j.ijbiomac.2012.11.012
13. Li M, Shan BE, Liang WJ, Ren FZ. Experimental study on the antimutagenic and mutagenic activity of *Rhizoma menispermi* extracts. *Chin J Cancer Prev Treat.* (2006) 6:411–8. doi: 10.16073/j.cnki.cjcpt.2006.06.004
14. Zhang CJ, Guo JY, Cheng H, Lin LI, Yu HT. Spatial structure and anti-fatigue of polysaccharide from *Inonotus obliquus*. *Int J Biol Macromol.* (2020) 151:855–60. doi: 10.1016/j.ijbiomac.2020.02.147
15. Yang P, Zhang R, Zhai Y, Liu YH. Optimization of deproteinization process by response surface method and the neuroprotective activity study of *Rhizoma menispermi* crude polysaccharide. *Nat Prod Res Dev.* (2019) 31:579–86. doi: 10.16333/j.1001-6880.2019.4.004
16. Dubois M, Gilles KA, Hamilton JK, Rebers PA, Smith F. Colorimetric method for determination of sugars and related substances. *Anal Chem.* (1956) 28:350–6. doi: 10.1021/ac60111a017
17. Zhong M, Wang LH, Ma H. Effect of selenium-protein polysaccharide extracted from Se-rich *Cordyceps militaris* on tumor-bearing mice. *Chin J Chin Mat Med.* (2008) 33:2120–3.
18. Du BX, Fu YP, Wang X, Jiang HQ, Lv QT, Du RK, et al. Isolation, purification, structural analysis, and biological activities of water-soluble polysaccharide from *Glehniae radix*. *Int J Biol Macromol.* (2019) 128:724–31. doi: 10.1016/j.ijbiomac.2019.01.159
19. Needs PW, Selvendran RR. Avoiding oxidative degradation during sodium hydroxide/methyl oidine-mediated carbohydrate methylation in dimethyl sulfoxide. *Carbohydr Res.* (1993) 245:1–10. doi: 10.1016/0008-6215(93)80055-J
20. Liu YH, Liu CH, Jiang HQ, Zhou HL, Li PL, Wang FS. Isolation, structural characterization, and neurotrophic activity of a polysaccharide from *Phellinus ribis*. *Carbohydr Polym.* (2015) 127:145–51. doi: 10.1016/j.carbpol.2015.03.057
21. Wang M, Yang XB, Zhao JW, Lu CJ, Zhu W. Structural characterization and macrophage immunomodulatory activity of a novel polysaccharide from *Smilax glabra Roxb*. *Carbohydr Polym.* (2017) 156:390–402. doi: 10.1016/j.carbpol.2016.09.033
22. Huang XM, Zou YF, Lian L, Wu XJ, He XS, He XW, et al. Changes of T cells and cytokines TGF-β1 and IL-10 in mice during liver metastasis of colon carcinoma: implications for liver anti-tumor immunity. *J Gastroint Surg.* (2013) 17:1283–91. doi: 10.1007/s11605-013-2194-5
23. Zhi F, Yang T, Wang Q, Jiang B, Wang Z, Zhang J, et al. Isolation, structure and activity of a novel water-soluble polysaccharide from *Dioscorea opposita* Thunb. *Int J Biol Macromol.* (2019) 133:1201–9. doi: 10.1016/j.ijbiomac.2019.04.087
24. Wang Y, Tian Y, Shao J, Shu X, Jia J, Ren X, et al. Macrophage immunomodulatory activity of the polysaccharide isolated from *Collybia radicata* mushroom. *Int J Biol Macromol.* (2017) 108:300–6. doi: 10.1016/j.ijbiomac.2017.12.025
25. Schepetkin IA, Quinn MT. Botanical polysaccharides: macrophage immunomodulation and therapeutic potential. *Int Immunopharmacol.* (2006) 6:317–33. doi: 10.1016/j.intimp.2005.10.005
26. Yu Y, Zhang Y, Hu C, Zou X, Lin Y, Xia Y, et al. Chemistry and immunostimulatory activity of a polysaccharide from *Undaria pinnatifida*. *Food Chem Toxicol.* (2019) 128:119–28. doi: 10.1016/j.fct.2019.03.042
27. Sorimachi K, Akimoto K, Hattori Y, Ieiri T, Niwa A. Secretion of TNF-alpha, IL-8, and nitric oxide by macrophages activated with polyanions, and involvement of interferon-gamma in the regulation of cytokine secretion. *Cytokine.* (1999) 11:571–8. doi: 10.1006/cyto.1998.0472
28. Ren Y, Zheng G, You L, Wen L, Li C, Fu X, et al. Structural characterization and macrophage immunomodulatory activity of a polysaccharide isolated from *Gracilaria lemaneiformis*. *J Func Food.* (2017) 33:86–296. doi: 10.1016/j.jff.2017.03.062
29. Han L, Meng M, Guo M, Cheng D, Shi L, Wang X, et al. Immunomodulatory activity of a water-soluble polysaccharide obtained from highland barley on immunosuppressive mice models. *Food Funct.* (2019) 10:304–14. doi: 10.1039/C8FO01991F
30. Bao X, Duan J, Fang X, Fang J. Chemical modifications of the (1→ 3)-α-d-glucan from spores of *Ganoderma lucidum* and investigation of their physicochemical properties and immunological activity. *Carbohydr Res.* (2001) 336:127–40. doi: 10.1016/S0008-6215(01)00238-5
31. Yang X, Wei S, Lu X, Qiao X, Li N, A. neutral polysaccharide with a triple helix structure from ginger: characterization and immunomodulatory activity. *Food Chem.* (2021) 350:129261. doi: 10.1016/j.foodchem.2021.129261
32. Nair P, Rodriguez S, Ramachandran R, Alamo A, Melnick SJ, Escalon E. Immune stimulating properties of a novel polysaccharide from the medicinal plant *Tinospora cordifolia*. *Int Immunopharmacol.* (2004) 4:1645–59. doi: 10.1016/j.intimp.2004.07.024
33. Zhao G, Kan J, Li Z, Chen Z. Characterization and immunostimulatory activity of a (1→ 6)-α-D-glucan from the root of ipomoea batatas. *Int Immunopharmacol.* (2005) 5:1436–45. doi: 10.1016/j.intimp.2005.03.012
34. Yang J, Tu J, Liu H, Wen L, Jiang Y, Yang B. Identification of an immunostimulatory polysaccharide in banana. *Food Chem.* (2019) 277:46–53. doi: 10.1016/j.foodchem.2018.10.043

Conflict of Interest: BD was employed by Sishui Siheyuan Culture and Tourism Development Company, Ltd.

The remaining authors declare that the research was conducted in the absence of any commercial or financial relationships that could be construed as a potential conflict of interest.

Publisher's Note: All claims expressed in this article are solely those of the authors and do not necessarily represent those of their affiliated organizations, or those of the publisher, the editors and the reviewers. Any product that may be evaluated in this article, or claim that may be made by its manufacturer, is not guaranteed or endorsed by the publisher.

Copyright © 2022 Yang, Jin, Ma, Wang, Li, Duan, Zhang and Liu. This is an open-access article distributed under the terms of the Creative Commons Attribution License (CC BY). The use, distribution or reproduction in other forums is permitted, provided the original author(s) and the copyright owner(s) are credited and that the original publication in this journal is cited, in accordance with accepted academic practice. No use, distribution or reproduction is permitted which does not comply with these terms.

frontiers | Frontiers in Nutrition

ORIGINAL RESEARCH
published: 21 June 2022
doi: 10.3389/fnut.2022.934073

Inhibitory Effect of Fermented *Flammulina velutipes* Polysaccharides on Mice Intestinal Inflammation

Sheng Ma[1,2], *Jianxiong Xu*[1,2]*, *Ting Lai*[1,2], *Weina Xu*[1,2], *Jing Zhang*[1,2], *Hongcai Zhang*[1,2]* *and Weiyi Zhang*[3]*

[1] School of Agriculture and Biology, Shanghai Jiao Tong University, Shanghai, China, [2] Shanghai Key Laboratory for Veterinary and Biotechnology, Shanghai, China, [3] Shanghai Center of Agri-Products Quality and Safety, Shanghai, China

To investigate the effect of *Flammulina velutipes* polysaccharides (FVPs) on mice intestinal inflammation, FVPs were extracted from *Flammulina velutipes* (FV) using a solid anaerobic fermentation technique. The antioxidant and anti-inflammatory capacities of FVP and fermented FVP (FFVP) induced by lipopolysaccharide (LPS) were investigated *in vitro* and *in vivo*. The results showed that the yield of FFVP (9.44%) was higher than that of FVP (8.65%), but the molecular weight (MW) of FFVP (15,702 Da) was lower than that of FVP (15,961 Da). The antioxidant and anti-inflammatory capacities of FFVP were higher than that of FVP in preventing mice diarrhea, enhancing antioxidant capacities, and reducing the secretion and mRNA expression of interleukin-1β (IL-1β), IL-6, IL-18, and tumor necrosis factor-α (TNF-α). The anti-inflammatory mechanisms of FVP and FFVP were analyzed by inhibiting the activation of the NLRP3 signaling pathway using an LPS-induced mice model. This study indicated that FFVP could be used as a functional antioxidant, indicating a potential application in functional food and health products.

Keywords: ***Flammulina velutipes*** **polysaccharides, solid anaerobic fermentation, anti-inflammatory capacities, NLRP3 signaling pathway, antioxidant capacities**

OPEN ACCESS

Edited by:
Bin Du,
Hebei Normal University of Science and Technology, China

Reviewed by:
Wenyi Kang,
Henan University, China
Guang Xin,
Shenyang Agricultural University, China

***Correspondence:**
Hongcai Zhang
hczhang@sjtu.edu.cn
Jianxiong Xu
jxxu1962@sjtu.edu.cn
Weiyi Zhang
zhangharewei@163.com

Specialty section:
This article was submitted to Nutritional Immunology, a section of the journal Frontiers in Nutrition

Received: *02 May 2022*
Accepted: *16 May 2022*
Published: *21 June 2022*

Citation:
Ma S, Xu J, Lai T, Xu W, Zhang J, Zhang H and Zhang W (2022) Inhibitory Effect of Fermented Flammulina velutipes Polysaccharides on Mice Intestinal Inflammation. Front. Nutr. 9:934073. doi: 10.3389/fnut.2022.934073

HIGHLIGHTS

- First report the extraction of fermented *Flammulina velutipes* polysaccharides (FFVP).
- FFVP with low molecular weight has higher anti-inflammatory capacities than FVP.
- FFVP regulates inflammatory response by inhibiting NLRP3 signal pathway activation.

INTRODUCTION

Flammulina velutipes (FV), as one of the four major cultivated edible fungi, is widely artificially cultivated in the world (1). It is well-known that FV mainly contains abundant polysaccharides and proteins, and among them, FV polysaccharides (FVP) have shown many excellent biological activities, including antioxidant, antimicrobial, anti-aging, anti-tumor, and immunomodulatory properties (2, 3). For instance, previous studies have reported that FVP could improve antioxidant capacities and anti-inflammatory properties by increasing the immunoglobulin and immune factors in mice serum (4, 5), and play an immunomodulatory role in regulating the intestinal environment and improving the balance of flora (6).

It is well-known that the preparation and purification of polysaccharides are critical to investigating their functional capacities. The traditional extraction methods of polysaccharides include hot water extraction (HWE), enzyme extraction (EE), chemistry assisted extraction (CAE), and pressurized liquid extraction (PLE) (7). However, the low extraction efficacy, high cost, and environmental pollution are the pitfalls of these methods. Recently, microbial fermentation has been widely employed to extract bioactive compounds and is applied in food, agriculture, environment, and medicine fields (8). Moreover, the solid-state fermentation, one of the most common forms of microbial fermentation, is an alternative method to produce large amounts of fungal polysaccharides, which has the advantages of a shorter production cycle, less environmental pollution, higher yield, and better product quality (9, 10). For instance, polysaccharides were extracted from *Monascus purpureus* using microbial fermentation, which enhanced immunomodulatory capacities by significantly improving pinocytic and phagocytic capacities (11). Moreover, polysaccharides were extracted from *Inonotus hispidus* using solid-state fermentation, showing that they had high yields and antioxidant capacities and could reduce H_2O_2-induced oxidative damage to cells *in vitro* (12).

NLRP3 (Nucleotide- binding oligomerization domain, leucine- rich repeat and pyrin domain- containing 3) inflammasome is a multiprotein complex located in the cytoplasm and has been proven to be closely related to the pathological process of intestinal inflammation (13). Cui et al. (14) reported that colitis could be ameliorated by polysaccharides from *Scutellaria baicalensis Georgi via* suppressing NLRP3 inflammasome activation. Thus, FVP has excellent antioxidant and anti-inflammatory capacities. There has few research on the extraction of fermented FVPs and their antioxidant and anti-inflammatory capacities. Therefore, we hypothesized that FVP extracted using microbial fermentation has higher extraction efficacy and biological functions than unfermented ones *in vitro* and *in vivo*. In this work, the yields and molecular weight (MW) of FFVP and unfermented FVP were compared, and anti-inflammatory capacities were studied using lipopolysaccharide (LPS)-induced mice model. This study could provide a new idea for developing a functional additive to alleviate intestinal inflammation.

Abbreviations: FV, *Flammulina velutipes*; FVP, *Flammulina velutipes* polysaccharides; FFVP, fermented *Flammulina velutipes* polysaccharides; LFVP, low dose FVP group; HFVP, high dose FVP group; LFFVP, low dose FFVP group; HFFVP, high dose FFVP group; LPS, lipopolysaccharide; SDS-PAGE, sodium dodecyl sulfate polyacrylamide gel electrophoresis; PVDF, polyvinylidene fluoride; TBST, Tris buffered saline tween; RIPA, radio immunoprecipitation assay; ECL, electrochemical luminescence; HWE, hot water extraction; EE, enzyme extraction; CAE, chemistry assisted extraction; PLE, pressurized liquid extraction; MW, molecular weight; MDA, Malondialdehyde; CAT, catalase; GSH-Px, Glutathioneperoxidase; SOD, Super oxide dismutase; T-AOC, total antioxidant capacity; H&E, hematoxylin and eosin; V/C, villi height to crypt depth; HRP, horse radish peroxidase; NCVP, *Nostoc commune Vauch* polysaccharides; PEDV, porcine epidemic diarrhea virus; GPP, *Gynostemma pentaphyllum herb* polysaccharides.

TABLE 1 | The ratio of villus height to crypt depth (V/C value).

	Group	Villus height (μm)	Crypt depth (μm)	V/C value
Jejunum	CON	354.50±35.24^{a}	62.30±2.86^{e}	5.69±1.23^{a}
	LPS	206.56±21.37^{e}	99.23±6.02^{a}	2.08±0.31^{d}
	LFVP	241.62±23.94^{d}	93.26±5.68^{b}	2.59±0.17^{d}
	HFVP	281.47±23.58^{c}	88.29±4.06^{b}	3.19±0.32^{c}
	LFFVP	260.05±24.31^{d}	90.44±4.27^{b}	2.88±0.26^{d}
	HFFVP	283.19±31.45^{c}	85.42±4.31^{c}	3.32±0.51^{c}
Ileum	CON	238.96±31.25^{a}	60.38±6.15^{c}	3.96±0.58^{a}
	LPS	123.23±24.98^{e}	89.72±8.24^{a}	1.37±0.09^{d}
	LFVP	142.67±25.01^{d}	86.22±7.51^{a}	1.65±0.74^{cd}
	HFVP	161.57±24.14^{c}	78.71±7.18^{b}	2.05±0.14^{b}
	LFFVP	149.90±25.67^{d}	84.33±7.04^{a}	1.78±0.82^{c}
	HFFVP	165.88±27.36^{c}	78.04±7.23^{b}	2.13±0.36^{b}
Colon	CON	341.61±36.18^{a}	61.02±2.86^{e}	5.60±1.20^{a}
	LPS	229.58±26.49^{e}	95.61±6.02^{a}	2.40±0.12^{d}
	LFVP	257.12±19.84^{d}	91.03±5.68^{b}	2.82±0.25^{d}
	HFVP	275.13±12.04^{c}	86.04±4.16^{b}	3.20±0.87^{c}
	LFFVP	268.71±22.57^{d}	85.64±4.27^{b}	3.14±1.03^{d}
	HFFVP	284.37±21.24^{c}	82.77±4.19^{c}	3.44±0.69^{c}

The same letters (a–e) in the same column indicate no significant difference ($P > 0.05$), while the different letters in the same column indicate significant difference ($P < 0.05$). CON, control group; LFVP, low dose FVP group; HFVP, high dose FVP group; LFFVP, low dose FFVP group; HFFVP, high dose FFVP group.

MATERIALS AND METHODS

Materials and Reagents

Flammulina velutipes was obtained by Shanghai Guangming Senyuan Biotechnology Co., Ltd., China. The microbial culture starter, including *Bacillus subtilis* CMCCB 63501, *Bifidobacterium longum* ATCC 15707, and *Saccharomyces cerevisiae* ATCC 9763, was a kind gift from Shanghai Chuangbo Ecological Engineering Co., Ltd., China (production batch No. CB08190529). LPS was obtained from Sigma–Aldrich (St. Louis, MO, United States). Other chemicals and reagents were of analytical grade and were purchased from Sigma–Aldrich (St. Louis, MO, United States).

Extraction of FFVP

Flammulina velutipes was pulverized using Waring blender (Shanghai Shibang Machinery Co., Ltd., China) and passed through a 0.75 mm sieve. Microbial culture starter (0.10%, v/w) was then added to the smashed FV and stirred (200 rpm) in a fermentation tank (Shanghai xiaohan industrial development co., Ltd., Shanghai, China) at the ambient room temperature. The optimal fermentation conditions, including the amounts of molasses contents (3%), temperature (28°C), moisture contents (40%), and culture time (10 days), were previously reported for the production of FFVP (15).

Ultrahigh pressure (HPP600/5L, Suzhou, China)–ultrasonic extraction method (HA131–50–01, Nantong supercritical extraction Co., Jiangsu, China) was used to extract the FVP and FFVP from FV and FFV, respectively. The optimized extraction conditions, including pH = 5, ultrahigh pressure of

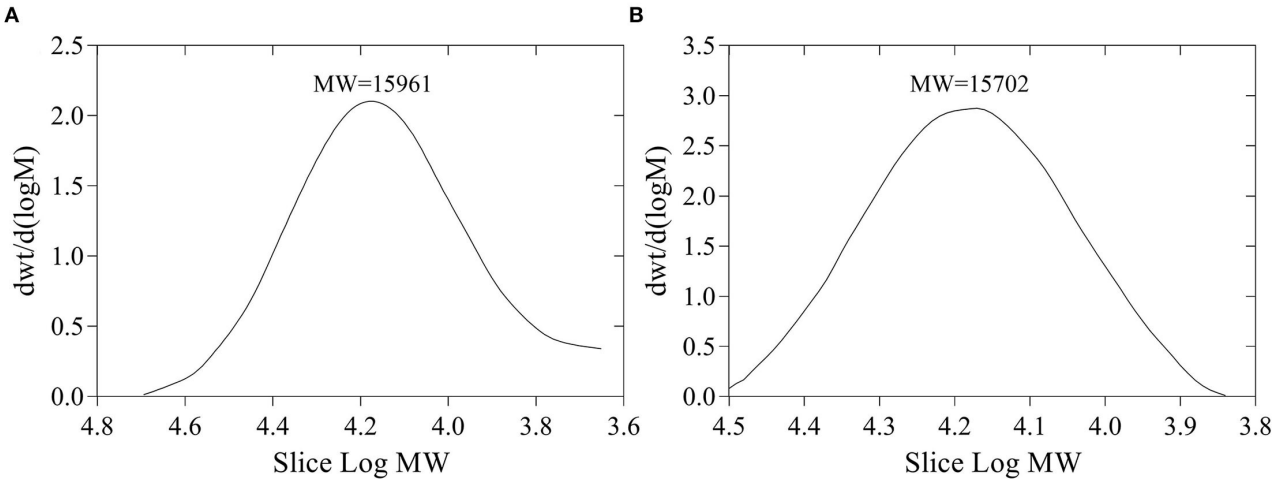

FIGURE 1 | Molecular weight (MW) of FVP **(A)** and FFVP **(B)**. FVP and FFVP are *Flammulina velutipes* polysaccharides and fermented *Flammulina velutipes* polysaccharides.

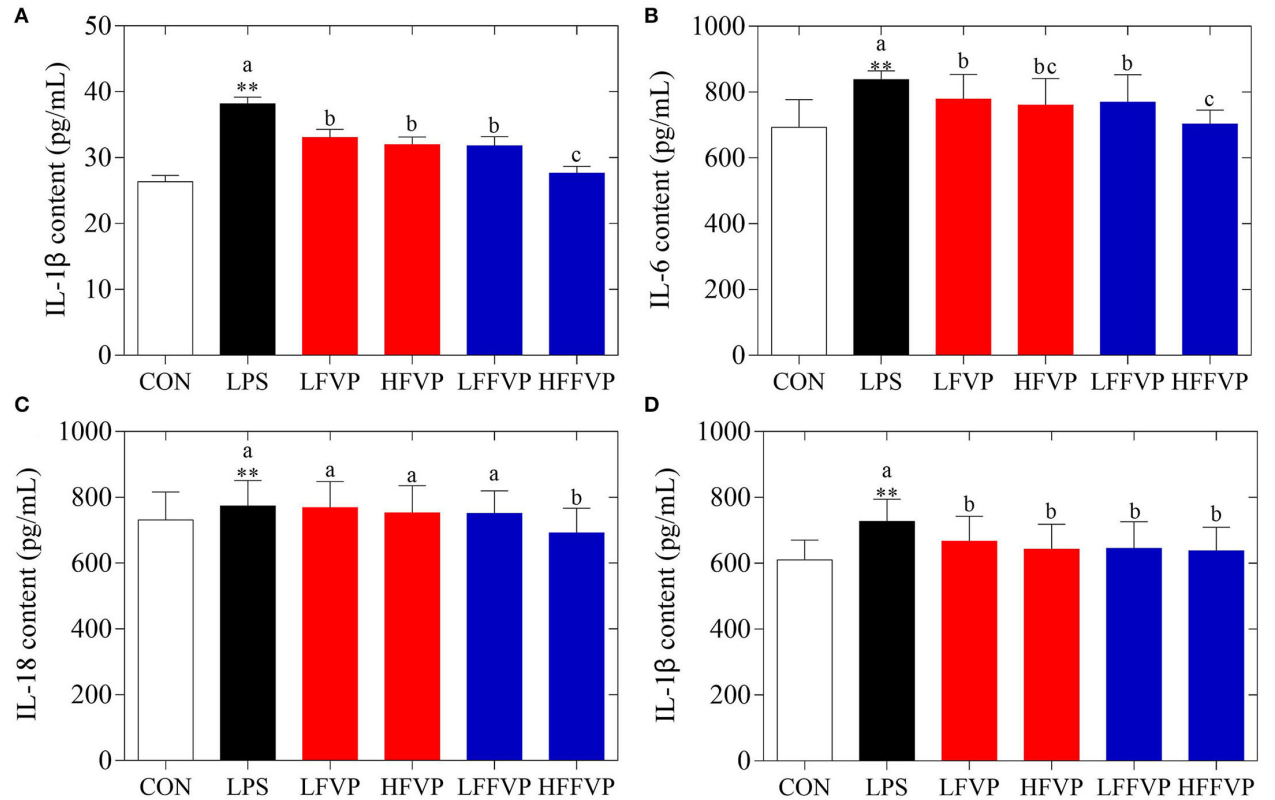

FIGURE 2 | Serum inflammatory factor contents, including IL-1β **(A)**, IL-6 **(B)**, IL-18 **(C)**, and TNF-α **(D)**. Mice were stimulated with 3 mg/kg LPS and/or 50 and 100 mg/kg FVP and FFVP. CON group, LPS group (3 mg/kg LPS), FVP and FFVP groups (50/100 mg/kg FVP and FFVP plus 3 mg/kg LPS). FV, *Flammulina velutipes*; FVP, *Flammulina velutipes* polysaccharides; CON, control group; LPS, lipopolysaccharide; LFVP, low dose FVP group; HFVP, high dose FVP group; LFFVP, low dose FFVP group; HFFVP, high dose FFVP group. $^{**}P < 0.01$ represents LPS vs. CON group; a, b and c ($P < 0.05$) represent FVP and FFVP groups vs. LPS treated mice.

360 MPa, ultrahigh pressure time of 5 min, ultrasonic power of 180 W, extraction temperature of 80°C, and extraction time of 40 min, have been reported based on a previous study (15). During the FVP extraction, lipids, pigments, and small molecular compounds were all washed out from FV first. The residues were then extracted with distilled water, and

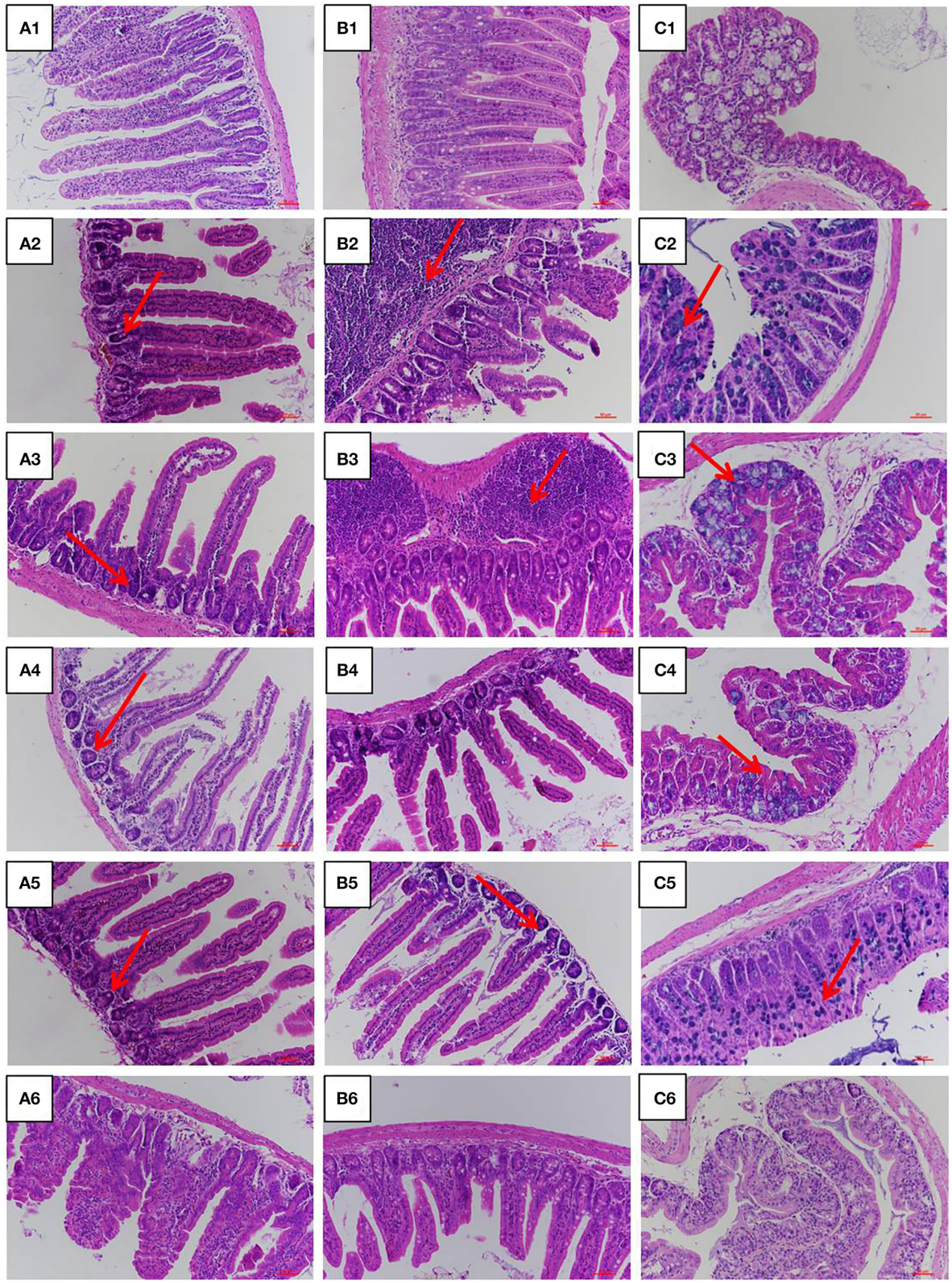

FIGURE 3 | Jejunum **(A)**, ileum **(B)**, and colon **(C)** intestinal morphology of CON group (1), LPS group (2), LFVP group (3), HFVP group (4), LFFVP group (5), HFFVP group (6). The magnification is 20×. FV, *Flammulina velutipes*; FVP, *Flammulina velutipes* polysaccharides; CON, control group; LPS, lipopolysaccharide; LFVP, low dose FVP group; HFVP, high dose FVP group; LFFVP, low dose FFVP group; HFFVP, high dose FFVP group.

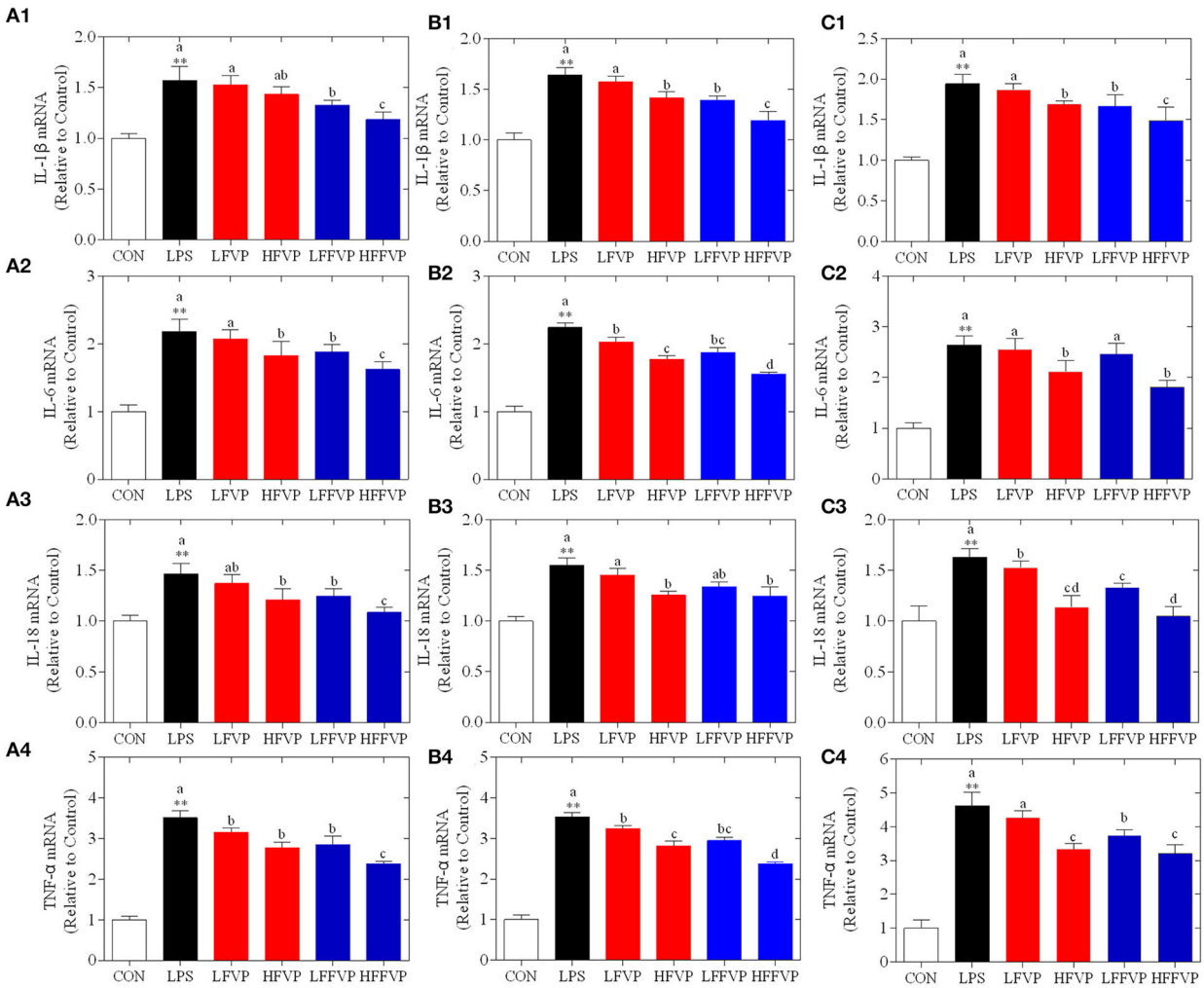

FIGURE 4 | LPS-induced IL-1β (1), IL-6 (2), IL-18 (3) and TNF-α (4) mRNA expression treated by FVP and FFVP in jejunum **(A)**, ileum **(B)**, and colon **(C)**. Mice were stimulated with 3 mg/kg LPS and/or 50 and 100 mg/kg FVP and FFVP. CON group, LPS group (3 mg/kg LPS), FVP and FFVP groups (50/100 mg/kg FVP and FFVP plus 3 mg/kg LPS). FV, *Flammulina velutipes*; FVP, *Flammulina velutipes* polysaccharides; CON, control group; LPS, lipopolysaccharide; LFVP, low dose FVP group; HFVP, high dose FVP group; LFFVP, low dose FFVP group; HFFVP, high dose FFVP group. $^{**}P < 0.01$ represents LPS vs. CON group; a, b and c ($P < 0.05$) represent FVP and FFVP groups vs. LPS treated mice.

the supernatant was filtered, combined, and concentrated. The crude polysaccharides were then precipitated by adding ethanol and washed successively with anhydrous ethanol, acetone, and petroleum ether (16). The extracted crude FVP was then harvested after deproteinization with Sevag solution (chloroform: butylalcohol = 5:1) and fractionated through diethylaminoethyl (DEAE)–Sepharose fast flow column (elution conditions: distilled water and 0.05, 0.1, 0.2, 0.3, and 0.5 mol/L NaCl gradient solutions) (1).

Molecular Weight Determination

The MW of FVP and FFVP was determined using HPLC (Waters Arc HPLC, Shanghai, China) equipped with a diode array and differential detector. Analyses were performed on a charged surface hybrid (CSH) C^{18} column (5 μm, 4.6 × 150 mm). The treatment conditions consisted of a mobile phase: 0.1% formic acid aqueous solution (A) and methanol (B), a flow rate of 0.6 ml/min, and an injection volume of 20 μl, respectively. A standard curve with the elution volume plotted against the logarithm of MW was constructed using the Dextran T standards and glucose according to Tang's method (17), and the MW of FVP/FFVP was calculated by the calibration curve equation based on their elution volume (18).

Animals and Experimental Design

Four-week-old male BALB/c mice obtained from Shanghai JieSiJie Laboratory Animals Co., Ltd. (Shanghai, China) were put in polypropylene cages. All mice were raised under standard conditions of 12 h light/dark cycle at 25 ± 2°C, with a relative humidity of 55 ± 5%. The mice had free access to a basal diet (Jiangsu Xietong Inc., Nanjing, China) and water. After one week adaption, 60 mice were randomly divided into 6 groups with 10

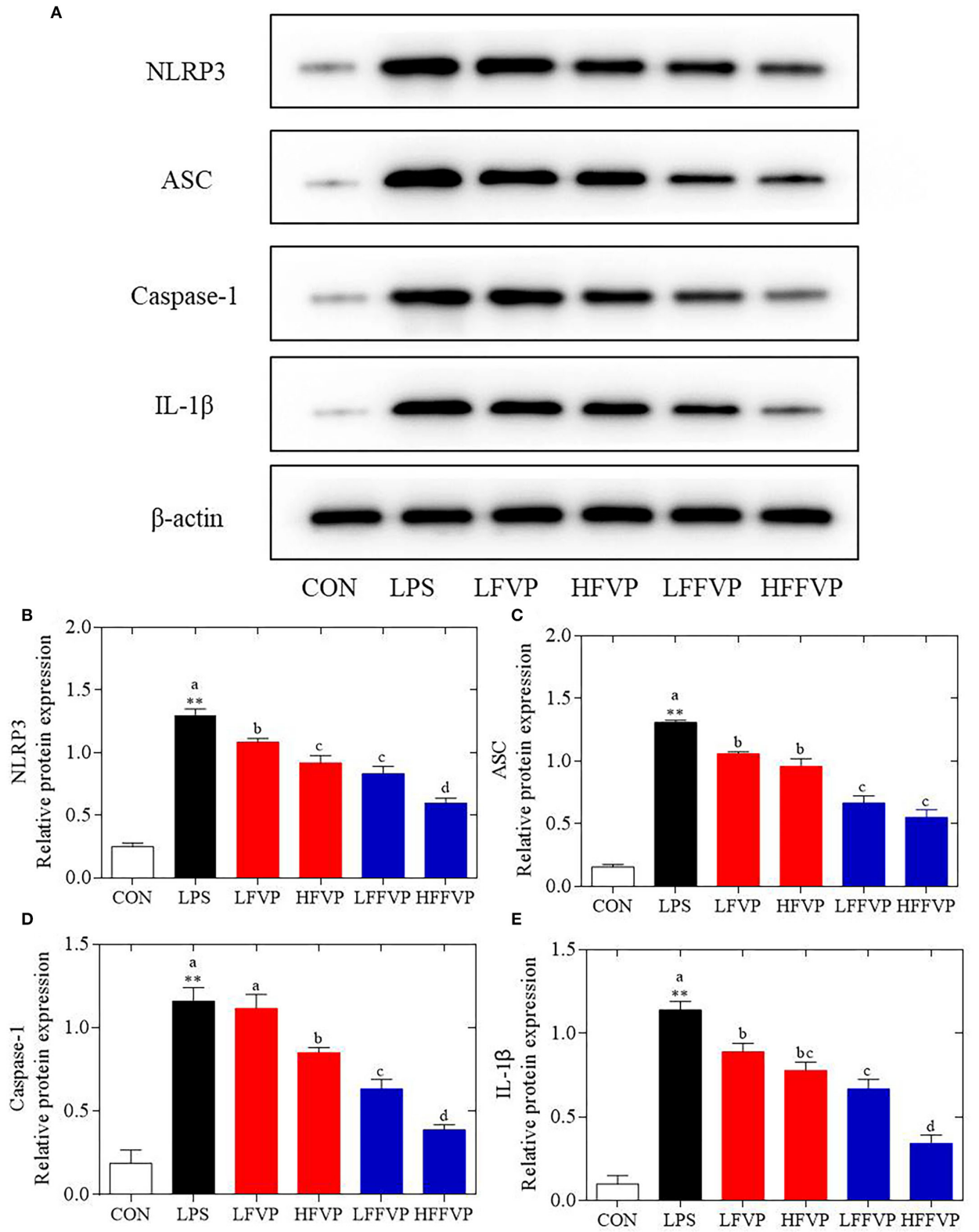

FIGURE 5 | LPS-induced NLRP3/β-actin **(A,B)**, ASC/β-actin **(A,C)**, Caspase-1/β-actin **(A,D)** and IL-1β/β-actin **(A,E)** protein expression treated by FVP and FFVP. FV, *Flammulina velutipes*; FVP, *Flammulina velutipes* polysaccharides; CON, control group; LPS, lipopolysaccharide; LFVP, low dose FVP group; HFVP, high dose FVP group; LFFVP, low dose FFVP group; HFFVP, high dose FFVP group. $^{**}P < 0.01$ represents LPS vs. CON group; a, b and c ($P < 0.05$) represent FVP and FFVP groups vs. LPS treated mice.

mice in each group and filled the stomachs with 2 mL sample everyday as follows: CON group (normal saline), LPS group (normal saline), LFVP group (50 mg/kg FVP), HFVP group (100 mg/kg FVP), LFFVP group (50 mg/kg FFVP) and HFFVP group (100 mg/kg FFVP). The experiment lasted for 60 days. On the last day, the CON group was injected intraperitoneally with normal saline (2 ml), while the LPS group, LFVP group, HFVP group, LFFVP group, and HFFVP group were injected intraperitoneally with LPS (2 ml, 3 mg/kg) to induce intestinal inflammation in mice (19). All experimental procedures were approved by the Institutional Animal Ethics Committee of Shanghai Jiao Tong University under animal protocol number 202101207.

Behavior and Appearance Observation of Mice

A total of three mice were randomly selected from each group and placed in a box after intraperitoneal injection. The behavior and appearance, including diarrhea occurrence and mice hair, were observed after 4 h (20).

Serum Oxidative Stress and Inflammatory Factor Analysis

Blood was collected from the eyeball of mice under anesthesia, and then the serum was obtained after centrifugation (5420, Eppendorf, Hamburg, Germany; 4,000 rpm, 10 min). The H_2O_2 and malondialdehyde (MDA) levels, catalase (CAT), glutathione peroxidase (GSH-Px), superoxide dismutase (SOD) capacities, and total antioxidant capacities (T-AOC) in serum were detected using an assay kit (Beyotime Biotechnology, Shanghai, China). Besides, the levels of interleukin-1β (IL-1β), IL-6, IL-18, and tumor necrosis factor-α (TNF-α) in serum were detected by enzyme linked immunosorbent assay method (ELISA) using ELISA Kit (Nanjing Jiancheng Bioengineering Institute, Nanjing, China).

Histological Analysis of Mice Intestine

The jejunum, ileum, and colon tissue sections were fixed in 10% formalin and embedded in paraffin to analyze the pathological changes. Sections (5 μm thick) were stained with a hematoxylin and eosin (H&E) stain kit (D006-1-1, Nanjing Jiancheng Bioengineering Institute, Nanjing, China) and observed under a light microscope (Eclipse Ci-L, Nikon, Tokyo, Japan). Image-Pro Plus 6.0 (Media Cybernetics, Rockville, MD, United States) was used for analysis. The height of intact villi and the depth of crypts in each section were measured, respectively, and the ratio of villi height to crypt depth (V/C value) was calculated ($n = 5$).

Quantitative Real-Time Polymerase Chain Reaction Analysis

Total RNA of intestinal samples was isolated with Trizol Reagent (Takara, Kyoto, Japan) after incubation for 24 h (21). RNA amount and quality were determined using the spectrophotometer (GeneQuant 1300 GE, Austin, TX, United States). The absorbance of samples between 1.8 and 2.0 at 260-280 nm was subjected to acceptable quality and integrity. The cDNA was synthesized with TransScript First-Strand complementary DNA synthesis SuperMix (AT341-01, Roche, Basel, Switzerland). The primer sequences are shown in **Supplementary Table 1**. Polymerase chain reaction (PCR) was performed in StepOnePlus Real-time PCR system (ABI, Carlsbad, CA, United States) using SYBR Green PCR Core Reagents (Roche, Basel, Switzerland). The housekeeping gene, β-actin, was used as a reference gene for normalization. Data were analyzed according to the $2^{-\Delta\Delta Ct}$ method. Results were expressed as relative mRNA levels.

Western Blot Analysis

The intestinal samples were lysed in radio immunoprecipitation assay (RIPA) buffer (Beyotime, Shanghai, China) with protease and phosphatase inhibitor cocktails (Sigma Co., St. Louis, MO, United States) for 10 min on a rocker at 4°C. Proteins of samples were analyzed using sodium dodecyl sulfate polyacrylamide gel electrophoresis (SDS-PAGE) and then transferred onto polyvinylidene fluoride (PVDF) membranes (0.45 μm, Millipore, Billerica, MA, United States). Each PVDF membrane was blocked with tris buffered saline tween (TBST; 100 mM Tris-HCl,150 mM NaCl, 0.05% Tween 20, pH 7.5) with 5% non-fat dried milk for 2 h, and then incubated with the following primary antibodies: NLRP3 (1:1,500), ASC (1:100), Caspase-1 (1:800), IL-1β (1:400), and β-actin (1: 5,000, Sungene biotech, China) overnight at 4°C on a shaker (SC390C, Shanghai Brave Construction Development co., Ltd., Shanghai, China). The goat anti-rabbit of 1:3000 (ZSGE-BIO, China) horse radish peroxidase (HRP) conjugate secondary antibody was then added and the WB results was observed through electrochemical luminescence (ECL) imaging system after adding the enhanced ECL reagent (Beyotime, Shanghai, China). The β-actin was used as a protein loading control. Quantitative analysis was carried out using Amersham Imager 600 (Cytiva, Montana, United States).

Statistical Analysis

All analysis was performed with the SPSS 22.0 software (SPSS Incorporated, Armonk, NY, United States), and statistical significance was analyzed using one-way ANOVA followed by an LSD test as a post-test. Data were expressed as mean ± standard error, and all measurements were conducted in triplicate. The values of $P < 0.05$ and $P < 0.01$ were considered significant and markedly significant, respectively, in different treatment groups.

RESULTS AND DISCUSSIONS

Physicochemical Analysis of FVP and FFVP

The yields of FVP and FFVP were 8.65 and 9.44%, respectively, and MW of 15,961 and 15,702 Da (**Figure 1**), respectively. Besides, the MW/MN (Weight-average Molecular Weight/Number-average Molecular Weight) of FVP and FFVP were 1.20 and 1.09 (**Supplementary Figure 2**), respectively, which was similar to a previous report (1.042) (16). A previous study has also reported that the contents and MW of tea polysaccharides, compared with the unfermented group, were, respectively, increased and decreased after fermentation treatment, and the biological capacities of fermented fractions were also better than unfermented ones (22). For instance, the MW of *Nostoc commune Vauch* polysaccharides (NCVP)

was higher than that of fermented ones, while the antioxidant capacities were significantly improved during *in vitro* digestion (23). Thus, microbial fermentation treatment could increase extraction yield and decrease MW of FVP, and the reason could be that one or more glycosidic bonds of FVP may be broken during the fermentation (24, 25).

Behavior and Appearance Observation of Mice

Diarrhea is a life-threatening condition and could cause extreme loss of fluid and salts from the animal body (26). Compared with the CON group, the mice of the LPS group had diarrhea with shaggy hair (**Supplementary Figure 1**). All of the LFVP group, HFVP group, LFFVP group, and HFFVP group did not have diarrhea, and only the LFVP group was shaggy. Besides, the mice of the CON group and HFFVP group were vigorous with shiny hair, while others gathered in the corner. A previous study has also reported that diarrhea could be prevented using plant polysaccharides including banana, guar, and soya polysaccharides (27). For instance, polysaccharides from *S. chinensis* could prevent diarrhea in rats by improving the ultrastructure of the gut (28). Besides, the polysaccharides from *Alpiniae oxyphyllae* and *Pogostemon cablin* also decreased diarrhea by inhibiting porcine epidemic diarrhea virus (PEDV) reproduction (29, 30).

Serum Antioxidant Capacities and Inflammatory Factor Contents of FVP and FFVP

Serum antioxidant capacities of FVP and FFVP are shown in **Supplementary Table 2**. Compared with the CON group, H_2O_2 (3.66 nmol/ml) and MDA (7.64 nmol/ml) contents of LPS group's serum was increased significantly ($P < 0.05$), while the CAT (0.49 U/ml), GSH-Px (1,319.61 U/ml), SOD (226.87 U/ml), and T-AOC (1.23 U/ml) were decreased significantly ($P < 0.05$). The antioxidant capacities gradually increased after FVP and FFVP gavage. Serum inflammatory factor contents of FVP and FFVP are shown in **Figure 2.** Compared with the CON group, the contents of IL-1β, IL-6, IL-18, and TNF-α in the LPS group's serum were increased significantly ($P < 0.05$). For instance, the IL-1β contents of the LPS group (38.17 pg/ml) were 1.45 times more than the CON group (26.34 pg/ml). Serum inflammatory factor content of the LFVP group, HFVP group, LFFVP group, and HFFVP group decreased significantly ($P < 0.05$) compared with the LPS group, whose IL-1β contents were 33.05, 31.97, 31.83, and 27.65 pg/ml, respectively. Besides, IL-1β, IL-6, and IL-18 contents of the HFFVP group were lower than that of the HFVP group.

Wang et al. (31) reported the antioxidant and anti-inflammatory effects of *Gynostemma pentaphyllum herb* polysaccharides (GPP) in diabetic mice, and the results indicated that GPP could enhance SOD, CAT and GSH-Px capacities, as well as decreasing MDA and IL-6 contents, which was consistent to the present study. Moreover, the antioxidant and anti-inflammatory activities of FFVP were also better than that of FVP. Jiang et al. (32) also reported that low MW *Enteromorpha prolifera* polysaccharides could enhance anti-inflammatory capacities and decrease inflammatory response through multiple signaling pathways, including TLR2/NF-κB, PKC/ERK/MAPK, and PI3K/Akt pathways (33, 34). Besides, low MW polysaccharides had higher antioxidant capacities than high MW ones (35).

Histological Analysis of Mice Intestine

The jejunum, ileum, and colon intestinal morphology are shown in **Figure 3** and the ratio of villus height to crypt depth (V/C value) is show in **Table 1**. For the LPS group, intestinal epithelial tissue structure was dissolved, most of the inflammatory cells were infiltrated, and mucosa was severely damaged with a large range of ulcers. Compared with the LPS group, intestinal epithelial tissue and intestinal villi were improved in the LFVP group, HFVP group, LFFVP group, and HFFVP group to varying degrees. Meanwhile, intestinal inflammatory damage in the LFVP and HFVP groups were more serious than that in the LFFVP and HFFVP groups, respectively. A previous study showed that FVP could ameliorate bowel inflammation and modulate the gut microbiota on dextran sulfate sodium (DSS)-induced inflammatory bowel disease (36). Besides, FVP could also improve the clinical symptoms and attenuate the mRNA and protein expressions of inflammatory cytokines and oxidative markers in colon tissue.

mRNA Expression of Inflammatory Factors

Lipopolysaccharide-induced IL-1β, IL-6, IL-18, and TNF-α mRNA expression treated by FVP and FFVP in jejunum, ileum, and colon are shown in **Figure 4**. The mRNA expression of inflammatory factors in the LPS group was significantly increased compared with the CON group ($P < 0.05$). The LFVP group, HFVP group, LFFVP group, and HFFVP group's mRNA expression of inflammatory factors were lower than that of the LPS group. For instance, IL-1β mRNA expression of the LPS group in the colon was 1.94, while in the LFVP group, HFVP group, LFFVP group, and HFFVP group were 1.87, 1.69, 1.67, and 1.49, respectively. Besides, HFVP's mRNA expressions of all four inflammatory factors were significantly higher than that of HFFVP's ($P < 0.05$). Han et al. (37) also reported that *Gracilaria Lemaneiformis* polysaccharides could prevent colitis in Balb/c mice and inhibited pro-inflammatory cytokines expression to attenuate acute inflammation, which was consistent with this study. Therefore, FVP and FFVP play an anti-inflammatory effect by inhibiting pro-inflammatory cytokines mRNA expression.

Protein Expression of NLRP3 Signaling Pathway

The NLRP3 signaling pathway was one of the most important anti-inflammatory signaling pathways (38). It could be activated by LPS and mediated by immune response of host to microbial infection and cell injury via agglomeration of NLRP3 inflammasome, resulting in producing activated Caspase-1 and mature IL-1β and IL-18 (39). As the colon was sensitive to LPS-induced inflammatory response, the colon was selected for the subsequent Western Blot test.

Compared with the CON group, protein expression of NLRP3, ASC, Caspase-1, and IL-1β were significantly increased in the LPS group. Protein expressions of LFVP, HFVP, LFFVP, and HFFVP groups were lower than that of the LPS group. At the same dose, protein expression of FFVP group was significantly lower than that of FVP group (**Figure 5**).

Pan et al. (40) reported that polysaccharides from *Smilax china* L. could ameliorate ulcerative colitis by inhibiting the galectin-3/NLRP3 inflammasome pathway. Besides, *Chayote* polysaccharides could also reduce active Caspase-1 protein levels and downregulate NLRP3 and IL-1β gene expression (41), suggesting that the NLRP3 inflammasome activation was dependent on the processing of inactive pro-Caspase-1 to active Caspase-1, which enhances IL-1β release, reactive oxygen species (ROS) production, and pyroptosis, an inflammatory form of programmed cell death (42). In this work, protein expression of NLRP3 ASC, Caspase-1 and IL-1β were significantly increased in the LPS group compared with CON group. Besides, these protein expression decreased after treated by FVP/FFVP compared with LPS group. Thus, the anti-inflammatory capacities of FVP and FFVP were also inhibited *via* activation of an NLRP3 signaling pathway.

CONCLUSION

The FFVP has higher antioxidant and anti-inflammatory capacities than FVP in preventing diarrhea, enhancing antioxidant capacities, and reducing the secretion and mRNA expression of IL-1β, IL-6, IL-18, and TNF-α. Besides, the anti-inflammatory capacities of FVP and FFVP are to inhibit the activation of an NLRP3 signaling pathway. This study indicated that FFVP could be used as functional additives and confered to its beneficial functions such as antioxidant and anti-inflammation.

DATA AVAILABILITY STATEMENT

The original contributions presented in the study are included in the article/**Supplementary Material**, further inquiries can be directed to the corresponding author/s.

ETHICS STATEMENT

The animal study was reviewed and approved by Institutional Animal Ethics Committee of Shanghai Jiao Tong University.

AUTHOR CONTRIBUTIONS

SM, WX, JZ, WZ, and JX: design and conceptualization. SM, HZ, and JX: manuscript writing and proofreading. SM, TL, WX, JZ, HZ, WZ, and JX: experimental work, data analysis, and interpretation. JX: funding acquisition. All authors have read and agreed to the published version of the manuscript.

FUNDING

This research was funded by Shanghai Agriculture Applied Technology Development Program, China (Grant No. X2019-02-08-00-08-F01155) and National Natural Science Foundation of China (Grant No. 31872367).

SUPPLEMENTARY MATERIAL

The Supplementary Material for this article can be found online at: https://www.frontiersin.org/articles/10.3389/fnut.2022.934073/full#supplementary-material

REFERENCES

1. Hao Y, Liao X, Wang X, Lao S, Liao W. The biological regulatory activities of *Flammulina velutipes* polysaccharide in mice intestinal microbiota, immune repertoire and heart transcriptome. *Int J Biol Macromol*. (2021) 185:582–91. doi: 10.1016/j.ijbiomac.2021.06.175
2. Chen F, Zhang Q, Wu P, Zhao Y, Chen Y. Green fabrication of seedbed-like *Flammulina velutipes* polysaccharides–derived scaffolds accelerating full-thickness skin wound healing accompanied by hair follicle regeneration. *Int J Biol Macromol*. (2021) 167:117–29. doi: 10.1016/j.ijbiomac.2020.11.154
3. Zhang T, Ye J, Xue C. Structural characteristics and bioactive properties of a novel polysaccharide from *Flammulina velutipes*. *Carbohydr Polym*. (2018) 197:147–56. doi: 10.1016/j.carbpol.2018.05.069
4. Wu M, Luo X, Xu XY, Wei W, Yu MY, Jiang N, et al. Antioxidant and immunomodulatory activities of a polysaccharide from *Flammulina velutipes*. *J Tradit Chin Med*. (2014) 34:733–40. doi: 10.1016/S0254-6272(15)30089-3
5. Zhao RQ, Hu QH, Ma GX, Su AX, Xie MH, Li XF, et al. Effects of *Flammulina velutipes* polysaccharide on immune response and intestinal microbiota in mice. *J Funct Foods*. (2019) 56:255–64. doi: 10.1016/j.jff.2019.03.031
6. Liang QX, Zhao QC, Hao XT, Wang JM, Ma CY, Xi XF, et al. The effect of *Flammulina velutipes* polysaccharide on immunization analyzed by intestinal flora and proteomics. *Front Nutr*. (2022) 9:1–17. doi: 10.3389/fnut.2022.841230
7. Hao W, Wang SF, Zhao J, Li SP. Effects of extraction methods on immunology activity and chemical profiles of *Lycium barbarum* polysaccharides. *J Pharmaceut Biomed*. (2020) 185:113219. doi: 10.1016/j.jpba.2020.113219
8. Jiang Z, Mao J, Huang J, Wu Y, Cai C, Fan Y. Changes in antioxidant activity of blueberry-ferment during natural fermentation process, *Sci Technol Food Ind*. (2013) 2:194–201. doi: 10.13386/j.issn1002-0306.2013.02.059.
9. Meshram V, Saxena S, Paul K, Gupta M, Kapoor N. Production, purification and characterization of a potential fibrinolytic protease from endophytic Xylaria curta by solid substrate fermentation. *Appl Biochem Biotechnol*. (2016) 181:1–17. doi: 10.1007/s12010-016-2298-y
10. Singhania RR, Patel AK, Soccol CR, Pandey A. Recent advances in solid-state fermentation. *Biochem Eng J*. (2009) 44:13–8. doi: 10.1016/j.bej.2008.10.019
11. Xie LM, Huang ZB, Meng H, Shi XY, Xie JH. Immunomodulation effect of polysaccharides from liquid fermentation of *Monascus purpureus* 40269 *via* membrane TLR-4 to activate the MAPK and NF-κB signaling pathways. *Int J Biol Macromol*. (2022) 201:480–91. doi: 10.1016/j.ijbiomac.2022.01.045
12. Liu X, Hou RL, Xu KQ, Chen L, Wu XP, Lin WX, et al. Extraction, characterization and antioxidant activity analysis of the polysaccharide from the solid-state fermentation substrate of *Inonotus hispidus*. *Int J Biol Macromol*. (2019) 123:468–76. doi: 10.1016/j.ijbiomac.2018.11.069
13. Bauer C, Duewell P, Mayer C, Lehr HA, Fitzgerald KA, Dauer M, et al. Colitis induced in mice with dextran sulfate sodium (DSS) is mediated by

the NLRP3 inflammasome. *Gut*. (2010) 59:1192–9. doi: 10.1136/gut.2009.197822
14. Cui L, Wang W, Luo Y, Ning Q, Xia Z, Chen J, et al. Polysaccharide from *Scutellaria baicalensis Georgi* ameliorates colitis *via* suppressing NF-κB signaling and NLRP3 inflammasome activation. *Int J Biol Macromol*. (2019) 132:393–405. doi: 10.1016/j.ijbiomac.2019.03.230
15. Ma S, Shen C, Xu JX. Extraction, structure and antioxidant activity of polysaccharide from fermented *Flammulina velutipes* root. *Food Sci Technol*. (2021) 46:147–54. doi: 10.13684/j.cnki.spkj.2021.03.026
16. Liang ZH, Zheng KW, Zhao QC, Shao WJ, Li CQ, Wang JM, et al. Structural identification and coagulation effect of *Flammulina velutipes* polysaccharides. *Appl Sci*. (2021) 11:1736. doi: 10.3390/app11041736
17. Tang W, Lin LH, Xie JH, Wang ZJ, Wang H, Dong YJ, et al. Effect of ultrasonic treatment on the physicochemical properties and antioxidant activities of polysaccharide from *Cyclocarya paliurus*. *Carbohydr Polym*. (2016) 151:305–12. doi: 10.1016/j.carbpol.2016.05.078
18. Xie JH, Liu X, Shen MY, Nie SP, Zhang H, Li C, et al. Purification, physicochemical characterization and anticancer activity of a polysaccharide from *Cyclocarya paliurus* leaves. *Food Chem*. (2013) 136 1453–60. doi: 10.1016/j.foodchem.2012.09.078
19. Liu R, Xiao N, Tian K. The role of PMN apoptosis delay in acute lung injury induced by administrating LPS. *Zhonghua Yi Xue Za Zhi*. (2001) 81:617–21. (in Chinese).
20. Lainiol M, Linden AM, Aitta-aho T. Behavioral responses of mGluR3-KO mice to the lipopolysaccharide-induced innate inflammatory reaction. *Pharmacol Biochem Behav*. (2020) 190:172852. doi: 10.1016/j.pbb.2020.172852
21. Wei MJ, Wang ZN, Yang Y, Zhang SJ, Bi CL. Selenium attenuates *S. aureus*-induced inflammation by regulation TLR2 signaling pathway and NLRP3 inflammasome in RAW 264.7 macrophages. *Biol Trace Elem Res*. (2021) 2021:1–7. doi: 10.1007/s12011-021-02676-4
22. Qin H, Huang L, Teng J, Wei B, Xia N, Ye Y. Purification, characterization, and bioactivity of *Liupao* tea polysaccharides before and after fermentation. *Food Chem*. (2021) 353:129419. doi: 10.1016/j.foodchem.2021.129419
23. Li HL, Liu S, Liu Y, Li WN, Niu AJ, Ren P, et al. Effects of *in vitro* digestion and fermentation of *Nostoc commune Vauch*. polysaccharides on properties and gut microbiota. *Carbohyd Polym*. (2022) 281:119055. doi: 10.1016/j.carbpol.2021.119055
24. Wu D, Yuan Q, Guo H, Fu Y, Li F, Wang S, et al. Dynamic changes of structural characteristics of snow chrysanthemum polysaccharides during *in vitro* digestion and fecal fermentation and related impacts on gut microbiota. *Food Res Int*. (2021) 141:109888. doi: 10.1016/j.foodres.2020.109888
25. Luo Z, Wang L, Zhou P, Feng R, Li X. Effect of *in vitro* simulated gastrointestinal digestion on structural characteristics and anti-proliferative activities of the polysaccharides from the shells of Juglans regia L. *Food Chem Toxicol*. (2021) 150:112100. doi: 10.1016/j.fct.2021.112100
26. Qi X, Tester RF. Starch containing formulations for diarrhea therapy. *Clin Nutr ESPEN*. (2018) 122:572–7. doi: 10.1016/j.clnesp.2018.08.003
27. Qi X, Tester RF. Utilization of dietary fiber (non-starch polysaccharide and resistant starch) molecules for diarrhea therapy: a mini-review. *Int J Biol Macromol*. (2019) 122:572–7. doi: 10.1016/j.ijbiomac.2018.10.195
28. Qi YL, Chen LX, Gao K, Shao ZJ, Huo XH. Effects of *Schisandra chinensis* polysaccharides on rats with antibiotic-associated diarrhea. *Int J Biol Macromol*. (2019) 124:627–34. doi: 10.1016/j.ijbiomac.2018.11.250
29. Chen Y, Zhang Y, Luo QY, Zhu YJ, Du HJ, Liao SY, et al. Inhibition of porcine epidemic diarrhea virus by *Alpiniae oxyphyllae fructus* polysaccharide 3. *Res Vet Sci*. (2021) 141:146–55. doi: 10.1016/j.rvsc.2021.10.026
30. Chen Y, Luo QY, Li SM, Li CH, Liao SY, Yang X, et al. Antiviral activity against porcine epidemic diarrhea virus of *Pogostemon cablin* polysaccharide. *J Ethnopharmacol*. (2020) 259:113009. doi: 10.1016/j.jep.2020.113009
31. Wang Z, Wang Z, Huang W, Suo J, Zhang H. Antioxidant and anti-inflammatory activities of an anti-diabetic polysaccharide extracted from *Gynostemma pentaphyllum* herb. *Int J Biol Macromol*. (2020) 145:484–91. doi: 10.1016/j.ijbiomac.2019.12.213
32. Jiang F, Ding YY, Tian Y, Yang RX, Quan ML, Tong ZY, et al. Hydrolyzed low-molecular-weight polysaccharide from *Enteromorpha prolifera* exhibits high anti-inflammatory activity and promotes wound healing. *Mater Sci Eng C Mater Biol Appl*. (2021) 112637. doi: 10.1016/j.msec.2021.112637
33. Huang L, Shen M, Morris GA, Xie J. Sulfated polysaccharides: immunomodulation and signaling mechanisms. *Trends Food Sci Technol*. (2019) 92:1–11. doi: 10.1016/j.tifs.2019.08.008
34. Hou C, Chen L, Yang L, Ji X. An insight into anti-inflammatory effects of natural polysaccharides. *Int J Biol Macromol*. (2020) 153:248–55. doi: 10.1016/j.ijbiomac.2020.02.315
35. Zhang L, Ma L, Pan Y, Zheng X, Qiao H. Effect of molecular weight on the antibacterial activity of polysaccharides produced by *Chaetomium globosum* CGMCC 6882 *Int J Biol Macromol*. (2021) 188:863–9. doi: 10.1016/j.ijbiomac.2021.08.059
36. Tsopmejio ISN, Ding M, Wei JL, Zhao C, Jiang Y, Li YT, et al. Auricularia polytricha and *Flammulina velutipes* ameliorate inflammation and modulate the gut microbiota *via* regulation of NF-κB and Keap1/Nrf2 signaling pathways on DSS-induced inflammatory bowel disease. *Food Biosci*. (2022) 47:101426. doi: 10.1016/j.fbio.2021.101426
37. Han R, Wang L, Zhao ZG, You LJ, Pedisićd S, Kulikouskaya V, et al. Polysaccharide from *Gracilaria Lemaneiformis* prevents colitis in Balb/c mice *via* enhancing intestinal barrier function and attenuating intestinal inflammation. *Food Hydrocoll*. (2020) 109:106048. doi: 10.1016/j.foodhyd.2020.106048
38. He Y, Hara H, Núez G. Mechanism and regulation of NLRP3 inflammasome activation. *Trends Biochem Sci*. (2016) 41:1012–21. doi: 10.1016/j.tibs.2016.09.002
39. Hou B, Zhang Y, Liang P, He Y, He X. Inhibition of the NLRP3-inflammasome prevents cognitive deficits in experimental autoimmune encephalomyelitis mice *via* the alteration of astrocyte phenotype. *Cell Death Dis*. (2020) 11:377. doi: 10.1038/s41419-020-2565-2
40. Pan XL, Wang HY, Zheng ZM, Huang X, Yang LL, Liu JX, et al. Pectic polysaccharide from Smilax China L. ameliorated ulcerative colitis by inhibiting the galectin-3/NLRP3 inflammasome pathway *Carbohyd Polym*. (2022) 277:118864. doi: 10.1016/j.carbpol.2021.118864
41. Castro-Alves VC, Shiga TM, Nascimento JRO. Polysaccharides from chayote enhance lipid efflux and regulate NLRP3 inflammasome priming in macrophage-like THP-1 cells exposed to cholesterol crystals. *Int J Biol Macromol*. (2019) 127:502–10. doi: 10.1016/j.ijbiomac.2019.01.048
42. Rajamäki K, Lappalainen J, Oörni K, Välimäki E, Matikainen S, Kovanen PT, et al. Cholesterol crystals activate the NLRP3 inflammasome in human macrophages: a novel link between cholesterol metabolism and inflammation. *PLoS ONE*. (2010) 5:11765. doi: 10.1371/journal.pone.0011765

Conflict of Interest: The authors declare that the research was conducted in the absence of any commercial or financial relationships that could be construed as a potential conflict of interest.

Publisher's Note: All claims expressed in this article are solely those of the authors and do not necessarily represent those of their affiliated organizations, or those of the publisher, the editors and the reviewers. Any product that may be evaluated in this article, or claim that may be made by its manufacturer, is not guaranteed or endorsed by the publisher.

Copyright © 2022 Ma, Xu, Lai, Xu, Zhang, Zhang and Zhang. This is an open-access article distributed under the terms of the Creative Commons Attribution License (CC BY). The use, distribution or reproduction in other forums is permitted, provided the original author(s) and the copyright owner(s) are credited and that the original publication in this journal is cited, in accordance with accepted academic practice. No use, distribution or reproduction is permitted which does not comply with these terms.

frontiers | Frontiers in Immunology

ORIGINAL RESEARCH
published: 23 June 2022
doi: 10.3389/fimmu.2022.911390

Modulation of T Cell Responses by Fucoidan to Inhibit Osteogenesis

Hailin Huang[1,2], Fangze Guo[1,2], Xuyang Deng[1,2], Mingzhe Yan[3], Danyang Wang[1,2,3], Zhanyi Sun[4], Changqing Yuan[1,2] and Qihui Zhou[1,2,3,5]*

[1] Department of Stomatology, The Affiliated Hospital of Qingdao University, Qingdao University, Qingdao, China, [2] School of Stomatology, Qingdao University, Qingdao, China, [3] Institute for Translational Medicine, The Affiliated Hospital of Qingdao University, Qingdao University, Qingdao, China, [4] State Key Laboratory of Bioactive Seaweed Substances, Qingdao Bright Moon Seaweed Group Co., Ltd., Qingdao, China, [5] School of Rehabilitation Sciences and Engineering, University of Health and Rehabilitation Sciences, Qingdao, China

Fucoidan has sparked considerable interest in biomedical applications because of its inherent (bio)physicochemical characteristics, particularly immunomodulatory effects on macrophages, neutrophils, and natural killer cells. However, the effect of fucoidan on T cells and the following regulatory interaction on cellular function has not been reported. In this work, the effect of sterile fucoidan on the T-cell response and the subsequent modulation of osteogenesis is investigated. The physicochemical features of fucoidan treated by high-temperature autoclave sterilization are characterized by UV–visible spectroscopy, X-ray diffraction, Fourier transform infrared and nuclear magnetic resonance analysis. It is demonstrated that high-temperature autoclave treatment resulted in fucoidan depolymerization, with no change in its key bioactive groups. Further, sterile fucoidan promotes T cells proliferation and the proportion of differentiated T cells decreases with increasing concentration of fucoidan. In addition, the supernatant of T cells co-cultured with fucoidan greatly suppresses the osteogenic differentiation of MC3T3-E1 by downregulating the formation of alkaline phosphatase and calcium nodule compared with fucoidan. Therefore, our work offers new insight into the fucoidan-mediated T cell and osteoblast interplay.

Keywords: marine polysaccharide, fucoidan, T cell, osteogenesis, osteoimmunology

OPEN ACCESS

Edited by:
Bin Du,
Hebei Normal University of Science and Technology, China

Reviewed by:
Chao Zhao,
Fujian Agriculture and Forestry University, China
Lei Chen,
Guangdong Ocean University, China

***Correspondence:**
Changqing Yuan
yuancq@qdu.edu.cn
Qihui Zhou
qihuizhou@qdu.edu.cn

Specialty section:
This article was submitted to Nutritional Immunology, a section of the journal Frontiers in Immunology

Received: *02 April 2022*
Accepted: *30 May 2022*
Published: *23 June 2022*

Citation:
Huang H, Guo F, Deng X, Yan M, Wang D, Sun Z, Yuan C and Zhou Q (2022) Modulation of T Cell Responses by Fucoidan to Inhibit Osteogenesis. Front. Immunol. 13:911390. doi: 10.3389/fimmu.2022.911390

1 INTRODUCTION

Due to their distinctive (bio)physicochemical features, such as outstanding biocompatibility, bioactivity, immunomodulation, and structural functions, marine polysaccharides have gained increasing attention in nutraceutical and biomedicine in recent decades (1–8). It is noteworthy that fucoidan is a sulfated polysaccharide extracted from brown algae with a variety of biological

Abbreviations: NK, natural killer; HFD, Fucoidan sterilized by high-temperature autoclave; Mw, Molecular weight; AxV, Annexin V-fluorescein-5-isothiocyanate; PI, propidium iodide; CFSE, 5-(and-6)-Carboxyfluorescein diacetate, succinimidyl ester; DMEM, Dulbecco's modified Eagle's medium; CCK8, Cell Counting Kit-8; ARS, Alizarin red S; UFD, unsterilized fucoidan; HPLC, high performance liquid chromatography; XRD, X- ray diffraction; NMR, Nuclear magnetic resonance; FT-IR, Fourier transform-infrared spectroscopy; OD, The optical density; MC3T3-E1, The murine osteoblastic cell line; ALP, Alkaline phosphatase.

activities, such as immunomodulatory activity, osteogenesis, anti-inflammatory, anti-tumor, anti-bacterial, anti-viral, anti-oxidant, anti-coagulant, anti-thrombotic, and anti-fibrotic (3, 9–12). Particularly, it has a critical option for a range of biological applications due to its immunomodulatory characteristic. For instance, fucoidan prevented the development of macrophages into foam cells and the migration of smooth muscle cells into the intimal layer of the aorta, thereby inhibiting the formation of atherosclerotic plaques (10). Intraperitoneal administration of fucoidan has been reported to accelerate the recovery of leukocytes and neutrophils with activity exceeding that of recombinant human granulocyte colony-stimulating factor (11). Fucoidan also significantly restores cytotoxicity and granzyme B release levels in natural killer (NK) cells (13). Furthermore, intranasal fucoidan treatment increased the activation of dendritic cells, and NK cells, in the mediastinal lymph node (14). Fucoidan as a dietary supplement has been reported to promote the activation of tumor-infiltrating T cells and thus may be used synergistically with immune checkpoint blockade in the treatment of malignancies (15). Thus, it is critical to elicit how fucoidan modulates the immune cells, particularly T cells.

The immune system is known to be implicit in tissue repair and regeneration, where adaptive immunity, especially T cells, plays a critical role in modulating surrounding (stem) cell behavior and function/differentiation (16–21). It has been suggested that the mechanism by which T cells promote tissue repair and regeneration may be related to the control of neutrophil behavior and the regulation of inflammation (22–25). In particular, the ability of bone to heal without scar tissue formation has led to widespread interest in T cell-related bone repair and regeneration (26, 27). In studies of cyclosporine A-induced osteoporosis, it has been reported that the lack of T-lymphocyte function led to the formation of demineralized bone matrix and the loss of existing bone tissue density (28). And, it has been demonstrated that T cells had an inhibitory effect on osteoclast formation and changes in bone resorption, which is mediated by interferon- γ produced by T cells acting by interfering with the RANKL-RANK signaling pathway (29). In addition, studies on osteogenic differentiation of human mesenchymal stromal cells confirmed that media derived from CD4 T cells could increase osteogenic mineralization *in vitro* (30). Several studies have reported that T cells had an effect on osteogenesis and fucoidan had a modulating effect on a wide range of immune cells. However, the effect of fucoidan on T cells *in vitro* has not been studied. Considering the effect of T cells on osteogenesis, it is necessary to elucidate the role of fucoidan on T cells and consequently the subsequent effects on osteogenesis.

Fucoidan sterilized by high-temperature autoclave (HFD) was employed in this study to explore its influence on T cell responses. It was found that that although high-temperature autoclave treatment resulted in fucoidan depolymerization, there were no changes in its key bioactive groups. The proliferative effect of HFD on T cell proliferation increased with an increasing concentration within a certain range (0.4–50 mg/mL). On the contrary, HFD inhibited the differentiation of T cells, and the higher the concentration, the more pronounced the inhibitory effect. HFD could inhibit osteogenesis by affecting T cells. This is the first report of fucoidan being employed *in vitro* to modulate T cell responses and thereby research its effects on osteogenesis, to the best of our knowledge.

2 EXPERIMENTAL SECTION

2.1 Materials

Fucoidan [Molecular weight (Mw) = 276 kDa, purity ≥95%, sulfate: 29.65%] was provided by Qingdao Bright Moon Seaweed Group Co., Ltd. (China). EasySep™ Mouse T Cell Isolation Kit was acquired from Stemcell Technologies (Vancouver, BC, Canada). The anti-mouse CD3 (Clone 17A2) and anti-mouse CD28 (Clone 37.51) were acquired from BioGems. Annexin V-fluorescein-5-isothiocyanate (AxV), propidium iodide (PI), anti-mouse CD8α, phycoerythrin-cyanine 7 (PE-Cy7, Clone: 53-6.7), anti-mouse CD4, PE (Clone: GK1.5) and Flow cytometry Straining buffer were supplied by Multi Sciences (LianKe) Biotech,CO.,LTD. 5-(and-6)-Carboxyfluorescein diacetate, succinimidyl ester (CFSE) was provided by Abbkine Bioadvisers. RPMI 1640 and Tris-(hydroxymethyl) aminomethane (Tris) was purchased from Solarbio. Dulbecco's modified Eagle's medium (DMEM), fetal bovine serum and penicillin/streptomycin were acquired from Biological Industries, Israel. Cell Counting Kit-8 (CCK-8) was provided by MedChemExpress Co.Ltd (Shanghai, China). Alizarin red S (ARS) staining kit for osteogenesis was purchased from Beyotime (Shanghai, China). All the experimental water was deionized water.

2.2 Chemical Composition Analysis

Unsterilized fucoidan (UFD) was dried in a lyophilizer after being treated with high-temperature autoclave sterilization (121°C, 20 min). The composition of monosaccharides was determined using high performance liquid chromatography (HPLC1260, Agilent, USA). Specific experimental methods are as follows: chromatographic conditions: C column, 250mm × 4.6mm, 5hm, or equivalent; The column temperature was 40 °C The flow rate was 1.0 mL/min; Mobile phase: solvent A: acetonitrile-0.05mol/L potassium dihydrogen phosphate buffer (15 + 85), solvent B: acetonitrile-0.05mol/L potassium dihydrogen phosphate buffer (40 + 60).

2.3 UV–Visible Spectroscopy Analysis

2 mg of UFD and HFD were completely dissolved in 2.5 mL deionized water respectively and the spectrum was measured in the range of 200–450 nm using UV–vis spectrophotometer (UV-1800 spectrophotometer, Shimadzu, Japan).

2.4 X-Ray Diffraction (XRD) Analysis

XRD spectroscopy was performed using DX2700 (Dandong, China) to examine the crystal structure of fucoidan. The

samples were tested between 10° and 70°, at a voltage of 40 kV, a current of 30 mA, and Cu Kα radiation (λ=1.5418 Å) at a scan rate of 0.05° (2θ)/min.

2.5 Nuclear Magnetic Resonance (NMR) Analysis

^{1}H NMR analysis was performed using a Sophisticated Spectrometer (400 MHz Bruker model). Simply, 5 mg of UFD and HFD were dissolved in 0.55 mL of deuterium oxide and placed in NMR tubes respectively. NMR spectrum was analyzed at 27°C and proton chemical shifts were expressed in parts per million (ppm).

2.6 Fourier Transform Infrared (FT-IR) Analysis

The functional groups of UFD and HFD were analyzed in the FT-IR spectroscopy (Nicolet iS10, Thermo Scientific, USA). The infrared spectrum was measured in the wavenumber range of 4000-500 cm^{-1}.

2.7 Primary T Lymphocytes Extraction and Activation

Murine cells were acquired from adult (6–12 week old) C57BL/6 mice spleens, approved by the Ethics Committee of the Affiliated Hospital of Qingdao University (approval number: QYFYWZLL 26850) (31, 32). T lymphocytes were isolated from splenocytes by negative selection using EasySep™ Mouse T Cell Isolation Kit according to the manufacturer's instructions. Plate fixed anti-mouse CD3 (1 μg/mL) and free anti-mouse CD28 (1 μg/mL) were used overnight at 4°C to activate primary T cells. The purity of extracted T cells is tested by the anti-mouse CD3e Antibody, Clone 145-2C11 and is sufficient for subsequent experiments. T cells were cultured in the T cell culture media (RPMI 1640 supplemented with phenol sulfonphthalein, hepes, Sodium Pyruvate, L- glutamine, D-glucose, sodium bicarbonate, 10% fetal bovine serum and 1% penicillin/streptomycin), in a humidified incubator of 5% CO_2 at 37°C.

2.8 Cell Proliferation

T cells were cultured in 96-well plates at a density of 1×10^6 cells/mL, and different concentrations of HFD (0.4, 2, 10, and 50 mg/mL) were added to the medium. A simple medium without HFD was used as a control and incubated for 1, 3 and 5 d, respectively. Subsequently, 10% CCK-8 was added to the medium and incubated for 4 h at 37°C. The optical density (OD) values of the medium at 450 nm were measured using a microplate reader (SynergyH1/H1M, Bio-Tek, China). In addition to this, the cells were stained using CFSE according to the instructions of the manufacturer before culturing, and after co-culture with different concentrations of HFD for 3 d, they were washed and analyzed using a BD FACSCanto (BD Bioscience, USA).

2.9 Cell Apoptosis

Potential toxic effects of HFD were tested using flow cytometry. Different concentrations of HFD were used to co-culture with T cells for 2 d as described previously, also with the normal medium as a control. Cells were stained using a mixture containing 0.5 μL/mL of AxV and 0.5 μL/mL of PI and incubated for 15 minutes at room temperature protected from light. The cells were then washed twice with phosphate buffer solution and assayed using flow cytometry.

2.10 Cell Differentiation

For cell differentiation analysis, after spreading the plates and culturing the cells for 5 d as described previously, the cells were resuspended using flow cytometry staining buffer and stained with anti-CD4, anti-CD8, both at a concentration of 0.5 μL/mL and incubated for 15 minutes at room temperature and under protection from light. Cells were washed with flow cytometry staining buffer and resuspended again before being detected using flow cytometry.

2.11 MC3T3-E1 Cell Viability

The murine osteoblastic cell line (MC3T3-E1) was provided by the Cell Culture Centre of Shanghai Institutes for Biological Science Chinese Academy of Sciences (Shanghai, China). MC3T3-E1 cells were grown at a density of 5×10^4 cells/mL in 96-well plates, DMEM medium was used as the control group (CON), while the remaining three groups were added with 20% of 0.4 mg/mL HFD supernatant (HFD), 20% of T cell supernatant (T) and 20% of supernatant from co-culture of T cells with HFD (CM), respectively. After 1 and 3 d of incubation, 10% of the Cell Counting Kit 8 (Absin Bioscience Inc., China) was added to the culture medium and incubated for 1 h at 37°C. The OD values of the medium at 450 nm were measured using a microplate reader (SynergyH1/H1M, Bio-Tek, China).

2.12 Alkaline Phosphatase (ALP) Staining and Activity

To obtain conditioned medium (CM), T cells were inoculated into 6-well plates at a density of 1×10^6 cells/mL and co-cultured with 0.4 mg/mL HFD. Cell suspensions were collected after 24 h, centrifuged, and the supernatants were collected and stored in a -80°C freezer until use. For ALP staining, MC3T3-E1 cells were inoculated at a density of 2×10^4 cells per well in 24-well plates and treated with osteogenic induction medium (0.1 mM dexamethasone,10 mM β-glycerophosphate and 50 μg/mL L-ascorbic acid in basic DMEM medium) containing CM at 20% concentration. The osteogenic induction medium alone group (CON), the group containing 20% 0.4 mg/mL HFD supernatant (HFD) and the group containing 20% T cell supernatant (T) were used as controls, and HFD, T, and CM were added at each medium change (33). Following the manufacturer's instructions, the ALP activity of MC3T3-E1 cells was determined using an

ALP assay kit (Nanjing Jiancheng Bioengineering Institute, Nanjing, China) after 14 days of incubation. Inverted Fluorescence Microscopy (Nikon A1 MP, Japan) was used to capture the photos. The ALP staining positive rate was quantified using ImageJ software. For standardization, total cellular protein concentration was determined by the BCA protein assay kit (Beyotime, Shanghai, China). ALP activity was shown as total cellular protein content (king unit/g prot). The ALP staining positive rate was quantified using ImageJ software. For standardization, total cellular protein concentration was determined by the BCA protein assay kit (Beyotime, Shanghai, China). ALP activity was shown as total cellular protein content (king unit/g prot).

2.13 ARS Staining

Calcium accumulation was determined by ARS staining. MC3T3-E1 cells were treated and cultured in the same way as before. After 14 d of incubation, the cells were treated with 70% (v/v) ice-cold ethanol for 1 h at 4°C, stained with 40 mM ARS solution, and imaged using a microscope.

2.14 Statistical Analysis

All data points were displayed as mean values ± standard deviation (SD). Graphpad Prism 8 or Origin 9 were used to evaluate all statistical analysis. To determine differences between groups, a one-way analysis of variance (ANOVA) with Tukey's test was used. Statistical significance was defined as a value of $p < 0.05$.

3 RESULTS AND DISCUSSION

3.1 Physicochemical Characterization of Fucoidan

In general, biomaterial sterilization is an essential part of microbial eradication in biomedical applications. Because of its capacity to remove nanoscale bacteria (e.g., virus and mycoplasma), a high-temperature autoclave was used to sterilize the aqueous solution of fucoidan in this situation.

The impact of a high-temperature autoclave on the Mw of fucoidan was examined using HPLC, as indicated in **Table 1**. The chemical composition of HFD remained unchanged, however, the Mw and the ratio of the components changed. The result shows that the MW of the HFD (14 kDa) was significantly lower than that of the UFD (223 kDa), indicating that the high-temperature autoclave treatment led to the depolymerization of the fucoidan. Studies have reported that low-molecular-weight fucoidan has higher absorption and bioavailability than high-molecular fucoidan, so autoclaved fucoidan may be more beneficial for our subsequent cellular experiments (7). The total sugar content of UFD was 78.61%, sulfate group content was 28.42%, and uronic acid content was 0.9%. Compared with UFD, the total sugar content of HFD decreased significantly, sulfate group content increased slightly and uronic acid content increased greatly.

TABLE 1 | The Mw and chemical composition of UFD and HFD.

Samples	Mw (kDa)	Total sugar (%)	Sulfate (%)	Uronic acid (%)
UFD	223	78.61	28.42	0.9
HFD	14	70.91	30.23	10.7

UV–visible spectroscopy, XRD, ^{1}HNMR, and FT-IR measurements were used to further evaluate the physicochemical characterizations of fucoidan. Both UFD and HFD appeared the typical absorbance peak at 260 nm within the UV–visible which indicates the covalent holding of aromatic compounds with the polysaccharides (**Figure 1A**). Additionally, the absorption band of fucoidan suggested fucose enriched sulfated polysaccharides (34). The changes in microstructure were determined by XRD analysis. As shown in **Figure 1B**, both the UFD and HFD powder at 23° showed a low overall crystallinity, which indicates that it could be a semicrystalline polymer, in line with previous research findings (35, 36).. In addition, NMR spectroscopy has served as a useful tool for studying the anomeric configuration and sulphation modes of polysaccharides. In this study, the ^{1}HNMR spectrum of UFD and HFD is shown in **Figure 1C**. Signals at 4.32 and 4.66 ppm corresponded to α-L-fucose and 3-linked α-L-fucose, which were the primary components of fucoidan (34, 37). The 3-linked β-D-galactose was represented by the signal at 4.00 ppm. The presence of α-L-rhamnopyranosyl residues was suggested by the signal at 3.70 ppm (38). FT-IR was used to investigate the influence of high-temperature autoclave sterilization on the chemical group of fucoidan. The key characteristic peaks (3440, 2937, 1640, 1250, 1053, and 840 cm^{-1}) were found in the FT-IR spectra of UFD and HFD, as shown in **Figure 1D**. The O-H group stretching vibrations related to a large peak between 3600 and 3000 cm^{-1}. Signals at 2936 and 1632 cm-1 were ascribed to C-H and C═O stretching vibration, and the band at 2936 cm^{-1} was recognized as the typical absorption of polysaccharides (39, 40). The band at 1250 cm^{-1} was considered to correlate to the S═O stretching vibration, which was regarded as the most prominent feature of fucoidan, indicating the existence of sulfate groups. The peak at 832 cm^{-1} was attributed to the C-O-S bending vibration, which indicated sulfate groups at the axial C-4 position of fucose (3, 34). Taken together, these results indicate that although high-temperature autoclave treatment resulted in fucoidan depolymerization, there were no changes in its key bioactive groups.

3.2 The Interactions Between HFD and T Lymphocytes

CCK-8 was used to detect the effect of fucoidan on T cell viability. CCK-8 viability was measured after 1, 3 and 5 d of co-cultured with HFD. As presented in **Figure 2A**, on the first day, the addition of HFD resulted in a significant increase in cell viability, and the higher the concentration, the more significant the increase in cell viability. On days 3 and 5, the addition of

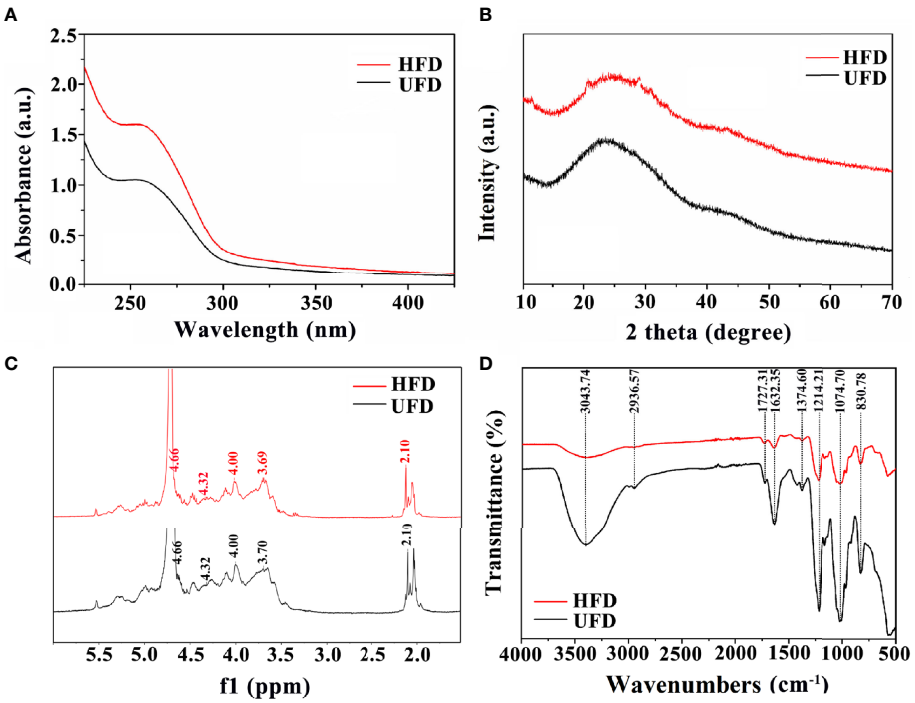

FIGURE 1 | **(A)** UV-visible spectroscopy, **(B)** XRD diffraction patterns, **(C)** ^{1}HNMR spectrum, and **(D)** FT-IR spectra of UFD and HFD.

HFD still had an increasing effect on cell viability, and the higher concentration groups (i.e., 10, and 50 mg/mL) still greatly increased cell viability. Furthermore, T cell proliferation was assessed by flow cytometry and CFSE staining. CFSE was chosen because the two acetate groups made it more cell-permeable and non-fluorescent than CFSE (41). Intracellular esterase cleaved the acetate groups of CFSE, resulting in the luminous, non-cell permeable CFSE. This dye was uniformly distributed between the two daughter cells during each cell division, resulting in a 50% reduction in CFSE fluorescence intensity with each cell division. The proliferation of the cells could be tracked in this way, and the flow cytometry results for 3 d following stimulation are presented in **Figure 2B**. The HFD group at 50 mg/mL showed a double peak, proving that this group had the best proliferation-promoting effect. Collectively, these data demonstrated that HFD greatly enhanced the growth of T cells.

Apoptotic and necrotic cells were detected with AxV and PI. As shown in **Figure 3**, the percentage of viable cells in the control group was 19.8% after 3 d of incubation. The addition

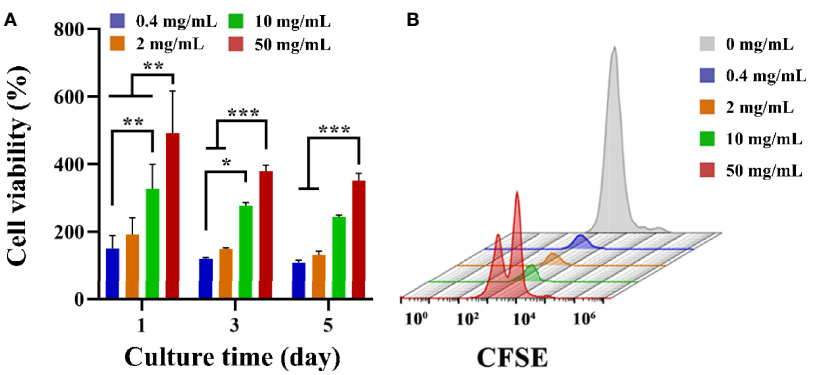

FIGURE 2 | **(A)** T cell viability on different groups treated with HFD after 1, 3 and 5 d. Data are mean ± SD (n = 3) (*$p < 0.05$, **$p < 0.01$, ***$p < 0.001$). **(B)** Representative CFSE diagram on various samples.

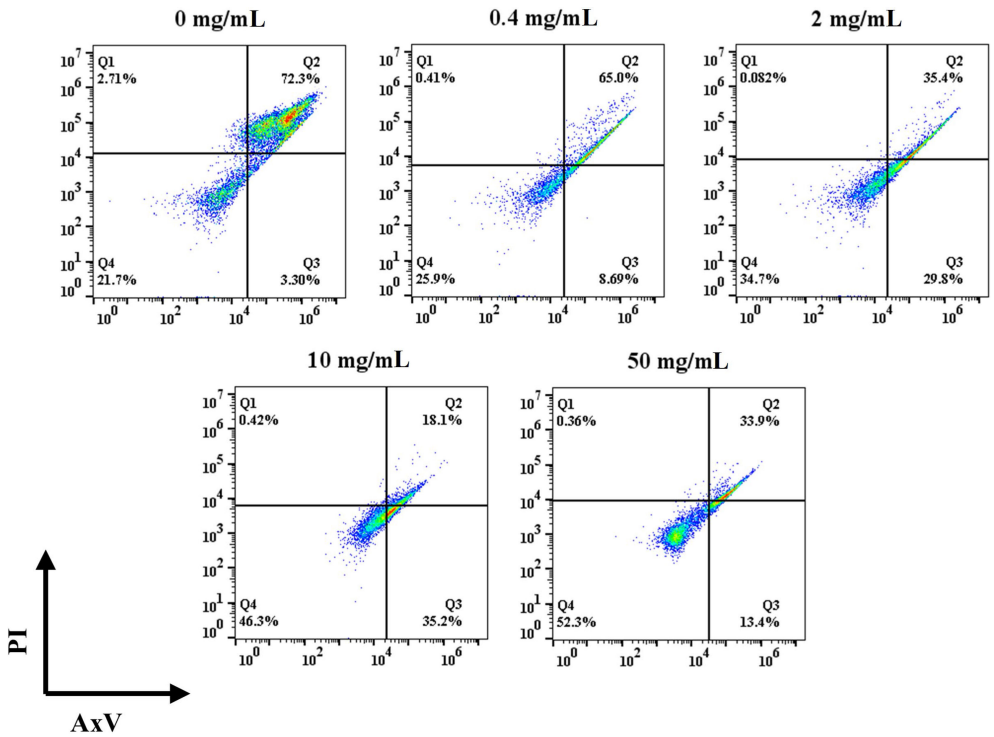

FIGURE 3 | Effect of HFD on the viability of mouse primary T cells.

of HFD increased the percentage of viable cells, and it gradually increased with the increase of HFD concentration. In details, the percentages of viable cells at 0.4, 2, 10, and 50 mg/mL of HFD were 25.9%, 30.6%, 46.1% and 52.6%, respectively. In addition, the addition of HFD resulted in a decrease in the ratio of late apoptotic to necrotic cells. To be specific, the ratios of late apoptotic and necrotic cells in the control, 0.4, 2, 10, and 50 mg/mL fucoidan were 75.4%, 65.2%, 38.3%, 18.8% and 27.2% respectively. The low overall percentage of live cells may be since IL-2 is not added to the cultures as it has been reported that T cells themselves can produce IL-2 to participate in certain feedback loops (42–45). Therefore, our results demonstrate that HFD reduces T cell apoptosis even in the absence of IL-2.

Differentiation experiments were performed on day 5 after seeding to evaluate the phenotype of the T cells after proliferation. Specifically, naïve T ($CD4^-/CD8^-$), $CD4^+$, and $CD8^+$ T cells were identified by flow cytometry. In the control group, the naïve T cells ratio was 27.9% and the ratio of $CD4^+$ to $CD8^+$ cells was 1.53 (**Figure 4**). The ratio of $CD4^+$ to $CD8^+$ did not show a trend with concentration after the addition of HFD, but the ratio of initial T cells gradually increased with the increase of HFD addition, with the ratios of 37.9%, 68%, 56.5%, and 82.0%, respectively. The 0.4 mg/mL HFD group had the greatest effect on T cell differentiation, and the ratio of $CD4^+$ to $CD8^+$ cells was 1.66. Differentiated T cells in this group may produce more cytokines, which may have the greatest effect on subsequent osteogenic differentiation.

3.3 MC3T3-E1 Cell Viability and Osteogenic Differentiation

Based on the differentiation of T cells above, 0.4 mg/mL HFD was chosen for the following experiments. In conjunction with studies by others, supernatants from one day after co-culture of HFD with T cells were used as CM (33). After 1 and 3 d of culture, we examined the effect of CM on MC3T3-E1 cell activity by CCK-8. As shown in **Figure 5**, MC3T3-E1 cell activity increased significantly with time in all groups. However, compared with the CON, the CM group did not significantly increase the viability of MC3T3-E1 cells. Therefore, HFD did not contribute to the viability of MC3T3-E1 cells by regulating T cells.

ALP has been regarded as an important biochemical marker for osteogenic differentiation and new bone production (46–49). **Figure 6A** represented microscopic photographs of cellular ALP expression in CON, HFD, T, and CM after 14 d of culture. It was found that the area of ALP staining was larger in the HFD and T compared with the CON, while the area of ALP staining was significantly reduced in the CM compared to other groups. To better understand the ALP staining results, we quantified the stained area (**Figure 6B**). Quantitative analysis of ALP staining also confirmed these results above.

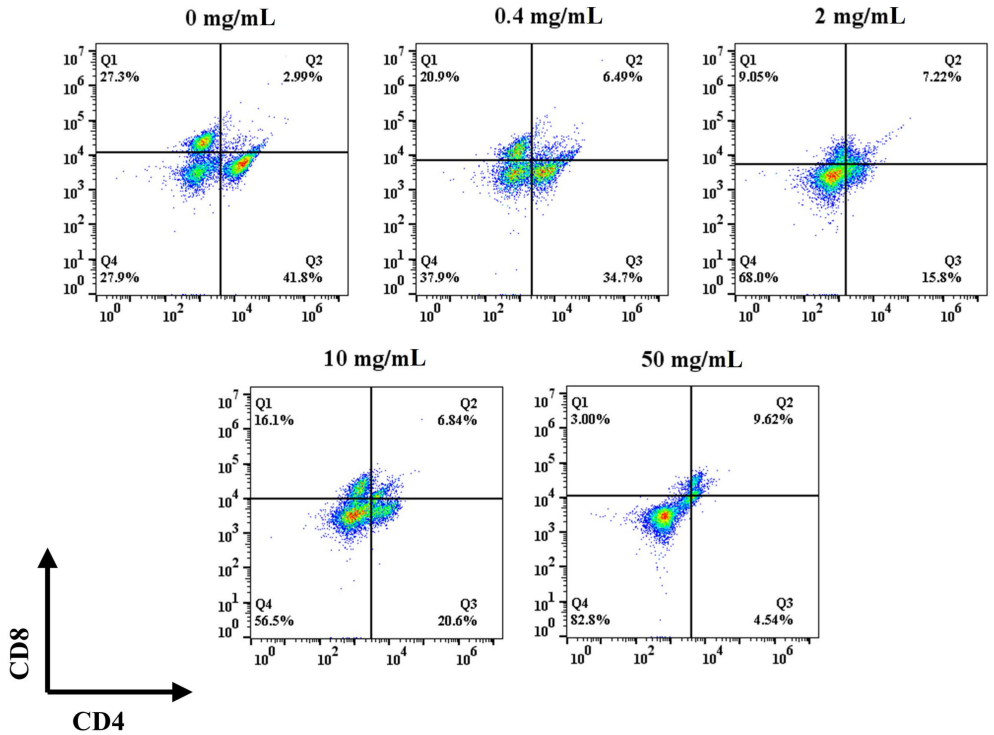

FIGURE 4 | Effect of HFD on the mouse primary T cells differentiation.

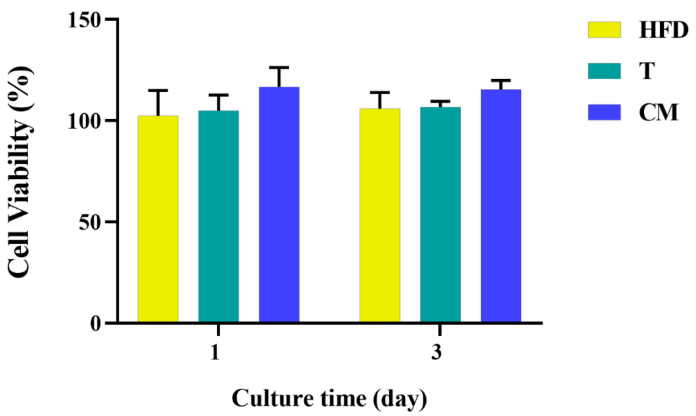

FIGURE 5 | MC3T3-E1 cell viability on various samples for 1 and 3 d. HFD: the group containing HFD; T: the group containing T cell supernatant; CM: supernatant from co-culture of T cells with HFD.

HFD or T alone slightly promoted the expression of ALP compared with the CON, while CM caused a decrease in ALP expression. **Figure 6C** presented the cellular ALP activities of each group using the ALP assay kit. ALP expression decreased in the CM group compared with other groups. Further, ARS, a dye that binds to Ca ions, was used to color mineralized nodules generated by extracellular matrix Ca deposition (50). As shown in **Figure 6D**, in all groups, the ARS staining revealed a brilliant red color of calcified nodules. The area stained with ARS was less in the CM group compared with the

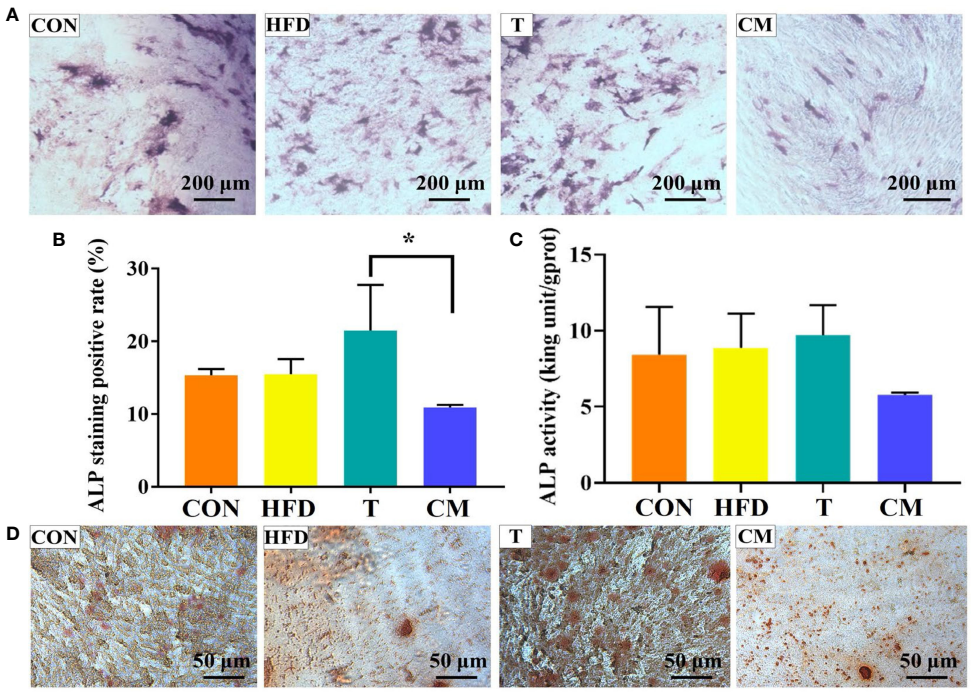

FIGURE 6 | **(A)** ALP activity of MC3T3-E1 cells on different groups after 14 d of culture. **(B)** ImageJ was used to quantify the ALP staining results (*$p < 0.05$). **(C)** ALP test after 14 d for each group using the ALP assay kit. **(D)** The mineralized nodules were stained with ARS after 14 d.

control group. Taken together, our results demonstrate that HFD could inhibit the osteogenic differentiation of MC3T3-E1 cells by regulating T cells.

4 CONCLUSIONS

In summary, high-temperature autoclave sterilization had no negative effect on the bioactive group of UFD. The molecular weight of UFD was reduced due to depolymerization. HFD modulated the proliferation and differentiation of T cells, and the proliferative effect of HFD on T cell proliferation increased with an increasing concentration within a certain range (0.4–50 mg/mL). On the contrary, HFD inhibited the differentiation of T cells, and the higher the concentration, the more pronounced the inhibitory effect. HFD could inhibit osteogenesis by affecting T cells. Thus, our findings provide new insight into the fucoidan-mediated T cells and the following regulatory on osteogenesis.

DATA AVAILABILITY STATEMENT

The original contributions presented in the study are included in the article/**Supplementary Material**. Further inquiries can be directed to the corresponding author.

ETHICS STATEMENT

The animal study was reviewed and approved by The Ethics Committee of the Affiliated Hospital of Qingdao University.

AUTHOR CONTRIBUTIONS

QZ and CY contributed to conception and design of the study. HH, FG, XD, DW, and ZS performed the experiments. HH, MY and CY performed the statistical analysis. HH, CY, and FG wrote the first draft of the manuscript. QZ reviewed the draft of the manuscript. QZ and CY provided the funding. All authors contributed to manuscript revision, read, and approved the submitted version.

FUNDING

The authors are very grateful for the financial support by National Natural Science Foundation of China (Grant No. 31900957), Shandong Provincial Natural Science Foundation (Grant No. ZR2019QC007), Innovation and technology program for the excellent youth scholars of higher education of Shandong province (Grant No. 2019KJE015), and Traditional Chinese Medicine Science and Technology Project of Shandong province (Grant No. 2021Q069).

REFERENCES

1. Zheng W, Hao Y, Wang D, Huang H, Guo F, Sun Z, et al. Preparation of Triamcinolone Acetonide-Loaded Chitosan/Fucoidan Hydrogel and its Potential Application as an Oral Mucosa Patch. *Carbohydr Polym* (2021) 272:118493. doi: 10.1016/j.carbpol.2021.118493
2. He Y, Zhao W, Dong Z, Ji Y, Li M, Hao Y, et al. A Biodegradable Antibacterial Alginate/Carboxymethyl Chitosan/Kangfuxin Sponges for Promoting Blood Coagulation and Full-Thickness Wound Healing. *Int J Biol Macromol* (2021) 167:182–92. doi: 10.1016/j.ijbiomac.2020.11.168
3. Zhu Y, Liu L, Sun Z, Ji Y, Wang D, Mei L, et al. Fucoidan as a Marine-Origin Prebiotic Modulates the Growth and Antibacterial Ability of Lactobacillus Rhamnosus. *Int J Biol Macromol* (2021) 180:599–607. doi: 10.1016/j.ijbiomac.2021.03.065
4. Hao Y, Zhao W, Zhang L, Zeng X, Sun Z, Zhang D, et al. Bio-Multifunctional Alginate/Chitosan/Fucoidan Sponges With Enhanced Angiogenesis and Hair Follicle Regeneration for Promoting Full-Thickness Wound Healing. *Mater Des* (2020) 193:108863. doi: 10.1016/j.matdes.2020.108863
5. Chiang CS, Lin YJ, Lee R, Lai YH, Cheng HW, Hsieh CH, et al. Combination of Fucoidan-Based Magnetic Nanoparticles and Immunomodulators Enhances Tumour-Localized Immunotherapy. *Nat Nanotechnol* (2018) 13:746–54. doi: 10.1038/s41565-018-0146-7
6. Geller JB, Darling JA, Carlton JT. Annual Review of Marine Science. *Genet Perspect Mar Biol Invasions* (2020) 2:367–93. doi: 10.1146/annurev-marine-032020-012810
7. Ganesan AR, Tiwari U, Rajauria G. Food Science and Human Wellness Seaweed Nutraceuticals and Their Therapeutic Role in Disease Prevention. *Food Sci Hum Wellness* (2019) 8:252–63. doi: 10.1016/j.fshw.2019.08.001
8. Li Y, Li M, Xu B, Li Z, Qi Y, Song Z, et al. The Current Status and Future Perspective in Combination of the Processing Technologies of Sulfated Polysaccharides From Sea Cucumbers: A Comprehensive Review. *J Funct Foods* (2021) 87:104744. doi: 10.1016/j.jff.2021.104744
9. Chen M, Zhang Y, Zhou P, Liu X, Zhao H, Zhou X, et al. Substrate Stiffness Modulates Bone Marrow-Derived Macrophage Polarization Through NF-κb Signaling Pathway. *Bioact Mater* (2020) 5:880–90. doi: 10.1016/j.bioactmat.2020.05.004
10. Xu Y, Xu J, Ge K, Tian Q, Zhao P, Guo Y. Anti-Inflammatory Effect of Low Molecular Weight Fucoidan From Saccharina Japonica on Atherosclerosis in apoE-Knockout Mice. *Int J Biol Macromol* (2018) 118:365–74. doi: 10.1016/j.ijbiomac.2018.06.054
11. Li C, Niu Q, Li S, Zhang X, Liu C, Cai C, et al. Fucoidan From Sea Cucumber Holothuria Polii: Structural Elucidation and Stimulation of Hematopoietic Activity. *Int J Biol Macromol* (2020) 154:1123–31. doi: 10.1016/j.ijbiomac.2019.11.036
12. Park SJ, Lee KW, Lim DS, Lee S. The Sulfated Polysaccharide Fucoidan Stimulates Osteogenic Differentiation of Human Adipose-Derived Stem Cells. *Stem Cells Dev* (2012) 21:2204–11. doi: 10.1089/scd.2011.0521
13. Yoo HJ, You DJ, Lee KW. Characterization and Immunomodulatory Effects of High Molecular Weight Fucoidan Fraction From the Sporophyll of Undaria Pinnatifida in Cyclophosphamide-Induced Immunosuppressed Mice. *Mar Drugs* (2019) 17:447. doi: 10.3390/md17080447
14. Zhang W, Hwang J, Yadav D, An EK, Kwak M, Lee PCW, et al. Enhancement of Immune Checkpoint Inhibitor-Mediated Anti-Cancer Immunity by Intranasal Treatment of Ecklonia Cava Fucoidan Against Metastatic Lung Cancer. *Int J Mol Sci* (2021) 22:9125. doi: 10.3390/ijms22179125
15. Yang J, Yang X, Pan W, Wang M, Lu Y, Zhang J, et al. Fucoidan-Supplemented Diet Potentiates Immune Checkpoint Blockage by Enhancing Antitumor Immunity. *Front Cell Dev Biol* (2021) 9:1–16. doi: 10.3389/fcell.2021.733246
16. Li J, Tan J, Martino MM, Lui KO. Regulatory T-Cells: Potential Regulator of Tissue Repair and Regeneration. *Front Immunol* (2018) 9:585. doi: 10.3389/fimmu.2018.00585
17. Hofmann U, Beyersdorf N, Weirather J, Podolskaya A, Bauersachs J, Ertl G, et al. Activation of CD4 + T Lymphocytes Improves Wound Healing and Survival After Experimental Myocardial Infarction in Mice. *Circulation* (2012) 125:1652–63. doi: 10.1161/CIRCULATIONAHA.111.044164
18. D'Alessio FR, Tsushima K, Aggarwal NR, West EE, Willett MH, Britos MF, et al. CD4+CD25+Foxp3+ Tregs Resolve Experimental Lung Injury in Mice and are Present in Humans With Acute Lung Injury. *J Clin Invest* (2009) 119:2898–913. doi: 10.1172/JCI36498
19. Volfson-Sedletsky V, Jones IVA, Hernandez-Escalante J, Dooms H. Emerging Therapeutic Strategies to Restore Regulatory T Cell Control of Islet Autoimmunity in Type 1 Diabetes. *Front Immunol* (2021) 12:814. doi: 10.3389/fimmu.2021.635767
20. Geng J, Li J, Zhu F, Chen X, Du B, Tian H, et al. Plant Sprout Foods: Biological Activities, Health Benefits, and Bioavailability. *J Food Biochem* (2022) 46: e13777. doi: 10.1111/jfbc.13777
21. Du B, Zhu F, Xu B. An Insight Into the Anti-Inflammatory Properties of Edible and Medicinal Mushrooms. *J Funct Foods* (2018) 47:334–42. doi: 10.1016/j.jff.2018.06.003
22. Lewkowicz N, Klink M, Mycko MP, Lewkowicz P. Neutrophil - CD4+CD25+ T Regulatory Cell Interactions: A Possible New Mechanism of Infectious Tolerance. *Immunobiology* (2013) 218:455–64. doi: 10.1016/j.imbio.2012.05.029
23. Santamaria JC, Borelli A, Irla M. Regulatory T Cell Heterogeneity in the Thymus: Impact on Their Functional Activities. *Front Immunol* (2021) 12:294. doi: 10.3389/fimmu.2021.643153
24. Brand IM, Gilberg L, Bruger JM, Garí M, Wieser A, Eser TM, et al. Broad T Cell Targeting of Structural Proteins After SARS-CoV-2 Infection: High Throughput Assessment of T Cell Reactivity Using an Automated Interferon Gamma Release Assay. *Front Immunol* (2021) 12:1825. doi: 10.3389/fimmu.2021.688436
25. Alvarez C, Abdalla H, Sulliman S, Rojas P, Wu Y-C, Almarhoumi R, et al. RvE1 Impacts the Gingival Inflammatory Infiltrate by Inhibiting the T Cell Response in Experimental Periodontitis. *Front Immunol* (2021) 12:1547. doi: 10.3389/fimmu.2021.664756
26. Wu D, Cline-Smith A, Shashkova E, Perla A, Katyal A, Aurora R. T-Cell Mediated Inflammation in Postmenopausal Osteoporosis. *Front Immunol* (2021) 12:2413. doi: 10.3389/fimmu.2021.687551
27. Knecht RS, Bucher CH, Van Linthout S, Tschöpe C, Schmidt-Bleek K, Duda GN. Mechanobiological Principles Influence the Immune Response in Regeneration: Implications for Bone Healing. *Front Bioeng Biotechnol* (2021) 9:81. doi: 10.3389/fbioe.2021.614508
28. Buchinsky J, Mann N, Bryer P, Romero F, Jee SS, City SL. T Lymphocytes Play a Critical Role in the Development of Cyclosporin A-Induced Osteopenia. *Endocrinology* (2015) 137:2278–85. doi: 10.1210/endo.137.6.8641176
29. Takayanagi H, Ogasawara K, Hida S, Chiba T, Murata S, Sato K, et al. T-Cell-Mediated Regulation of Osteoclastogenesis by Signalling Cross-Talk Between RANKL and IFN-γ. *Nature* (2000) 408:600–5. doi: 10.1038/35046102
30. Fomby P, Cherlin AJ, Hadjizadeh A, Doillon CJ, Sueblinvong V, Weiss DJ, et al. Stem Cells and Cell Therapies in Lung Biology and Diseases: Conference Report. *Ann Am Thorac Soc* (2010) 12:181–204. doi: 10.1002/term.1727
31. Pruitt HC, Lewis D, Ciccaglione M, Connor S, Smith Q, Hickey JW, et al. Collagen Fiber Structure Guides 3D Motility of Cytotoxic T Lymphocytes. *Matrix Biol* (2020) 85–86:147–59. doi: 10.1016/j.matbio.2019.02.003
32. Kureel AK, Saini S, Singh B, Singh K, Rai AK. Compromised Levels of CD6 and Reduced T Cell Activation in the Aged Immune System. *Biomarkers* (2021) 26:483–90. doi: 10.1080/1354750X.2021.1921030
33. Croes M, Öner FC, van Neerven D, Sabir E, Kruyt MC, Blokhuis TJ, et al. Proinflammatory T Cells and IL-17 Stimulate Osteoblast Differentiation. *Bone* (2016) 84:262–70. doi: 10.1016/j.bone.2016.01.010
34. Manikandan R, Parimalanandhini D, Mahalakshmi K, Beulaja M, Arumugam M, Janarthanan S, et al. Studies on Isolation, Characterization of Fucoidan From Brown Algae Turbinaria Decurrens and Evaluation of It's *In Vivo* and *In Vitro* Anti-Inflammatory Activities. *Int J Biol Macromol* (2020) 160:1263–76. doi: 10.1016/j.ijbiomac.2020.05.152
35. Chen Y, Zhu H, Hao Y, Sun Z, Shen P, Zhou Q. Preparation of Fucoidan-Based Electrospun Nanofibers and Their Interaction With Endothelial Cells. *Front Bioeng Biotechnol* (2021) 9:1–10. doi: 10.3389/fbioe.2021.739209
36. Saravana PS, Cho YJ, Park YB, Woo HC, Chun BS. Structural, Antioxidant, and Emulsifying Activities of Fucoidan From Saccharina Japonica Using Pressurized Liquid Extraction. *Carbohydr Polym* (2016) 153:518–25. doi: 10.1016/j.carbpol.2016.08.014
37. Palanisamy S, Vinosha M, Marudhupandi T, Rajasekar P, Prabhu NM. Isolation of Fucoidan From Sargassum Polycystum Brown Algae: Structural

Characterization, *In Vitro* Antioxidant and Anticancer Activity. *Int J Biol Macromol* (2017) 102:405–12. doi: 10.1016/j.ijbiomac.2017.03.182
38. Seedevi P, Moovendhan M, Sudharsan S, Vasanthkumar S, Srinivasan A, Vairamani S, et al. Structural Characterization and Bioactivities of Sulfated Polysaccharide From Monostroma Oxyspermum. *Int J Biol Macromol* (2015) 72:1459–65. doi: 10.1016/j.ijbiomac.2014.09.062
39. Casu B, Scovenna G, Cifonelli AJ, Perlin AS. Infrared Spectra of Glycosaminoglycans in Deuterium Oxide and Deuterium Chloride Solution: Quantitative Evaluation of Uronic Acid and Acetamidodeoxyhexose Moieties. *Carbohydr Res* (1978) 63:13–27. doi: 10.1016/S0008-6215(00)80925-8
40. Kozarski M, Klaus A, Nikšić M, Vrvić MM, Todorović N, Jakovljević D, et al. Antioxidative Activities and Chemical Characterization of Polysaccharide Extracts From the Widely Used Mushrooms Ganoderma Applanatum, Ganoderma Lucidum, Lentinus Edodes and Trametes Versicolor. *J Food Compos Anal* (2012) 26:144–53. doi: 10.1016/j.jfca.2012.02.004
41. Quah BJC, Parish CR. The Use of Carboxyfluorescein Diacetate Succinimidyl Ester (CFSE) to Monitor Lymphocyte Proliferation. *J Vis Exp* (2010), 44:4–7. doi: 10.3791/2259
42. Zenke S, Palm MM, Braun J, Gavrilov A, Meiser P, Böttcher JP, et al. Quorum Regulation *via* Nested Antagonistic Feedback Circuits Mediated by the Receptors CD28 and CTLA-4 Confers Robustness to T Cell Population Dynamics. *Immunity* (2020) 52:313–27.e7. doi: 10.1016/j.immuni.2020.01.018
43. Boyman O, Sprent J. The Role of Interleukin-2 During Homeostasis and Activation of the Immune System. *Nat Rev Immunol* (2012) 12:180–90. doi: 10.1038/nri3156
44. Ross SH, Cantrell DA. Signaling and Function of Interleukin-2 in T Lymphocytes. *Annu Rev Immunol* (2018) 36:411–33. doi: 10.1146/annurev-immunol-042617-053352
45. Kalia V, Sarkar S. Regulation of Effector and Memory CD8 T Cell Differentiation by IL-2—A Balancing Act. *Front Immunol* (2018) 9:2987. doi: 10.3389/fimmu.2018.02987
46. Li X, Huang Q, Hu X, Wu D, Li N, Liu Y, et al. Evaluating the Osteoimmunomodulatory Properties of Micro-Arc Oxidized Titanium Surface at Two Different Biological Stages Using an Optimized *In Vitro* Cell Culture Strategy. *Mater Sci Eng C* (2020) 110:110722. doi: 10.1016/j.msec.2020.110722
47. Wang Z, Mei L, Liu X, Zhou Q. Hierarchically Hybrid Biocoatings on Ti Implants for Enhanced Antibacterial Activity and Osteogenesis. *Colloids Surfaces B Biointerfaces* (2021) 204:111802. doi: 10.1016/j.colsurfb.2021.111802
48. Wang Z, Wang X, Wang Y, Zhu Y, Liu X, Zhou Q. NanoZnO-Modified Titanium Implants for Enhanced Anti-Bacterial Activity, Osteogenesis and Corrosion Resistance. *J Nanobiotechnol* (2021) 19:1–23. doi: 10.1186/s12951-021-01099-6
49. Yan M, Pan Y, Lu S, Li X, Wang D, Shao T, et al. Chitosan-CaP Microflowers and Metronidazole Loaded Calcium Alginate Sponges With Enhanced Antibacterial, Hemostatic and Osteogenic Properties for the Prevention of Dry Socket After Tooth Removal. *Int J Biol Macromol* (2022) 212:134–45. doi: 10.1016/j.ijbiomac.2022.05.094
50. Guo F, Yuan C, Huang H, Deng X, Bian Z, Wang D, et al. Regulation of T Cell Responses by Nano-Hydroxyapatite to Mediate the Osteogenesis. *Front Bioeng Biotechnol* (2022) 10:2022.884291. doi: 10.3389/fbioe.2022.884291

Conflict of Interest: Author ZS is employed by Qingdao Bright Moon Seaweed Group Co., Ltd.

The remaining authors declare that the research was conducted in the absence of any commercial or financial relationships that could be construed as a potential conflict of interest.

Publisher's Note: All claims expressed in this article are solely those of the authors and do not necessarily represent those of their affiliated organizations, or those of the publisher, the editors and the reviewers. Any product that may be evaluated in this article, or claim that may be made by its manufacturer, is not guaranteed or endorsed by the publisher.

Copyright © 2022 Huang, Guo, Deng, Yan, Wang, Sun, Yuan and Zhou. This is an open-access article distributed under the terms of the Creative Commons Attribution License (CC BY). The use, distribution or reproduction in other forums is permitted, provided the original author(s) and the copyright owner(s) are credited and that the original publication in this journal is cited, in accordance with accepted academic practice. No use, distribution or reproduction is permitted which does not comply with these terms.

frontiers | Frontiers in Nutrition

ORIGINAL RESEARCH
published: 15 July 2022
doi: 10.3389/fnut.2022.944390

Research on the Mechanism of HRP Relieving IPEC-J2 Cells Immunological Stress Based on Transcriptome Sequencing Analysis

Muyang Li[1], *Lu Chen*[2], *Yiran Zhao*[3], *Hui Sun*[4]* *and Lei Zhao*[1]*

[1] College of Animal Science and Veterinary Medicine, Heilongjiang Bayi Agricultural University, Daqing, China, [2] Shanxi Animal Husbandry and Veterinary School, Taiyuan, China, [3] College of Food Science, Heilongjiang Bayi Agricultural University, Daqing, China, [4] College of Animal Science and Technology, Jilin Agricultural University, Changchun, China

Early weaning increased the economic benefits of piglets. However, early weaning damages the intestinal barrier of piglets and causes immunological stress. The mechanism by which *Hippophae rhamnoides* polysaccharide (HRP) alleviates lipopolysaccharide (LPS)-induced intestinal porcine epithelial cells (IPEC-J2) inflammatory damage was investigated using proteomics in our previous studies. In this study we employed RNA-sequencing (RNA-seq) to determine the level and function of differentially expressed genes (DEGs) and further explore the mechanism of the HRP anti-inflammatory and immune process. The differential expression analysis indicated that 3622, 1216, and 2100 DEGs in the IPEC-J2 cells were identified in C vs. L, L vs. H6-L, and C vs. H6-L, respectively. The Kyoto Encyclopedia of Genes and Genomes (KEGG) enrichment analysis foundsix identified pathways related to the immune system. Additionally, we used the Science, Technology, Engineering, and Math (STEM) program to categorize the 3,134 DEGs that were differentially expressed in H2-L, H4-L and H6-L into eight possible expression profiles, in which 612 were clustered into two profiles. The accuracy and consistency of RNA-seq data were validated by the results of qRT-PCR of the nuclear factor of kappa light polypeptide gene enhancer in B-cells 2 (NFKB2), MAP kinase interacting serine/threonine kinase 2 (MKNK2), mitogen-activated protein kinase kinase 1 (MAP2K1), mitogen-activated protein kinase kinase kinase 8 (MAP3K8), Ras-related protein R-Ras (RRAS), TNF receptor-associated factor 1 (TRAF1), NF-kappa-B inhibitor alpha (NFKBIA), interleukin 8 (IL8), tumor necrosis factor, alpha-induced protein 3 (TNFAIP3), and transforming growth factor beta-1 (TGFB1). Transcriptome sequencing also indicated that HRP reduced the expression levels of related DEGs and inhibited the activation of the mitogen-activated protein kinase (MAPK)/nuclear factor kappa-B (NF-κB) signaling pathway. Our findings indicate that the application of HRP in piglet diets during the early weaning period can improve intestinal epithelial function and integrity, and relieve intestinal damage, and improve piglet health.

Keywords: IPEC-J2 cells, HRP, anti-inflammatory, MAPK/NF-κB signaling pathway, transcriptome

OPEN ACCESS

Edited by:
Baojun Xu,
United International College, China

Reviewed by:
Utoomporn Surayot,
Chiang Mai University, Thailand
Susmita Barman,
University of Nebraska Medical Center, United States

***Correspondence:**
Lei Zhao
zlhljbyau@126.com
Hui Sun
shjlau@163.com

Specialty section:
This article was submitted to Nutritional Immunology, a section of the journal Frontiers in Nutrition

Received: *15 May 2022*
Accepted: *13 June 2022*
Published: *15 July 2022*

Citation:
Li M, Chen L, Zhao Y, Sun H and Zhao L (2022) Research on the Mechanism of HRP Relieving IPEC-J2 Cells Immunological Stress Based on Transcriptome Sequencing Analysis. Front. Nutr. 9:944390. doi: 10.3389/fnut.2022.944390

INTRODUTION

With the acceleration of the large-scale and intensified process of pig production, early weaning techniques for piglets have been gradually implemented (1). Weaned piglets are affected by stresses such as nutrition, immunity, and environment, and piglets have early weaning syndromes such as reduced feed utilization, poor growth, and diarrhea (2, 3). Piglet weaning is accompanied by the occurrence of intestinal inflammation, which causes a series of negative reactions in the incompletely developed intestinal tracts of piglets, such as intestinal mucosal injury, intestinal villi damage, and intestinal wall injury, Intestinal inflammation also affects the digestive and absorptive function of the intestinal tract in piglets and leads to sluggish growth, diarrhea, and even death, causing great economic losses to the swine industry (4). The intestinal mucosa is the host's first line of defense against pathogenic microorganisms. Intestinal epithelial cells (IECs) are an important part of the intestinal mucosal barrier (5, 6). Injury to IECs is an important pathological basis for intestinal dysfunction. IECs can produce severe immune stress in a variety of physiological, pathological, dietary, or environmental conditions, and the accumulation of excessive inflammatory cytokines can damage intestinal epithelial cells, resulting in intestinal dysfunction. Therefore, the key to reducing the diarrhea rate and improving the production performance of weaned piglets is to reduce weaning stress and protect the intestinal structure and function of piglets (7). Seeking immunostimulants to promote growth and reduce the intestinal inflammation caused by weaning has become a hot scientific issue.

In recent years, plant extracts as immunomodulators have received worldwide attention due to their nutritional and medicinal potential (8, 9). *Hippophae rhamnoides L.* (sea buckthorn) is a traditional medicinal plant (10). *H.rhamnoides* extracts have shown antioxidant, anti-inflammatory, and anti-viral effects by decreasing cytotoxicity and reactive oxygen species (ROS) generation (11, 12). A recent study showed that *Hippophae rhamnoides* polysaccharide (HRP) protected mice livers from CCl_4-induced damage through its anti-inflammatory effect and the modulation of the balance between anti-inflammatory cytokines inimmune cells (13). The protective mechanism of chitosan oligosaccharide against LPS-induced inflammatory responses in IPEC-J2 and in mice with DSS dextran sulfate sodium-induced colitis is reported (14). In our previous study, the role of several key regulatory genes and proteins involved in HRP immunoregulation was examined (15, 16). However, the composition and mechanisms of the underlying global regulatory networks at the transcriptome levels are still poorly understood. To confirm the pre-protective effect of HRP on lipopolysaccharide (LPS)-induced intestinal porcine epithelial cells (IPEC-J2) in terms of anti-inflammatory or immunoregulatoryproperties, the pathways enriched by differentially expressed genes (DEGs) should be biologically validated. We employed RNA-sequencing (RNA-seq) to determine the abundance and function of genes (17, 18) and lay the foundation for further study of the anti-inflammatory immune response of HRP in order to provide a theoretical basis and technical support for the treatment and prevention of diseases such as diarrhea caused by intestinal damage in early-weaned piglets.

TABLE 1 | Summary statistics for sequence quality and alignment information of IPEC-J2 cells sample in every group.

Sample	Group	Raw reads	Clean reads	BF_Q30 (%)	AF_Q30 (%)	BF_GC (%)	AF_GC (%)	Total_Mapped	Mapping_ rate (%)	Unique_Mapped	Multiple_Mapped
C-1	C	2,08,95,136	2,08,62,498	93.87	93.99	57.06	57.06	2,03,31,961	97.78	1,97,11,071	6,20,890
C-2		2,10,28,580	2,09,87,072	93.43	93.54	55.14	55.13	2,03,48,751	97.45	1,97,28,826	6,19,925
C-3		2,25,18,532	2,247,2688	93.48	93.61	55.32	55.32	2,17,40,753	97.47	2,10,55,186	6,85,567
L-1	L	2,03,00,292	20262572	93.65	93.79	56.17	56.16	1,95,66,822	97.52	1,88,75,343	6,91,479
L-2		2,37,73,966	2,37,31,954	93.68	93.81	56.09	56.09	2,30,56,064	97.61	2,22,76,195	7,79,869
L-3		2,36,25,640	2,35,82,598	93.51	93.63	55.97	55.96	2,29,31,153	97.66	2,21,51,500	7,79,653
H2-L-1	H2-L	2,11,43,164	2,11,06,066	93.9	94.02	56.49	56.49	2,04,55,400	97.63	1,97,62,846	6,92,554
H2-L-2		2,24,45,906	2,23,96,564	93.19	93.32	56.14	56.14	21629948	97.26	2,09,15,053	7,14,895
H2-L-3		2,46,04,618	2,45,58,736	93.66	93.78	56.04	56.03	2,37,74,066	97.56	2,29,82,487	7,91,579
H4-L-1		2,87,80,540	2,87,16,008	93.13	93.27	56.38	56.38	2,77,37,540	97.33	2,68,17,089	9,20,451
H4-L-2	H4-L	2,45,62,664	2,45,06,630	92.95	93.1	56.62	56.63	2,37,01,504	97.27	2,29,11,180	7,90,324
H4-L-3		2,77,16,820	2,76,60,210	93.49	93.61	55.68	55.68	2,67,26,026	97.32	2,58,29,866	8,96,160
H6-L-1		2,68,24,310	2,67,75,974	93.44	93.56	56.13	56.13	2,58,68,459	97.4	2,50,02,306	8,66,153
H6-L-2	H6-L	2,55,24,164	2,54,70,010	93.45	93.6	56.27	56.27	2,45,00,614	97.06	2,36,43,298	8,57,316
H6-L-3		2,31,67,684	2,31,17,728	93.37	93.5	55.93	55.92	2,23,36,845	97.25	2,15,99,289	7,37,556

C1–C3 represent the control-group IPEC-J2 cells without treatment, L1-L3 represent the replicates of treatment IPEC-J2 cells induced by LPS with 10 μg/mL, H2-L-1- H2-L-3 represent the replicates of pre-treatment IPEC-J2 cells with 200 μg/mL HRP and followed by co-treatment with 10 μg/mL LPS, H4-L-1- H4-L-3 represent the replicates of pre-treatment IPEC-J2 cells with 400 μg/mL HRP and followed by co-treatment with 10 μg/mL LPS, and H6-L-1- H6-L-3 represent the replicates of pre-treatment IPEC-J2 cells with 600 μg/mL HRP and followed by co-treatment with 10 μg/mL LPS.

MATERIALS AND METHODS

Materials

HRP, ≥98% (HPLC) purchased from Nanjing Zelang Biological Technology Co., Ltd., China. HRP was extracted by water decoction and alcohol precipitation as described previously (19, 20). The protein in the filtrate was removed primarily by the Sevage method, HRP was purified on a Sephadex G150 gel (Pharmacia) and the purity was also verified by HPLC. HRP consists of 70% carbohydrate and 14.2% uronic acid. The polysaccharide is composed of mannose, arabinose, glucose, galactose and rhamnose with a ratio of 2.02:1.02:4.24:1:9.22 as the indication of chromatographic analysis of HRP (19).

Cell Culture and Treatment

The IPEC-J2 cell line source and cells culture method was as described in our previous study (21). HRP was pretreated for 24 h. Subsequently, cells were exposed to LPS for 16 h. The cells were collected, and quickly frozen in liquid nitrogen, and stored at −80°C for future transcriptome analysis. This study included five treatments C represents the control group IPEC-J2 cells without treatment. L represents the treatment group of IPEC-J2 cells induced by 10 μg/mL LPS. H2-L, H4-L, and H6-L represent the pre-treatment of IPEC-J2 cells with 200, 400, and 600 μg/mL HRP, respectively, followed by treatment with 10 μg/mL LPS. The HRP and LPS concentrations used were based on the results of our previous articles (16, 17).

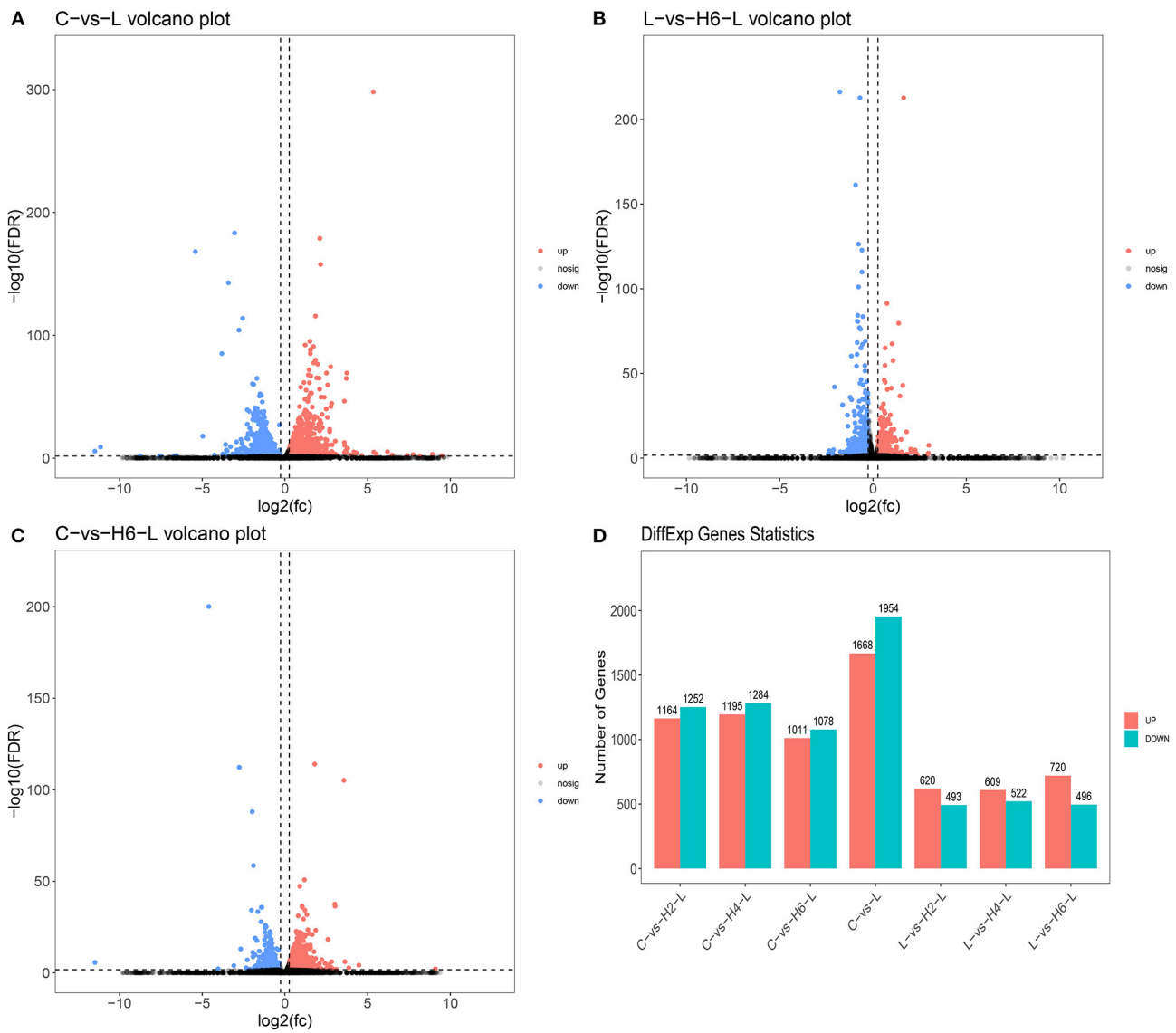

FIGURE 1 | Analysis of the volcano plotof DEGs **(A–C)**. Upregulated genes are shown in red, down-regulated genes are shown in blue, and genes with no significant difference in expression are indicated in black, significance was indicated by $P < 0.05$. DEGs statistics in the comparison group **(D)**.

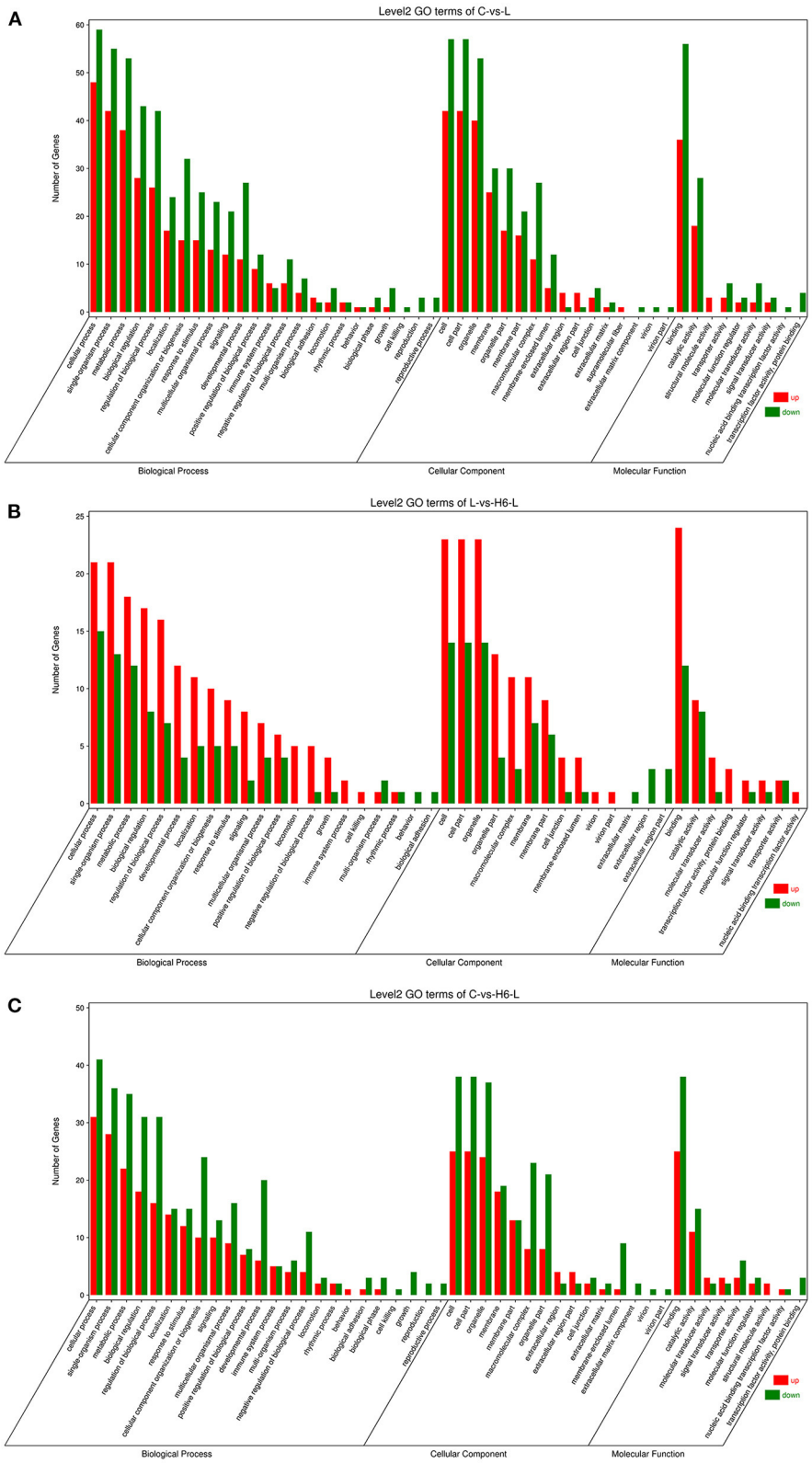

FIGURE 2 | The GO analysis of the DEGs in IPEC-J2 cells. Classification of identified genes based on functional annotations using GO analysis are shown for comparisons between the L treatment and C **(A)**, H6-L treatment and L alone **(B)**, H6-L treatment and C **(C)**.

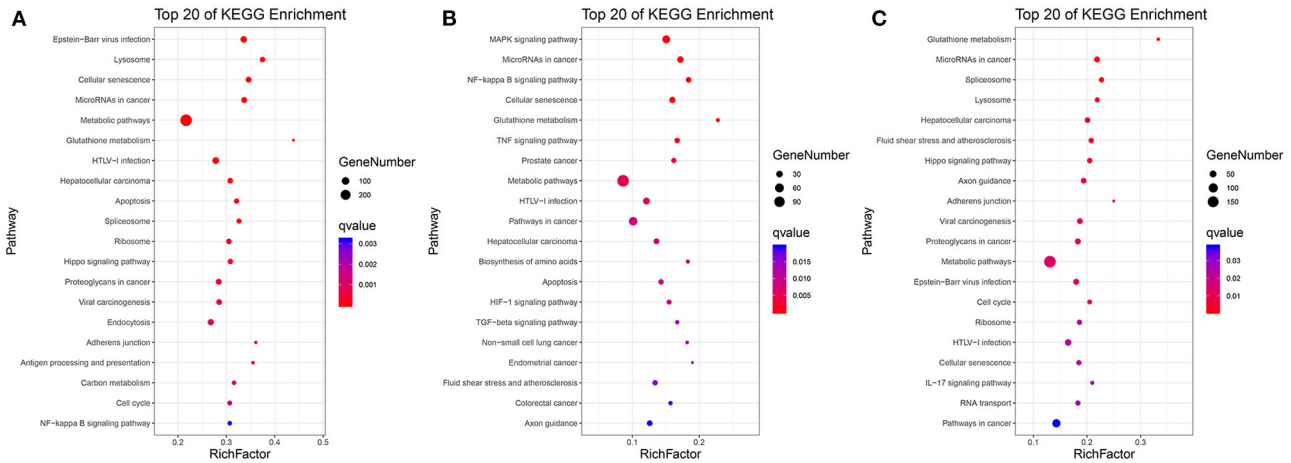

FIGURE 3 | Top 20 pathway enrichment in KEGG pathway analysis. **(A)** C vs. L. **(B)** L vs. H6-L. **(C)** C vs. H6-L. The greater the rich factor, the higher the degree of enrichment. The Q value ranges from 0 to 1 and the closer it is to zero, the more significant.

Total RNA Extraction, cDNA Library Construction, and RNA-seq

According to the manufacturer's instructions, TRIzol reagent was used to extract RNA from the IPEC-J2 cells in different groups. cDNA library construction and RNA-seq were as described by Shao et al. (17).

Bioinformatics Analysis

High quality clean reads were obtained by removing reads containing adapters, more than 10% unknown nucleotides (N), and low-quality reads containing more than 50% low quality (Q-value ≤20) bases. The short reads alignment tool Bowtie2 (22) was used to map reads to the ribosome RNA (rRNA) database. The rRNA mapped reads were removed. The remaining reads were further used in the assembly and analysis of the transcriptome. Gene abundances were quantified by the RSEM software (23). Transcript abundance was normalized to fragments per kilobase of exon model per million mapped reads (FPKM). DEGs between groups were analyzed using the DEGs R package (http://www.rproject.org/). Genes with fold change (FC) >1.2 and a false discovery rate (FDR) <0.02 were considered significant. Significant enrichment of the Kyoto Encyclopedia of Genes and Genomes (KEGG) pathways determined the most important biochemical metabolic pathways and signal transduction pathways that the protein participated in. The KEGG website (http://www.kegg.jp/kegg/) was used to query the immune-related signal pathways involved in significantly differently changed genes, and heat map analysis was performed on the significantly differentially expressed genes involved in immune-related signal pathways. For each treatment group, it is included three replicates to increase reliability of the data.

Verification of Transcriptome Data Using qRT-PCR

To validate the accuracy of the RNA-seq data, the DEG expressions for the nuclear factor of kappa light polypeptide gene enhancer in B-cells 2 (NFKB2), MAP kinase interacting serine/threonine kinase 2 (MKNK2), mitogen-activated protein kinase kinase 1 (MAP2K1), mitogen-activated protein kinase kinase kinase 8 (MAP3K8), Ras-related protein R-Ras (RRAS), TNF receptor-associated factor 1 (TRAF1), NF-kappa-B inhibitor alpha (NFKBIA), interleukin 8 (IL8), tumor necrosis factor, alpha-induced protein 3 (TNFAIP3), and transforming growth factor beta-1 (TGFB1) were determined by qRT-PCR analyses as described previously (16). We focused on the 600 μg/mL concentration of *H. rhamnoides* polysaccharide to pre-treat the IPEC-J2 cells in the following results (16, 21). The primers for the selected genes are listed in **Supplementary Table S1**.

Statistical Analysis

For the qPCR analysis, all data analyses were performed by using SPSS software (SPSS version 20.0, Chicago, IL, USA). Tukey's multiple range test was used to compare the mean values ($P < 0.05$) to indicate significant differences and the results were expressed as mean ± SD.

RESULTS

Transcriptome Profiles

The aggregate of 356,912,016 raw reads were accumulated by using the High-throughput RNA sequencing to do the paired-end sequencing of the fifteen constructed libraries. After quality control, assessment of contaminated rRNA and low-quality sequences, 356,207,308 qualified Illumina reads were obtained. Approximately 97.44% of the clean reads were mapped to the reference genome and then used for further gene expression analysis (**Table 1**). We focused on C, L, and H6-L samples in the following experiment.

DEGs were identified using digital gene expression tags. The expression analysis indicated that 3,622, 1,216, and 2,100 DEGs

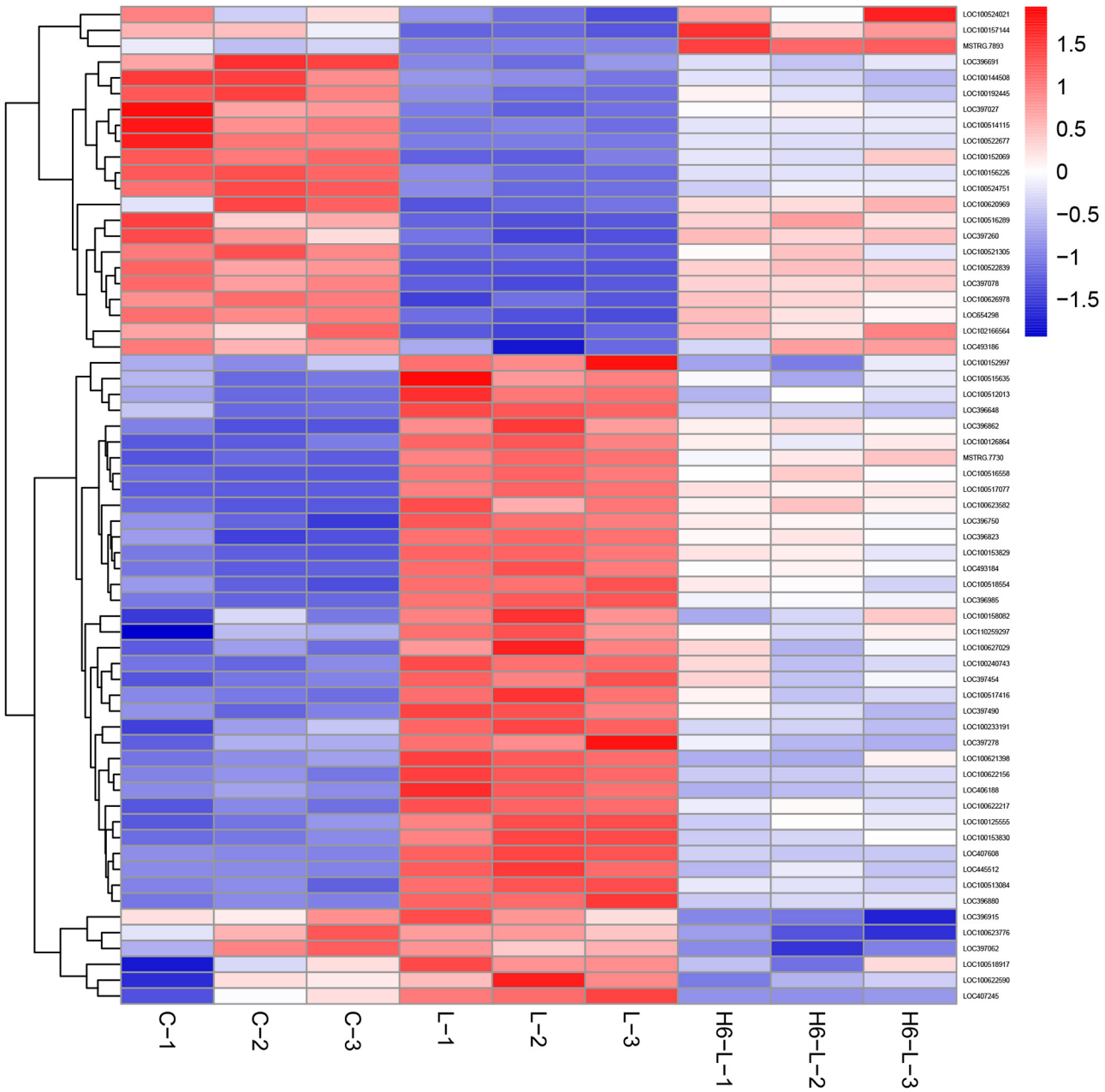

FIGURE 4 | A heat map of the DEGs related to immune pathways in IPEC-J2 cells. The sample gene expression of the C (C1–C3) and L (L1–L3), L (L1–L3) and H6–L (H6-L-1-H6-L-3), C (C1–C3), and H6-L (H6-L-1-H6-L-3) groups is shown using a pseudo color scale, with high levels of expression shown in red and low levels shown in blue.

in the IPEC-J2 cells were identified in C vs. L, L vs. H6-L, and C vs. H6-L, respectively (FC >1.2 and FDR <0.02) The most DEGs were identified from C to L (**Figures 1A–D** and **Supplementary Tables S2–S4**). These results demonstrated that number of inflammatory cytokines were accentuated after LPS induction. However, number of inflammatory cytokines in HRP pre-treated groups were significantly reduced. The volcano plot shows that HRP plays an important role in the immune regulation of cellular inflammatory damage.

Functional Enrichment of DEGs

DEGs were categorized into three Gene Ontology (GO) groups: biological process, cellular component, and molecular function. In the biological process group, many DEGs were categorized as the cellular process, single-organism process, and metabolic process. In the cellular component group, many DEGs were categorized as the cell, cell part and organelle. In the molecular function group, many DEGs were categorized as the binding,

TABLE 2 | Significant differentially expressed genes related to the main immune pathways in the L-vs-H6-L comparison group.

Gene ID	Gene name	Description
LOC100153829	NFKB2	Nuclear factor of kappa light polypeptide gene enhancer in B-cells 2
LOC100517077	MKNK2	MAP kinase interacting serine/threonine kinase 2
LOC100233191	MAP2K1	Mitogen-activated protein kinase kinase 1
LOC396648	HSPA1s	Heat shock 70kda protein 1/2/6/8
LOC100158082	PPP3C	Serine/threonine-protein phosphatase 2B catalytic subunit
LOC100152997	GADD45	Growth arrest and dna-damage-inducible protein
LOC100622217	MAP3K8	Mitogen-activated protein kinase kinase kinase 8
LOC100240743	DDIT3	DNA damage-inducible transcript 3
LOC493184	HSPB1	Heat shock protein beta-1
LOC100513084	CSF1	Macrophage colony-stimulating factor 1
LOC100516558	RRAS	Ras-related protein R-Ras
LOC110259297	RRAS2	Ras-related protein R-Ras2
LOC396985	PLAU	urokinase plasminogen activator
LOC100627029	TRAF1	TNF receptor-associated factor 1
LOC406188	NFKBIA	NF-kappa-B inhibitor alpha
LOC100125555	LY96	Lymphocyte antigen 96
LOC100623776	TRIF	Toll-like receptor adapter molecule 1
LOC396750	ICAM1	Intercellular adhesion molecule 1
LOC100153830	MALT1	Mucosa-associated lymphoid tissue lymphoma translocation protein 1
LOC396880	IL8	Interleukin 8
LOC100518917	PARP	Poly
LOC100622156	TNFAIP3	Tumor necrosis factor, alpha-induced protein 3
LOC100622590	BIRC2_3	Baculoviral IAP repeat-containing protein 2/3
LOC100515635	CREB5	Cyclic amp-responsive element-binding protein 5
LOC396915	EDN1	Endothelin-1
LOC397454	ITPR1	Inositol 1,4,5-triphosphate receptor type 1
LOC397278	PMAIP1	Phorbol-12-myristate-13-acetate-induced protein 1
LOC407245	LDH	L-lactate dehydrogenase
LOC396823	GAPDH	Glyceraldehyde 3-phosphate dehydrogenase
LOC445512	HMOX1	Heme oxygenase 1
LOC407608	PGK	Phosphoglycerate kinase
LOC100512013	ALDO	Fructose-bisphosphate aldolase, class I
LOC100126864	IFNGR2	Interferon gamma receptor 2
LOC397062	TFRC	Transferrin receptor
LOC396862	TIMP1	Metallopeptidase inhibitor 1
LOC100623582	NBL1	Neuroblastoma suppressor of tumorigenicity 1
LOC397490	INHBB	Inhibin beta B chain
LOC100518554	INHBE	Inhibin beta e chain
MSTRG.7730	PDGFB	Platelet-derived growth factor subunit b
LOC100517416	DUSP10	Dual specificity phosphatase 10
LOC397260	SMAD2_3	Mothers against decapentaplegic homolog 2/3
LOC100152069	SMAD6	Mothers against decapentaplegic homolog 6
LOC100522839	ID1	DNA-binding protein inhibitor ID1
LOC100522677	E2F4_5	Transcription factor e2f4/5
LOC396691	BMPR1B	Bone morphogenetic protein receptor type-1b
LOC654298	ID2	DNA-binding protein inhibitor ID2
LOC100626978	ID3	DNA-binding protein inhibitor ID3
LOC100144508	ID4	DNA-binding protein inhibitor ID4
LOC100521305	SMAD7	Mothers against decapentaplegic homolog 7
LOC100516289	PFKFB3	6-phosphofructo-2-kinase / fructose-2,6-biphosphatase 3
LOC100156226	EP300	E1A/CREB-binding protein
LOC100192445	PDPK1	3-phosphoinositide dependent protein kinase-1
LOC397027	CAPN1	Calpain-1
LOC493186	SOCS3	Suppressor of cytokine signaling 3
LOC100621398	MRAS	Ras-related protein M-Ras
LOC100620969	EREG	Epiregulin
LOC397078	TGFB1	Transforming growth factor beta-1
LOC100524751	RIPK1	Receptor-interacting serine/threonine-protein kinase 1
LOC100157144	DUSP	Dual specificity MAP kinase phosphatase
MSTRG.7893	NR4A1	Nuclear receptor subfamily 4 group A member 1
LOC100524021	CACNB3	Voltage-dependent calcium channel beta-3
LOC102166564	PDGFRB	Platelet-derived growth factor receptor beta
LOC100514115	FGFR3	Fibroblast growth factor receptor 3
LOC654328	MET	Proto-oncogene tyrosine-protein kinase Met

catalytic activity, and transporter activity (**Figures 2A–C** and **Supplementary Tables S5–S7**).

As shown in **Figures 3A–C** and **Supplementary Tables S8–S10**, in C vs. L, 1,442 DEGs were mapped into 322 KEGG pathways. The key pathways were Apoptosis (ko04210) and the NF-kappa B signaling pathway (ko04064). In L vs. H6-L, 531 DEGs were mapped into 307 KEGG pathways. The key pathways were MAPK (ko04010), NF-kappa B (ko04064), TNF (ko04668), Apoptosis (ko04210), HIF-1 (ko04066), and the TGF-beta signaling pathway (ko04350). In C vs. H6-L, 892 DEGs were mapped into 318 KEGG pathways. The key pathway was the IL-17 signaling pathway (ko04657).

Heat Map of the DEGs Related to Immune Pathways in L vs. H6-L

In **Figure 4** and **Table 2**, the sample gene expression of the C and L, L and H6-L, C and H6-L groups is shown using a pseudo color scale, with high levels of expression shown in red and low levels shown in blue. The results showed that most of the gene expression levels were down-regulated after HRP pre-treatment compared with the LPS group. The Log2-fold change and *p*-value statistics of DEGs related to the main immune pathways in the L-vs.-H6-L group are shown in **Table 3**. This data indicated that genes were significantly expressed in six immune pathways.

Cluster Analysis of DEGs Among the Three HRP Concentrations

To determine the gene expression trajectories, we used the STEM program to categorize the 3,134 DEGs that were

TABLE 3 | Log2-fold change and *p*-value statistics of significant differentially expressed genes related to the main immune pathways in the L-vs-H6-L group.

Gene ID	Gene name	Log2 fold change		*P*-value	
		C-vs-L	L-vs-H6-L	C-vs-L	L-vs-H6-L
LOC100153829	NFKB2	1.16	−0.43	9.63E-39	2.65E-18
LOC100517077	MKNK2	1.16	−0.35	5.10E-65	2.88E-39
LOC100233191	MAP2K1	0.61	−0.45	2.23E-12	3.99E-12
LOC396648	HSPA1s	0.82	−0.59	2.61E-19	7.87E-114
LOC100158082	PPP3C	0.48	−0.29	5.85E-07	0.00045
LOC100152997	GADD45	2.28	−2.18	9.91E-06	8.74E-06
LOC100622217	MAP3K8	1.77	−0.76	1.82E-22	5.36E-09
LOC100240743	DDIT3	1.61	−0.76	2.11E-23	8.35E-09
LOC4 93184	HSPB1	1.98	−0.65	4.03E-80	1.82E-68
LOC100513084	CSF1	2.07	−1.01	8.41E-28	1.90E-11
LOC100516558	RRAS	1.40	−0.42	4.76E-52	5.56E-15
LOC110259297	RRAS2	0.61	−0.29	4.70E-12	3.17E-13
LOC396985	PLAU	1.28	−0.57	1.14E-58	1.10E-70
LOC100627029	TRAF1	2.28	−0.88	2.27E-11	0.00050
LOC406188	NFKBIA	0.97	−0.77	4.03E-21	5.22E-21
LOC100125555	LY96	1.79	−0.84	2.07E-16	1.29E-07
LOC100623776	TRIF	0.02	−0.48	0.28430	0.00119
LOC396750	ICAM1	0.82	−0.33	9.75E-18	1.23E-11
LOC100153830	MALT1	1.49	−0.78	1.83E-17	1.33E-08
LOC396880	IL8	1.71	−0.98	4.04E-37	2.07E-18
LOC100518917	PARP	0.40	−0.35	0.00013	0.00022
LOC100622156	TNFAIP3	1.58	−0.99	4.94E-37	4.43E-28
LOC100622590	BIRC2_3	0.50	−0.61	0.00108	1.80E-05
LOC100515635	CREB5	2.53	−1.27	5.95E-17	4.61E-07
LOC396915	EDN1	0.11	−0.68	0.02909	6.20E-11
LOC397454	ITPR1	0.81	−0.39	1.26E-19	2.07E-08
LOC397278	PMAIP1	0.90	−0.69	1.34E-09	1.72E-07
LOC407245	LDH	0.24	−0.32	1.53E-07	3.24E-28
LOC396823	GAPDH	0.71	−0.28	3.78E-19	8.99E-41
LOC445512	HMOX1	2.38	−1.37	6.68E-53	2.62E-28
LOC407608	PGK	0.59	−0.44	4.28E-23	4.92E-58
LOC100512013	ALDO	0.98	−0.60	3.18E-17	2.34E-12
LOC100126864	IFNGR2	1.39	−0.50	9.80E-31	5.24E-10
LOC397062	TFRC	0.03	−0.61	0.07717	8.04E-21
LOC396862	TIMP1	0.81	−0.28	1.02E-16	4.82E-06
LOC100623582	NBL1	1.29	−0.34	1.58E-22	0.00014
LOC397490	INHBB	1.95	−0.99	7.16E-10	6.23E-05
LOC100518554	INHBE	0.80	−0.37	4.79E-15	2.46E-08
MSTRG.7730	PDGFB	1.40	−0.40	1.78E-26	1.14E-05
LOC100517416	DUSP10	2.11	−1.00	5.37E-25	1.01E-10
LOC397260	SMAD2_3	−0.46	0.39	5.08E-06	3.01E-17
LOC100152069	SMAD6	−1.57	0.99	1.65E-13	6.05E-07
LOC100522839	ID1	−1.89	1.64	2.86E-63	3.67E-217
LOC100522677	E2F4_5	−0.90	0.38	7.12E-11	2.86E-06
LOC396691	BMPR1B	−1.08	0.41	2.31E-14	2.66E-05
LOC654298	ID2	−1.34	1.03	3.63E-13	2.60E-12
LOC100626978	ID3	−1.07	0.81	2.45E-19	5.13E-26
LOC100144508	ID4	−1.75	0.66	8.12E-18	0.00041
LOC100521305	SMAD7	−0.97	0.63	7.04E-07	9.90E-05
LOC100516289	PFKFB3	−0.80	0.68	3.84E-06	2.42E-11
LOC100156226	EP300	−1.15	0.52	3.85E-19	3.15E-08
LOC100192445	PDPK1	−0.73	0.31	3.17E-07	0.00189
LOC397027	CAPN1	−0.66	0.36	2.47E-06	1.36E-13
LOC493186	SOCS3	−1.11	0.94	0.00058	1.46E-06
LOC100621398	MRAS	2.52	−1.47	2.76E-06	0.00043
LOC100620969	EREG	−0.76	1.81	2.39E-06	0.00046
LOC397078	TGFB1	−0.56	0.43	2.25E-05	5.57E-13
LOC100524751	RIPK1	−0.81	0.35	1.44E-08	0.00057
LOC100157144	DUSP	−0.26	0.35	0.41187	6.08E-05
MSTRG.7893	NR4A1	−0.29	0.85	0.39207	7.41-17
LOC100524021	CACNB3	−0.27	0.36	0.39343	0.00266
LOC102166564	PDGFRB	−1.20	1.13	0.00016	8.65E-06
LOC100514115	FGFR3	−1.20	0.57	8.41E-21	3.70E-35
LOC654328	MET	−1.04	0.48	5.19E-23	2.23E-17

differentially expressed in H2-L, H4-L, and H6-L into eight possible expression profiles ($P < 0.05$) (**Figures 5A,B**, **6A–H**, and **Supplementary Table S11**), in which 612 were clustered into two profiles ($P \leq 0.05$), including two up-regulated patterns (Profile 6 and Profile 7). Profile 6 and 7 contained 452 and 160 DEGs, respectively. The consistent up-regulation of genes of Profile 6 in H2-L, H4-L, and H6-L indicated that DEGs may contribute to stimulatory functions during the polysaccharide anti-inflammatory function. The up-regulated genes of Profile 7 between only H2-L and H4-L revealed that these DEGs played a key role in the anti-inflammatory process. There was no significant difference in the up-regulated genes between H4-L and H6-L.

KEGG Pathway Enrichment Analysis of Differentially Expressed Genes Among the Three HRP Concentrations

A total of 11.1% (940/8,499) of the DEGs could be annotated. As shown in **Table 4**, the metabolic pathways (ko01100), Cytokine-cytokine receptor interaction (ko04060), Neuroactive ligand-receptor interaction (ko04080), Pathways in cancer (ko05200), Olfactory transduction (ko04740), PI3K-Akt signaling pathway (ko04151), Calcium signaling pathway (ko04020), Human papillomavirus infection (ko05165), Jak-STAT signaling pathway (ko04630), and Systemic lupus erythematosus (ko05322) pathways were significantly enriched. The 13 genes among 125 DEGs (22.40%) in Profile 6, and five genes accounting for 11.63% of 43 DEGs in Profile 7 were annotated to the cytokine-cytokine receptor interaction. The three genes among 125 DEGs (2.40%) in Profile 6, and two genes accounting for 4.65% of 43 DEGs in Profile 7 were annotated to the PI3K-Akt signaling pathway. The seven genes among 125 DEGs (5.60%) in Profile 6, and two genes accounting for

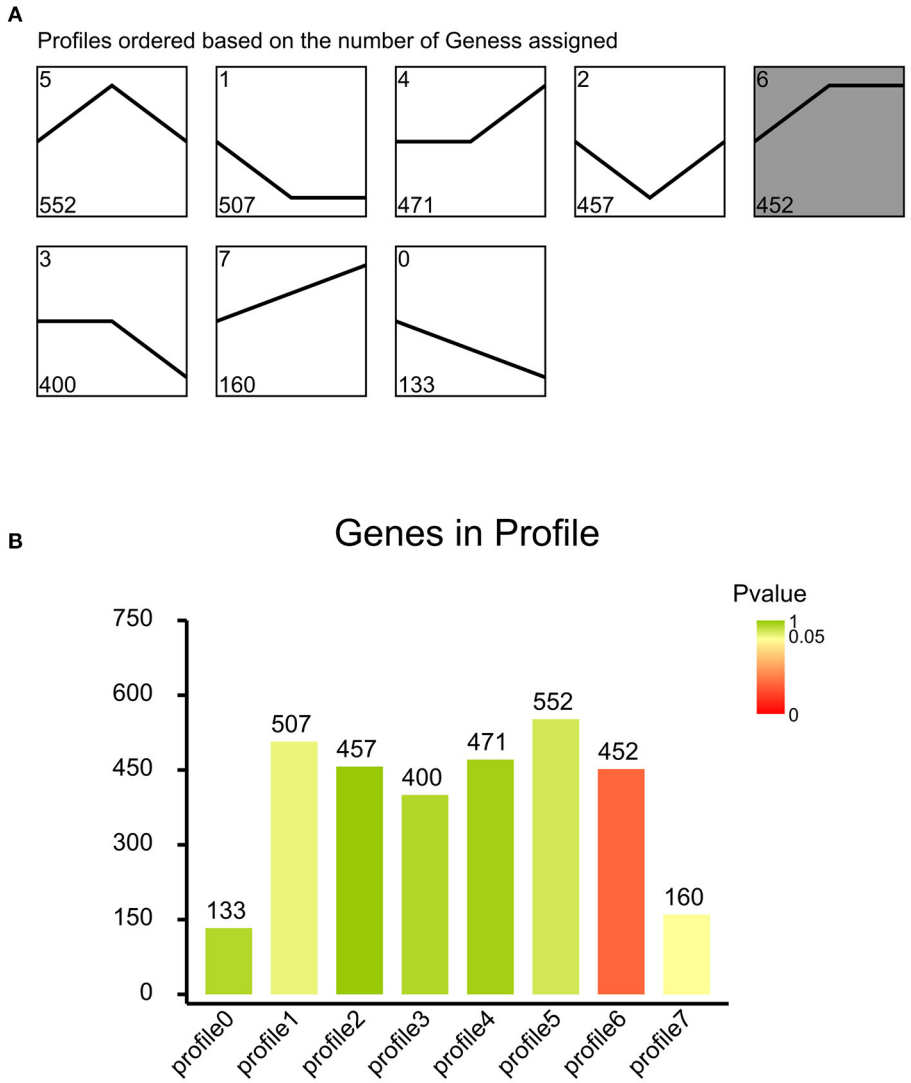

FIGURE 5 | (A) Eight profiles of DEGs with unique expression alterations over H2-L, H4-L, and H6-L. The profile number and the number of genes are shown on top of each square. The number of genes assigned is used to order the profiles. The profiles with color ($P < 0.05$): significant enrichment trend. The profiles without color: non-significant enrichment trend. **(B)** Trend DEGs number and *P*-value histogram. X-axis indicates the eight profiles; Y-axis shows DEGs number of every profile. The color of the column represents *P*-value.

4.65% of 43 DEGs in Profile 7 were annotated to the Jak-STAT signaling pathway.

Validation of RNA-seq Data Using qRT-PCR

Ten genes (NFKB2, MKNK, MAP2K1, MAP3K8, RRAS, TRAF1, NFKBIA, IL8, TNFAIP3, and TGFB1) were selected for qRT-PCR analysis.The results showed a strong correlation between the RNA sequencing data and the qRT-PCR data (**Figure 7**). This suggested that the expression results generated by RNA sequencing were reliable.

DISCUSSION

In the current piglet production system, early weaning is an important means to improve the efficiency of pig production (24, 25). However, early weaning is very stressful to piglets, and can easily cause piglet immune stress and affect the healthy growth of piglets. How to alleviate the immune stress of piglets has become an area of concerning the piglet industry (26, 27). *Hippophae rhamnoides* extracts are widely used to enhancing immunity in both healthy and diseased animals (28). Polysaccharide is the main active ingredient of *H.rhamnoides*. HRP has been shown to have immunomodulatory effects (10). No research has been conducted on the molecular mechanism of HRP in piglets by transcriptome sequencing. Variation in gene expression may provide a key to uncovering the mechanisms of diseases. Transcriptome sequencing, also called RNA-seq, provides a new technique to quantify whole-genome expression profiling in any organism. It promises digital transcriptome profiling with high resolution and is rapidly replacing microarray technology (29, 30). Studies have used RNA-seq technology to explore the protective mechanism of IPEC-J2 cells stimulated

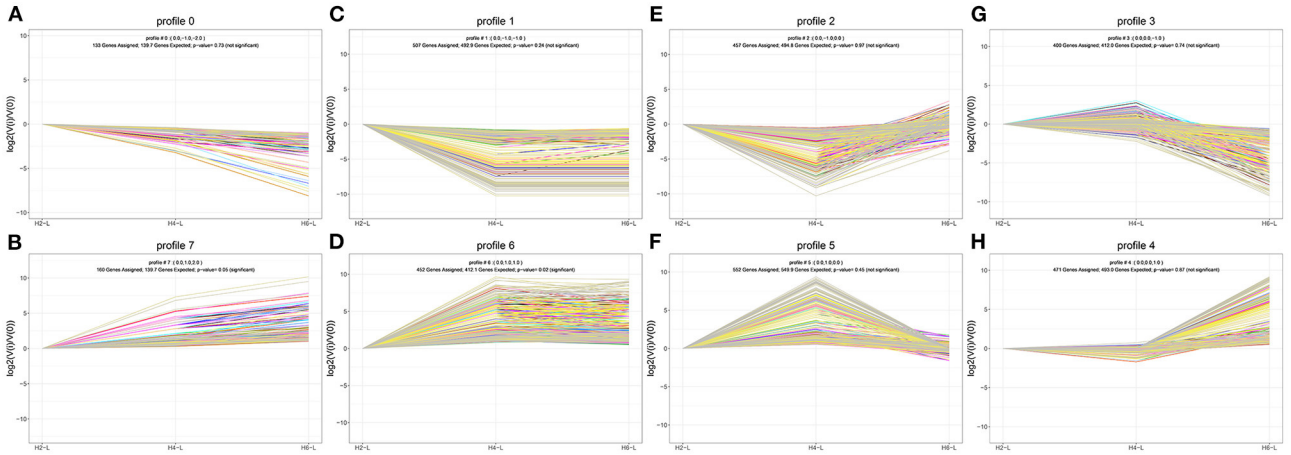

FIGURE 6 | DEGs expression profiles **(A–H)** in the IPEC-J2 cells induced by LPS after HRP pre-treatment. **(A,B)**, **(C,D)**, **(E,F)**, and **(G,H)** are two antagonistic profiles of DEGs curves, respectively. Each X-axis indicates the concentration of HRP pre-treated IPEC-J2 cells (H2-L, H4-L, and H6-L), Y-axis shows expression changes.

by LPS after astragalus polysaccharide (APS) pretreatment. APS relieves cell damage by inhibiting the activation of the MAPK and NF-κB inflammatory pathways, thereby reducing intestinal inflammation (31). Cluster analysis revealed 3134 DEGs that were differentially expressed in H2-L, H4-L, and H6-L into eight possible expression profiles, in which 168 were clustered into two profiles. The up-regulated genes of Profile 6, only between H2-L and H4-L, revealed that these DEGs played a key role in the anti-inflammatory process. The consistent up-regulation of genes of the Profile 7 in H2-L, H4-L, and H6-L indicated that DEGs may contribute to stimulatory functions during the polysaccharide anti-inflammatory process. KEGG enrichment analysis found that the six identified pathways were related to the immune system. Among the six identified pathways related to the immune system, the MAPK signaling pathway and NF-κB signaling pathway play important immunomodulatory roles in our study. Finally, we selected 10 DEGs (NFKB2, MKNK2, MAP2K1 (MEK1), MAP3K8, RRAS, TRAF1, NFKBIA, IL8, TNFAIP3, and TGFB1) related to the main immune pathways to validate the RNA-Seq data using qRT-PCR.

The downstream signal transduction pathways mediated by LPS mainly include the NF-κB signal transduction pathway and the MAPK signal transduction pathway (32). Extracellular regulated protein kinases (ERK), c-Jun N-terminal kinase (JNK), and p38 mitogen-activated protein kinase (p38 MAPK) belong to the three subtypes of the MAPK signaling pathway (33). The Ras/Mitogen-activated protein kinase kinase (MEK)/ERK pathway is one of the most important signal transduction pathways among the MAPK pathways. The Ras/MEK/ERK pathway involves the regulation of a variety of physiological functions of cells and plays a key role in the pathogenesis and pathophysiology of various diseases (34). The activation of ERK is a key step in transferring signals from surface receptors to the nucleus. The activation of ERK induced by LPS leads to the secretion of large amounts of tumor necrosis factor-alpha (TNF-α), as well as interleukin-6 (IL-6) and IL-8, and increases the expression of inducible nitric oxide synthase and nitric oxide. Son of Sevenless (SOS) binds to RRAS-Guanosine diphosphate (GDP), prompting guanosine triphosphate (GTP) to replace GDP on RRAS and activate RRAS protein, then activate MEK and ERK sequentially. In recent years, some initial reports on targeting SOS to inhibit the activation of RRAS, thereby inhibiting the activation of the MAPK signaling pathway, have also achieved satisfactory results (35). The activation of ERK promotes the secretion of MKNK. MKNK is an important downstream protein kinase of ERK that has an important immunomodulatory function. MKNK dysfunction can inhibit the inflammatory signal of upstream ERK and affect downstream eIf4E and CREB and other effector proteins, thereby preventing cell inflammation. MAP3K8

TABLE 4 | 10 top KEGG pathways with high representation of the DEGs.

pathways	No. of DEGs with pathway annotation			Pathway ID
	All profiles (940)	Profile 6 (125)	Profile 7 (43)	
Metabolic pathways	162 (17.23%)	28 (22.40%)	5 (11.63%)	ko01100
Cytokine-cytokine receptor interaction	81 (8.62%)	13 (10.40%)	4 (9.30%)	ko04060
Neuroactive ligand-receptor interaction	73 (7.77%)	9 (7.20%)	1 (2.33%)	ko04080
Pathways in cancer	69 (7.34%)	5 (4.00%)	4 (9.30%)	ko05200
Olfactory transduction	67 (7.13%)	8 (6.40%)	3 (6.98%)	ko04740
PI3K-Akt signaling pathway	48 (5.11%)	3 (2.40%)	2 (4.65%)	ko04151
Calcium signaling pathway	42 (4.47%)	5 (4.00%)	1 (2.33%)	ko04020
Human papillomavirus infection	42 (4.47%)	2 (1.60%)	4 (9.30%)	ko05165
Jak-STAT signaling pathway	40 (4.26%)	7 (5.60%)	2 (4.65%)	ko04630
Systemic lupus erythematosus	37 (3.94%)	5 (4.00%)	1 (2.33%)	ko05322

is essential for the activation of the intracellular MAPK/ERK pathway induced by LPS in cells (36). Therefore, MAP3K8 is a critical factor for the production of pro-inflammatory cytokines during immune responses (37). Therefore, in our study, the results showed that MKNK2, MAP2K1, MAP3K8, and RRAS gene expression levels were down-regulated after HRP pre-treatment compared with the LPS group. The reduction of MKNK2, MAP2K1, MAP3K8, and RRAS gene levels plays an important immuno-regulatory role in HRP alleviating LPS-induced cell damage.

LPS, a trigger of inflammation, can activate the NF-κB signaling pathway (38). NFKBIA is a specific inhibitor of NF-κB that binds to NF-κB at a resting state to cause NF-κB to enter an inactive state. Phosphorylated NFKBIA is separated from NF-κB, and NF-κB is activated. Activated NF-κB migrates to the nucleus, where NF-κB nuclear transcription factor can up-regulate the levels of inflammation-related genes TNF, IL-6, and IL-8 and down-regulate the level of TGFB1 (39). Studies have proven that LPS promotes the degradation of NFKBIA, activates the DNA binding ability of NF-κB, and regulates the gene expression level of cytokines (40). Moreover, TRAFs are key regulatory proteins in NF-κB signaling pathways. TRAF1 enhances the activation of TNF-R2 induced by NF-κB (41), therefore promoting the release of a large number of inflammatory cytokines. A previous study showed that TRAF1 is over-expressed in a variety of lymphoma and leukemia cell lines and is a crucial mediator of diverse oncogenic signaling in the development of lymphoid malignancies. TNFAIP3 is a cytokine-induced protein that inhibits apoptosis and activates NF-κB (42). The main function of TNFAIP3 is to inhibit the activity of NF-κB and inhibit TNF-mediated apoptosis, thereby having an important impact on immune regulation and inflammatory processes (43, 44). The release of NFKB2, TRAF1, NFKBIA, IL8, and TNFAIP3, as important regulatory genes of NF-κB, can activate the upstream pathway NF-κB. Jayashankar et al. found that the intervention of supercritical carbon dioxide extract from seabuckthorn leaves can inhibit the expression levels of TNF-α and IL-6 after LPS-induced inflammatory damage, inhibit the activation of the MAPK/NF-κB signaling pathway, reduce inflammation, and play a immunomodulatory role (45). Our study indicated that NFKB2, TRAF1, NFKBIA, IL8, and TNFAIP3were increased and TGFB1 was reduced after LPS induction. However, after HRP pre-treatment, the gene expression level showed the opposite trend and they played an important immune-regulatory role in HRP alleviating LPS-induced cell damage, which provided more targets and prevention directions for theoretical and basic research on intestinal health. Studies have shown that APS may block radiation-induced bystander effects (RIBE) in bone mesenchymal stem cells (BMSCs) induced by the irradiated A549 through regulating the MAPK/NF-κB pathway (46).

CONCLUSIONS

This study was the first using a RNA-Seq technique to establish a dynamic transcriptomic profile of three stages (C, L, and H6-L)

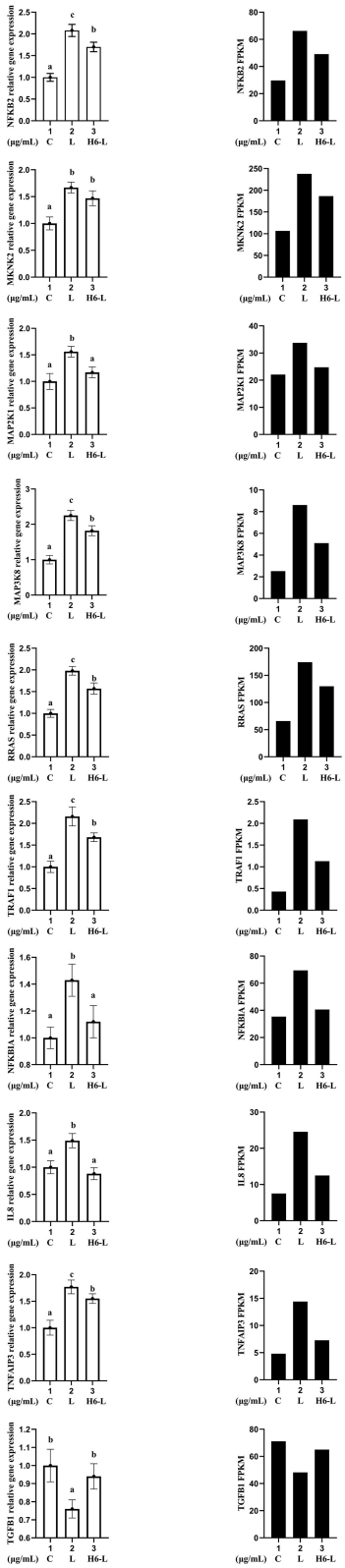

FIGURE 7 | Candidate unigene expression levels revealed by qRT-PCR (left side) and RNA-seq (right side). Data from qRT-PCR are means of five replicates and bars represent SD.

related to pre-treatment with HRP followed by challenge with LPS in IPEC-J2 cells. Subsequently, bioinformatics analysis (GO, KEGG, and series cluster) helped us to identify key regulatory genes (IL8 and NFKB2, among others.) related IPEC-J2 cellular immune regulation. Transcriptome analysis also showed that HRP protected IPEC-J2 cells from LPS-induced inflammation and decreased the expression of inflammatory cytokines by mainly inhibiting the MAPK/NF-κB signaling pathway. This study does not only provide the useful transcriptomic reference for HRP to effectively protect LPS-induced inflammatory damage in IPEC-J2 cells, but also provides a benchmark for the discovery of biomarkers related to HRP immune regulation.

DATA AVAILABILITY STATEMENT

The data presented in the study are deposited in the following repository: https://www.ncbi.nlm.nih.gov/Traces/study/, accession number PRJNA854604.

AUTHOR CONTRIBUTIONS

ML, HS, and LZ contributed to conception, design of study, drafting the manuscript, and critical revision. YZ conducted acquisition of data. LC conducted analysis of data. All authors read and approved the final manuscript.

FUNDING

This project was supported by grant from the National Key Research and Development Program of China (2017YFD0500506) and the Personnel Foundation of Heilongjiang Bayi Agricultural University (NO. XYB202015).

SUPPLEMENTARY MATERIAL

The Supplementary Material for this article can be found online at: https://www.frontiersin.org/articles/10.3389/fnut.2022.944390/full#supplementary-material

REFERENCES

1. He Q, Tang H, Ren P, Kong X, Wang Y. Dietary supplementation with l-arginine partially counteracts serum metabonome induced by weaning stress in piglets. *J Prot Res*. (2011) 10:5214–21. doi: 10.1021/pr200688u
2. Shanahan F. Probiotics in inflamatory bowel disease. *Gut*. (2001) 48:609. doi: 10.1136/gut.48.5.609
3. Hoque MA, Skerratt LF, Rahman MA, Rabiul Alam Beg ABM, Debnath NC. Factors limiting traditional household duck production in Bangladesh. *Trop Ani Health Prod*. (2010) 42:1579–87. doi: 10.1007/s11250-010-9609-z
4. Lakatos L, Rednik A. Astroenterologic sub-acute care unit at the hospital department of internal medicine letter. *Orvosi Hetilap*. (1997) 138:1668.
5. Berschneider, M. Development of a normal cultured small intestinal epithelial cell line which transport na and cl. *Gastroenterology*. (1989) 96:A41.
6. Hermes RG, Manzanilla EG, Susana, M. Martín-Orúe, José F, Pérez, et al. Influence of dietary ingredients on *in vitro* inflammatory response of intestinal porcine epithelial cells challenged by an enterotoxigenic escherichia coli (k88). *Compar Immunol Microbiol Infect Dis*. (2011) 34:479–88. doi: 10.1016/j.cimid.2011.08.006
7. Pan L, Qin G, Zhao Y, Wang J, Liu F, Che D. Effects of soybean agglutinin on mechanical barrier function and tight junction protein expression in intestinal epithelial cells from piglets. *Int J Molecul*. (2013) 14:21689–704. doi: 10.3390/ijms141121689
8. Mlot C. Antidotes for antibiotic use on the farm. *BioScience*. (2000) 50, 955–960. doi: 10.1641/0006-3568(2000)050(0955:AFAUOT)2.0.CO;2
9. VanCott JL, Kobayashi T, Yamamoto M, Pillai S, McGhee JR, Kiyono H. Induction of pneumococcal polysaccharide-specific mucosal immune responses by oral immunization. *Vaccine*. (1996) 14:392–8. doi: 10.1016/0264-410X(95)00198-A
10. Zhang A, Sun H, Wang X. Recent advances in natural products from plants for treatment of liver diseases. *Eur J Med Chem*. (2013) 63:570–7. doi: 10.1016/j.ejmech.2012.12.062
11. Wang X, Liu J, Zhang X, Zhao S, Zou K, Xie J. Seabuckthorn berry polysaccharide extracts protect against acetaminophen induced hepatotoxicity in mice via activating the Nrf-2/HO-1-SOD-2 signaling pathway. *Phytomedicine*. (2018) 38:90–7. doi: 10.1016/j.phymed.2017.11.007
12. Suryakumar G, Gupta A. Medicinal and therapeutic potential of sea buckthorn (*hippophae rhamnoides l.*). *J Ethnopharmacol*. (2011) 138:268–78. doi: 10.1016/j.jep.2011.09.024
13. Zhang W Zhang X, Zou K, Xie J, Zhao S, Liu J. Seabuckthorn berry polysaccharide protects against carbon tetrachloride-induced hepatotoxicity in mice via anti-oxidative and anti-inflammatory activities. *Food Func*. (2017) 8:3130–38. doi: 10.1039/C7FO00399D
14. Shi L, Fang B, Yong Y, Li X, Gong D, Li J. Chitosan oligosaccharide-mediated attenuation of LPS-induced inflammation in IPEC-J2 cells is related to the TLR4/NF-κB signaling pathway. *Carbohyd Poly*. (2019) 219:269–79. doi: 10.1016/j.carbpol.2019.05.036
15. Zhao L, Li M, Su S, Geng T, Sun H. Hippophae rhamnoides Linn polysaccharide enhances antioxidant enzyme activity, cytokine level and related mRNA expression in intestinal porcine epithelial cells. *Canadian J Ani Sci*. (2020) 100:193–204. doi: 10.1139/cjas-2019-0134
16. Zhao L, Li M, Sun K, Su S, Geng T, Sun, H. Hippophae rhamnoides polysaccharides protect ipec-j2 cells from lps-induced inflammation, apoptosis and barrier dysfunction in vitro via inhibiting tlr4/nf-κb signaling pathway. *Int J Biol Macromol*. (2020) 155:1202–15. doi: 10.1016/j.ijbiomac.2019.11.088
17. Shao D, Hu Y, Wang Q, Tong H, Shi S. Transcriptome sequencing reveals genetic mechanisms of reproduction performance stimulated by dietary daidzein in laying breeder *Hens Theriogenol*. (2019) 142:120–30. doi: 10.1016/j.theriogenology.2019.09.040
18. Gao Y, Li S, Bao X, Luo C, Yang H, Wang J. Transcriptional and proteomic analysis revealed a synergistic effect of aflatoxin m1 and ochratoxin a mycotoxins on the intestinal epithelial integrity of differentiated human Caco-2 cells. *J Prot Res*. (2018) 17:3128–42. doi: 10.1021/acs.jproteome.8b00241
19. Liu H, Zhang W, Dong S. Protective effects of sea buckthorn polysaccharide extracts against LPS/d-GalN-induced acute liver failure in mice via suppressing TLR4-NF-κB signaling. *J Ethnopharmacol*. (2015) 176(Complete):69–78. doi: 10.1016/j.jep.2015.10.029
20. Ni W, Gao T, Wang H, Du Y, Li J, Li, C. Anti-fatigue activity of polysaccharides from the fruits of four Tibetan plateau indigenous medicinal plants. *J Ethnopharmacol*. (2013) 150:529–535. doi: 10.1016/j.jep.2013.08.055
21. Zhao L, Geng T, Sun K, Su S, Zhao Y, Bao N. Proteomic analysis reveals the molecular mechanism of Hippophae rhamnoides polysaccharide intervention in LPS-induced inflammation of IPEC-J2 cells in piglets. *Int J Biol Macromol*. (2020) 164:3294–304. doi: 10.1016/j.ijbiomac.2020.08.235
22. Langmead B, Salzberg SL. Fast gapped-read alignment with Bowtie 2. *Nat Meth*. (2012) 9:357–9. doi: 10.1038/nmeth.1923
23. Li B, Dewey CN. RSEM: accurate transcript quantification from RNA-Seq data with or without a reference genome. *BMC Bioinform*. (2011) 12:1. doi: 10.1186/1471-2105-12-323
24. Bomba L, Minuti A, Moisá SJ, Trevisi E, Eufemi E, Lizier M. Gut response induced by weaning in piglet features marked changes in

immune and inflammatory response. *Func Int Genom*. (2014) 14:657–71. doi: 10.1007/s10142-014-0396-x
25. Khafipour E, Munyaka PM, Nyachoti CM, Krause DO, Rodriguez-Lecompte JC. Effect of crowding stress and escherichia coli k88+ challenge in nursery pigs supplemented with anti-escherichia coli k88+ probiotics. *J Animal Sci*. (2014) 92:2017–29. doi: 10.2527/jas.2013-7043
26. Pluske JR, Hampson DJ, Williams IH. Factors influencing the structure and function of the small intestine in the weaned pig: a review. *Livestock Prod Sci*. (1997) 51:215–36. doi: 10.1016/S0301-6226(97)00057-2
27. Xiao T. Innate immune recognition of nucleic acids. *Immunol Res*. (2009) 43:98–108. doi: 10.1007/s12026-008-8053-x
28. Tanwar H, Shweta, Singh D, Singh SB, Ganju L. Anti-inflammatory activity of the functional groups present in Hippophae rhamnoides (*Seabuckthorn*) leaf extract. *Inflammopharmacology*. (2017) 26:291–301. doi: 10.1007/s10787-017-0345-0
29. Herwig R. Predictive network modelling with toxicogenomics data. *Toxicol Lett*. (2014) 229:S4–S21. doi: 10.1016/j.toxlet.2014.06.043
30. Davoli R, Zambonelli P, Hedeegard J, Hornshoj H, Nanni Costa L, Stella A. Transcriptome analysis of skeletal muscle tissue to identify genes involved in pre-slaughter stress response in pigs. *Italian J Anil Sci*. (2009) 8:69–71. doi: 10.4081/ijas.2009.s2.69
31. Dong N, Li X, Xue C, Zhang L, Wang C, Xu X. Astragalus polysaccharides alleviates lps-induced inflammation via the nf-κb/mapk signaling pathway. *J Cell Physiol*. (2020) 235:1–16. doi: 10.1002/jcp.29452
32. Wu CX, Sun H, Liu Q, Guo H, Gong JP. Lps induces hmgb1 relocation and release by activating the nf-κb-cbp signal transduction pathway in the murine macrophage-like cell line raw264.7. *J Surg Res*. (2012) 175:88–100. doi: 10.1016/j.jss.2011.02.026
33. Costa AP, Lopes MW, Rieger DK, Barbosa SGR, Gonçalves FM, Xikota JC. Differential activation of mitogen-activated protein kinases, ERK 1/2, 38MA.PK and JNK p54/p46 during postnatal development of rat hippocampus. *Neurochem Res*. (2015) 41:1160–9. doi: 10.1007/s11064-015-1810-z
34. Okano JI, Snyder LC, Rustgi AK. Paclitaxel induces prolonged activation of the ras/mek/erk pathway independently of activating the programmed cell death machinery. *Gastroenterology*. (2011) 120:A661–2. doi: 10.1016/S0016-5085(01)83290-X
35. Zhao H, Li YY, Fucini RV, Ross SE, Pessin JE, Koretzky GA. T cell receptor-induced phosphorylation of sos requires activity of cd45, lck, and protein kinase c, but not erk. *J Biol Chem*. (1997) 272:21625–34. doi: 10.1074/jbc.272.34.21625
36. Santag S, Siegel F, Wengner AM, Lange C, Petersen K. Abstract 341: preclinical mode of action and anti-tumor efficacy of the selective mknk1 inhibitor bay 11,43,269 in nsclc models. *Cancer Res*. (2016) 76(14 Supplement):341. doi: 10.1158/1538-7445.AM2016-341
37. Wei R, Yang Q, Han B, Li Y, Yao K, Yan, X. Microrna-375 inhibits colorectal cancer cells proliferation by downregulating jak2/stat3 and map3k8/erk signaling pathways. *Oncotarget*. (2017) 8:16633–41. doi: 10.18632/oncotarget.15114
38. Shishodia S, Koul D, Aggarwal BB. Cyclooxygenase (cox)-2 inhibitor celecoxib abrogates tnf-induced nf-κb activation through inhibition of activation of iκbα kinase and akt in human non-small cell lung carcinoma: correlation with suppression of cox-2 synthesis. *J Immunol*. (2004) 173:2011–22. doi: 10.4049/jimmunol.173.3.2011
39. Koh Y. Inhibition of SRC Tyrosine kinases suppresses activation of nuclear factor-κB, and Serine and Tyrosine Phosphorylation of IκB-α in Lipopolysaccharide-stimulated Raw 264.7 macrophages. *J Toxicol Environ Health, Part A*. (2005) 68:1643–62. doi: 10.1080/15287390500192114
40. Li MY, Sun L, Niu XT, Chen XM, Tian JX, Kong YD, et al. Astaxanthin protects lipopolysaccharide-induced inflammatory response in Channa argus through inhibiting NF-κB and MAPKs signaling pathways. *Fish Shellfish Immunol*. (2019) 86:280–6. doi: 10.1016/j.fsi.2018.11.011
41. Tang X, Zhang L, Wei W. Roles of TRAFs in NF-κB signaling pathways mediated by BAFF. *Immunol Lett*. (2018) 196:113–8. doi: 10.1016/j.imlet.2018.01.010
42. Rhee L, Murphy SF, Kolodziej LE, Grimm,WA, Weber CR, Lodolce JP. Expression of TNFAIP3 in intestinal epithelial cells protects from DSS- but not TNBS-induced colitis. *Am J Physiol-Gastroint Liver Physiol*. (2012) 303:G220–7. doi: 10.1152/ajpgi.00077.2012
43. Gui J, Yue Y, Chen R, Xu W, Xiong S. A20 (TNFAIP3) alleviates CVB3-induced myocarditis via inhibiting NF-κB signaling. *PLoS ONE*. (2012) 7:e46515. doi: 10.1371/journal.pone.0046515
44. Varfolomeev E, Goncharov T, Maecker H, Zobel K, Komuves LG, Deshayes K, et al. Cellular inhibitors of apoptosis are global regulators of NF- B and MAPK activation by members of the TNF family of receptors. *Sci Signal*. (2012) 5:ra22. doi: 10.1126/scisignal.2001878
45. Jayashankar B, Mishra KP, Kumar MSY, Udayasankar K, Misra K, Ganju L, et al. A supercritical CO2 extract from seabuckthorn leaves inhibits pro-inflammatory mediators via inhibition of mitogen activated protein kinase p38 and transcription factor nuclear factor-κB. *Int Immunopharmaco*l. (2012) 13:461–7. doi: 10.1016/j.intimp.2012.05.011
46. Zhang L, Luo Y, Lu Z, He J, Liu Y. Astragalus polysaccharide inhibits ionizing radiation-induced bystander effects by regulating mapk/nf-kb signaling pathway in bone mesenchymal stem cells (bmscs). *Med Mon Int Med J Exp Clin Res*. (2018) 24:4649. doi: 10.12659/MSM.909153

Conflict of Interest: The authors declare that the research was conducted in the absence of any commercial or financial relationships that could be construed as a potential conflict of interest.

Publisher's Note: All claims expressed in this article are solely those of the authors and do not necessarily represent those of their affiliated organizations, or those of the publisher, the editors and the reviewers. Any product that may be evaluated in this article, or claim that may be made by its manufacturer, is not guaranteed or endorsed by the publisher.

Copyright © 2022 Li, Chen, Zhao, Sun and Zhao. This is an open-access article distributed under the terms of the Creative Commons Attribution License (CC BY). The use, distribution or reproduction in other forums is permitted, provided the original author(s) and the copyright owner(s) are credited and that the original publication in this journal is cited, in accordance with accepted academic practice. No use, distribution or reproduction is permitted which does not comply with these terms.

Frontiers in Nutrition

Explores what and how we eat in the context of health, sustainability and 21st century food science

A multidisciplinary journal that integrates research on dietary behavior, agronomy and 21st century food science with a focus on human health.

Discover the latest Research Topics

See more →

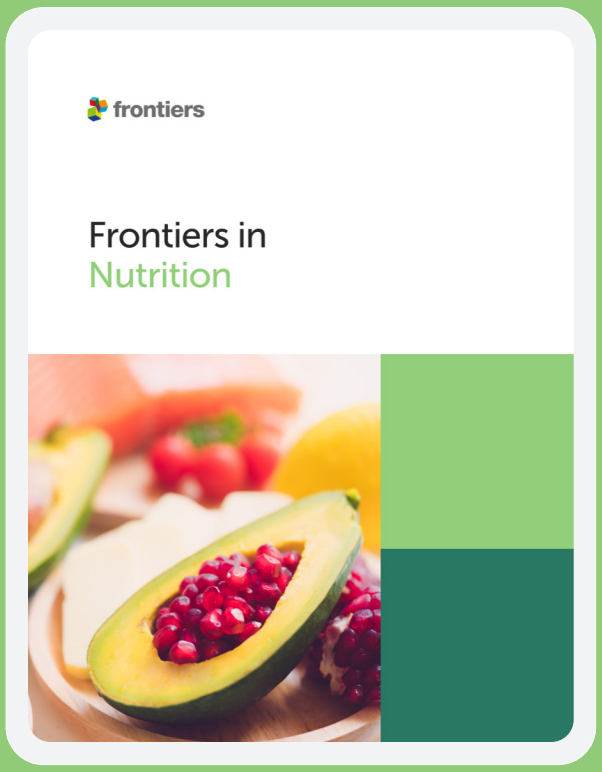

Frontiers

Avenue du Tribunal-Fédéral 34
1005 Lausanne, Switzerland
frontiersin.org

Contact us

+41 (0)21 510 17 00
frontiersin.org/about/contact